



**HELLENIC REPUBLIC
UNIVERSITY OF IOANNINA
SCHOOL OF ENGINEERING
DEPARTMENT OF MATERIALS SCIENCE AND ENGINEERING**

**A hybrid modeling framework for simulating plasma-surface interactions of rough
polymeric substrates**

George Memos

PhD Dissertation

Ioannina 2021



**ΕΛΛΗΝΙΚΗ ΔΗΜΟΚΡΑΤΙΑ
ΠΑΝΕΠΙΣΤΗΜΙΟ ΙΩΑΝΝΙΝΩΝ
ΠΟΛΥΤΕΧΝΙΚΗ ΣΧΟΛΗ
ΤΜΗΜΑ ΜΗΧΑΝΙΚΩΝ ΕΠΙΣΤΗΜΗΣ ΥΛΙΚΩΝ**

**Υβριδικό υπολογιστικό πλαίσιο προσομοίωσης αλληλεπιδράσεων πλάσματος-επιφανειακής
τραχύτητας σε πολυμερικά υποστρώματα**

Γεώργιος Μέμος

Διδακτορική Διατριβή

Ιωάννινα 2021

Η έγκριση της διδακτορικής διατριβής από το Τμήμα Μηχανικών Επιστήμης Υλικών της Πολυτεχνικής Σχολής του Πανεπιστημίου Ιωαννίνων δεν υποδηλώνει αποδοχή των γνώμών του συγγραφέα Ν. 5343/32, άρθρο 202, παράγραφος 2

Ημερομηνία αίτησης του κ. Γεώργιου Μέμου: 22-12-2015

Ημερομηνία ορισμού Τριμελούς Συμβουλευτικής Επιτροπής: 9-2-2016

Μέλη Τριμελούς Συμβουλευτικής Επιτροπής:

Επιβλέπων

Ελευθέριος Λοιδωρίκης, Καθηγητής του Τμήματος Μηχανικών Επιστήμης Υλικών της Πολυτεχνικής Σχολής του Πανεπιστημίου Ιωαννίνων

Μέλη*

Αγγελική Τσερέπη, Δ/ντρια Ερευνών του Ινστιτούτου Νανοεπιστήμης και Νανοτεχνολογίας του ΕΚΕΦΕ «ΔΗΜΟΚΡΙΤΟΣ»

Ευάγγελος Γογγολίδης, Δ/ντης Ερευνών του Ινστιτούτου Νανοεπιστήμης και Νανοτεχνολογίας του ΕΚΕΦΕ «ΔΗΜΟΚΡΙΤΟΣ»

Ημερομηνία ορισμού θέματος: 9-2-2016

«Προσομοίωση ηλεκτρικών εκκενώσεων πλάσματος χαμηλής θερμοκρασίας πλάσματος σε πολλαπλές χωρικές κλίμακες»

Ημερομηνία τροποποίησης θέματος: 15-7-2020

«Υβριδικό υπολογιστικό πλαίσιο προσομοίωσης αλληλεπιδράσεων πλάσματος-επιφανειακής τραχύτητας σε πολυμερικά υποστρώματα (A hybrid modeling framework for simulating-plasma surface interactions of rough polymeric substrates)»

ΔΙΟΡΙΣΜΟΣ ΕΠΤΑΜΕΛΟΥΣ ΕΞΕΤΑΣΤΙΚΗΣ ΕΠΙΤΡΟΠΗΣ : 21/10/20

1. Ελευθέριος Λοιδωρίκης, Καθηγητής του Τμήματος Μηχανικών Επιστήμης Υλικών της Πολυτεχνικής Σχολής του Πανεπιστημίου Ιωαννίνων

2. Αγγελική Τσερέπη, Δ/ντρια Ερευνών του Ινστιτούτου Νανοεπιστήμης και Νανοτεχνολογίας του ΕΚΕΦΕ «ΔΗΜΟΚΡΙΤΟΣ»

3. Ευάγγελος Γογγολίδης, Δ/ντης Ερευνών του Ινστιτούτου Νανοεπιστήμης και Νανοτεχνολογίας του ΕΚΕΦΕ «ΔΗΜΟΚΡΙΤΟΣ»

4. Βασίλειος Κωνσταντούδης, Ερευνητή Β του Ινστιτούτου Νανοεπιστήμης και Νανοτεχνολογίας του ΕΚΕΦΕ «ΔΗΜΟΚΡΙΤΟΣ»


5. Δημήτριος Φωτιάδης, Καθηγητής του Τμήματος Μηχανικών Επιστήμης Υλικών της Πολυτεχνικής Σχολής του Πανεπιστημίου Ιωαννίνων

6. Δημήτριος Παπαγεωργίου, Αναπληρωτής Καθηγητής του Τμήματος Μηχανικών Επιστήμης Υλικών της Πολυτεχνικής Σχολής του Πανεπιστημίου Ιωαννίνων

7. Χριστίνα Λέκκα, Αναπληρώτρια Καθηγήτρια του Τμήματος Μηχανικών Επιστήμης Υλικών της Πολυτεχνικής Σχολής του Πανεπιστημίου Ιωαννίνων

Έγκριση Διδακτορικής Διατριβής με βαθμό «ΑΡΙΣΤΑ» στις 23/04/2021

Ο Πρόεδρος του Τμήματος


Απόστολος Αυγερόπουλος
Καθηγητής



Η Γραμματέας του Τμήματος


Μαρία Κόντου

*Σημείωση. Την διδακτορική διατριβή συνεπίβλεψε ο Δρ. Γεώργιος Κόκκορης, Συνεργαζόμενος Ερευνητής του Ινστιτούτου Νανοεπιστήμης και Νανοτεχνολογίας του ΕΚΕΦΕ Δημόκριτος

Date of Application of Mr George Memos: 22-12-2015

Date of Appointment of PhD Advisory Committee: 9-2-2016

Members of the Three-Member Advisory Committee:

Thesis Advisor

Elefterios Lidorikis, Professor, Department of Materials Science and Engineering, School of Engineering, University of Ioannina

Members*

Angeliki Tserepi, Director of Research, Institute of Nanoscience and Nanotechnology, NCSR «DEMOKRITOS»

Evangelos Gogolides, Director of Research, Institute of Nanoscience and Nanotechnology, NCSR «DEMOKRITOS»

Date of dissertation topic definition: 9-2-2016

«Multiscale modeling of low temperature plasma discharges»

Date of dissertation topic modification: 15-7-2020

«A hybrid modeling framework for simulating-plasma surface interactions of rough polymeric substrates»

DATE OF APPOINTMENT OF THE SEVEN-MEMBER EXAMINATION COMMITTEE:

21/10/20

1. **Elefterios Lidorikis**, Professor, Department of Materials Science and Engineering, School of Engineering, University of Ioannina

2. **Angeliki Tserepi**, Director of Research, Institute of Nanoscience and Nanotechnology, NCSR «DEMOKRITOS»

3. **Evangelos Gogolides**, Director of Research, Institute of Nanoscience and Nanotechnology, NCSR «DEMOKRITOS»

4. **Vassilios Constantoudis**, Senior Researcher, Institute of Nanoscience and Nanotechnology, NCSR «DEMOKRITOS»


5. **Dimitrios Fotiadis**, Professor, Department of Materials Science and Engineering, School of Engineering, University of Ioannina

6. **Dimitrios Papageorgiou**, Associate Professor, Department of Materials Science and Engineering, School of Engineering, University of Ioannina

7. **Christina Lekka**, Associate Professor, Department of Materials Science and Engineering, School of Engineering, University of Ioannina

The PhD Dissertation was approved with the grade of «Excellent » on 23/04/2021

The Chairman of the Department


Apostolos Avgeropoulos
Professor



The Secretary of the Department


Maria Kontou

***Note.** The PhD Dissertation was co-supervised by Dr. **George Kokkoris**, Research Associate, Institute of Nanoscience & Nanotechnology, NCSR «DEMOKRITOS»

ABSTRACT

Introduction

Plasma etching,¹ in addition to its traditional use for pattern transfer in microelectronics, is utilized in nanotechnology to functionalize polymers by improving their surface properties through the modification of the chemical composition and the morphology of the surface. The former is achieved through the creation of reactive centers at which plasma gas fragments or atoms can stick as new functional groups while the latter through the removal of material in chemical and/or physical ways. An outcome of this plasma-induced change, which has attracted much attention lately both experimentally and theoretically is surface roughness.

Plasma induces micro/nano roughness on the surface of the polymeric substrates, a factor that has major importance in the surface properties (e.g. wetting behavior, interaction of surfaces with cells). It is critical to study the mechanisms that affect surface roughness and, ultimately, to design “recipes” delivering desired surface roughness. However, plasma-surface interactions are complex and the process design is usually based on a trial and error procedure.

Many studies to date have pinpointed several potential mechanisms for roughness formation and evolution, such as scattering/reflection of ions within the topographic features of the rough profile, change of etching yield with the angle of incidence, deposition of material engendered in the plasma as well as re-deposition of material ejected by etching, to name a few. There is also significant overlapping among such mechanisms; usually, a roughness experimental measurement can be interpreted by invoking more than one physical mechanism. These mechanisms take place concurrently during plasma etching, and the expectation for segregating their effects via experiment is low. Modifying the process conditions to diminish the effect of one phenomenon will commonly intensify another. However, for efficient process design and optimization, it is essential to understand the mechanisms influencing the etched rough profile.

The only approach which enables to examine the effect of a mechanism on surface roughness during etching either independently or jointly with other mechanisms is **numerical simulation**. The latter is of major interest for giving indications about the physics governing various processes and to ultimately pinpoint the etching control mechanisms as far as the roughness evolution is concerned. It can consequently provide aid for specifying the ideal operating conditions for the desired roughness, thus, enabling the optimization of a given etching process.

¹Plasma, an outstanding “tool” in microelectronics and nanotechnology, is created in reactors operating at low pressures. An electromagnetic field is imposed on the reactor gas leading to an electrical discharge. The electrons of the discharge, due to their small mass, acquire high velocities, and as a result, their energy reaches a few eVs (1eV corresponds to 11600 K) while the gas is kept at a low temperature (300-450 K), i.e. the term “low temperature plasma” is used. The high energy electrons, through collisions with the neutral particles of the plasma, produce ions and reactive neutrals which are crucial in the etching process. Another consequence of the electrons high velocity is that they reach the inner walls of the reactor faster than the ions. This leads to a potential gradient arising from the difference in the concentration of ions and electrons in the vicinity of the reactor inner walls. The corresponding electric field in this region (plasma sheath) points from the plasma to the walls. In this way, electrons are held back to the plasma (self-confining mechanism for plasma) while ions are accelerated rapidly toward the walls. This ion bombardment energy can be used for many applications in material processing.

Dissertation aims

Given its importance in nanotechnology and in other fields, there is a strong motivation to understand and manipulate plasma induced surface roughness of polymeric substrates. Toward the comprehension and, finally, the control of plasma induced surface roughness, in this dissertation, plasma-surface interactions on rough polymeric substrates are studied from a computational point of view.

For this purpose, a hybrid modeling framework, coupling stochastic and deterministic modules, for profile evolution of unconventional, rough polymeric surfaces under plasma etching is developed. Although the components of the framework may differ depending on the case study, the cornerstone of the framework is a surface etching model that combines the local flux, energy, and the angle of incidence of the plasma species with the local etching yield and rate. The local etching rate calculated by the surface etching model is then fed to a profile evolution module which computes the successive positions of the profile.

The **first model system** being used for the investigations includes **Argon (Ar) plasma** etching of poly(methyl methacrylate) (PMMA) substrates with an initially sinusoidal profile resembling a rough profile. The main focus, filling the relevant gap in the literature, is to record how charging is developed on the rough profile being etched and how it affects the evolving roughness of the profile, in the presence of ion reflection and secondary electron-electron emission (SEEE). This is the first time in the literature that this interplay is examined. Even if plasma induced surface charging on conventional – with respect to the semiconductor industry – structures, i.e., trenches or holes, has been studied in previous works and its artifacts, such as notching, microtrenching, etching lag, and twisting have been examined both experimentally, theoretically, and computationally, there is a lack of studies on surface charging of rough polymeric surfaces.

The **second model system** is plasma etching of PMMA with **oxygen (O₂) chemistry**. O₂ and O₂-containing plasmas offer a great potential for the surface functionalization of polymeric substrates: thermal reactive neutral species are combined with high energy ions to alter both micro/nanomorphology and composition of polymeric surfaces in a dry means of processing. Towards comprehensive process design, by addressing both effects of plasmas on polymeric surfaces (alteration of surface morphology and composition), the dissertation investigates the effect of operating conditions and model parameters on O₂-plasma-induced surface roughening of PMMA. The potential of the framework to address changes of the surface wettability during plasma etching is also demonstrated; the framework can simulate changes of surface morphology (roughness) and O₂ surface coverage (linked to O₂ functional groups), the combination of which determines the wetting state of the surface.

Contents and results of the dissertation

Chapter 1 is an introduction to the topic of plasma-surface interactions and processing of polymeric materials, the field in which the dissertation belongs to. The general theoretical background of the dissertation is presented: we make a brief introduction to the plasma reactor and to the basic plasma etching mechanisms. Some of the most significant examples of plasma-surface interactions encountered in plasma processing of polymers are also discussed. Being a core subject of the present dissertation, much of this chapter is devoted to a review of the

literature concerning plasma induced roughness and its amplification/attenuation mechanisms with an emphasis to computational works. Surface functionalization and etching, generally occurring together, are discussed for O₂ plasma. The reason for this selection is not only that O₂ plasma provokes strong effects in both mechanisms, but that it also has much technological interest in industrial processing. Particular importance is also attached to the review of the literature concerning plasma induced surface charging on conventional dielectric microstructures in microelectronics, mainly, from a modeling point of view. This because one of the main ideas of this dissertation is that surface charging is critical not only for microelectronics but also for unconventional polymeric surface morphologies, where the term unconventional stands for the roughness produced on initially flat polymeric substrates during plasma etching. Finally, the aims of this dissertation are presented.

Chapter 2 includes the description of the computational tools developed during this dissertation. The tools cooperate with each other through a hybrid modeling framework implemented by homemade codes. To model the temporal evolution of a surface over a short time interval, the framework mainly implements the following three steps: (1) it calculates the fluxes of ions, electrons, neutrals to each point of the surface, (2) it specifies the local etching rate for each surface point from the given fluxes, and (3) it utilizes the local etching rates to predict the surface profile after a short time. The ultimate surface profile for **any etching mechanism** may be predicted in this fashion. **The components of the framework are discussed through its application to two different case-studies, namely Ar and O₂ plasma etching of PMMA, involving different etching mechanisms.** Specifically, Ar plasmas cannot chemically react with the polymer and the interaction is restricted to ion bombardment effects, i.e. energetic ions drive atoms off the surface of a solid material (i.e. physical sputtering). In this case study, the framework consists of:

- A **charging module** consisting of models for the calculation of a) ion and electron trajectories (Newton equations), b) the surface charge density, and c) the charging potential (Laplace equation).
- A **model for ion reflection** as well as an **original model for the SEEE mechanism**, developed for PMMA substrates in the energy range which is of interest in plasma etching.
- A **surface etching model** able to calculate the angle and energy dependence of the etching (sputtering) yield of PMMA by Ar ions (Ar⁺), devised by combining **experimental measurements** and numerical calculations.
- A **profile evolution module**, which is based on a continuum description of the profile and the level set method;² the latter module has been developed by Dr. George Kokkoris and has been used for conventional (microelectronic) structures in previous works not only for plasma etching but also for wet etching and chemical vapor deposition. In this dissertation, it is modified in order to handle also the evolution of unconventional (rough) profiles.

² In the level set method, the surface profile is “embedded” in an implicit function, namely the level set function, $\varphi(x,t)$. The surface profile is the zero contour of φ . The level set method tracks the evolution of the surface profile implicitly through the evolution of φ : instead of a profile, a surface is tracked.

In O₂ plasmas, except from mechanical ion induced effects (i.e. sputtering), there are also chemical ion induced effects as ions promote chemical reactions between the O₂ reactive species and the polymeric substrate (i.e. ion enhanced etching). Due to the high computational complexity, charging phenomenon is not considered in this case study.

Thus, the framework for O₂ plasmas consists of:

- A **kinetic Monte Carlo (kMC) surface etching model**, considering the nonlinear synergy of neutral species and ions for the calculation of the local etching rate in the case of O₂ plasma etching, taking into account the surface morphology through the calculation of the trajectories of the species joining the surface reactions.
- A **profile evolution module** described above, modified to treat a fundamental weakness of the level set method, and generally of all methods using an implicit representation of the surface profile, namely the tracking of local profile properties during evolution.

kMC models usually refer to small length and time scales and as a consequence it is of stochastic nature and cannot be readily used for the larger length and time scales manageable by the profile evolution module. There is a set of computational assignments to carry out for the implementation of the hybrid modeling framework, discussed in this chapter. First, in order to couple the different length scales, a coarse grained adjustment of the surface is used by adopting coarse cells that encompass a number of sites under the local mean field approximation.³ In this fashion, the local etching rate is forged in terms of population coverages of species adsorbates in the coarse cells. An atomistic representation of the surface would impose noise to the local etching rate, which would be practically unmanageable by a deterministic profile evolution module. Second, in order to couple the different time scales, the focus is on the computational efficiency: the time step for the profile evolution should be as high as possible and the time interval for the kMC simulation should be as low as possible. The high bound of the former is posed by the Courant–Friedrichs–Lewy (CFL) criterion while the low bound of the latter is posed by the time required to get the local etching rate to steady state. The transport of the local properties from the current profile to the next decreases the time to reach the steady state and shifts the low bound of the time interval for the kMC simulation downward. **This chapter has been published as a part of the following articles:**

- a) G. Memos, G. Kokkoris, Modeling of Charging on Unconventional Surface Morphologies of PMMA Substrates during Ar Plasma Etching, *Plasma Processes and Polymers* 13 (2016) 565-578.
- b) G. Memos, E. Lidorikis, G. Kokkoris, The interplay between surface charging and microscale roughness during plasma etching of polymeric substrates, *J Appl Phys* 123 (2018) 073303.
- c) G. Memos, E. Lidorikis, G. Kokkoris, Roughness evolution and charging in plasma-based surface engineering of polymeric substrates: The effects of ion reflection and secondary electron emission, *Micromachines* 9 (2018).
- d) G. Memos, E. Lidorikis, E. Gogolides and G. Kokkoris, (2021), A hybrid modeling framework for the investigation of surface roughening of polymers during oxygen plasma etching, *Journal of Physics D: Applied Physics*, 54 (2021) 175205

³ Uniform distribution of particles is presumed and any local correlations among particles in a coarse cell are omitted.

Chapter 3 focuses on the calculation of the charging potential, the local ion and electron fluxes, and the local etching rate on a snapshot of the evolving rough polymeric surface. Profile evolution is out of the scope of this chapter. The case study is Ar plasma etching of a PMMA substrate with a sinusoidal profile resembling a rough profile, i.e. a case where the etching mechanism is physical sputtering with a strong dependence of the etching yield and rate on the angle of ion incidence. Etching rate calculations with and without charging are performed; it is shown that charging affects the etching rate mainly due to the decrease of the ion energy. Calculations are performed for sinusoidal profiles of different amplitude (roughness); as the amplitude increases, the ion energy decreases and the angle of ion incidence increases contributing competitively to the etching rate. The charging time, i.e., the time required for reaching a steady state charging potential, is calculated in the order of milliseconds. The latter is crucial for the calculations in the following chapter, Chapter 4; we deduce that the charging phenomenon evolves very fast and arrives at steady state in a time much lower than the time step of the evolution of the surface profile, thus, the solution of the charging module can be decoupled from the solution of the profile evolution module facilitating the calculations. **This chapter has been published as a part of the following articles:**

- a) G. Memos, G. Kokkoris, Modeling of Charging on Unconventional Surface Morphologies of PMMA Substrates during Ar Plasma Etching, *Plasma Processes and Polymers* 13 (2016) 565-578.
- b) G. Memos, E. Lidorikis, G. Kokkoris, The interplay between surface charging and microscale roughness during plasma etching of polymeric substrates, *J Appl Phys* 123 (2018) 073303.

Regarding (a), this publication was the first publication in the field of plasma-induced roughness, revealing that charging is really present on rough surfaces of polymeric substrates being etched by plasma. It received compliments by Prof. Riccardo D' Agostino, past editor in chief of *Plasma Processes and Polymers*, and pioneer in plasma etching and modification of polymers.

Results of the Chapter 3 shows that it is necessary to take charging into account during the evolution simulation of rough polymeric - and generally rough dielectric- surfaces during plasma etching. Thus, in **Chapter 4**, the evolution of initially rough profiles during plasma etching is calculated by taking into account as well as by neglecting charging. It is revealed, on the one hand, that the surface charging contributes to the suppression of roughness and, on the other hand, that the decrease of the surface roughness induces a decrease of the charging potential. Besides roughness, charging also decreases the etching rate of rough dielectric substrates. This practically reveals a mechanism which contributes to the decrease of surface roughness of dielectric substrates; this mechanism is not present in the case of conductive materials. The effect of charging on roughness is intense when the etching yield depends solely on the ion energy, and it is mitigated when the etching yield additionally depends on the angle of ion incidence. When ion reflection is taken into account, the results show that the surface charging contributes to a faster decrease of the roughness compared to the case without charging. Ion reflection sustains roughness; without ion reflection, roughness is eliminated. Either with or without ion reflection, the effect of SEEE on the evolution of the rms roughness over etching time is marginal. Ultimately, the mutual interaction of the roughness and the charging potential is revealed through the correlation of the charging potential with a parameter suitably combining statistical

properties of the profile such as rms roughness⁴ and skewness.⁵ Regardless of the mechanisms and the phenomena taken into account, the charging potential shows an almost monotonic behavior with this parameter, something that reveals the mutual interaction between surface charging and profile roughness. **This chapter has been published as a part of the following articles:**

- a) G. Memos, E. Lidorikis, G. Kokkoris, The interplay between surface charging and microscale roughness during plasma etching of polymeric substrates, J Appl Phys 123 (2018) 073303.
- b) G. Memos, E. Lidorikis, G. Kokkoris, Roughness evolution and charging in plasma-based surface engineering of polymeric substrates: The effects of ion reflection and secondary electron emission, Micromachines 9 (2018).

In **Chapter 5**, the hybrid modeling framework, is applied to the investigation of O₂-plasma-induced surface roughening of PMMA. In O₂ plasmas, thermal reactive neutral species are combined with high energy ions to alter both micro/nanomorphology and composition of polymeric surfaces. Through the implementation of a novel kMC surface etching model, the framework can address both effects of O₂ plasma on the PMMA surface. The first aim of the chapter is the evaluation of the accuracy of the kMC model through a comparison to the analytical equations describing the ion-enhanced kinetics as well as the proper adjustment of critical parameters of the kMC model in order to cope with computational and accuracy issues. Then, we track how the operating conditions of the reactor, such as the output power (or equivalently the ratio of O atom flux over the O⁺ flux at the flat region), the DC bias voltage (or equivalently the ion energy) and the etching time, as well as the model parameters, such as the re-emission of oxygen atoms (O) and the reflection of oxygen ions (O⁺) on the surface, intertwine with the evolution of morphology and, ultimately, how their interwoven effects determine the evolution of roughness. The framework is also able to replicate experimental roughness evolution trends found in the literature in high density plasma reactors under the effect of different operating conditions. For instance, given the output power is large, the roughness is subjected to changes in the growth mode with the etching time and/or it increases with the increase of bias. Given the bias is constant, the roughness increases with the output power. Ultimately, the potential of the modeling framework to address changes of the surface wettability during plasma etching is demonstrated. The framework can simulate changes of surface morphology (roughness) and O surface coverage (linked to O functional groups), the combination of which determines the wetting state of the surface. **This chapter has been published as a part of the following article:**

G. Memos, E. Lidorikis, E. Gogolides and G. Kokkoris, (2021), A hybrid modeling framework for the investigation of surface roughening of polymers during oxygen plasma etching, Journal of Physics D: Applied Physics, 54 (2021) 175205

Chapter 6 summarizes the novelties of the dissertation as well as the utility and capabilities of the developed hybrid modeling framework. Some interesting future extensions arising from the dissertation are also suggested. In a nutshell, some key contributions are: a) The significance of

⁴ It evaluates the vertical fluctuations of the surface morphology. It is equivalent to the standard deviation of heights.

⁵ It quantifies the asymmetry of the surface morphology, is utilized to pinpoint the kind of pattern on the surface: Positive skewness means that bumps dominate on the surface morphology, while if skewness is negative, holes prevail.

the effect of surface charging in the design of recipes for producing or eliminating surface roughness, b) the development of an original model for the SEEE mechanism on PMMA substrates, c) the development of a kMC surface etching model able to take into consideration the surface morphology, d) the use of the level set method for the transport of local properties of the profile from a time step to the next and e) the ability of the framework to simulate changes of both surface morphology and surface chemical composition. Some future research suggestion arising out of this dissertation are: a) The application of the framework to other polymeric substrates and/or other plasmas as well as its application to plasma etching of conventional structures in the semiconductor industry such as trenches or to address cases of 3d surface morphologies from micro- to nanoscale. b) The extension of the framework to include additional mechanisms, which can affect roughness evolution or the coupling of the framework to a reactor scale model. c) Interesting extension are to analyze all scales of surface roughness and focus on the prediction of wetting state of the surface (e.g. Wenzel or Cassie-Baxter or hybrid states) or to clarify the relationship between roughness and charge retention on the surface of a polymer as well as the influence of the charge on the properties of the etched surfaces with a focus on possible applications that may arise from such a technology.

ΠΕΡΙΛΗΨΗ

Εισαγωγή

Η εγχάραξη με πλάσμα,⁶ εκτός της παραδοσιακής χρήσης της για την μεταφορά σχήματος στην μικροηλεκτρονική, χρησιμοποιείται στην νανοτεχνολογία για την ενεργοποίηση της επιφάνειας των πολυμερών μέσω της τροποποίησης της χημικής σύνθεσης και της μορφολογίας της επιφάνειας. Το πρώτο επιτυγχάνεται μέσω της προσκόλλησης ατόμων ή μορίων που παράγονται στον κύριο όγκο του πλάσματος στην επιφάνεια και δημιουργίας νέων λειτουργικών ομάδων, ενώ το δεύτερο μέσω της αφαίρεσης υλικού (εγχάραξη) με χημικούς ή / και φυσικούς τρόπους. Ένα αποτέλεσμα της αλλαγής που προκαλείται από το πλάσμα, η οποία έχει προσελκύσει μεγάλη προσοχή τον τελευταίο καιρό τόσο πειραματικά όσο και θεωρητικά, είναι η δημιουργία επιφανειακής τραχύτητας.

Το πλάσμα προκαλεί μικρο/νανο-τραχύτητα στην επιφάνεια των πολυμερικών υποστρωμάτων, έναν παράγοντα που έχει μεγάλη σημασία στις επιφανειακές ιδιότητες (π.χ. συμπεριφορά διαβροχής, αλληλεπίδραση επιφανειών με κύτταρα). Είναι λοιπόν σημαντικό να μελετηθούν οι μηχανισμοί που επηρεάζουν την τραχύτητα στην επιφάνεια και, τελικά, να σχεδιαστούν «συνταγές» που να παρέχουν την επιθυμητή τραχύτητα. Ωστόσο, οι αλληλεπιδράσεις πλάσματος-επιφάνειας είναι πολύπλοκες και ο σχεδιασμός της πειραματικής διαδικασίας βασίζεται συνήθως σε εφαρμογή μεθόδων δοκιμής και σφάλματος.

Πολλές μελέτες μέχρι σήμερα έχουν εντοπίσει αρκετούς πιθανούς μηχανισμούς για το σχηματισμό και την εξέλιξη της τραχύτητας, όπως, μεταξύ άλλων, την ανάκλαση ιόντων εντός των μορφολογικών χαρακτηριστικών του τραχιού προφίλ, την αλλαγή της απόδοσης εγχάραξης με τη γωνία πρόσπτωσης των ιόντων, την απόθεση υλικού προερχόμενο από το πλάσμα ή την απόθεση υλικού που εκτοξεύεται με την εγχάραξη του υποστρώματος στην επιφάνεια. Υπάρχει επίσης σημαντική αλληλοεπικάλυψη μεταξύ αυτών των μηχανισμών. Συνήθως, μια πειραματική μέτρηση τραχύτητας μπορεί να ερμηνευθεί με την επίκληση περισσότερων του ενός φυσικών μηχανισμών. Αυτοί οι μηχανισμοί λαμβάνουν χώρα ταυτόχρονα κατά τη εγχάραξη με πλάσμα και η προσδοκία για τον διαχωρισμό των επιδράσεων τους μέσω πειράματος είναι χαμηλή. Η τροποποίηση των συνθηκών της πειραματικής διαδικασίας για τη μείωση της επίδρασης ενός μηχανισμού θα εντείνει συνήθως ένα άλλο. Ωστόσο, για αποτελεσματικό σχεδιασμό και

⁶ Το πλάσμα ως «εργαλείο» της νανοτεχνολογίας δημιουργείται σε αντιδραστήρες χαμηλής πίεσης με την επιβολή ηλεκτρομαγνητικών πεδίων σε αέρια που οδηγεί σε ηλεκτρική εκκένωση. Τα ηλεκτρόνια της εκκένωσης λόγω της μικρής μάζας τους, αποκτούν μεγάλες ταχύτητες, με αποτέλεσμα η ενέργειά τους να φτάνει μερικά eVs (1 eV αντιστοιχεί σε 11600 K) ενώ το αέριο διατηρείται σε χαμηλή θερμοκρασία (300-450 K), από όπου προέρχεται και ο χαρακτηρισμός «πλάσμα χαμηλής θερμοκρασίας». Τα ενεργητικά ηλεκτρόνια, μέσω συγκρούσεων με τα ουδέτερα συστατικά του πλάσματος, παράγουν τα – κρίσιμα για τη διεργασία της εγχάραξης – ιόντα και δραστικά ουδέτερα συστατικά. Μια ακόμη συνέπεια της μεγάλης ταχύτητας των ηλεκτρονίων είναι ότι φτάνουν ταχύτερα από τα ιόντα στις εσωτερικές επιφάνειες του αντιδραστήρα. Η διαφορά συγκεντρώσεων ηλεκτρονίων - θετικών ιόντων στη γειτονιά των επιφανειών δημιουργεί την οριακή στοιβάδα πλάσματος στην οποία αναπτύσσεται ηλεκτρικό πεδίο με κατεύθυνση προς τις επιφάνειες. Με αυτόν τον τρόπο, τα ηλεκτρόνια συγκρατούνται πίσω στο πλάσμα ενώ τα ιόντα επιταχύνονται γρήγορα προς τα τοιχώματα. Η ενέργεια βομβαρδισμού των ιόντων μπορεί να χρησιμοποιηθεί για πολλές εφαρμογές στην επεξεργασία των υλικών.

βελτιστοποίηση της διαδικασίας, είναι σημαντικό οι μηχανισμοί που επηρεάζουν το εγχαρασόμενο τραχύ προφίλ να είναι κατανοητοί.

Η μόνη προσέγγιση που επιτρέπει την εξέταση της επίδρασης ενός μηχανισμού στην τραχύτητα της επιφάνειας κατά τη εγχάραξη με πλάσμα είτε ανεξάρτητα είτε από κοινού με άλλους μηχανισμούς είναι η αριθμητική προσομοίωση. Η τελευταία έχει μεγάλο ενδιαφέρον για την παροχή ενδείξεων σχετικά με τη φυσική που διέπει την πειραματική διαδικασία και για τον τελικό προσδιορισμό των μηχανισμών που ελέγχουν την εξέλιξη της τραχύτητας. Μπορεί συνεπώς να παρέχει βοήθεια για τον καθορισμό των ιδανικών συνθηκών για την επιθυμητή τραχύτητα, επιτρέποντας έτσι τη βελτιστοποίηση της πειραματικής διαδικασίας εγχάραξης.

Στόχοι της διδακτορικής διατριβής

Δεδομένης της σπουδαιότητάς της στη νανοτεχνολογία, υπάρχει ισχυρό κίνητρο για την διερεύνηση της επιφανειακής τραχύτητας πολυμερικών υποστρωμάτων που προκαλείται από την εγχάραξη με πλάσμα. Με στόχο την κατανόηση και, τέλος, τον έλεγχο της επιφανειακής τραχύτητας, σε αυτήν την διδακτορική διατριβή, πραγματοποιείται υπολογιστική μελέτη αλληλεπιδράσεων πλάσματος επιφανειακής τραχύτητας σε πολυμερικά υποστρώματα.

Για το σκοπό αυτό, αναπτύσσεται ένα υβριδικό πλαίσιο προσομοίωσης, το οποίο συνδέει στοχαστικά και ντετερμινιστικά μοντέλα, για την εξέλιξη του προφίλ μη συμβατικών, τραχιών πολυμερικών επιφανειών κατά την εγχάραξή τους με πλάσμα. Παρόλο που τα στοιχεία του πλαισίου ενδέχεται να διαφέρουν ανάλογα με τη μελέτη περίπτωσης, ο ακρογωνιαίος λίθος του πλαισίου είναι ένα μοντέλο εγχάραξης επιφάνειας το οποίο συνδυάζει την τοπική ροή, την ενέργεια και τη γωνία πρόσπτωσης των σωματιδίων που προέρχονται από το πλάσμα με την τοπική απόδοση και τον ρυθμό εγχάραξης. Ο τοπικός ρυθμός εγχάραξης που υπολογίζεται από το μοντέλο επιφανειακής εγχάραξης τροφοδοτείται στη συνέχεια στο μοντέλο εξέλιξης μορφολογίας το οποίο υπολογίζει τις διαδοχικές θέσεις του προφίλ της επιφάνειας.

Η πρώτη μελέτη περίπτωσης περιλαμβάνει την εγχάραξη με πλάσμα Αργού (Ar) ενός υποστρώματος πολυ (μεθακρυλικού μεθυλεστέρα) (PMMA) με αρχικά ημιτονοειδές προφίλ το οποίο προσομοιάζει ένα τραχύ προφίλ. Αρχικά διερευνάται, με στόχο την συμπλήρωση του σχετικού κενού στη βιβλιογραφία, ο τρόπος ανάπτυξης την επιφανειακής φόρτισης στην αναπτυσσόμενη τραχύτητα και στην συνέχεια το πώς η φόρτιση επηρεάζει την τραχύτητα, παρουσία των μηχανισμών ανάκλασης των ιόντων και δευτερογενούς εκπομπής ηλεκτρονίων στα μορφολογικά χαρακτηριστικά της επιφάνειας του υποστρώματος.. Σημειώνεται ότι είναι η πρώτη φορά στη βιβλιογραφία που εξετάζεται αυτή η αλληλεπίδραση. Αν και η επιφανειακή φόρτιση που προκαλείται από το πλάσμα σε συμβατικές - σε σχέση με τη βιομηχανία ημιαγωγών - δομές, δηλαδή αυλάκια ή οπές, έχει μελετηθεί σε προηγούμενες εργασίες και οι αποκλίσεις από την επιθυμητή δομή, όπως η δημιουργία εσοχών ή πτυχώσεων στα άκρα της βάσης της δομής, η συστροφή των πλάγιων τοιχωμάτων της δομής και η υστέρηση εγχάραξης έχουν εξεταστεί τόσο πειραματικά όσο και υπολογιστικά, υπάρχει έλλειψη μελετών σχετικά με την επιφανειακή φόρτιση τραχιών πολυμερικών επιφανειών από το πλάσμα.

Η δεύτερη μελέτη περίπτωσης είναι η εγχάραξη πολυμερικού υποστρώματος PMMA με πλάσμα χημείας οξυγόνου (O₂). Το τελευταίο προσφέρει μεγάλες δυνατότητες για την ενεργοποίηση των

επιφανειών πολυμερικών υποστρωμάτων: Ουδέτερα είδη συνδυάζονται με ιόντα υψηλής ενέργειας για να μεταβάλουν τόσο τη μικρο/νανομορφολογία όσο και την χημική σύνθεση της επιφάνειας. Με χρήση του υπολογιστικού πλαισίου, το οποίο μπορεί να διαχειρίζεται και τις δύο αυτές επιδράσεις του πλάσματος O_2 στην πολυμερική επιφάνεια (μεταβολή της επιφανειακής μορφολογίας και της χημικής σύνθεσης), η διατριβή διερευνά την επίδραση των συνθηκών λειτουργίας και των παραμέτρων του πλαισίου στην εξέλιξη της επιφανειακής τραχύτητας του PMMA. Παρουσιάζεται η δυνατότητα του πλαισίου να μπορεί να διαχειρίζεται αλλαγές στις ιδιότητες διαβροχής της επιφάνειας κατά την εγχάραξη τους με πλάσμα O_2 . Το πλαίσιο μπορεί να προσομοιώσει αλλαγές στην επιφανειακή μορφολογία (τραχύτητα) και την κάλυψη της επιφάνειας σε οξυγόνου (που συνδέεται με λειτουργικές ομάδες οξυγόνου), ο συνδυασμός των οποίων καθορίζει την κατάσταση διαβροχής της επιφάνειας.

Περιεχόμενα και αποτελέσματα της διατριβής

Το **Κεφάλαιο 1** είναι μια εισαγωγή στο θέμα της επεξεργασίας των πολυμερών με πλάσμα, το πεδίο στο οποίο ανήκει η διατριβή. Παρουσιάζεται το γενικό θεωρητικό υπόβαθρο της διατριβής: δίνεται μια σύντομη εισαγωγή στον αντιδραστήρα πλάσματος και στους βασικούς μηχανισμούς εγχάραξης με πλάσμα. Συζητούνται μερικά από τα πιο σημαντικά παραδείγματα αλληλεπιδράσεων πλάσματος-επιφάνειας που συναντώνται στην επεξεργασία των πολυμερών με πλάσμα. Όντας βασικό θέμα της παρούσας διατριβής, μεγάλο μέρος αυτού του κεφαλαίου αφιερώνεται σε μια ανασκόπηση της βιβλιογραφίας σχετικά με τους μηχανισμούς ενίσχυσης/ εξασθένησης της τραχύτητας που προκαλείται από το πλάσμα με έμφαση σε υπολογιστικές εργασίες. Η ενεργοποίηση και η εγχάραξη της πολυμερικής επιφάνειας, οι οποίες λαμβάνουν χώρα ταυτόχρονα, συζητούνται για την περίπτωση πλάσματος O_2 . Ο λόγος για αυτήν την επιλογή δεν είναι μόνο ότι το πλάσμα O_2 έχει ισχυρή επίδραση και στους δύο μηχανισμούς, αλλά και το ότι έχει επίσης μεγάλο τεχνολογικό ενδιαφέρον. Ιδιαίτερη σημασία αποδίδεται επίσης στην ανασκόπηση της βιβλιογραφίας σχετικά με την επιφανειακή φόρτιση που προκαλείται από πλάσμα σε συμβατικές δομές μικροηλεκτρονικής, κυρίως, υπολογιστών εργασιών. Αυτό επειδή μία από τις βασικές ιδέες αυτής της διατριβής είναι ότι η επιφανειακή φόρτιση είναι κρίσιμη όχι μόνο για συμβατικές δομές μικροηλεκτρονικής, όπως αυλάκια και οπές, αλλά και για μη συμβατικές, τραχιές πολυμερικές επιφανειακές μορφολογίες που συναντώνται στην νανοτεχνολογία. Τέλος, παρουσιάζονται οι στόχοι αυτής της διατριβής.

Το **Κεφάλαιο 2** περιλαμβάνει την περιγραφή των μοντέλων που αναπτύχθηκαν κατά τη διάρκεια αυτής της διατριβής. Τα μοντέλα «συνεργάζονται» μεταξύ τους μέσω ενός υβριδικού υπολογιστικού πλαισίου. Για να μοντελοποιηθεί η χρονική εξέλιξη του προφίλ της επιφάνειας, το πλαίσιο εφαρμόζει κυρίως τα ακόλουθα τρία βασικά βήματα: (1) υπολογίζει τις ροές ιόντων, ηλεκτρονίων, ουδέτερων σε κάθε σημείο του προφίλ, (2) καθορίζει τον τοπικό ρυθμό εγχάραξης για κάθε σημείο του προφίλ από τις δεδομένες ροές, και (3) χρησιμοποιεί τους τοπικούς ρυθμούς εγχάραξης για να προβλέψει το προφίλ της επιφάνειας μετά από ένα ορισμένο χρονικό βήμα. Το τελικό προφίλ της επιφάνειας μπορεί να προβλεφθεί με αυτόν τον τρόπο για οποιονδήποτε μηχανισμό εγχάραξης. Τα μοντέλα του υπολογιστικού πλαισίου περιγράφονται μέσω της εφαρμογής του σε δύο διαφορετικές μελέτες περίπτωσης, συγκεκριμένα, εγχάραξη PMMA με πλάσμα Ar και πλάσμα O_2 , οι οποίες περιλαμβάνουν διαφορετικούς μηχανισμούς εγχάραξης. Το πλάσμα Ar δεν μπορεί να αντιδράσει χημικά με την πολυμερική επιφάνεια και η αλληλεπίδραση

πλάσματος-επιφάνειας περιορίζεται στον βομβαρδισμό της επιφάνειας από ενεργητικά ιόντα που οδηγεί στην μηχανική απομάκρυνση υλικού από την επιφάνεια του πολυμερούς (ιονοβολή).

Σε αυτήν την μελέτη περίπτωσης, το πλαίσιο αποτελείται από:

- Μοντέλο επιφανειακής φόρτισης το οποίο αποτελείται από μοντέλα για τον υπολογισμό α) των τροχιών ιόντων και ηλεκτρονίων (εξισώσεις Νεύτωνα), β) της τοπικής επιφανειακής πυκνότητας φόρτισης και του γ) του δυναμικού φόρτισης που προκαλείται από το επιφανειακό φορτίο (εξίσωση Laplace).
- Μοντέλο ανάκλασης των ιόντων στην επιφάνεια του πολυμερικού υποστρώματος καθώς επίσης και πρωτότυπο μοντέλο για τον συντελεστή απόδοσης και οπισθοσκέδασης της δευτερογενούς εκπομπής ηλεκτρονίων για υποστρώματα PMMA στην ενεργειακή περιοχή που αφορά την εγχάραξη με πλάσμα.
- Μοντέλο εγχάραξης επιφάνειας που λαμβάνει υπόψη την γωνιακή και ενεργειακή εξάρτηση της απόδοσης εγχάραξης του PMMA από ιόντα Αργού (Ar^+) με βάση τη σύζευξη μετρήσεων από πειράματα ιονοβολής και υπολογισμούς με διαθέσιμο κώδικα.
- Ντεντερμινιστικό μοντέλο εξέλιξης μορφολογίας, το οποίο βασίζεται σε συνεχή περιγραφή του προφίλ και την μέθοδο των ισοϋψών.⁷ Το μοντέλο αυτό έχει αναπτυχθεί από τον Δρ. Γεώργιο Κόκκορη και έχει χρησιμοποιηθεί σε προηγούμενες εργασίες για συμβατικές δομές μικροηλεκτρονικής (όπως αυλάκια και οπές) όχι μόνο σε περιπτώσεις εγχάραξης με πλάσμα αλλά επίσης για την μοντελοποίηση διεργασιών υγρής εγχάραξης και απόθεσης. Σε αυτήν την διδακτορική διατριβή, τροποποιείται για να χειριστεί την εξέλιξη μη συμβατικών (τραχιών) προφίλ.

Στο πλάσμα O_2 , εκτός από φυσική αλληλεπίδραση με την επιφάνεια (ιονοβολή), υπάρχει επίσης και χημική αλληλεπίδραση καθώς τα ιόντα προάγουν χημικές αντιδράσεις μεταξύ των ατόμων του οξυγόνου (O) που προέρχονται από το πλάσμα και του πολυμερικού υποστρώματος (εγχάραξη υποβοηθούμενη από ιόντα). Με χρήση αυτής της χημείας πλάσματος, υπάρχει (μη γραμμική) συνέργεια μεταξύ ιόντων και ουδετέρων συστατικών στο μηχανισμό εγχάραξης. Λόγω της υψηλής υπολογιστικής πολυπλοκότητας, το φαινόμενο φόρτισης δεν λαμβάνεται υπόψη σε αυτή τη μελέτη περίπτωσης.

Σε αυτήν την μελέτη περίπτωσης, το πλαίσιο αποτελείται από:

- Στοχαστικό μοντέλο επιφανειακής εγχάραξης στο οποίο εφαρμόζεται πρωτότυπη κινητική μέθοδος Μόντε Κάρλο (kinetic Monte Carlo ή kMC) λαμβάνοντας υπόψη την μορφολογία της επιφάνειας στον υπολογισμό του ρυθμού μιας διεργασίας.
- Ντεντερμινιστικό μοντέλο εξέλιξης μορφολογίας που περιγράφεται στην προηγούμενη μελέτη περίπτωσης, τροποποιημένο ωστόσο για να αντιμετωπίσει μια θεμελιώδη αδυναμία της μεθόδου των ισοϋψών και γενικά όλων των μεθόδων που χρησιμοποιούν πεπλεγμένη αναπαράσταση του επιφανειακού προφίλ, δηλαδή την παρακολούθηση των τοπικών ιδιοτήτων του προφίλ κατά την εξέλιξη.

⁷ Η μέθοδος των ισοϋψών συνιστά αλγόριθμο εξέλιξης συνόρου που βασίζεται στην πεπλεγμένη (implicit) απεικόνιση του συνόρου. Το σύνоро ορίζεται έμμεσα ως η ισοϋψής μηδέν πεπλεγμένης συνάρτησης, της λεγόμενης συνάρτησης ισοϋψών, $\phi(\mathbf{x}, t)$. Η εξέλιξη του συνόρου παρακολουθείται έμμεσα από την εξέλιξη αυτής της συνάρτησης, η οποία αποτελεί την πεπλεγμένη απεικόνιση του συνόρου.

Τα μοντέλα kMC αναφέρονται συνήθως σε μικρές χωρικές και χρονικές κλίμακες και κατά συνέπεια είναι στοχαστικής φύσης και δεν μπορούν εύκολα να συζευχθούν με τις μεγαλύτερες αντίστοιχες κλίμακες που διαχειρίζεται το ντετερμινιστικό μοντέλο εξέλιξης μορφολογίας. Υπάρχει ένα σύνολο υπολογιστικών εργασιών για την υλοποίηση του υβριδικού πλαισίου προσομοίωσης, που συζητείται σε αυτό το κεφάλαιο. Αρχικά για τη σύζευξη των διαφορετικών χωρικών κλιμάκων του στοχαστικού και ντετερμινιστικού μοντέλου, υλοποιείται αδροποίηση της επιφάνειας με την δημιουργία ομάδων θέσεων προσρόφησης υπό την προσέγγιση του μέσου πεδίου.⁸ Με αυτόν τον τρόπο, ο τοπικός ρυθμός εγχάραξης διαμορφώνεται με βάση την κάλυψη του πληθυσμού των προσροφημένων ατόμων οξυγόνων στους αδρούς κόκκους της επιφάνειας. Μια ατομική αναπαράσταση της επιφάνειας θα επέβαλλε θόρυβο στον τοπικό ρυθμό εγχάραξης, ο οποίος θα ήταν πρακτικά μη διαχειρίσιμος από το ντετερμινιστικό μοντέλο εξέλιξης μορφολογίας. Στην συνέχεια, για τη σύζευξη των διαφορετικών χρονικών κλιμάκων του στοχαστικού και ντετερμινιστικού μοντέλου, γίνεται εστίαση στην μείωση του χρόνου προσομοίωσης: το χρονικό βήμα για την εξέλιξη του προφίλ είναι όσο το δυνατόν υψηλότερο και το χρονικό διάστημα για την προσομοίωση kMC είναι όσο το δυνατόν χαμηλότερο. Το όριο του πρώτου τίθεται από το κριτήριο Courant – Friedrichs – Lewy (CFL) ενώ το όριο του τελευταίου τίθεται από τον απαιτούμενο χρόνο για να έρθει το τοπικό κλάσμα κάλυψης της επιφάνειας από οξυγόνο, κι επομένως ο τοπικός ρυθμός εγχάραξης, σε μόνιμη κατάσταση. Η μέθοδος των ισοϋψών χρησιμοποιείται για τη μεταφορά των τοπικών μεταβλητών της κάλυψης της επιφάνειας από οξυγόνο από το τρέχον προφίλ στο προφίλ του επόμενου βήματος ως καινοτόμος μεθοδολογία για την αποτελεσματική μείωση του χρόνου προσομοίωσης kMC. **Το κεφάλαιο αυτό έχει δημοσιευτεί ως μέρος των παρακάτω άρθρων:**

- a) G. Memos, G. Kokkoris, Modeling of Charging on Unconventional Surface Morphologies of PMMA Substrates during Ar Plasma Etching, Plasma Processes and Polymers 13 (2016) 565-578.
- b) G. Memos, E. Lidorikis, G. Kokkoris, The interplay between surface charging and microscale roughness during plasma etching of polymeric substrates, J Appl Phys 123 (2018) 073303.
- c) G. Memos, E. Lidorikis, G. Kokkoris, Roughness evolution and charging in plasma-based surface engineering of polymeric substrates: The effects of ion reflection and secondary electron emission, Micromachines 9 (2018).
- d) G. Memos, E. Lidorikis, E. Gogolides and G. Kokkoris, (2021), A hybrid modeling framework for the investigation of surface roughening of polymers during oxygen plasma etching, Journal of Physics D: Applied Physics, 54 (2021) 175205

Το **Κεφάλαιο 3** επικεντρώνεται στον υπολογισμό του δυναμικού φόρτισης, των τοπικών ροών ιόντων και ηλεκτρονίων και του τοπικού ρυθμού εγχάραξης σε ένα στιγμιότυπο του προφίλ της πολυμερικής επιφάνειας. Η εξέλιξη του προφίλ είναι εκτός του σκοπού αυτού του κεφαλαίου. Συγκεκριμένα η μελέτη περίπτωσης είναι εγχάραξη με πλάσμα Ar υποστρώματος PMMA που φέρει επιφάνεια με ημιτονοειδές (τραχύ) προφίλ, δηλαδή περίπτωση όπου ο μηχανισμός εγχάραξης είναι ιονοβολή με ισχυρή εξάρτηση της απόδοσης και του ρυθμού εγχάραξης από τη γωνία πρόσπτωσης των ιόντων. Πραγματοποιούνται υπολογισμοί ρυθμού εγχάραξης με και χωρίς φόρτιση. Φαίνεται ότι η φόρτιση επηρεάζει το ρυθμό εγχάραξης κυρίως λόγω της μείωσης της ενέργειας των ιόντων. Πραγματοποιούνται επίσης υπολογισμοί για ημιτονοειδή προφίλ

⁸ Θεωρείται ότι η κατανομή των σωματιδίων μέσα σε ένα κελί της επιφάνειας ακολουθεί ομοιόμορφη κατανομή και τυχόν τοπικές αλληλεπιδράσεις μεταξύ τους παραλείπονται.

διαφορετικού πλάτους (διαφορετικής τραχύτητας). Καθώς το πλάτος αυξάνεται, η ενέργεια των ιόντων μειώνεται ενώ η γωνία πρόσπτωσης τους αυξάνεται συμβάλλοντας ανταγωνιστικά στη διαμόρφωση του ρυθμού εγχάραξης. Ο χρόνος φόρτισης, δηλαδή ο χρόνος που απαιτείται για την επίτευξη δυναμικού φόρτισης σε σταθερή κατάσταση, υπολογίζεται στην κλίμακα των χιλιοστών του δευτερολέπτου. Το τελευταίο είναι σημαντικό για τους υπολογισμούς στο επόμενο κεφάλαιο (Κεφάλαιο 4). Συμπεραίνουμε ότι το φαινόμενο φόρτισης εξελίσσεται πολύ γρήγορα και φτάνει σε σταθερή κατάσταση σε χρόνο πολύ μικρότερο από το χρονικό βήμα της εξέλιξης του προφίλ της επιφάνειας, επομένως, μπορεί να πραγματοποιηθεί αποσύζευξη της επίλυσης του μοντέλου επιφανειακής φόρτισης από την επίλυση του μοντέλου εξέλιξης μορφολογίας κάτι που διευκολύνει σημαντικά τους υπολογισμούς.

Το κεφάλαιο αυτό έχει δημοσιευτεί ως μέρος των παρακάτω άρθρων:

a) G. Memos, G. Kokkoris, Modeling of Charging on Unconventional Surface Morphologies of PMMA Substrates during Ar Plasma Etching, Plasma Processes and Polymers 13 (2016) 565-578.

b) G. Memos, E. Lidorikis, G. Kokkoris, The interplay between surface charging and microscale roughness during plasma etching of polymeric substrates, J Appl Phys 123 (2018) 073303.

Όσον αφορά το (α), αυτή η δημοσίευση ήταν η πρώτη δημοσίευση στον επιστημονικό πεδίο της τραχύτητας που προκαλείται από πλάσμα, που αποκάλυψε ότι η φόρτιση είναι πραγματικά παρούσα σε τραχιές επιφάνειες πολυμερικών υποστρωμάτων που εγχαράσσονται από πλάσμα. Έλαβε πολύ θετικά σχόλια από τον καθηγητή Riccardo D'Agostino, πρώην αρχισυντάκτη του Plasma Processes and Polymers, και πρωτοπόρο στη εγχάραξη και τροποποίηση πολυμερών με πλάσμα.

Τα αποτελέσματα του κεφαλαίου 3 δείχνουν ότι είναι απαραίτητο να ληφθεί υπόψη η φόρτιση κατά την προσομοίωση της εξέλιξης τραχιών πολυμερικών - και γενικά διηλεκτρικών επιφανειών κατά τη εγχάραξη τους με πλάσμα. Έτσι, στο **Κεφάλαιο 4**, υπολογίζεται η εξέλιξη τραχιών προφίλ λαμβάνοντας υπόψη και αμελώντας τη φόρτιση. Αποκαλύπτεται ότι η φόρτιση συμβάλει στην μείωση της τραχύτητας και την ίδια στιγμή η μείωση της τραχύτητας προκαλεί μείωση του δυναμικού φόρτισης. Εκτός από την τραχύτητα, η φόρτιση μειώνει επίσης το ρυθμό εγχάραξης των τραχιών πολυμερικών (διηλεκτρικών) υποστρωμάτων. Η μελέτη αυτή αποκαλύπτει πρακτικά έναν μηχανισμό που συμβάλει στη μείωση της τραχύτητας της επιφάνειας διηλεκτρικών υποστρωμάτων. Αυτός ο μηχανισμός δεν υπάρχει στην περίπτωση των αγωγικών υποστρωμάτων. Η επίδραση της φόρτισης στην τραχύτητα είναι έντονη όταν η απόδοση εγχάραξης έχει εξάρτηση αποκλειστικά από την ενέργεια των ιόντων, ενώ αμβλύνεται, όταν η απόδοση έχει εξάρτηση επιπλέον από την γωνία πρόσπτωσης. Ειδικά όταν η ανάκλαση των ιόντων λαμβάνεται υπόψη, η επιφανειακή φόρτιση συμβάλει στην ταχύτερη εξάλειψη της τραχύτητας σε σύγκριση με την περίπτωση χωρίς φόρτιση. Η ανάκλαση των ιόντων διατηρεί την τραχύτητα. Χωρίς την ανάκλαση των ιόντων η τραχύτητα εξαλείφεται. Με ή χωρίς τον μηχανισμό της ανάκλασης των ιόντων, η επίδραση της δευτερογενούς εκπομπής ηλεκτρονίων στην εξέλιξη της τραχύτητας κατά την διάρκεια της εγχάραξης είναι οριακή. Το δυναμικό φόρτισης συσχετίζεται για πρώτη φορά στην βιβλιογραφία με την τραχύτητα του προφίλ μέσω παραμέτρου, η οποία συνδυάζει κατάλληλα στατιστικές ιδιότητες της επιφάνειας όπως η root mean square (rms)⁹ τραχύτητα και η ασυμμετρία της επιφάνειας (skewness)¹⁰. Ανεξάρτητα από

⁹ Μέση τυπική απόκλιση των υψών της επιφάνειας από την μέση τιμή τους.

τους μηχανισμούς και τα φαινόμενα που λαμβάνονται υπόψη, το δυναμικό φόρτισης δείχνει μια σχεδόν μονοτονική συμπεριφορά με την παράμετρο αυτή, κάτι που αποκαλύπτει την αμοιβαία αλληλεπίδραση μεταξύ επιφανειακής φόρτισης και τραχύτητας του προφίλ. **Το κεφάλαιο αυτό έχει δημοσιευτεί ως μέρος των παρακάτω άρθρων:**

a) G. Memos, E. Lidorikis, G. Kokkoris, The interplay between surface charging and microscale roughness during plasma etching of polymeric substrates, J Appl Phys 123 (2018) 073303.

b) G. Memos, E. Lidorikis, G. Kokkoris, Roughness evolution and charging in plasma-based surface engineering of polymeric substrates: The effects of ion reflection and secondary electron emission, Micromachines 9 (2018).

Στο **Κεφάλαιο 5**, το υβριδικό υπολογιστικό πλαίσιο προσομοίωσης, εφαρμόζεται στην διερεύνηση της επιφανειακής τραχύτητας σε υπόστρωμα PMMA που προκαλείται από πλάσμα O_2 . Στο τελευταίο, ουδέτερα είδη συνδυάζονται με ιόντα υψηλής ενέργειας για να μεταβάλουν τόσο τη μικρο/νανομορφολογία όσο και την χημική σύνθεση της επιφάνειας. Μέσω της ανάπτυξης ενός καινοτόμου μοντέλου επιφανειακής εγχάραξης στο οποίο εφαρμόζεται πρωτότυπη μέθοδος kMC, το πλαίσιο μπορεί να διαχειριστεί και τις δύο επιδράσεις του πλάσματος O_2 στην επιφάνεια PMMA. Ο πρώτος στόχος του κεφαλαίου είναι η αξιολόγηση της ακρίβειας του μοντέλου επιφανειακής εγχάραξης μεθόδου kMC μέσω σύγκρισης με τις αναλυτικές εξισώσεις που περιγράφουν την κινητική του μηχανισμού εγχάραξης υποβοηθούμενης από ιόντα, καθώς και τη σωστή προσαρμογή των κρίσιμων παραμέτρων του μοντέλου kMC προκειμένου να αντιμετωπιστούν θέματα υπολογιστικής ακρίβειας. Στη συνέχεια, διερευνάται το πώς οι συνθήκες λειτουργίας του αντιδραστήρα, όπως η ισχύς εξόδου (ή ισοδύναμα ο λόγος της ροής O προς την ροή ιόντων οξυγόνου (O^+) σε επίπεδη επιφάνεια), η τάση πόλωσης DC (ή ισοδύναμα η ενέργεια ιόντων) και ο χρόνος εγχάραξης, καθώς και οι παράμετροι του μοντέλου, όπως η επανεκπομπή O και η ανάκλαση των O^+ στην επιφάνεια, συνυφαίνονται με την εξέλιξη της τραχύτητας και, τελικά, πώς οι αλληλένδετες επιδράσεις τους καθορίζουν την εξέλιξη της τραχύτητας. Το πλαίσιο είναι επίσης ικανό να αναπαράγει πειραματικές τάσεις της εξέλιξης της τραχύτητας που συναντώνται στη βιβλιογραφία σε αντιδραστήρες πλάσματος υψηλής πυκνότητας υπό την επίδραση διαφορετικών συνθηκών λειτουργίας. Για παράδειγμα, δεδομένου ότι η ισχύς εξόδου είναι μεγάλη, η τραχύτητα υπόκειται σε αλλαγές στον τρόπο (εκθέτη) αύξησης με τον χρόνο εγχάραξης ή/ και αυξάνεται με την αύξηση της τάσης πόλωσης. Επίσης, η τραχύτητα αυξάνεται με την ισχύ. Παρουσιάζεται επίσης η δυνατότητα του πλαισίου να μπορεί να διαχειρίζεται αλλαγές στις ιδιότητες διαβροχής της επιφάνειας κατά την εγχάραξή τους με πλάσμα O_2 . Το πλαίσιο μπορεί να προσομοιώσει αλλαγές στην επιφανειακή μορφολογία (τραχύτητα) και την κάλυψη της επιφάνειας σε οξυγόνου (που συνδέεται με λειτουργικές ομάδες οξυγόνου), ο συνδυασμός των οποίων καθορίζει την κατάσταση διαβροχής της επιφάνειας.

Το κεφάλαιο αυτό έχει δημοσιευτεί ως μέρος του παρακάτω άρθρου:

G. Memos, E. Lidorikis, E. Gogolides and G. Kokkoris, (2021), A hybrid modeling framework for the investigation of surface roughening of polymers during oxygen plasma etching, Journal of Physics D: Applied Physics, 54 (2021) 175205

¹⁰ Φανερώνει το μοτίβο της επιφάνειας (για αρνητικές τιμές, κυριαρχούν κοιλότητες στην εγχαρασόμενη επιφάνεια, ενώ για θετικές τιμές, η επιφάνεια παρουσιάζει κορυφές).

Στο **Κεφάλαιο 6**, συνοψίζονται η καινοτομία της μελέτης που πραγματοποιήθηκε στο πλαίσιο της διατριβής όπως επίσης και η χρησιμότητα και οι δυνατότητες του υβριδικού υπολογιστικού πλαισίου προσομοίωσης που αναπτύχθηκε. Επίσης προτείνονται ορισμένες ενδιαφέρουσες μελλοντικές προεκτάσεις που προκύπτουν από την διατριβή. Επιγραμματικά, οι βασικές συνεισφορές που αναφέρονται στο κεφάλαιο αυτό είναι: α) Η ανάδειξη της σημασίας της επιφανειακής φόρτισης στο σχεδιασμό “συνταγών” για την παραγωγή ή την εξάλειψη της τραχύτητας της επιφάνειας ενός πολυμερικού (ή διηλεκτρικού) υποστρώματος, β) η ανάπτυξη πρωτότυπου μοντέλου για τον συντελεστή απόδοσης και οπισθοσκέδασης της δευτερογενούς εκπομπής ηλεκτρονίων για υποστρώματα PMMA, γ) η ανάπτυξη στοχαστικού μοντέλου επιφανειακής εγχάραξης στο οποίο εφαρμόζεται πρωτότυπη μέθοδος kMC λαμβάνοντας υπόψη την επιφανειακή μορφολογία, δ) η μεταφορά τοπικών ιδιοτήτων του προφίλ (κλάσμα κάλυψης επιφάνειας από οξυγόνο) από το ένα χρονικό βήμα στο επόμενο με τη μέθοδο των ισοϋψών, ε) η δυνατότητα του πλαισίου να «παρακολουθεί» τόσο αλλαγές στη μορφολογία (τραχύτητα) όσο και την χημική σύσταση της επιφάνειας. Ενδιαφέρουσες μελλοντικές προεκτάσεις που αναφέρονται στο κεφάλαιο αυτό είναι: α) Η εφαρμογή του υπολογιστικού πλαισίου προσομοίωσης σε άλλα πολυμερικά υποστρώματα ή/και σε άλλες χημείες πλάσματος όπως επίσης η εφαρμογή του στην εγχάραξη με πλάσμα συμβατικών δομών μικροηλεκτρονικής που συναντώνται στην βιομηχανία ημιαγωγών, όπως αυλάκια και οπές, ή ακόμα και σε τρισδιάστατες μορφολογίες. β) Η επέκταση του πλαισίου με τη συμπερίληψη πρόσθετων μηχανισμών που μπορούν να επηρεάσουν την εξέλιξη της τραχύτητας. γ) Η σύνδεση του πλαισίου με ένα μοντέλο προσομοίωσης πλάσματος στην κλίμακα του αντιδραστήρα. δ) Ακόμα η ανάλυση της επιφανειακής τραχύτητας σε πολλαπλές χωρικές κλίμακες με στόχο την πρόβλεψη της κατάστασης διαβροχής της επιφάνειας (π.χ. Wenzel ή Cassie-Baxter ή υβριδική κατάσταση). ε) Η μελέτη της σχέσης τραχύτητας - διατήρησης επιφανειακού φορτίου στην επιφάνεια ενός πολυμερούς σε συνδυασμό με το πώς επηρεάζονται οι επιφανειακές ιδιότητες από το επιφανειακό φορτίο (εφόσον αυτό διατηρείται μετά την εγχάραξη) με στόχο την διερεύνηση πιθανών εφαρμογών που δύναται να προκύψουν από μια τέτοια τεχνολογία.

Acknowledgements

I wish to express my sincere thanks to Professor Elefterios Lidorikis, my dissertation supervisor, for his guidance and encouragement throughout this investigation. The helpful advice and support of the rest of the dissertation committee, Dr. Angeliki Tserepi, Director of Research Institute of Nanoscience & Nanotechnology - NCSR “Demokritos”, and Dr. Evangelos Gogolides, Director of Research at the Institute of Nanoscience & Nanotechnology - NCSR “Demokritos”, are gratefully appreciated. I also wish to thank Dr. George Kokkoris, Research Associate at the Institute of Nanoscience & Nanotechnology-NCSR “Demokritos”. Without his effective mentoring and supervising, the completion of this dissertation would not have been possible. I also want to acknowledge all people of Plasma Group of Institute of Nanoscience and Nanotechnology - NCSR “Demokritos”, providing me any help whenever I needed. Finally, I would like to thank my family for their support and encouragement.

Publications

The results of the dissertation were published in four international peer-reviewed journals (Journal of Physics D: Applied Physics Impact Factor (IF) 3.169, Micromachines IF 2.523, Journal of Applied Physics IF 2.286, Plasma Processes and Polymers IF 3.065). They were also presented at 6 international scientific conferences. The impact of the publications has been reflected in the international scientific community so far with 30 citations in google scholar.

International peer-reviewed journals

- G. Memos, E. Lidorikis , E. Gogolides and G. Kokkoris, (2021), A hybrid modeling framework for the investigation of surface roughening of polymers during oxygen plasma etching, Journal of Physics D: Applied Physics, 54 (2021) 175205, DOI: 10.1088/1361-6463/abdb0b
- G. Memos, E. Lidorikis, G. Kokkoris, (2018) Roughness evolution and charging in plasma-based surface engineering of polymeric substrates: The effects of ion reflection and secondary electron emission, Micromachines, 9 (8), 415, DOI: 10.3390/mi9080415
- G. Memos, E. Lidorikis, G. Kokkoris, (2018) The interplay between surface charging and microscale roughness during plasma etching of polymeric substrates, Journal of Applied Physics, 123 (7), 073303, DOI: 10.1063/1.5018313
- G. Memos and G. Kokkoris, (2016), Modeling of charging on unconventional surface morphologies of PMMA substrates during Ar plasma etching, Plasma Processes and Polymers, 13: 565-578, DOI: 10.1002/ppap.201500176

International peer-reviewed conferences

- George Memos, Elefterios Lidorikis, E. Gogolides, George Kokkoris, A hybrid modeling framework for the investigation of roughness formation during plasma etching of polymeric surfaces, 45th International Conference on Micro & Nano Engineering, Rhodes Greece, September 23rd - 26th, 2019
- George Kokkoris, George Memos, Elefterios Lidorikis, A modeling framework for profile evolution during etching of rough polymeric surfaces with low pressure oxygen plasma, 24th International symposium on plasma chemistry, Naples(Italy), June 9-14, 2019
- George Kokkoris, George Memos, Elefterios Lidorikis, Evangelos Gogolides, Modeling the evolution of rough profiles of polymeric substrates during plasma etching: The interaction between surface charging and roughness, 17th International Conference on Plasma Surface Engineering, Garmisch-Partenkirchen, Germany, September 6- 11, 2018
- George Memos, George Kokkoris, Athanasios Smyrnakis, Elefterios Lidorikis, Evangelos Gogolides, " Simulation of profile evolution of rough polymeric substrates taking into account surface charging ", 10th Plasma Etch and Strip for Microtechnology workshop (PESM), Leuven, Belgium, IMEC, October 19-20th, 2017
- G. Memos and G. Kokkoris, "A modeling framework for the calculation of plasma induced surface charging on unconventional or rough polymeric substrates", 7th

International Symposium on Plasma Nanoscience (iPlasmaNano-VII), Vravrona, Greece, October 16-20, 2016

- G. Kokkoris, G. Memos, "Does charging affect surface roughness evolution of plasma etched polymeric substrates?", 15th International Conference on Plasma Surface Engineering, Garmisch-Partenkirchen, Germany, September 12 - 16, 2016

Contents

ABSTRACT.....	1
ΠΕΡΙΛΗΨΗ	8
Acknowledgements	16
Publications	17
Contents	19
1. Introduction: basic theory, literature review & dissertation aims.....	22
1.1 Introduction.....	22
1.2 Plasmas and Polymers.....	22
1.3 Plasma state.....	24
1.3.1 Plasma etching in nanotechnology: the plasma reactor	25
1.3.2 Mechanisms of plasma etching	29
1.4 Interaction of plasma with polymer surfaces	32
1.4.1 Plasma induced surface roughness of polymeric substrates.....	38
1.4.1.2 Modeling of plasma induced surface roughness	39
1.4.1.3 Statistical parameters to characterize surface roughness	43
1.4.2 O ₂ plasma chemistry and polymers.....	44
1.4.2.1 Surface functionalization and etching.....	44
1.4.2.2 Models of etching of polymers in O ₂ plasmas	46
1.5 The plasma induced surface charging phenomenon	47
1.5.1 Surface charging of conventional microstructures in microelectronics	47
1.5.2 Computational studies on surface charging of conventional microstructures in microelectronics	49
1.6 The aims of this dissertation	51
2. Description of the modeling framework	55
2.1 Introduction.....	55
2.2 Description of the Modeling Framework: application to sputtering of PMMA with Ar plasma.....	56
2.2.1 The surface charging module.....	56
2.2.1.1 Particle Trajectory Model	57
2.2.1.2 Secondary Electron-Electron Emission Model	61
2.2.1.3 Ion Reflection Model	64

where θ is the angle of ion incidence with respect to the normal to the surface	64
2.2.1.4 Surface Charge Density Model	64
2.2.1.5 Charging Potential Model	65
2.2.2 Surface Etching Model.....	66
2.2.2.1 etching (sputtering) yield based on Yoshimura et al. experimental measurement and TRIM simulations	67
2.2.2.2 etching (sputtering) yield based on Bruce experimental measurements	69
2.2.3 Profile evolution module.....	71
2.3 Description of the Modeling Framework: application to ion enhanced etching of PMMA with O ₂ plasma	73
2.3.1 Surface processes during ion enhanced etching of PMMA with O ₂ plasma.....	75
2.3.2 The kinetic Monte Carlo surface model.....	77
2.3.2.1 Coarse graining	77
2.3.2.2 Estimation of the transition probabilities by a particle trajectory module	78
2.3.2.3 The algorithm.....	79
2.3.3 Transport of local variables of the evolving surface profile	80
2.3.4 The time intervals (scales) of the framework.....	82
2.4 Implementation	82
2.5 Conclusions.....	83
3. Modeling of charging on unconventional surface morphologies of PMMA substrates during Ar plasma etching	85
3.1 Introduction.....	85
3.2 Surface charging module verification	86
3.3 Surface charging on rough surfaces with sinusoidal profiles.....	88
3.4 The effect of profile AR on surface charging	93
3.5 The effect of substrate thickness on charging.....	97
3.6 Conclusions.....	100
4. The intertwined effects of surface charging, ion reflection, and secondary electron-electron emission on roughness evolution during Ar plasma etching of polymeric substrates.....	102
4.1 Introduction.....	102
4.2 Case Study	103
4.3 Evolution of the surface profile with and without charging	103

4.3.1 Results for energy dependent etching yield	104
4.3.2. Results for angle and energy dependent etching yield.....	106
4.4 The effects of ion reflection and secondary electron emission	109
4.5 Conclusions.....	115
5. Investigation of roughness evolution during O₂ plasma etching of polymeric surfaces	116
5.1 Introduction.....	116
5.2 Case study	117
5.3 Evaluation and verification of the kMC model.....	117
5.3.1 Evolution of the surface coverage and the etching rate	117
5.3.2 What is the proper choice of t_{kMC} ?	119
5.3.3 The update of the transition probabilities and the sticking coefficient of O atoms.....	122
5.4 The evolution of the surface profile and rms roughness	123
5.5 Comparison to measurements	125
5.6 The potential of the hybrid framework to study the wetting behavior of plasma etched polymeric surfaces	126
5.7 Conclusions.....	128
6 Conclusions.....	129
7. Appendices.....	133
A. The directionality difference between ions and electron fluxes at the wafer and the electron shadowing effect.....	133
B. A brief review on kinetic Monte Carlo schemes	137
B.1 Introduction - the master equation.....	137
B.2 Direct kMC.....	138
B.3 n-fold direct kMC.....	139
B.4 Coarse grain kMC	140
B.5 τ -leap method.....	141
C. The effect of different coarse-graining levels in the z-direction <i>and</i> along the arclength of the surface profile.....	141
C.1 The effect of coarse-graining level in the z direction	141
C.2 The effect of coarse-graining level along the arclength of the surface profile.....	142
D. The effect of dielectric thickness on the charging time through an analytical approach	147
8. References.....	149

1. Introduction: basic theory, literature review & dissertation aims

1.1 Introduction

Plasma etching, in addition to its traditional use for pattern transfer in microelectronics, is utilized in nanotechnology to control surface roughness and surface chemical composition of polymeric substrates. Plasma induces both micro/nano roughness and functional groups¹¹ on the surface of the substrates, factors that have major importance in the surface properties (e.g. wetting behavior, interaction of surfaces with cells). It is critical to study the parameters that affect these factors and ultimately to design “recipes” delivering desired surface characteristics. However, plasma-surface interactions are complex and the process design is usually based on a trial and error procedure. Towards comprehensive process design, in this dissertation, the interaction of plasmas with the surface of polymeric substrates is studied by utilizing a hybrid modeling framework, addressing both effects of plasmas, i.e. alteration of the surface morphology and composition.

This chapter is an introduction in plasma-surface interactions and processing of polymeric materials, the field in which the dissertation belongs to. Basic concepts of the topics of a) surface functionalization, b) etching in plasma reactors and c) surface modeling and simulation are presented. Particular importance is also attached to plasma induced surface charging on conventional dielectric microstructures in microelectronics. This because **one of the main ideas** of this dissertation is that surface charging is critical not only for microelectronics but also for the developing roughness on the surface of polymeric substrates during plasma etching. The chapter concludes by discussing the aims of the dissertation.

1.2 Plasmas and Polymers

Nowadays, polymeric materials are used for a wide variety of applications, e.g. thermoplastic objects, coatings, films, membranes, fibers, textiles, and biomaterials, in various industrial areas, e.g. automotive, packaging, filtration, clothing, and biomedical technology. For many applications, the polymer surface properties are of major importance. Indeed, highly functionalized surface polymers are much desired to applications ranging from wetting control [1], antireflective coatings [2], and waveguide [3] applications, to protein and cell adsorption enhancement [4], stem cell differentiation [5-7] and pressure-driven or electroosmotic flow tuning in micro- or nanofluidics [8, 9]. However, polymers usually do not own a priori the special surface properties needed for the above mentioned plethora of applications [10, 11]. For

¹¹ Functional groups are assemblages of atoms that fasten to the carbon skeleton of an organic molecule and provide particular properties. A functional group can take part to specific chemical reactions through the development of different bonds. Functional groups are commonly categorized as hydrophobic or hydrophilic relying on their charge or polarity.

instance, many polymers¹² are chemically inert and cannot strongly interact with other materials due to the absence of functional groups in their surface structure. In this case, they can be characterized by a low wettability¹³ and/or poor adhesion¹⁴ properties. Generally, polymers have exceptional bulk physical and chemical properties, are inexpensive, and are not difficult to process [10, 11]. So how these materials can be transformed into highly valuable finished products? An efficient, easy, clean and comfortable option is plasma processing, a method that has been extensively employed **to functionalize polymers by improving their surface properties through the modification of the chemical composition and the morphology of the surface**. The former is achieved through the creation of reactive centers at which plasma gas fragments or atoms can stick as new functional groups while the latter through the removal of material in chemical and/or physical ways. The removal of the polymeric material, under particular conditions, which have to do both with the type of the feeding gas and the process parameters as well as the nature of the polymer that is treated, can promote either the fabrication of stochastic [15] or ordered nanostructures [16, 17] (see Figure 1).

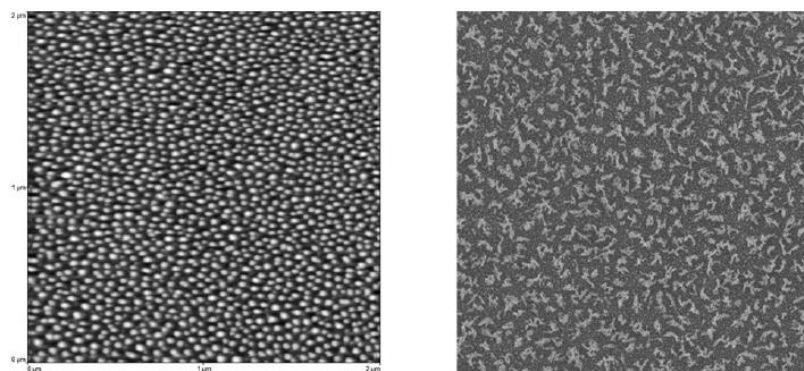


Figure 1.1: Poly(methyl methacrylate) (PMMA) surfaces after plasma treatment. (a) Ordered structures and (b) stochastic structures. Taken from [18].

Plasma processing of polymeric surfaces is a well-established technique for many applications because of its competitive advantages: the dry character, the low temperature processing,¹⁵ and mainly, the flexibility to perform three different processes, i.e. etching, deposition, and treatment, on polymeric surfaces, without modifying bulk properties (e.g. strength, toughness, biodegradability). A shower of different species (energetic neutrals, ions, electrons and photons)

¹² For example, polyolefins such as polyethylene and polypropylene have inadequate adhesion properties owing to the lack of polar groups in their surface [12] J. Friedrich, *The Plasma Chemistry of Polymer Surfaces: Advanced Techniques for Surface Design*, Wiley-VCH Verlag & Co. KGaA, Weinheim, Germany, 2012.

¹³ Functional groups able to augment the wettability of a polymer surface to which they adhere are the carbonyl group, the hydroxyl group and the carboxyl group [13] J.R. Roth, *Industrial Plasma Engineering*, IOP Publishing 2001.

¹⁴ Increase of polymer surface adhesion can be seen as a generalization of the augmentation of wettability [14] A. Fridman, *Plasma Chemistry*, Cambridge University Press 2008. The presence of O – containing functional polar groups at polyolefin surfaces render the polyolefins wettable by polar liquids and also by metal layers [12] Friedrich, *The Plasma Chemistry of Polymer Surfaces: Advanced Techniques for Surface Design*. High polar contributions to surface energy are preconditions for strong adhesion.

¹⁵ Heat-sensitive polymeric materials can be effectively treated by plasmas.

present in the plasma bombards the polymeric surface. A result of this bombardment is the attachment of atoms or molecular fragments of the dissociated plasma gas at the polymer chain; in this way, it is possible to interlock certain functional groups on the polymeric surface for specific interaction with other functional groups.

Plasma treatment does not only cause a modification of surface chemical composition; it can also modify the surface morphology dramatically through ion energy bombardment. The ions can gain enough energy to penetrate relatively deeply (1-10nm) [19] into the polymer material. Such ions would not only be implanted into the material, but would also cause ion enhance etching¹⁶ and sputtering.¹⁷ The special issue of this plasma-induced change, which has attracted much attention lately both experimentally and theoretically [20, 21], is surface roughness. For instance, the highly hydrophilic character of polymers is often achieved by using an oxygen (O₂) plasma and it is attributed to both the appearance of oxygen (O)-containing functional groups on the surface as well as on the surface roughness [9, 22-24]. With regard to the adhesion properties of polymers, roughness also increases the surface area of the polymeric target, inducing more interactions, and better adhesive bond strength [24]. However, plasma induced surface roughness must be precisely controlled in rather narrow bounds so as to deliver the desirable outcome [25].

Conclusively, by adjusting the gas phase chemistry and the ion-bombardment energy, an amount of commercially valuable functional properties of the polymeric surfaces immersed in plasma can be tuned.

1.3 Plasma state

Plasma is a gaseous mixture of positive ions and electrons. Plasmas can be fully ionized, as the plasma of the Sun, or partially ionized, as the plasma reactors that are used in microfabrication. Specifically, the plasma which is useful to ultra large scale integration (ULSI) processing is a weakly ionized plasma, i.e. a plasma where the ionization fraction is less than 1% [26].

In order for the plasma to be formed, the atoms or molecules within a gas must be heated to or beyond the ionization energy. The result is a huge number of charged particles that interact by electric forces. This is in contrast to a neutral gas where particles interact only during a collision, i.e. when two gas atoms "feel" the short-range Van der Waals force,¹⁸ which decays with the inter-particle distance (r) as r^{-6} . This means that two neutral atoms are not affecting one another until they collide. On the other hand, the electrostatic interaction decays as r^{-2} which makes it a long range force. Considering this situation, in the plasma state, charged particles produce a long-range field (like Coulomb field), which can affect many particles at a distance. In this sense, the plasma state is able to react to an external stimulation in a collective manner [27].

¹⁶ Ions from the plasma promotes chemical reactions between a neutral gas and the substrate.

¹⁷ Energetic ions drive atoms off the surface of a solid material.

¹⁸ From a physics point of view, the Van der Waals force is the spontaneous formation of dipoles due to distortion of electron clouds of adjacent atoms.

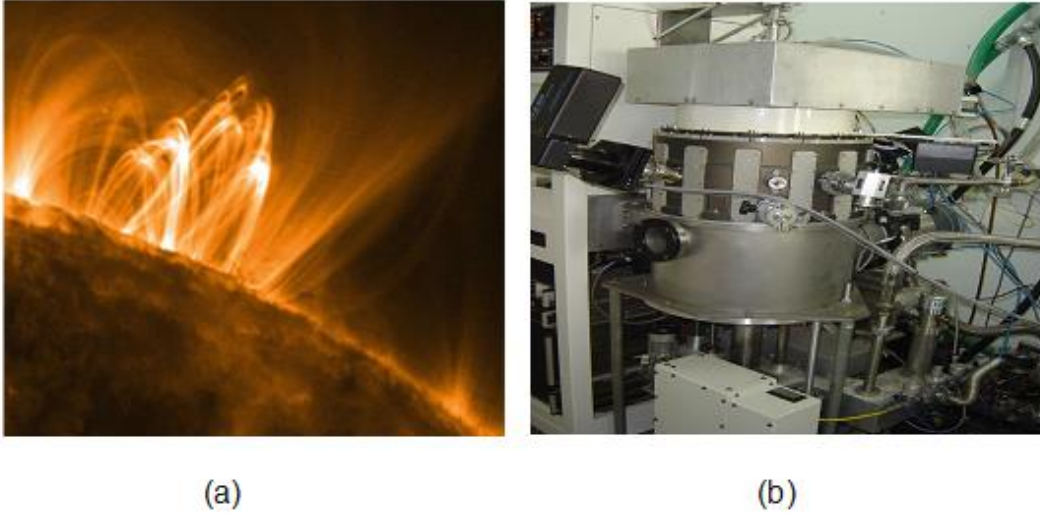


Figure 1.2: Examples of plasmas. (a) Coronal loops filled with hot plasma that emits in the soft X-ray regime. Observed at 17.1 nm wavelength by the Transition Region and Coronal Explorer (TRACE) satellite [27]. (b) Inductively coupled plasma reactor for microfabrication processing (Institute of Nanoscience & Nanotechnology, National Center for Scientific Research “Demokritos”) [28].

Several varieties of plasmas exist, characterized by their electron densities and temperatures. Figure 1.3 shows the ranges of electron temperature, electron density, and Debye length¹⁹ [29] for typical plasmas found in nature and in technological applications [30].

1.3.1 Plasma etching in nanotechnology: the plasma reactor

Industrial plasma is created by imposing an electromagnetic field to a volume of gas in the reactor chamber. This field provides energy to the free electrons present in the gas rendering them energetically capable to provoke gas ionization. Specifically, the high energy electrons a) liberate more electrons from the gas atoms by detaching them from their atomic orbital shell, b) excite bound electrons to higher-level orbits and c) lead to the formation of molecular and atomic radicals. Ultimately, a distinctive glow is generated as species excited by high energy electrons go through relaxation to lower energy levels and re-emit the energy as photons (see Figure 1.4).

¹⁹ The Debye length, λ_{De} , tells us how rapidly a potential perturbation is attenuated in the plasma. Over a distance λ_{De} , the perturbation is reduced to 1/e of its initial value. In particular, the variation of the potential around a

perturbation is given by $\Delta V(x) = \Delta V_0 \exp(-\frac{|x|}{\lambda_{De}})$.

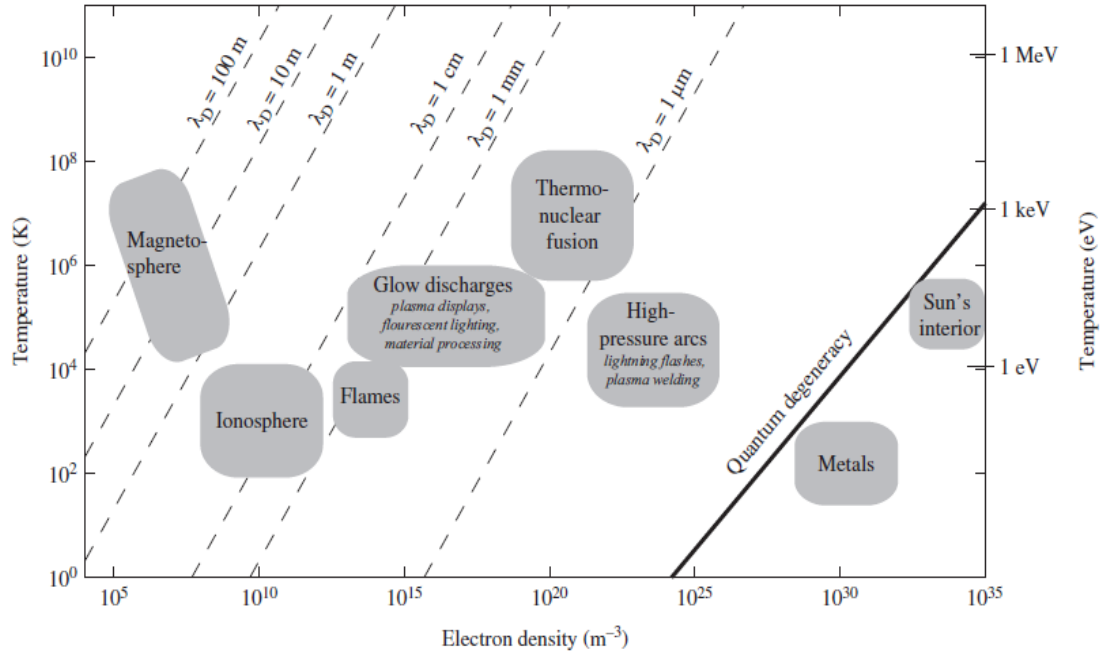


Figure 1.3: Range of temperature, electron density, and Debye length for typical plasmas in nature and in technological applications. It should be mentioned that only states to the left of the quantum degeneracy line are considered plasmas and can be treated with formulations from classical physics. Reproduced from [30].

A plasma is macroscopically neutral, with balanced populations of positively and negatively charged species. But how is plasma sustained? Ions and electrons are lost to all surfaces within the chamber. To maintain a steady state of electron and ion densities in the bulk of the plasma, the loss processes must be balanced by an ionization process, i.e. an external energy source is required. In practice, this energy source is the above mentioned electric field which can act directly on the charged particles only. Provided that the ion mass is much larger than the electron mass, it is obvious that the action of the field is primarily to give energy to the electrons (2-8 eV) [29].²⁰

Although electrons collide with neutral atoms and ions, only a very small energy transfer to the heavy particle can take place [29].²¹ This is also the reason why the containing vessel of the plasma is not melting. Indeed, only a small amount of energy is transferred to the reactor walls or the wafer atoms. Ultimately, since the ions are able to receive some energy from the external field, their temperature is above the ambient temperature.

²⁰ The work done by the electric field on an initially stationary particle with mass m , and hence the energy transferred to this particle can be easily proved that is equal to $\frac{(Eet)^2}{2m}$, where E is the magnitude of the electric field, e is the electronic charge, and t is the time.

²¹The energy transfer from an electron to an ion is expressed by the equation $\frac{E_{\text{ion}}}{E_{\text{electron}}} = \frac{4m_{\text{electron}}m_{\text{ion}}}{(m_{\text{electron}} + m_{\text{ion}})^2} \cos^2 \theta$, where θ is the angle of incidence.

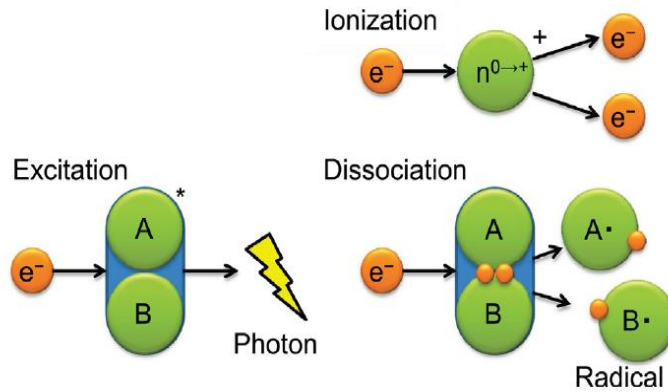
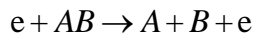
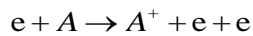


Figure 1.4: The ionization, dissociation, and excitation of molecules. When an electron collides with a molecule (bonded A and B atoms), excitation of the molecule generates an excited state molecule (metastable) and subsequent de-excitation, accompanied by the emission of photons. Another process is dissociation, leading to rupture of the chemical bonds and the generation of A and B atoms. The ionization process generates an additional electron and the target molecule is ionized. Taken from [31].

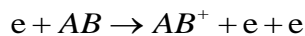
The types of processes that may arise in the plasma can be differentiated as dissociation



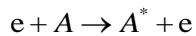
atomic ionization



molecular ionization



atomic excitation



and molecular excitation



where e denotes an electron, AB denotes a molecule of a neutral gas and the superscript (*) denotes that a species is at an excited state. Dissociated atoms (or fragments of AB molecule) like A and B are called radicals. Radicals have an incomplete bonding state and are extremely reactive. Ions are charged atoms or molecules such as A^+ or AB^+ .

Confined plasmas form positively charged boundary layers known as *sheaths* when entering into contact with the confining surfaces. Sheaths are normally created to balance electron and ion losses to the confining surfaces. They are of particular interest for etching. However, they are far from simple and are often considered as an example of nonlinear physics. An oversimplified description of a plasma sheath follows. A rigorous mathematical description [32] of plasma sheaths are beyond the scope of this dissertation.

Let us imagine an ideal arrangement of a plasma slab between two alike parallel grounded surfaces (walls). Owing to charge neutrality, the electric field is zero everywhere. Nevertheless, since in this arrangement electrons are not constrained by any electric field, due to their greater mobility, they are quickly lost to the walls, inducing an abrupt alteration of charge concentration. Consequently, at the plasma–wall interface, charge neutrality is no longer met and the electrical potential turn up to be positive in the plasma (due to absence of negative charged particles) and quickly lessening within the space domain of plasma- sheath, ultimately, reaching zero adjacent to the walls. This charge imbalance and the ensuing formation of such a potential barrier²² constitutes a self-confining mechanism for electrons which are held back to the plasma by the corresponding electric field pointing from the plasma to the walls. On the other hand, ions that drift and diffuse to the edge of this region are accelerated rapidly toward the walls.

By the same token, an object putted in the plasma reactor, such as a wafer, acquires then the floating potential (V_f), which is lower than the potential of the plasma bulk (V_p). The sheath region adjacent to the wafer (and also adjacent to the reactor walls) will include much fewer electrons than the plasma bulk; due to electron depletion, this region precludes optical emission since excitation and relaxation do not take place as often there. Consequently, **the plasma sheath is a dark space**. Due to the potential difference ($V_p - V_f$), ions are accelerated across the sheath, creating a flux of high-energy particles with a nearly narrow angular distribution. The scale length of a sheath is much smaller than the plasma spatial expansion.

If the wafer is connected through an electrode to an oscillating power supply (which can also be the power supply for the plasma depending on the type of the reactor plasma source-vide infra), the ion energy is augmented further by the growth of self-bias at the electrode. This ion bombardment energy can be used in order to drive various surface processes. The consequent momentum transfer can lead to the ejection of subsurface species (i.e. sputtering) or it can promote chemical reactions so that weakly bound surface species are readily desorbed (i.e. ion enhanced etching). Concerning the latter, when neutral species are present at a solid surface, ion bombardment promotes the rate of surface processes such as reactant adsorption, reaction, and product desorption and etch directionality can be attained in the direction normal to the film/substrate surface deposited on the wafer [33]. A more detailed description of the mechanisms of plasma etching follows in Section 1.3.2.

The plasma density (number density of electrons) of a processing plasma varies from about 10^8 to 10^{13} per cm^3 , relying on the type of plasma source and the power level utilized. Reactive ion etchers (RIEs) are capacitively coupled plasmas in which the wafer is placed on the powered

²² The sheath region starts where charge neutrality begins to impart. The electric potential gradient turns into very steep on the boundary side of the sheath edge, and owing to the curvature of the potential, ions are accelerated toward the boundary while electrons are repelled from it.

electrode. The power on this electrode adjusts both the density of ions and their energies as they bombard the wafer. To prevent extremely high ion energy (which leads to the lowering of selectivity²³) low power and high pressure is utilized, which restricts the plasma density (and thus the etching rate).

However, the requirements for a) enhanced control of etched profiles (while preserving high etching rates), b) enhanced etching-rate uniformity across the wafer, and c) significant selectivity to material layers that are subjected to the plasma but that should not be etched have advanced the growth of low-pressure, high-density plasma sources. Low-pressure operation conditions are required to curtail collisions in the sheath. This leads to a narrower ion angular distribution, which in turn ensues in a more anisotropic etching process. The essential element of etching systems exploiting these sources is their capability to separately control the ion density and the ion energy via wafer radio frequency (RF) biasing, thus accomplishing high selectivity to the underlying substrate. Furthermore, high ion density permits high etching rate and, thus, high throughput.

The most popular commercial high-density source is made up of a coil above the roof of the reactor chamber. RF power applied to the coil couples to the plasma via a dielectric window (alumina or quartz). The amount of RF power applied to the coil regulates the ion density of the plasma. The wafer electrode is biased with an independent power supply that regulates the energy of the ions bombarding the surface. A typical picture of the architecture of such a plasma reactor is presented in Figure 1.5. In this example, an application of plasma processing is also depicted: the inductively coupled plasma (ICP) reactor is utilized in order to give to a polymeric substrate the desired morphology which is crucial in **the differentiation of stem cells into different cell types**; the critical role of substrate nanomorphology has been emphasized and attempts have been made to explain its role in differentiation in a series of recent studies [34-38].

1.3.2 Mechanisms of plasma etching

The mechanisms of plasma etching can be categorized into physical (mechanical) sputtering, pure chemical or spontaneous (thermal) etching, and ion-enhanced etching [39].

Physical sputtering results from the physical ejection of material due to bombarding with high energy ions. More precisely, when high energetic ions impact on a wafer surface, their kinetic energy is absorbed by the lattice atoms. In order for the crystal to dissipate this energy, a particle or more must be ejected from the solid. The number of particles that are removed per incident ion is expressed by the sputtering yield. The direction of etching is that of the bombarding ions. The selectivity of this mechanism is low.

²³ Etching selectivity of material A to B is the ratio of etching rates of A to B.

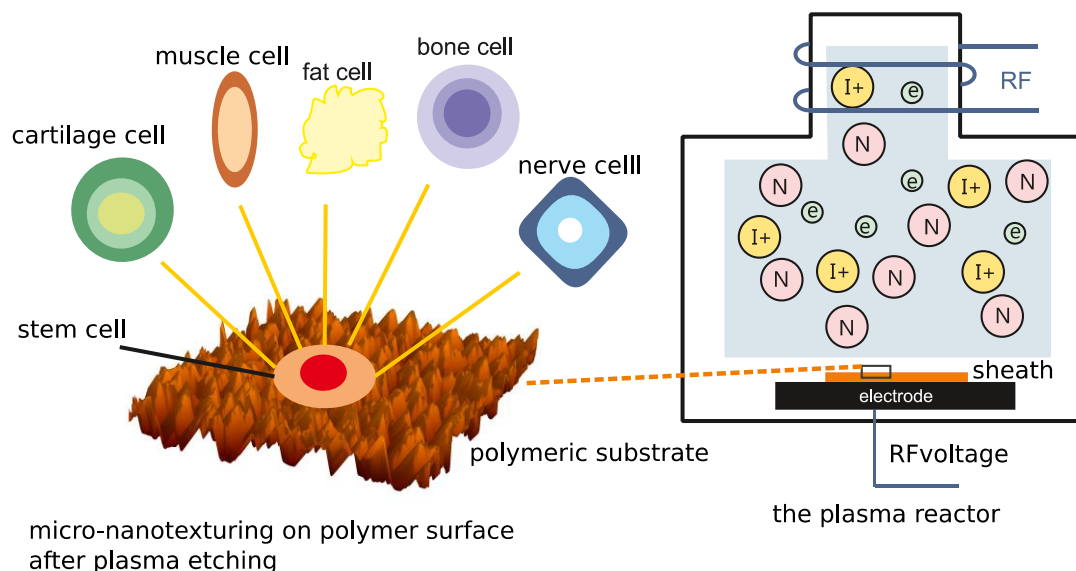


Figure 1.5: An inductively coupled plasma reactor creates micro-nanotexturing (i.e. micro-nanomorphology) on a polymeric surface which is then used for the differentiation of adipose tissue stem cells into different types of cells such bone cells, cartilage cells, fat cells, nerve and muscle cells. I+ is for ions, N is for neutrals and e is for electrons.

Pure chemical or spontaneous (thermal) etching occurs through a homogeneous or heterogeneous surface reactions between neutral species and volatile products. Typically, there is no significant difference with wet etching in the sense that both advance through chemical interaction with the surface. The selectivity of this mechanism is very high. Owing to their deficiency in directionality,²⁴ pure chemical etching is mainly utilized in cases where isotropic etching is needed.

As far as the ion-enhanced is concerned, interestingly enough, both chemical and physical surface interactions are important in this process. Indeed, Coburn and Winters showed that the chemical and physical attributes of ion-enhanced etching are not simply additive but act in synergy, something that is clearly illustrated in Figure 1.6 [40].

²⁴ Directionality describes the relative etch rates in the vertical and horizontal directions. An isotropic process etches at the same rate in all directions.

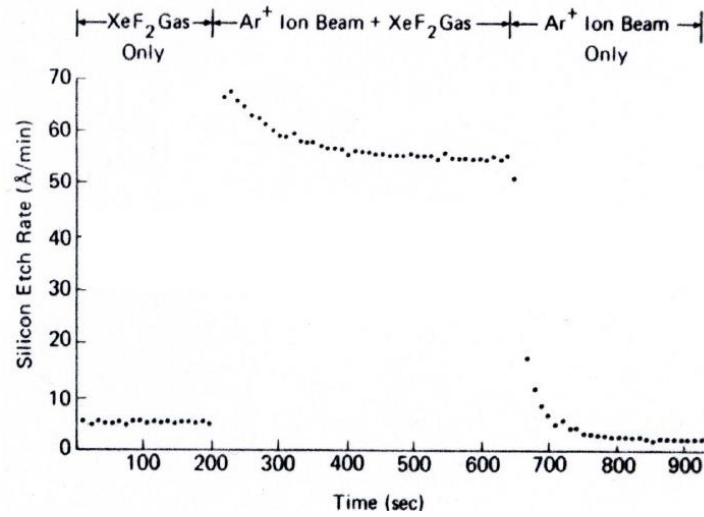


Figure 1.6: Coburn and Winters measured silicon (Si) etching rate under independent and concurrent exposure to XeF₂ gas and 450 eV Argon ion (Ar⁺) beams. They observed that the etching rate under simultaneous exposure to both the beams was nearly six times the sum of the etch rates under exposure to the individual beams. Taken from [40].

Ion-enhanced etching is an anisotropic etching process. The selectivity obtained in this occasion is significantly increased in comparison to a thermal process (see Figure 1.7).

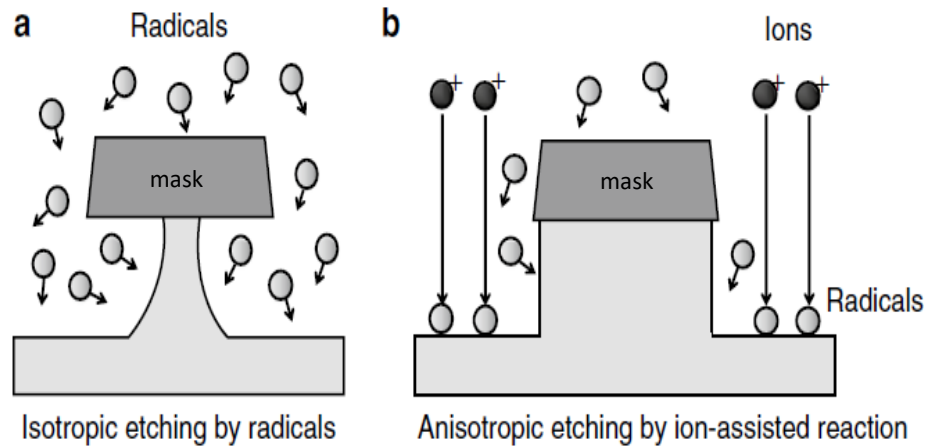


Figure 1.7: (a) Isotropic and (b) anisotropic etching. Plasma etching is a technology traditionally used for transferring circuit patterns developed with the resist, onto the underlying thin film. Plasma partly clears away the various thin films deposited on a wafer, with this resist utilized as a mask. Anisotropic etching advances in the vertical direction implementing processing that meticulously reproduces the mask patterns, thus, carrying out fine patterning. Taken from [41].

1.4 Interaction of plasma with polymer surfaces

Interaction mechanisms between a plasma and a polymer surface are too convoluted: for they involve physical bombardment by energetic particles like ions, electrons and ultraviolet photons, and chemical reactions at and below the surface caused by the presence of particles in excited states, molecular fragments, free radicals, dissociated atoms, and thermalized charged particles on the polymer surface. Several effects ensue from this, such as etching/ablation, interlocking of new chemical functionalities and charging, just to name a few. These take place simultaneously in a complex coaction, which relies on many parameters (e.g. ion energy, type of feeding gas chemistry, polymer type, treatment time).

Some of the most significant examples of these interactions encountered in plasma processing of polymers are listed below:

(1) Plasma etching/ablation of the polymer. When a polymer is plasma treated, the mechanical effects of ion bombardment produces physical sputtering which mechanically eject material (atoms/ions/molecular fragments) from the surface. For metal free polymers (i.e. polymers constituting mainly by carbon atoms (C), oxygen atoms (O) and hydrogen atoms (H)), the sputtering yield is determined [42, 43] by the “effective” carbon content in the material, i.e. the concentration of C not bounded to O.²⁵

The effect of neutral particles (e.g. free radicals) on etching is relied on their reactivity with the polymer. For example, O radicals in an O₂ plasma react with hydrocarbon-based polymers to produce volatile products that are afterwards pumped away from the surface. On the other hand, thermal neutrals in pure Ar discharges are inert, with a temperature close to room temperature, so there is no chemical etching.

In other words, in the case of reactive plasmas (and in contrast to inert gas plasmas), except from mechanical ion induced effects (i.e. sputtering), there are also chemical effects as well as chemical ion induced effects. For instance, in O₂ plasmas, the polymer carbon chain is dismantled by O chemical attack which can be accelerated by simultaneous ion bombardment.

(2) Surface roughening. Either the plasma is reactive or inert, beginning from a flat surface, within minutes of etching with plasma, a rough surface layer is formed, leading to a rough surface morphology (see Figure 1.8 and Figure 1.9). Depending on the reactor conditions, the feeding gas, the treatment time and the polymer utilized, the features of the surface morphology size from some tens of nm to several micrometers.

²⁵ As the sputtering yield of CO groups is much greater than that of carbon (since the sublimation heat of CO is very much less than the sublimation heat of carbon), the limiting step of the sputtering rate is then regulated by the concentration of carbon atoms not bounded to O [44] A. Bès, M. Koo, T.L. Phan, A. Lacoste, J. Pelletier, Oxygen plasma etching of hydrocarbon-like polymers: Part II experimental validation, *Plasma Processes and Polymers* 15 (2018).

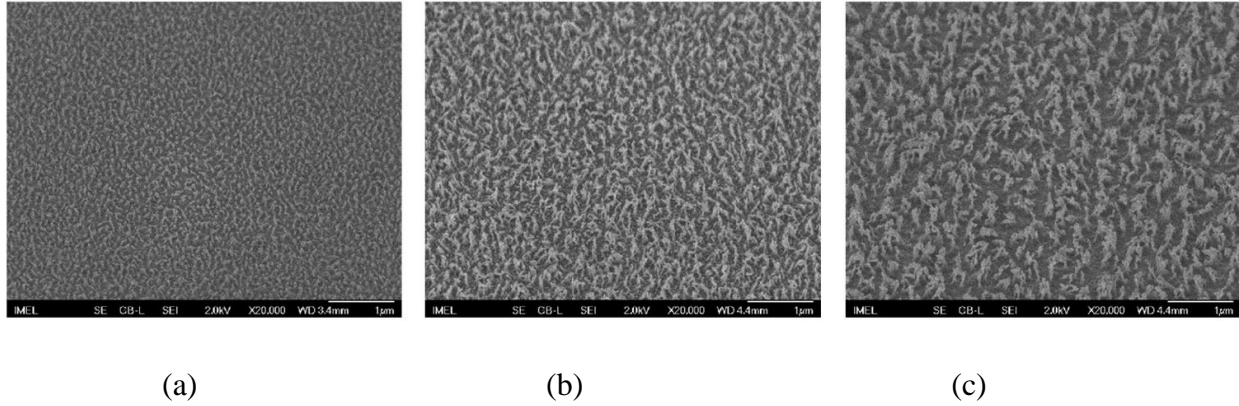


Figure 1.8: Tilted images (tilt = 45°) with characteristic micro-nano roughening on PMMA surfaces, after O₂ plasma etching for: (a) 60, (b) 90s and (c) 120s. Taken from [18]

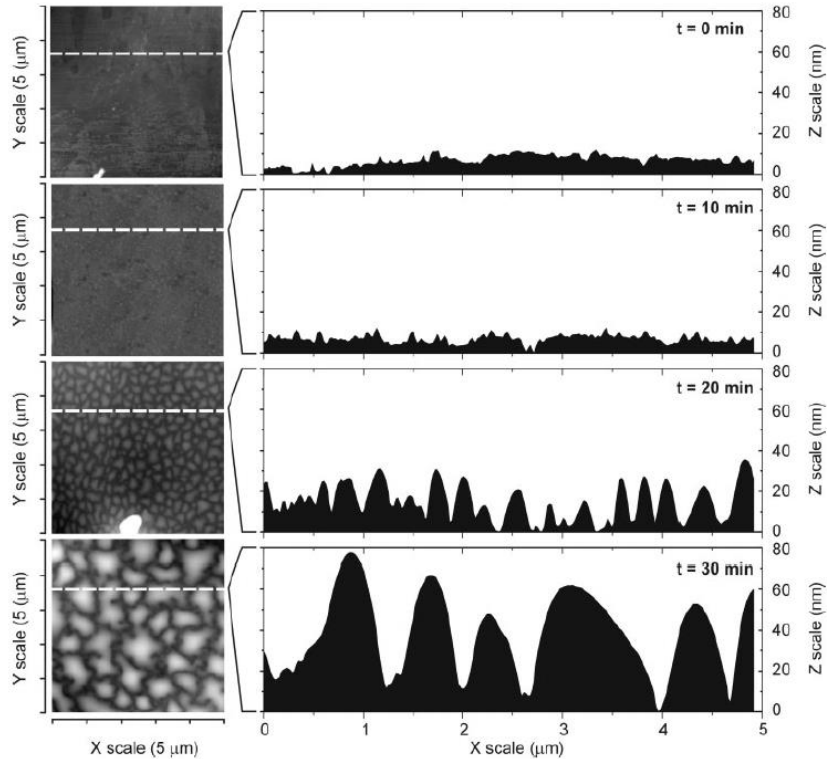


Figure 1.9. Roughness profiles of a polyurethane surface with different exposure times to O₂ plasma. Surface roughness increases as exposure time increases. Taken from [45].

(3) Surface chemical structure modification (functionalization). It is the process of importing new functional groups to the surface (e.g. amines, alcohols, ketones, esters) and can be separated into plasma activation and plasma passivation. The former is one of the most robust ways of boosting polymer wettability and polymer bond strength with another surface; it leads to the

enhancement of the surface free energy²⁶ through the integration/replacement of surface atoms and molecules.

A clear differentiation must be made between plasmas produced from inert gases (e.g. Ar, He, Ne, Xe) and reactive gases (e.g. O₂, N₂, CO₂, NH₃, ...). In case of reactive plasmas, there are two groups of active species existing in the plasma active region. **The first group** comprises of reactive neutrals such as O and nitrogen (N) radicals. These reactive species can be interlocked directly onto the surface as new functional groups. For example, in O₂ plasmas polar functional groups are added on the surface [i.e. hydroxyl (OH), carbonyl (C=O), and carboxyl (COOH) functional groups], which can dramatically enhance the surface free energy of the polymer (see Figure 1.10).

Specifically, oxidation is recognized to augment metal-polymer adhesion, while surface nitrogenation with nitrogen-containing plasmas imports basic functional groups that can increase dyeability with acid dyes, printability, or cell affinity in biocompatibility [46]. Plasma can also be utilized for surface fluorination and silylation, surface-chemical alterations which lead to greater hydrophobicity, i.e. reduced wettability and bond strength [46].

The second group comprises of nonreactive ions, nonreactive excited atoms, nonreactive molecules, photons and electrons, and have no direct chemical impact on surfaces. For plasmas produced from inert gases, only the second group of species exists. Such plasmas cannot chemically react with the polymer and the interaction is restricted to ion bombardment effects.

Ultimately, plasma passivation is the generic name for all plasma functionalization processes that lead to the lowering of the surface free energy by rendering the surface chemically inactive. The most commonly known example of plasma passivation is fluorine-based plasma functionalization (e.g. by CF₄ or C₄F₈ plasmas), ending in Teflon-like surface films.

²⁶ The surface energy is the work done against surface tension forces in forming a unit area of liquid on the surface at constant temperature and it is linked with the capability of water or liquids to wet surfaces. When the surface energy of a material is small, it is nearly *unwettable*, and water will bead up on the surface. If the surface energy is large, the surface will be *wettable*, and a water drop will cover a large area. Augmenting the surface energy can be achieved by modifying the chemical composition or the physical features of the surface with plasma active species. [13] Roth, Industrial Plasma Engineering.

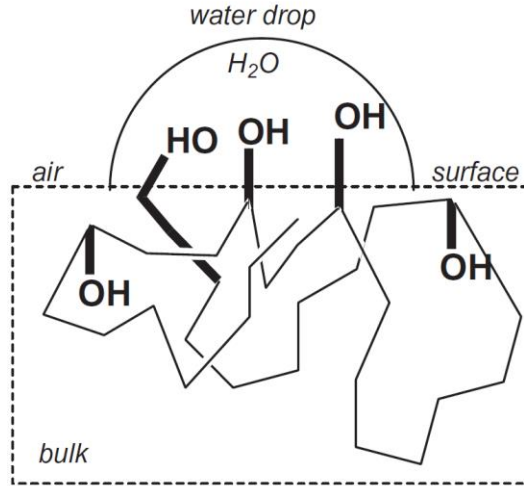


Figure 1.10: O_2 plasma induced polar groups on the polymer surface forming hydrogen bonds with water molecule. Taken from [12]

(4) **Surface charging** which has been attributed to the capture or trapping of ions by polar groups constituting the polymer surface, giving rise to the charging effect [18, 47]. The latter can also produce important effects as the pronounced hydrophilization of organic surfaces [18, 47].

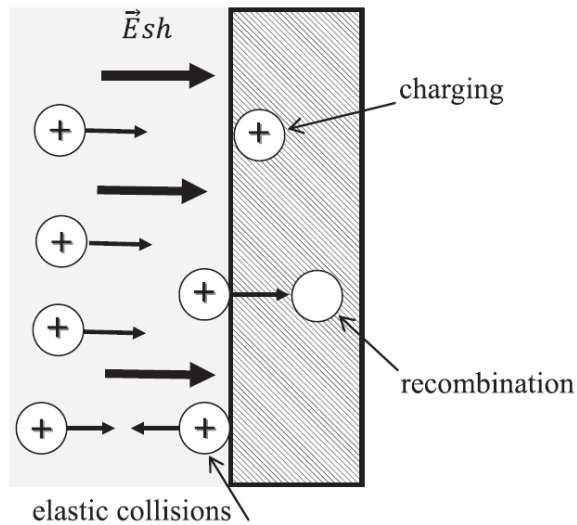


Figure 1.11: The events taking place under collisions of plasma ions accelerated by the sheath field (\vec{E}_{sh}) with the polymer surface: elastic collisions, recombination and trapping of ions, co-occurring with the electrical charging of the surface. Taken from [47].

(5) **Secondary electron emission** in which energetic primary species, including ions, electrons, neutrals, or photons drive electrons off the solid surface. The secondary electrons, once emitted, are then accelerated toward the plasma bulk owing to the sheath field. Because of their high

energy, these electrons can modify the dissociation and ionization processes near the processing surface [33].

(6) **Geometrical shadowing of neutral species and ions [48].** Shadowing indicates that a given point on the surface can obtain fewer particles than other points because adjacent surface features impede some of the impinging particles (see Figure 1.12). It is critical at low pressure conditions, where the Knudsen number (ratio to the mean free path over the dimension of the surface features) is much greater than 1, and the collisions between the species in the gas phase is negligible to the collisions of the species with the surface features. Shadowing effect is more pronounced for neutral species (i.e. radicals, inhibitors etc.) which enter the sheath having a Maxwellian energy distribution.²⁷ This means that they have the same velocity in any direction towards the plasma etched surface, thus their angular distribution is isotropic (i.e. large incidence angle θ , see Figure 1.12). Such particles have a lower flux in the valleys of surface morphology than at the peaks, which impede access to the valleys. Shadowing leads to either an increase or a decrease of roughness relying on whether the particles involved contribute to deposition or etching, respectively.

(7) **Diffusive and specular reemission of neutral species and ions [49].** Diffusive²⁸ reemission means that the impinging particles reach thermal equilibrium with the surface spontaneously and then are reemitted from the surface to the gaseous state with a Maxwellian distribution of velocities that depends on the surface temperature. In other words, the reemitted particle has no knowledge of its previous velocity (see Figure 1.12). Specular reemission (i.e. reflection) means that each incident particle is re-emitted at the same angle to the surface normal as the incident particle but on the opposing side of the surface normal in the plane formed by incident and re-emitted trajectories. It is assumed that ions rebound from the surface in a specular and elastic²⁹ manner, as expected for high energy particles incident close to grazing angles. Ions and neutral species are re-emitted from feature sidewalls, augmenting their relative flux at feature bottoms increasing roughness.

²⁷ Neutral species emerge from plasma into the sheath region due to random thermal motion. The Maxwellian distribution conveniently relates a characteristic neutral species temperature to the average energy of neutral species.

²⁸ The particle is scattered in a different direction that the law of specular reflection predicts.

²⁹ An elastic collision is one in which there is only an interchange of kinetic energy between the colliding bodies. An inelastic collision has no such restriction and internal (potential) energies change also. The latter can be in the form of electronic excitation, ionization, etc. Ultimately, in a non-interacting collision, the ions are specularly reflected on the surface with neither interchange of kinetic energy between the ion and the surface nor fractional transfer of the ion kinetic energy to the surface internal (potential) energy.

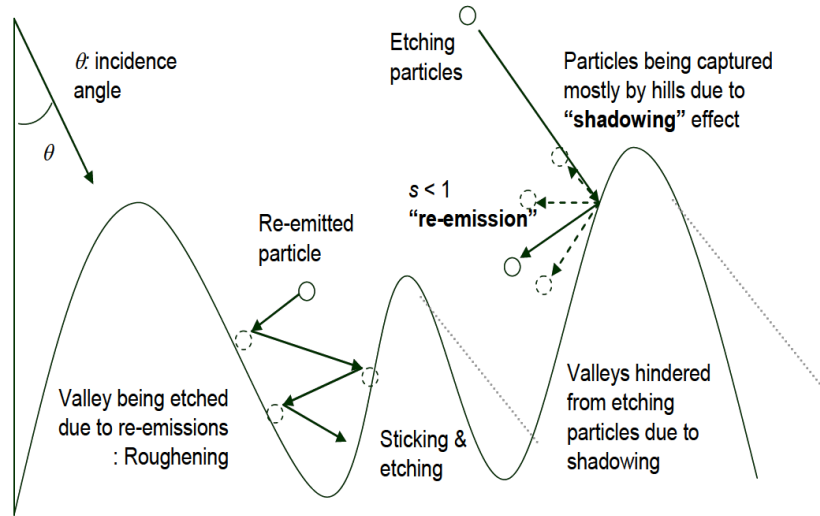


Figure 1.12. Shadowing and re-emission effects during plasma surface interaction. Etching particles with a non-unity sticking coefficient ($s < 1$), which outline the probability of etching a surface atom, desorb/rebound-off from the first collision point, re-emitted, and ultimately etch another surface point after numerous re-emission steps. Taken from [31].

(8) **Micromasking by etch inhibitors [50, 51].** Inhibitors can be classified as “hard” inhibitors, which can be dislodged from the surface only by ion sputtering and “soft” inhibitors, which can be dislodged from the surface by both ions and reactive neutrals. Potential sources for “hard” inhibitors are the material of the walls of the reactor, the material of the electrode, while potential sources of “soft” inhibitors are larger molecules or radicals emerging from the bulk plasma. Inhibitors can be deposited onto the surface being etched. There they act as an etch mask, and provoke lateral non- uniform etching. Termed micromasking, this mechanism consists a roughness enhancement mechanism as Figure 1.13 depicts.

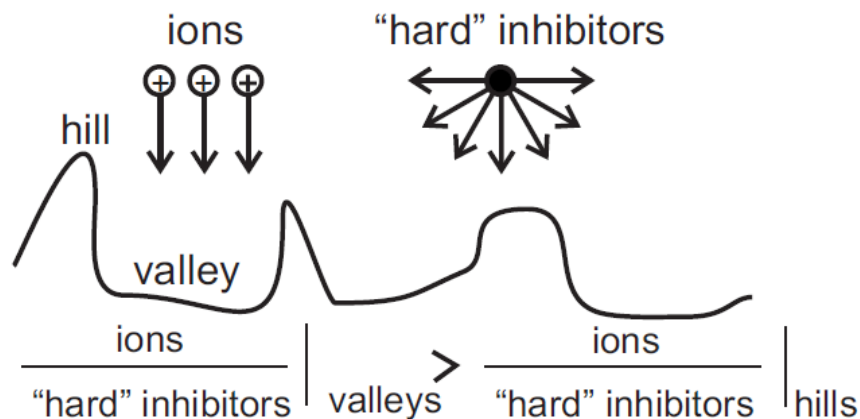


Figure 1.13: Example of roughness enhancement during plasma etching due to “hard” inhibitors: The ratio of ions to inhibitors is larger in the valleys than in the hills, owing to more severe

shadowing of inhibitors compared to the ions. Inhibitors have isotropic angular distribution while ions impinge nearly vertically the etched surface. Taken from [50, 51]

Being a core subject of the present dissertation, much of the remaining section is devoted to plasma induced roughness (Section 1.4.1) and its amplification/attenuation mechanisms. Surface functionalization and etching, generally occurring together, are discussed using O_2 plasma (Section 1.4.2). The reason for this selection is not only that O_2 plasma provokes strong effects in both mechanisms, but that it also has much technological interest in industrial processing.

1.4.1 Plasma induced surface roughness of polymeric substrates

Plasma etching results in surface roughening. The low-level surface roughening (stochastic roughening) at the initial stage of plasma exposure is widely believed to be caused by the noise or the non-uniformity of incident fluxes of ions and/or neutral species on surfaces at micro/nanoscale, where its degree depends on plasma conditions (such as the ion energy and the magnitude of ion and neutral flux). However, to sufficiently interpret the following evolution of roughness, one has to invoke a few interactions such as geometrical shadowing, neutral species and ion reemission, and micromasking by etch-inhibitors, as partly illustrated in Figure 1.14.

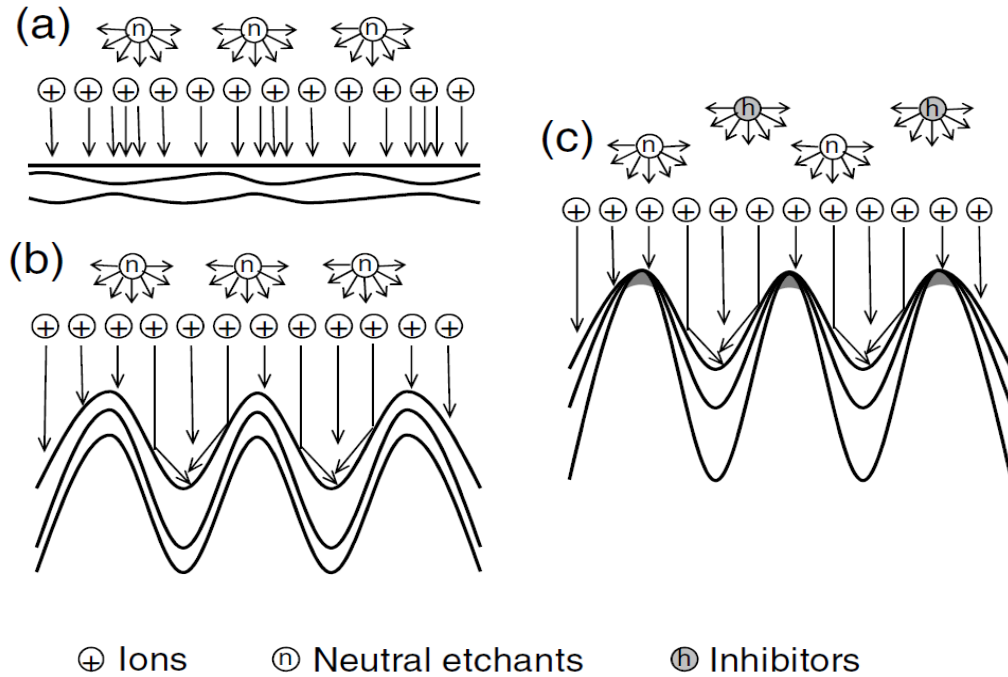


Figure 1.14. Schematic of the mechanisms responsible for surface roughening during plasma etching. a) **Stochastic roughening:** low-level roughening owing to temporal and spatial non-uniformity of the impinging flux and angle of ions and/or neutral etchants on surfaces at microscale. b) **Ion reflection-induced roughening:** the ion reflection from microscopically roughened feature surfaces on incidence generates the evolution of surface roughness, which tends to be restricted by geometrical shadowing effects of the feature for neutral etchants. (c)

Inhibitor-enhanced roughening: the impinging flux of etch inhibitors augments the roughness evolution, where they tend to form surface passivation layers (or micromasks) preferentially on top of the feature and inhibit etching thereon, owing to the shadowing effects for neutral inhibitors. Taken from [52].

The formation of surface roughness during plasma etching of polymeric substrates has been shown for different materials, plasma reactors, conditions, and gases [15, 53]. Surface roughness is a common side effect of the plasma etching process and can be crucial for several applications and related fields. In some of them, roughness is an artifact to be wiped out; for instance, surface roughness of polymeric substrates was and is still an artifact in the semiconductor industry [e.g. line edge roughness (LER) of a polymeric etching mask may affect the operation of the final device] [54-56]. In polymeric waveguide components, roughness may cause serious waveguide scattering loss and acutely hampers scaling down of waveguide dimensions [57]. In other, it is a beneficial property of the surface. For example, roughness affects the wetting properties of surfaces; a series of studies demonstrating the effect of plasma induced roughness on the wetting properties of polymeric surfaces can be found in the literature [22, 58-65]. In polymeric microfluidics fabrication, roughness may also influence the pressure drop [66] and the electrokinetic efficiency [67] in microfluidic channels. By the same token, the importance of roughness to stem cell differentiation [34-36] and, more generally, to cell-surface interactions [68-71], has also introduced plasma into the field of biomaterials and biomicrosystems.

Given its importance in the semiconductor industry and in other fields, there is a strong motivation to understand and manipulate plasma induced surface roughness of polymeric substrates. As a consequence, a series of previous works [15, 16, 25, 53, 72-78] focused either on the mechanisms of roughness formation or on recipes decreasing or increasing roughness.

1.4.1.2 Modeling of plasma induced surface roughness

Many studies to date have pinpointed several potential phenomena for roughness formation and evolution, such as scattering/reflection of ions within the *topographic* features of the rough profile [79, 80], change of etching yield with the angle of incidence [81], deposition of material engendered in the plasma as well as re-deposition of material ejected by ion-induced etching [50, 51], and deflection/attenuation of ions by charging of the surface [82-84], to name a few.

There is also significant overlapping among these phenomena; usually, a roughness experimental measurement can be interpreted by invoking more than one physical mechanism. These mechanisms take place concurrently during plasma etching, and the expectation for segregating their effects via experiment is low. Modifying the process conditions to diminish the effect of one phenomenon will commonly intensify another. However, for efficient process design and optimization, it is essential to understand the phenomena influencing the etched rough profile.

The only approach which enables to examine the effect of a mechanism during etching either independently or jointly with other mechanisms is **numerical simulation**. The latter is of major

interest for giving indications about the physics governing various processes and to ultimately pinpoint the etching control mechanisms as far as the roughness evolution is concerned. It can consequently provide aid for specifying the ideal operating conditions for the desired roughness, thus, enabling the optimization of a given etching process.

Modeling the temporal evolution of a surface over a short time interval comprises mainly of the following three steps: (1) calculating the fluxes of ions, electrons, neutrals and/or other important species (i.e. inhibitors) to each point of the surface, (2) specifying a local etching rate for each point from the given fluxes, and (3) utilizing the local etching rates to predict the surface profile after a short time. The ultimate surface profile for any etching mechanism may be predicted in this fashion. Different models and methods exist for each of these steps, but this section will focus on the various methods concerning the last step, i.e. the surface advancement step.

Profile evolution simulators have been used to predict the evolution and explore origins of the surface roughness during plasma etching: Cell-based methods [52, 85-93], molecular dynamics simulations [19, 94, 95] and the level set method [82, 83, 96-100] have been encompassed for the evolution of surface roughness.

The cell-based method is a stochastic algorithm based on a Monte Carlo model and the description of the surface morphology is discrete. The surface morphology consists of cubic cells each of which may contain more than one atom or molecule (coarse graining). Cells can be removed or added relying on etching or deposition probabilities as outlined by the etching yields and the sticking probabilities. Ono et al. used a cell-based method to study the formation mechanisms of surface roughness during plasma etching of Si in Cl_2/O_2 [52, 85, 89] and Cl_2 [86-88] plasmas. Surface roughening and rippling dynamics were detected to rely on the incident angles [87], energy [89] and reflection probability of ions [52, 88, 90], the incoming fluxes of neutral reactants [89], and O and etch byproducts [89]. The cell-based method was also used to investigate roughness evolution during etching of composite films. In particular, Zakka et al. [91] executed a systematic investigation of the roughness effects on a nonhomogeneous film consisting of two components (phases) randomly distributed in the material. The cell-based method was also utilized to study the roughness formation and evolution during simultaneous-to-etching deposition. Guo and Sawin [101] investigated the surface roughness of SiO_2 substrates etched with $\text{C}_4\text{F}_8/\text{Ar}$ plasmas with a 3-dimensional (3d) Monte Carlo profile evolution simulator; they focused on the effect of neutral-to-ion flux ratio. To interpret the roughness origins and explain the experimental findings concerning dual nanoscale roughness during Si etching by SF_6 plasma, Kokkoris et al. [92] proposed mechanisms for roughness evolution through an (1+1)d Monte Carlo simulation framework; the key elements in the nanoroughness evolution was the difference in the angular distributions and sticking probabilities of etch-inhibitors (depositing neutral species) and ions. The latter framework was extended to (2+1)d and was utilized to show that during ion-driven etching (ion-enhanced etching and physical sputtering), simultaneous deposition of etch-inhibitors could lead to the formation of periodic dots on the etched surfaces [93].

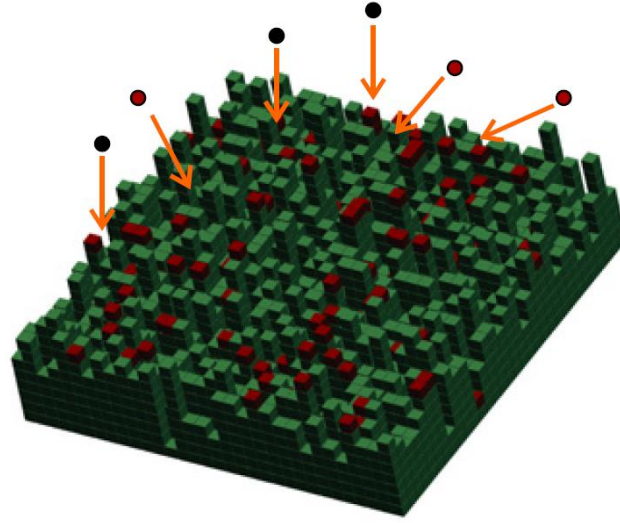


Figure 1.15. In a typical cell based method the etched film is depicted by a lattice of cubic cells; particles with user-defined energy and angular distributions bombard the cellular morphology. Taken from [50]

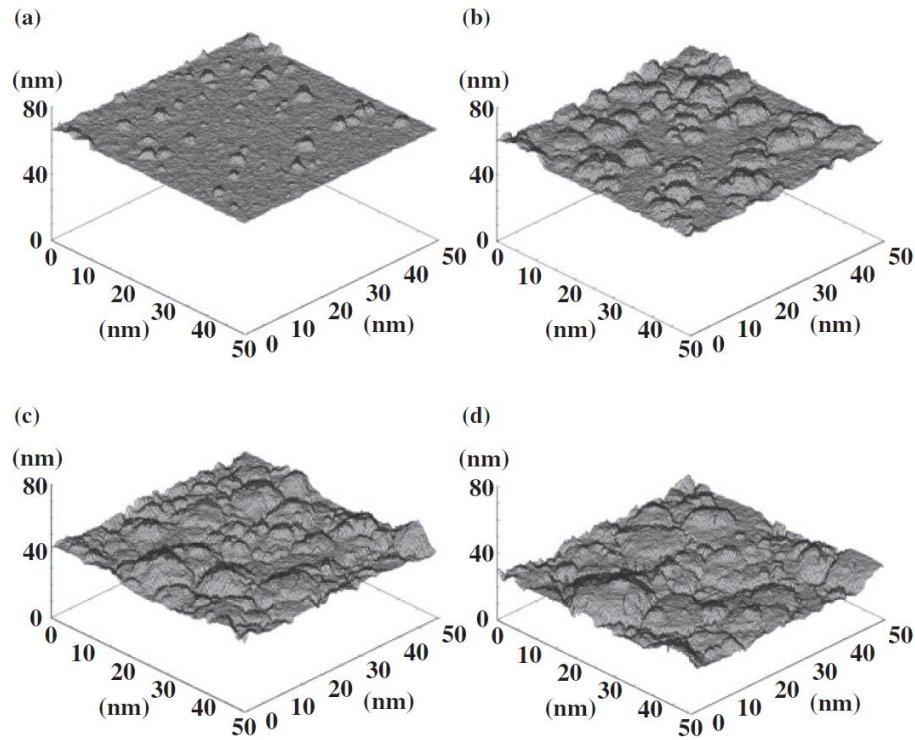


Figure 1.16: Evolution of 3d plots of the position of the outer Si atoms or substrate cells on etched surfaces at t equal to (a) 3, (b) 5, (c) 10, and (d) 15 s after the beginning of Si etching in Cl_2 plasmas utilizing the cell based method. Taken from [102].

Besides cell-based methods, **molecular dynamics (MD) simulations** were also used to investigate the formation of surface roughness. Concentrating on Si etching with monoenergetic Cl^+ and Br^+ beams, Ikawava et al. [94] illustrated that residual halogens inside the Si lattice was a pivotal ingredient for intensifying the surface roughness. Focusing on Si etching in Cl_2/O_2 plasmas, Tsuda et al. [95] pinpointed that roughness was provoked by local surface oxidation on convex roughened surfaces during etching. Although polymers with similar chemical composition could experience related sputtering characteristics at steady state, Vegh and Graves [19] showed that during the transient period prior to reaching steady-state, structural changes (cross-linking, chain-scission) could lead to different sputtering behavior, including smaller or larger fluctuations in mass removal from location to location on the polymer surface, something that was correlated with the formation and evolution of different degree of roughness among various polymers during plasma processing.

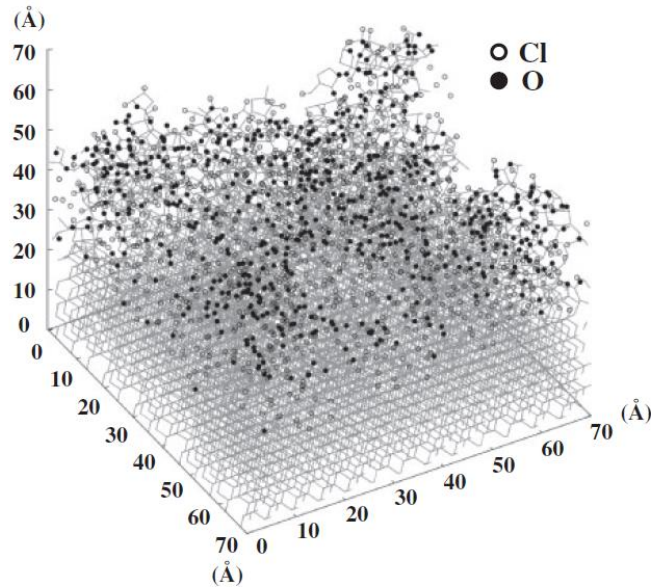


Figure 1.17. Diagram of the classical MD simulation of etching. Substrate or target Si atoms are deposited in the simulation cell. The case study is Si etching in Cl_2/O_2 plasmas. Taken from [103].

The level set method [104, 105] is a deterministic approach for the evolution of the surface morphology; the description of the surface morphology is continuum. It relies on the concept of the implicit function; the evolving profile or surface is determined as the zero contour of the level set function. By using the level set method, Radjenović et al. [96-99] studied the evolution of surface roughness (roughening or smoothing) during isotropic, anisotropic etching and physical sputtering of homogeneous and nonhomogeneous films.

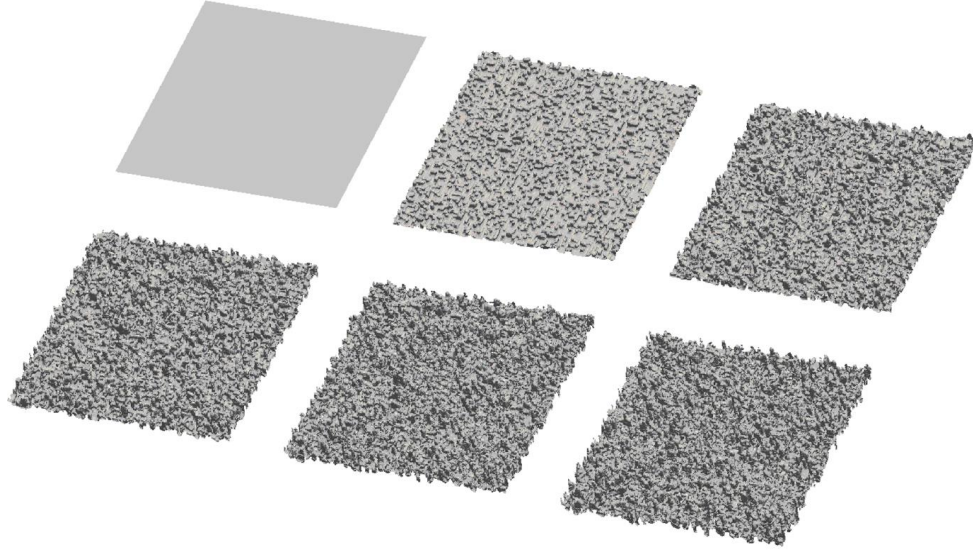


Figure 1.18: Illustrations of roughening with anisotropic etching of a substrate consisted of nanocomposite materials. The level set method is utilized for profile evolution. Taken from [106].

A more extensive review in recent developments in theoretical/numerical and experimental studies of the formation and evolution of surface roughness can be found elsewhere [52].

1.4.1.3 Statistical parameters to characterize surface roughness

The surface morphology characterization is crucial for the evaluation of a roughness mechanism. The statistical parameters utilized to characterize the surface morphologies, i.e. the outputs of the simulations or the experimental measurements, refer to the surface roughness, the existence of bumps on the surface, and the development of periodicity. Especially, the following statistical parameters are commonly encountered in the majority of literature on plasma induced roughness [107, 108]: The root mean square (rms) roughness or surface width, which evaluates the vertical fluctuations of the surface morphology. The correlation length, which describes the horizontal extent of the surface roughness; it is a measure of the mean width of the surface features (e.g. bumps). The roughness exponent, which gives the relative contribution of high-frequency roughness on the total roughness. Additionally, skewness and periodicity (order) have been also proposed [93]. The former quantifies the asymmetry of the surface morphology, is utilized to pinpoint the kind of pattern on the surface: Positive skewness means that bumps dominate on the surface morphology, while if skewness is negative, holes prevail. The latter is revealed by a peak in the power spectral density (PSD). This does not mean that the surface morphology features a flawless periodicity and only one wavelength. A prevailing or distinguishing wavelength usually exists. Further information on the statistical parameters of surface morphology as well as formulas for their calculations can be found in reference [109]. In this dissertation, the rms roughness of the evolving morphologies is mainly demonstrated.

1.4.2 O₂ plasma chemistry and polymers

1.4.2.1 Surface functionalization and etching

O₂ and O₂-containing plasmas are most commonly employed to improve polymer surface properties. An O₂ plasma can react with a wide range of polymers to produce a variety of O₂-containing functional groups³⁰ on the surface [10]. The formation of polar groups on the polymer surfaces, leads to growth of the polymer surface energy and significant increase of the polymers wettability³¹ and adhesion to metals and different organic compounds [14]. The maximum density of functional groups at the outermost polymer surface is completed after a few seconds, most often after only few seconds [12]. If plasma exposure to polymers is continued the process passes over to an etch process [11, 12].

Indeed, further interaction of the polymer with non-thermal O₂-containing plasma can result in further oxidation, formation of etching products³², and their transition to the gas phase [14]. A steady - state process between continuation of introduction of functional groups and polymer etching is then established [12]. The balance of these two processes depends on the operation parameters of the given experiment [10]. During the balance, the two processes occur simultaneously [10] etching of the polymer surface through the reactions of O with the surface carbon atoms, giving volatile products, and the formation of O-functional groups at the polymer surface through the reactions between the active species from the plasma and the surface atoms. The distinction between polymer etching (material removal) and modification is somewhat artificial and is usually a matter of degree of material removal **or** by virtue of the particular application [110] (e.g. cleaning,³³ pattern definition³⁴ in microelectronics, modification/functionalization). However, the mechanisms involved can be treated simultaneously [110].

³⁰ Peroxides, alcohols, ethers, and epoxies, aldehydes, ketones and carboxyl-acidic groups. [14] Fridman, Plasma Chemistry.

³¹ The wettability increase effect is correlated to plasma-stimulated creation of polar peroxide groups on the polymer surface. Specifically, the polar component of surface energy, which defines polar interactions between polymer surface and the liquid, expands during exposure in O₂ plasma. [14] *ibid*.

³² e.g. Carbon dioxide (CO₂) and water (H₂O)

³³ Plasma exposure is able to drive contaminants off the surfaces of thin solid films. [13] Roth, Industrial Plasma Engineering.

³⁴ The most regularly manipulated leverage of plasma processes is the capability to delimit high aspect ratio patterns in thin solid films. [111] Plasma deposition, treatment, and etching of polymers, Academic Press, Inc, San Diego, 1990.

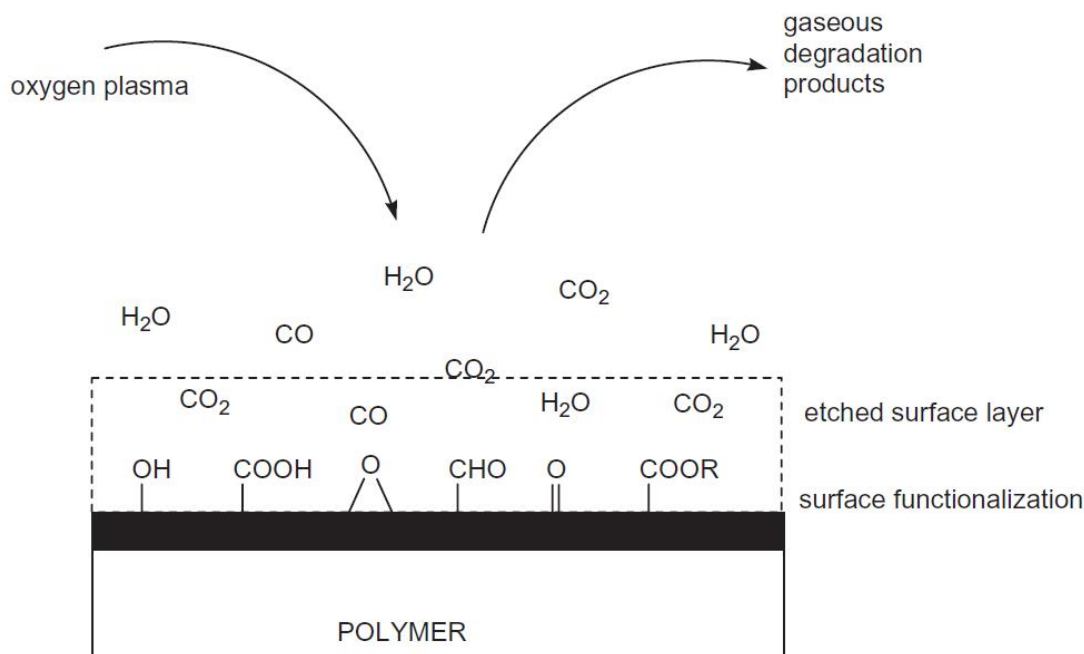


Figure 1.19: Interaction of the polymer with non-thermal O_2 -containing plasma. A steady - state process between continuation of introduction of functional groups and polymer etching is then established. Taken from [12].

With the increasing number of technical applications of plasma technologies for structuring, modification and deposition of polymer films, much effort has gone into trying to understand and optimize the basic physical and chemical processes. In particular, investigation of dry etching of polymers for multi-layer lithography, and of resist stripping, has significantly increased the understanding of plasma degradation of polymers. O radicals produced by electron impact in the plasma have turned out to be the essential chemical species necessary for decomposition of hydrocarbon polymers, and O_2 is, for that reason, the most often used process gas.³⁵ But what characteristics of O make it particularly suitable for etching of polymers? It is believed that two properties of O, its number of valence electrons and its high electronegativity, make it particularly suitable for the oxidative degradation of polymers [111].

At the polymer surface the reactions occur after previous adsorption of the reactive species from the gas phase [112]. This means that surface functionalization is the preliminary step followed by material ablation to form gaseous degradation products [12].

³⁵ Thus, to augment the etching of polymers in pure O_2 plasmas, plasma parameters should be altered to enhance the dissociation of O_2 to O, to lessen recombinative losses of O and to boost the flux of O from the plasma to the sample. By all means, concurrent impingement of energetic ions to the polymer surface is admitted to increase the etching of polymers in O_2 plasmas [111] *ibid.*

1.4.2.2 Models of etching of polymers in O₂ plasmas

The first experimental studies on plasma etching of polymers have allowed to identify the critical factors for the etching of polymers in O₂ plasmas and their respective influence on the etching kinetics [113-115]. These factors were the concentration of O in the gaseous phase, the current density and energy of ions bombarding the polymer surface, and the surface temperature. These experimental results have led the way to the first self-consistent models of etching of polymers in O₂ plasmas, which are based on a) a monolayer-type O adsorption on polymers [113, 116, 117], b) a negligible adsorption of O₂ compared to O [113, 114] and c) the balance of O fluxes (adsorption of O and desorption of reaction products) at the polymer surface [113-115]. Recently, the hypotheses and the mechanisms of the etching of polymers in O₂ plasmas were reinvestigated in order to take into account the specificity of the nature of polymers and their fundamental structure at the molecular level by Bes et al. [118]. Bes et al. updated the model of Pons et al. [114], which described correctly the kinetics of ion enhanced etching but only partially the kinetics of spontaneous etching, by including the terms arising from the thermal spontaneous desorption of CO above 100 °C (in addition to CO₂ desorption) and the involvement of UV photons in photo induced desorption of reaction products.

Ultimately, the latest modeling approach for the etching of polymers in O₂ plasmas of Bes et al. [118] includes two steps:

- a) An initial quick step of direct oxidation³⁶ and/or ion-induced desorption³⁷ of volatile elements (i.e. O and H atoms) grafted along the polymer chains segments and the subsequent transformation of the latter to bare carbon chain segments.
- b) Etching of the carbon chain segments which constitute the skeleton of the polymer chains. This step, which is considered as the rate determining step of the etching of polymer, governs the etching kinetics.

According to the abovementioned approach, under plasma etching conditions, any metal free polymer (i.e. a polymer constituting mainly by C, O and H) surface can be modeled as linear carbon chain segments consisting of single bonds between consecutive carbon atoms; then, the available adsorption sites of the carbon atoms may be incompletely or fully filled by the reactive atoms emerging from the plasma.

³⁶ The reactions are thermally activated by the sample temperature (thermal desorption).

³⁷ The energy transfer by ion bombardment is the energetically dominant activation mechanism (ion assisted desorption).

1.5 The plasma induced surface charging phenomenon

1.5.1 Surface charging of conventional microstructures in microelectronics

Surface charging has been extensively studied for conventional silicon on insulator (SOI) structures such as poly-Silicon (poly-Si) line and space patterns as well as exclusively dielectric structures such as trenches and holes met in micro- or nanoelectronics. Its root cause is the directionality difference between ion and electron fluxes impinging on the structure surface during plasma etching. Specifically, ions are accelerated through the plasma sheath, and so a robustly anisotropic ion angular distribution is developed on the processing wafer, while, on the other hand, electrons are decelerated in the sheath and so their angular distribution is considerably more isotropic. The origin of this difference was elaborated by Hwang and Giapis [119]. The interested reader can find more details on this subject in the Appendix A.

During plasma etching of a conventional dielectric structure, e.g. a trench, and in view of the aforementioned directionality difference, the flux of the isotropic electrons is restricted to the upper regions of the trench sidewalls (see Figure 1.20); indeed, by virtue of electron shadowing only a small fraction of electrons reaches the trench bottom. Simultaneously, the highly anisotropic (positive) ions accumulate at the trench bottom. Positive charge will continue to build up until the bottom dielectric surface obtains a potential large enough to repel a sufficient number of ions. This is because the ion and electron fluxes to the trench bottom must balance at the steady state. Owing to the electrostatic repulsion, ultimately, a vast amount of ions impinge at the trench sidewall surface or even return to the plasma bulk. Consequently, the ion deflection caused by surface charging, lead to profile irregularities such as notching [120], microtrenching [121], etching lag [122], and twisting [123, 124].

The notching effect describes the formation of long narrow wedge in a conductive material at the interface with an underlying insulator (Figure 1.21). It commonly appears at the inner sidewall foot of the outermost feature in a line and space pattern adjacent to an open area. Microtrenching concerns the appearance of narrow grooves at the edges of the feature bottom during ion bombardment (Figure 1.22). Etching lag describes the situation where the wider features are etched at a higher rate compared to the narrower ones. Twisting refers to the feature profile twisting, i.e. to a divergence from feature vertical etching (Figure 1.23). The voltage developed by the charge build-up may provoke breakage of thin gate oxide films as well as aspect ratio dependent etching (ARDE); the latter leads to nonuniform etching among features of different aspect ratio which is still a great challenge for the semiconductor industry [125, 126].

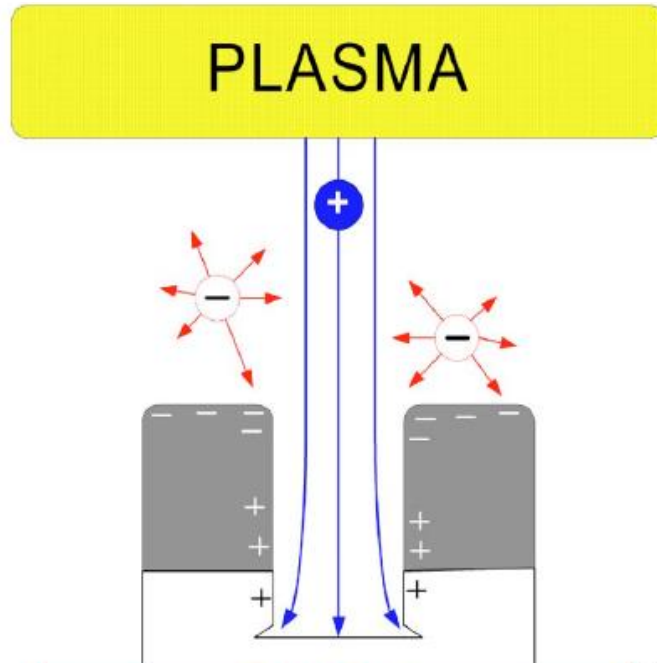


Figure 1.20: Microstructure charging process. High aspect ratio microstructures receive reduced electron flux at the lower trench sidewalls and bottom due to shadowing effects. For the case of insulating materials in either of these regions, surface charging is developed [127].

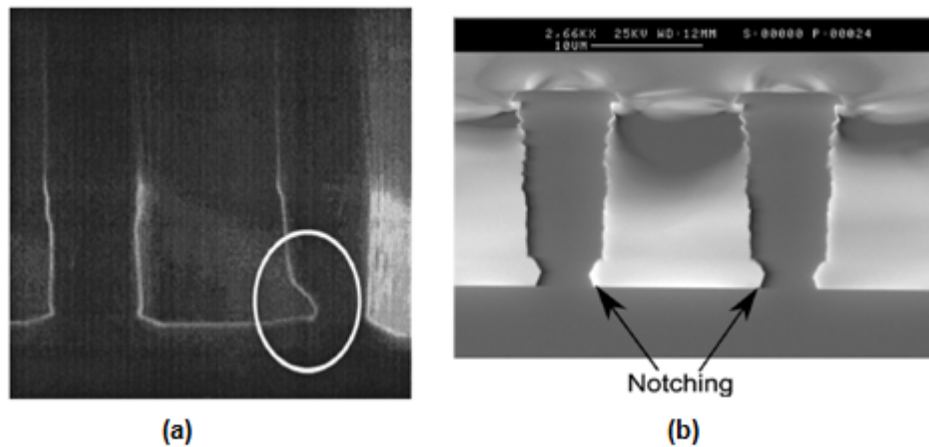


Figure 1.21: (a) Example of the notch which is the opening of a narrow groove in a conductive material at the interface with an underlying insulator. Taken from reference [128]. (b) Experimental results from Oxford Instruments Plasma technology, reproduced from the paper of Ishchuk et al. [129].

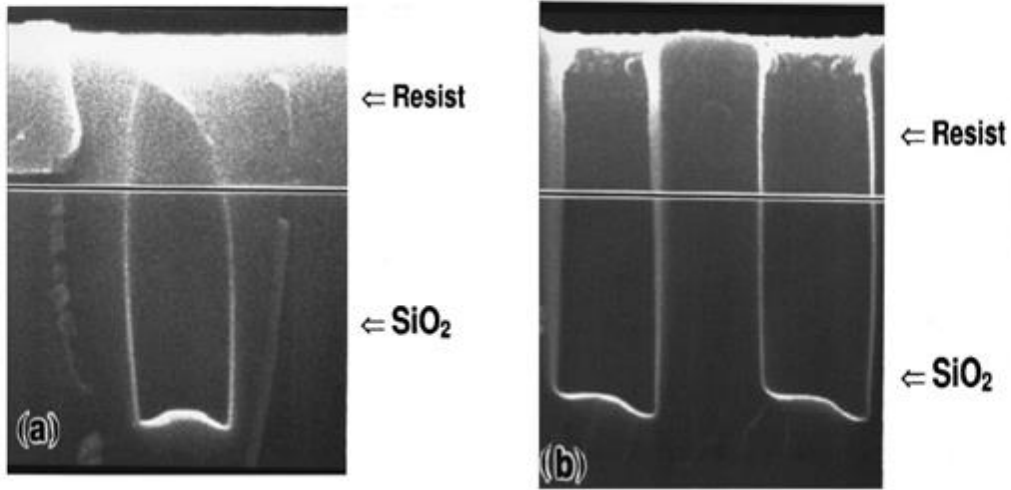


Figure 1.22: (a) Microtrenching profile due to the differential charging mechanism in the absence of a magnetic field. The local electric fields in the feature deflect ions from the centre towards the negatively charged sidewalls, resulting in symmetric microtrenching. (b) Schematic view of differential charging in the presence of a magnetic field. The Lorentz force F_L deflects electrons, resulting in an asymmetric electron angular distribution, resulting in asymmetric microtrenching. See reference [121] for more details.

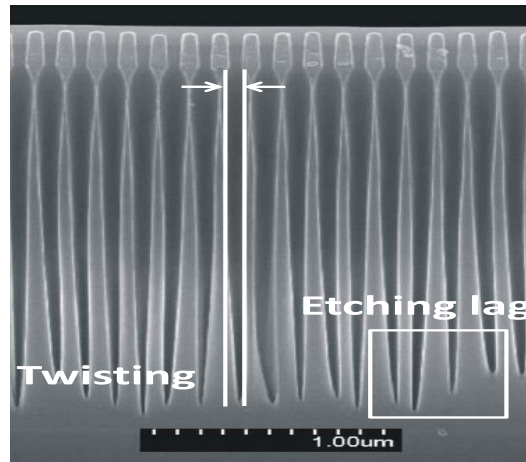


Figure 1.23: Scanning electron micrograph (SEM) of an HAR array of SiO₂ features etched in a commercially available capacitively coupled plasma chamber using a fluorocarbon gas mixture. There is errant twisting and varied etching rate among trenches. Taken from [130].

1.5.2 Computational studies on surface charging of conventional microstructures in microelectronics

The need to remedy these artifacts has been the motive for several theoretical and computational studies on surface charging. The majority of them focus on dielectric, mainly Silicon dioxide

(SiO₂) trenches or holes [130-141], some of them on Si trenches with a dielectric mask [142-144] and/or on SOI wafers [120, 145, 146].

In particular, Kinoshita et al. [145] numerically simulated the influence of a rising bottom potential on the trajectory of incident ions on a poly-Si line and space pattern adjacent to an open area. Hwang and Giapis [120] improved the simulation of Kinoshita et al. [145] by allowing the charge distribution in the poly-Si line to be affected by the positive potential on the oxide and by the negative charges on the resist. They also expanded their simulation to uncover the influence of different phenomena on pattern dependent etching and related profiles distortion effects [119, 142, 147-156].

Besides the study of charging of SOI, there are also modeling works on charging of structures consisting exclusively of dielectric materials. Arnold and Sawin [131] were the first to simulate the charging of an individual dielectric trench assuming monodirectional ion bombardment and an isotropic electron flux in a two-dimensional (2d) geometry. Hwang and Giapis [157], motivated by experimental results for SiO₂ etching, calculated charging potentials for dielectric surfaces. Matsui et al. [133] proposed a model with a small surface conductivity due to the thin fluorocarbon surface layer developed during etching of SiO₂ trenches by fluorocarbon chemistries. Park et al. [134] studied the impact of pressure on the microstructure charging during the etching of SiO₂ trenches. Ohtake et al. [124] implemented a charging model in which actual data from on-wafer monitoring sensors was involved in the computation; the focus was on the investigation of twisting during plasma etching of high aspect ratio (AR) SiO₂ holes. Kenney and Hwang [137] investigated the stochastic behavior of charging by studying the oscillation of charging potential in high AR dielectric nanostructures. Lee et al. [136] surmised that large electrostatic potential fluctuations due to stochastic charging could lead to profile irregularities as the trench size was reduced to nanometer scale. Zhang et al. [158-161] presented a computational research regarding plasma induced surface charging on the top surface of mask holes. Through the years they examined cases in which the mask pattern either was set as a perfect [161] or an arbitrarily shaped hole [159, 160] or cases with mask holes having rough edges [158]. The key idea was that if the shape of the mask hole was initially asymmetric or rough due to nonperfect mask fabrication, or/and nonuniform plasma sources), the distribution of the negative electric field on the hole edge (emerged from the isotropic electron flux restricted in the upper hole region) distorted correspondingly. This nonuniform electric field distribution could affect the trajectories of ions falling on the mask surface, further enhancing the asymmetry or roughness of the mask hole shape. Under the influence of a more asymmetric or rough mask, the etched hole shape would become more asymmetric or more rough. Additionally, the alignment of the holes in the mask array influenced the aforementioned field.

Among them, **only few works address the coupling of surface charging with profile (interface between the substrate and the plasma) evolution.** In particular, Hwang and Giapis [120] examined the relation among charging and notch evolution in a line and space Si pattern adjacent to an open area on a SOI wafer during the overetching step; they used a discrete description, i.e. a cellular topography, for the substrate and a Monte Carlo (MC) model for profile evolution. The same approach was used to investigate the effect of charging of a dielectric mask on the profile evolution of Si trenches [142]. Shimada et al. [139] presented a simulation study on the evolution of SiO₂ trenches in a fluorocarbon plasma under different operating conditions and at different positions on the wafer; they used a continuum description of the

profile and the level set method for the profile evolution. Wang and Kushner [130] investigated the role of charging on the twisting of high AR SiO₂ holes etched by fluorocarbon chemistries; they simulated the etching of high AR SiO₂ holes under a fluorocarbon (Tetrafluoromethane/Argon, CF₄/Ar) plasma using a discrete description of the substrate and a MC model for profile evolution. The same type of module for profile evolution was used by Zhao et al. [138] to simulate the evolution of SiO₂ trenches under different plasma conditions. Radmilović-Radjenović et al. [140] used a continuum description of the profile and the level set method for the profile evolution to study the effect of charging on the evolution of SiO₂ trenches under a fluorocarbon (CF₄/Ar) plasma. Ishchuk et al. [146] also used a continuum description of the interface and the string technique for the profile evolution; the objective was to investigate notching during plasma etching of a Si trench on a SOI wafer. The string technique was also utilized by Zhang et al. [158, 159] to investigate the evolution of the horizontal cross sectional profiles of mask holes with asymmetric [159] or rough [158] edges under the influence of the charging effect. Finally, Dai et al. [144] studied the effect of bias on the evolution of Si trenches under a Chlorine plasma by using a discrete description of the substrate and a MC model for the profile evolution. The charging module in all previous works included a model for the calculation of the ion and electron trajectories based on the equations of Newton. Except from [136, 159-161] where the charging potential was calculated by analytic gathering of the Coulomb interaction fields from discrete surface charges on the microstructure surface, a model for the calculation of the charging potential based on the Laplace equation was used in all previous works. Additionally, all but one [140] of the previous works addressed 2-dimensional (2d) geometries.

1.6 The aims of this dissertation

Toward the comprehension and, finally, the control of plasma induced surface roughness, in this dissertation, plasma-surface interactions on rough polymeric substrates are studied from a computational point of view.

The **first model system** being used for the investigations includes Argon (Ar) plasma etching of PMMA substrates with an initially sinusoidal profile resembling a rough profile; sinusoidal profiles have been used in previous works [74, 76] to model rough profiles. The main focus, filling the relevant gap in the literature, is to record how charging is developed on the rough profile being etched and how it affects the evolving roughness of the profile, in the presence of ion reflection and secondary electron-electron emission (SEEE).

This is the first time in the literature that this interplay is examined. Even if plasma induced surface charging on conventional – with respect to the semiconductor industry – structures, i.e., trenches or holes, has been studied in previous works and its artifacts, such as notching, microtrenching, etching lag, and twisting have been examined both experimentally, theoretically, and computationally, there is a lack of studies on surface charging of rough polymeric surfaces.

Is charging really present on rough surfaces of polymeric substrates being etched by plasma? The answer is yes: The substrate is dielectric to allow charge accumulation and the surface of the substrate is not perfectly flat. Due to the roughness there is a surface morphology which in combination with the directionality difference of positive ions and electrons impinging on the etched surface [119], enables the local imbalance of positive and negative charges. There

are measurements in previous studies verifying the existence of a surface charge density on the plasma etched polymeric substrates [47, 162].

The **second model system** is plasma etching of PMMA with O₂ chemistry. O₂ and O₂-containing plasmas offer a great potential for the surface functionalization of polymeric substrates: thermal reactive neutral species are combined with high energy ions to alter both micro/nanomorphology and composition of polymeric surfaces in a dry means of processing. Towards comprehensive process design, by addressing both effects of plasmas on polymeric surfaces (alteration of surface morphology and composition), the dissertation investigates of the effect of operating conditions and model parameters on O₂-plasma-induced surface roughening of PMMA. The potential to study surface wettability is demonstrated; the surface morphology and the O-functional groups (linked to the surface coverage by O) determine the wetting behavior of a surface.

The main research questions that this dissertation is called upon to answer, covering pertinent lacks in the literature, are summarized below:

- How charging is developed on a sinusoidal (resembling a rough) profile being etched? Is there a specific factor or factors that control(s) charging in such a profile?
- What is the effect of charging potential on the local ion flux, energy and the angle of ion incidence and thus on the local etching rate?
- Given that charging and etching occur simultaneously, what is the time scale of charging (the charging time)? In particular, based on the time scales, can the two phenomena, i.e. charging and etching, be studied decoupled?
- What is the effect of the thickness of the polymeric (dielectric) substrate on the charging time? Previous works for conventional structures in semiconductor industry addressed the effect of the aspect ratio [163, 164] and the surface conductivity of dielectric trenches [133] on the charging time.
- What is the interplay between surface charging and roughness during plasma etching of polymeric substrates? This is the first time in the literature that this interplay will be examined. It has to be noticed that there are few simulation works which take into account surface charging during profile evolution.³⁸ However, all of them refer to trenches and not on rough profiles.
- Is the charging effect on roughness evolution the same when a different etching mechanism is considered? To answer this question, two different mechanisms will be studied; in the first one, the etching yield will depend solely on the ion energy (similar to ion enhanced etching) while in the second one, besides the ion energy, it will depend on the angle of ion incidence (sputtering).
- What is the behavior of the evolving roughness of the profile if we add ion reflection and SEEE in the presence of surface charging? Ion reflection is expected to enhance

³⁸ Details in Section 1.5.2

roughness [165] by increasing the flux of ions at the valleys of the surface morphology. SEEE and the consequent electron redistribution on the dielectric surface could affect surface charging, as demonstrated in previous simulation studies on plasma etching of dielectric trenches [166, 167]. The secondary ion-electron emission (SIEE) is not considered in the current dissertation as it was found that, in the presence of SEEE, SIEE had an insignificant impact on the formation of the charging potential [167].

- Can we quantify the correlation between the surface roughness and the charging potential? The rough profiles emerging in plasma based surface engineering applications are random and not sinusoidal, thus, we will try to investigate, the scaling of the charging potential to a combination of suitable statistical properties of the surface roughness.
- What is the effect of operating conditions and model parameters on **O₂-plasma-induced** surface roughening of a polymeric substrate?
- In the case of plasma etching of a polymeric substrate with **O₂ chemistry**, can we determine the surface composition of the etched surface? This is crucial as both surface morphology and composition determine the wetting behavior of a surface.

The abovementioned research questions will be answered based on the following developed computational tools. The tools cooperate with each other through a hybrid modeling framework implemented by homemade codes.

- A **charging module** [84] consisting of models for the calculation of a) ion and electron trajectories (Newton equations), b) the surface charge density, and c) the charging potential (Laplace equation).
- A **model for ion reflection** [82] as well as an **original model for the SEEE mechanism** [82], developed for PMMA substrates in the energy range which is of interest in plasma etching.
- A **surface etching model** [84] able to calculate the angle and energy dependence of the etching (sputtering) yield of PMMA by Ar⁺ is devised combining **experimental measurements** [168] and calculations by **TRIM (transport of ions in matter) code** [169].
- A **kinetic Monte Carlo (kMC) surface etching model** [100], in order to consider the synergy of neutral species and ions for the calculation of the local etching rate in the case of O₂ plasma etching (i.e. ion enhanced etching), taking into account the surface morphology.
- A **profile evolution module** [170], which is based on a continuum description of the profile and the level set method; the latter module has been used for conventional (microelectronic) structures in previous works not only for plasma etching [170], but also for wet etching [53], and chemical vapor deposition [171]. In this dissertation, it is **modified** in order to α) handle also the evolution of unconventional (rough) profiles and

b) treat a fundamental weakness of the level set method, and generally of all methods using an implicit representation of the surface profile, namely the tracking of local profile properties during evolution [100].

2. Description of the modeling framework

2.1 Introduction

A hybrid modeling framework for profile evolution of unconventional, rough polymeric surfaces under plasma etching is developed and presented. The framework couples stochastic and deterministic modules. Although the components of the framework may differ depending on the case study, the cornerstone of the framework is that a surface etching model combines the local flux, energy, and the angle of incidence of the plasma species with the local etching yield and rate. The local etching rate calculated by the surface etching model is then fed to a profile evolution module which computes the successive positions of the profile.

The components of the framework are discussed through its application to two different case-studies (Ar and O₂ plasma). In the first case (Section 2.2), particular importance is attached to the effects of plasma induced surface charging on roughness evolution. The model system being used is Ar plasma etching of PMMA. The framework consists of models for the calculation of the ion and electron trajectories through a Monte Carlo scheme, the local surface charge density, the charging potential induced by the surface charge, and a surface etching model. An etching yield function is proposed based on the coupling of measurements from ion beam experiments with computational calculations. The framework is extended to include also SEEE and ion reflection on the PMMA surface.

The etching mechanism in the aforementioned system is physical sputtering. Thus, in order to apply the framework to ion enhanced etching (coming from the nonlinear synergy of ions with neutral species) of polymeric substrates, i.e. etching of PMMA with O₂ plasma (Section 2.3), it should be properly adopted. In this case, a kMC surface model is used for the calculation of the local etching rates which is then used for the profile evolution. To couple the different length scales of the kMC surface etching model and the deterministic profile evolution module, a coarse grained adjustment of the surface is used by adopting coarse cells that encompassed a number of sites under the local mean field approximation. The kMC model describes the surface processes during O₂ plasma etching (surface charging is not taken into account in this case study) and is used for the calculation of the local etching rate along the profile. The coupling of the two components of the framework allows the kMC surface model to take into consideration the profile shape (or the surface morphology) and extended the potential of previous kMC surface models in the literature which assume that the surface is flat.

The profile evolution module [170] is based on a continuum description of the profile and the level set method [172, 173]. The latter module has been used in previous works not only for plasma etching [170], but also for wet etching [53], and chemical vapor deposition [171]. Details for the module are included in Ref. [170]. Appropriate extensions are implemented in order for the module to treat unconventional surface profiles and to transport local surface properties from the current profile to the profile at the next time step.

2.2 Description of the Modeling Framework: application to sputtering of PMMA with Ar plasma

The modeling framework consists of a) the surface charging module, b) the surface etching model, and c) the profile evolution module [170]. The linking among modules of the framework is shown in the schematic diagram of Figure 2.1. The inputs are the energy and angular distributions of ions and electrons as well as the initial surface profile (e.g. sinusoidal profile). The simulation starts with the surface charging module (Section 2.2.1); in particular, the local ion flux as well as the distributions of ion energy and angle of ion incidence are calculated at steady state (when the charging potential reaches steady state) along the surface profile. The outputs of the surface charging module are utilized by the surface etching model (Section 2.2.2) to calculate the local etching rate. The evolution of the surface profile is realized by the feed of local etching rates to the profile evolution module (Section 2.2.3). The surface profile is updated and the procedure is repeated until the total etching time is reached. It has to be noticed that the solution of the charging module is decoupled from the solution of the profile evolution module as the charging phenomenon evolves very fast and arrives at steady state in a time much lower than the time step of the evolution of the surface profile, Δt (Chapter 4).

2.2.1 The surface charging module

The surface charging module is utilized to treat the dynamics of charged particles exposed to a local electric field. The source of the field is a perpetually changing surface charge density. Charge is dropped on the surface during plasma etching due to the ion and electron impingement on the surface. The module comprises (Figure 2.1) of a) a particle tracing model for the computation of ion and electron trajectories (**Model 1**), b) a SEEE model (**Model 2**), c) an ion reflection model (**Model 3**), d) a model for the computation of the local surface charge density (**Model 4**), and e) a model for the computation of the potential induced by the surface charge (**Model 5**). A sequential run of the five models (defined as charging step) is redone until the charging potential attains a steady state. An equal number of ions and electrons are released at the beginning of a charging step. Their trajectories are traced, then the surface charge density is calculated, and finally the electric potential and field are calculated. The electric field is taken into account in the next charging step for the calculation of particle trajectories. The steady state condition is fulfilled when the potential distribution along the surface no longer changes, i.e. the ion and electron fluxes are equal everywhere on the surface profile. A description of Model 1, Model 2 and Model 3 is included in Sections 2.2.1.1, 2.2.1.2, and 2.2.1.3. Model 4 and Model 5 are presented in Sections 2.2.1.4 and 2.2.1.5.

Before proceeding to the details of the surface charging module, the following points are clarified. First, surface currents, which have been attributed either to subsurface conduction in SiO₂ layers [155, 174] or to the conduction in a thin fluorocarbon layer formed on the dielectric surface during etching with fluorocarbon chemistries [124, 133] are not taken into account. The case study is Ar⁺ sputtering of PMMA, i.e. no fluorocarbon chemistry is employed; additionally, no subsurface conduction has been reported for PMMA. Second, the framework can be applied

to dielectric substrates, i.e. substrates with negligible conductivity. The substrates should be thick enough to avoid leakage currents. For SiO₂, the critical thickness for current leakage is 0.1 μm [119]. Third, the model surface for the calculations is a 2d sinusoidal surface. The profile of the surface is constant along the z axis (**Figure 2.2**), thus the surface charging should not vary along that direction [131, 146, 167]. The latter allows for calculations in 2d for both the particle trajectory and the electric potential. A real rough surface is a 3d surface which is not constant along z axis. For the real 3d surface, the shadowing of the electron flux may be altered, e.g. it will be reduced for a surface with pillars and increased for a surface with holes compared to a 2d surface; however, the shadowing of the isotropic electron flux, and thus surface charging, cannot be avoided. The use of a model 2d surface allows us to avoid the high computational cost of calculations for a real 3d rough surface without missing the qualitative effect of surface charging.

2.2.1.1 Particle Trajectory Model

In the Model 1, the trajectories of the particles, i.e. ions and electrons, inside the surface morphology are calculated. The simulation domain is a rectangular area (Figure 2.2). Particles are released from the top boundary or "inlet" of the simulation domain. A uniform distribution is used for the selection of the particle initial position at the inlet of the domain. User defined (coming either from measurements or from simulation) energy and angular distributions are sampled with the acceptance-rejection statistical method [175] to determine the particle initial velocity vector; the velocity coordinates of a particle that enters the domain are calculated by the following equations

$$u_x^2 + u_y^2 = \frac{2\varepsilon_p}{m_p} \quad (2.1)$$

and

$$\tan \theta = \frac{u_x}{u_y}, \quad (2.2)$$

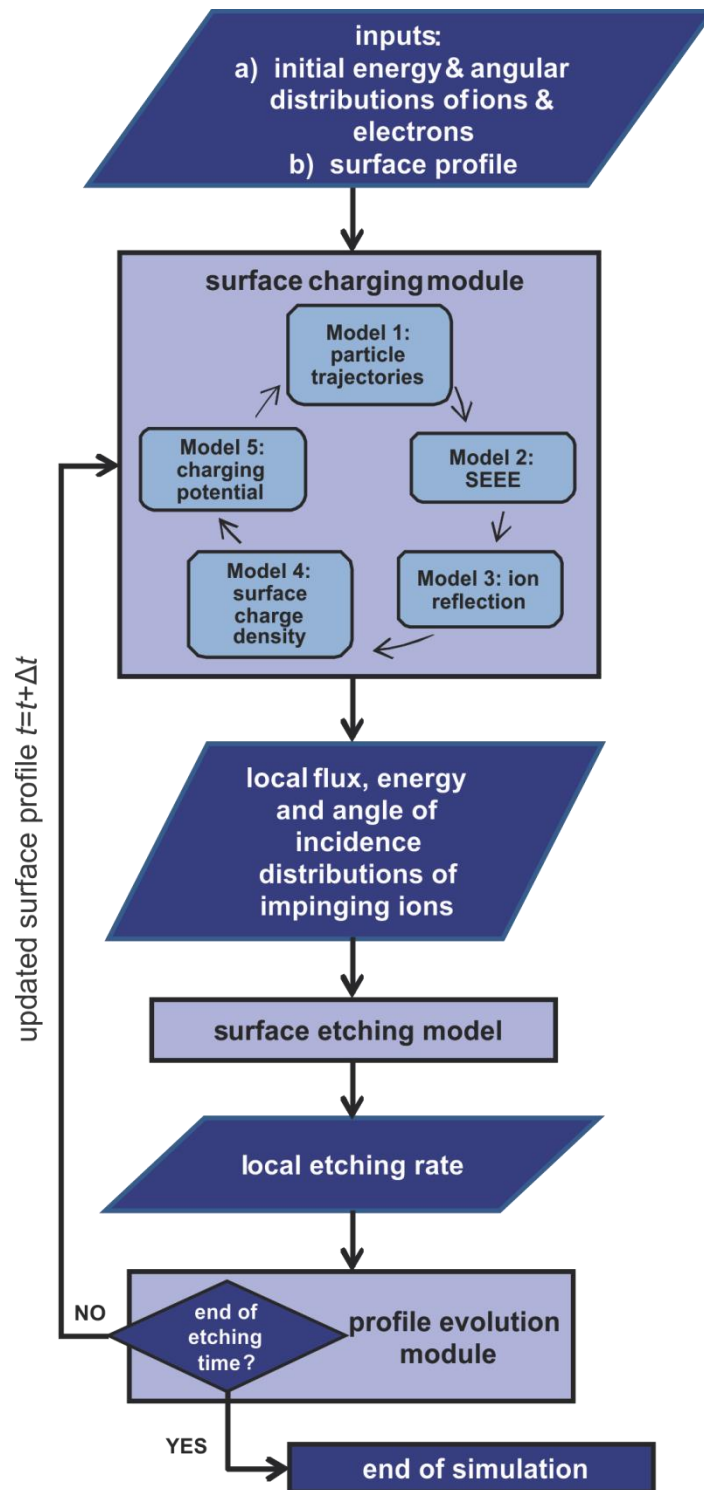


Figure 2.1. The modeling framework and the procedure of the computations. The coupling among modules of the framework, as well as the flow of data in the framework, is depicted.

where m_p and ε_p are the mass and the initial energy of the particle. θ is the angle of the initial velocity of the particle with respect to $-\mathbf{j}$.

The trajectory of a particle depends on both its initial velocity and position as well as the influence of the electric field. Precisely, the particle trajectory calculation is realized by the numerical solution of the following system of ordinary differential equations, derived by the second law of Newton,

$$\begin{aligned}\frac{d\mathbf{x}}{dt} &= \mathbf{u} \\ \frac{d\mathbf{u}}{dt} &= \frac{q_p}{m_p} \mathbf{E}\end{aligned}\tag{2.3}$$

where \mathbf{x} and \mathbf{u} are the vectors defining the position and the velocity of the particle, q_p is the charge of the particle, and \mathbf{E} is the spatially varying electric field vector calculated by Model 5 (cf. Section 2.2.1.5).

A particle trajectory is terminated on the surface profile, Γ (Figure 2.2). The termination condition is implemented by utilizing function φ , which is defined as the signed distance from the surface profile. The signed distance function φ is calculated by the solution of the Eikonal equation, i.e.

$$|\nabla \varphi(x, y)| = 1, \tag{2.4}$$

with the fast marching method [176]. The function φ for the surface profile of Figure 2.2 is shown in Figure 2.3. φ is negative inside the material (PMMA) and positive in vacuum. Thus, the particle trajectory is terminated when φ at the particle position is less or equal to zero. The use of the signed distance function provides a flexible termination condition, suitable for arbitrary surface profiles.

A trajectory termination can also occur on the upper boundary (inlet) of the computational domain; the electrostatic repulsion may cause the reverse of the sign of the particle velocity on the y axis.

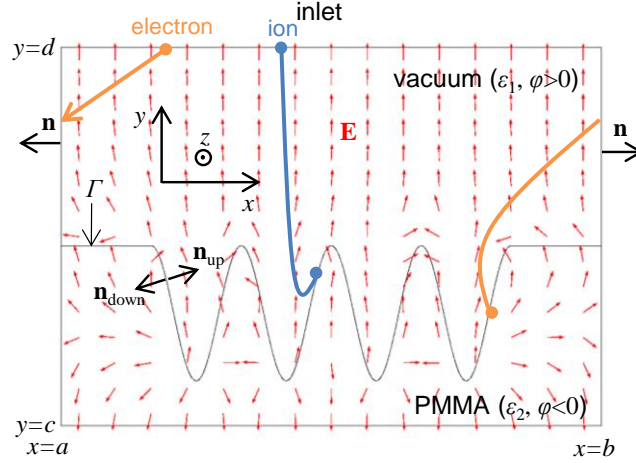


Figure 2.2. The simulation domain. ε_1 and ε_2 are the dielectric permittivities of the two media (vacuum, PMMA). φ is the signed distance function. \mathbf{E} is the space electric field. The surface profile is denoted with Γ . \mathbf{n} is the unit normal vector on the respective boundary. The curve starting from the right boundary demonstrates the particle trajectory continuity condition: A particle getting out of the left (right) boundary of the domain, will re-enter the domain from the right (left) boundary having the same velocity and the same y -coordinate.

When a particle reaches the left or right boundary of the simulation domain, the particle trajectory continuity condition is activated [120, 146]. More precisely, the trajectories of the particles, which abandon the simulation domain and traverse the left and right boundaries, are mirrored with respect to the y axis. This means that the tracing of the particle continues; its position is shifted to the opposite wall boundary, from the left to the right or from the right to the left.

It has to be noticed that every particle represents a cluster of particles or a superparticle. A superparticle will follow the same trajectory as a real particle would because the electric force depends on the charge to mass ratio (see Equation 3). By using superparticles, the calculations are tremendously hastened. The number of particles of each superparticle utilized in this application is 3×10^6 particles.

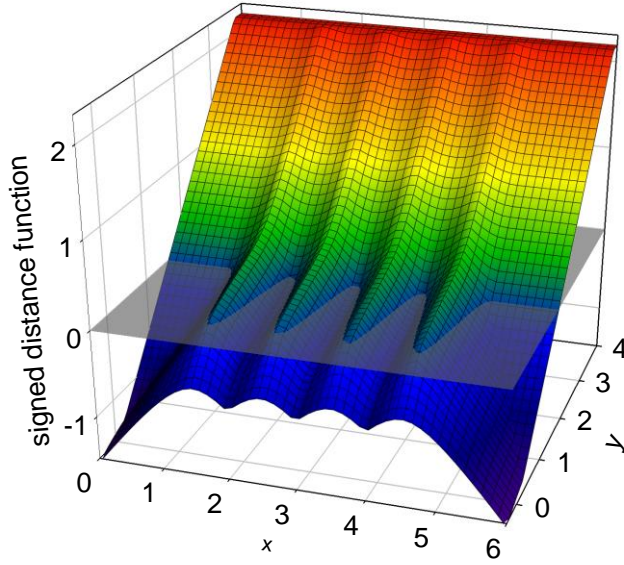


Figure 2.3. Signed distance function, ϕ , of the sinusoidal profile of Figure 2.2 as calculated by the solution of the Eikonal equation.

A final note on the dimensionality of the particle trajectory calculation is made. Given that the profile of the polymeric surface is constant along the z axis, the electric potential should not vary along that direction (Section 2.2.1.5). The latter means that the electric field parallel to z axis, E_z , is zero. For this, the z -component of the velocity, is also neglected; the thermal velocity of the particles, obtained from the plasma, is much smaller than their directional kinetic energy, obtained from the charging field [138]. Thus, a 2d approach is justified for the calculation of particle trajectories.

2.2.1.2 Secondary Electron-Electron Emission Model

When an electron impinges on the PMMA surface, there are three potential events: it may stick on the surface, it may be reflected or it may produce a secondary electron. This behavior can be described by the total electron yield σ_e , equal to $\delta + \eta$, which is commonly defined as the number of emitted electrons per incident (primary) electron. According to this definition, the yield includes three categories of emitted electrons [177]: a) elastically reflected primary electrons, b) inelastically reflected primary electrons, and c) true secondary electrons. δ is the secondary electron emission yield including (c) and η is the backscattering coefficient including (a) and (b). All coefficients, σ_e , δ , and η , may depend on the energy and the angle of incidence of the primary electrons as well as on the substrate material. In the following, a model for σ_e , δ , and η is described. It is based on available information in the literature for PMMA and other polymers in the energy range which is of interest in plasma etching.

The initial electron energy distribution function (EEDF) is a Maxwellian distribution with electron temperature equal to 4 eV (Section 3.2). The energy domain of such a distribution is

extended approximately to 25 eV (Section 3.2). Nevertheless, the energy of an electron can be increased further due to acceleration by the developed charging potential. Given the electrostatic attraction, it is predicted that the range of energies of the primary electrons bombarding the PMMA surface will be from 0 to 50 eV. The same energy domain was also assumed during plasma etching of a SiO₂ trench in view of SEEE [166, 167].

Unfortunately, literature is not deluged with publications describing δ and η for PMMA in the energy range from 0 to 50 eV. Few existing works concern mostly high energy electron bombardment of the PMMA surface. For instance, experimental data on δ for PMMA are available only for (primary electron) energies ranging from ~100 eV to several keV [178-180]. There is also one study including measurements of η in the energy range of 5 to 35 keV [177]. To the best of our knowledge, there are no experimental data that accurately portray the contribution of η to σ_e at low energies for PMMA. However, there are analytical expressions describing δ and η for the whole energy spectrum in the case of PMMA such as the Lin and Yoy law [181] for δ . Yu et al. [182] also proposed an analytical expression to describe δ and used an analytical equation derived by Burke [183] for η . Regarding the computational studies, Dapor et al. [184] developed a Monte Carlo model for the emission of secondary electrons from PMMA. They calculated δ in the energy domain ranging from few keV down to few tens of eV [184]. Dapor [185] also calculated the total electron yield σ_e as a function of the primary electron kinetic energy varying from 0 to 1500 eV. σ_e from the latter work is adopted in this work (Figure 2.4), as it is the only describing σ_e in the energy range of interest (0 – 50 eV).

In order to separate the backscattering proportion of electrons, we use the Burke's equation [183] for η ,

$$\eta = 0.115 \left(\frac{E_0}{10^3} \right)^{-0.223} \quad (2.5)$$

where E_0 is the energy of the primary electrons. Equation 5 was also utilized by Yu et al. [182] for PMMA. Generally, it expresses η in polymers consisting of H, C, N and O as a function of E_0 (eV). It should be mentioned that, in the energy range of interest (0 – 50 eV), we assume that η represents only elastically reflected electrons. This simplification is prompted by Monte Carlo calculations for Teflon demonstrating that only elastically reflected electrons contribute to η for energy lower than 50 eV [186].

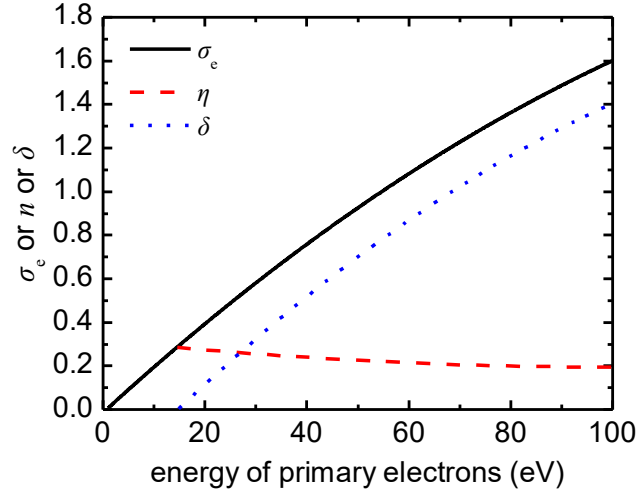


Figure 2.4. The total electron yield, σ_e , the secondary electron emission yield, δ , and the backscattering coefficient, η , being utilized in the SEEE model (Model 2).

η from Equation 5 blows up as the energy of the primary electron goes to zero and strictly speaking Equation 5 results into $\eta > \sigma_e$ for 0 to 16 eV, something that is not realistic. A compromise is to consider that n below 16 eV is equal to σ_e . Thus, δ , i.e. $\sigma_e - \eta$, is considered equal to zero for energy lower than 16 eV (Figure 2.4). It should be noted that the value of 16 eV is not far from the value of 12.6 eV, i.e. the average energy required to produce one secondary electron for PMMA [180]. It is also not far from the value of 10 eV, the general threshold for the secondary electron emission process [187]. For energy greater than 16 eV, δ is calculated as the difference of σ_e and η (Figure 2.4).

Although δ generally depends on the angle of electron incidence [184], this dependence is diminished in the energy range of interest (0 – 50 eV), as shown by both experimental [188] and simulation data [184]. Thus, it is considered that δ does not depend on the angle of electron incidence for energy range which is relevant for plasma etching.

Regarding the energy distribution of the secondary electrons, a typical secondary electron energy spectrum was presented by Dekker. [187]. Nobuo et al. [189] calculated that the average energy of secondary electrons from PMMA was 15 eV when the energy of the primary electrons was 5 keV. Seiler et al. stated [188] that the energy distribution of secondary electrons, released by primary electrons with energies more than 100 eV is essentially independent of the primary energy and proposed an energy distribution of secondary electrons typical for insulating materials. The latter distribution is used by Seggern [190] for secondary electrons from Teflon and by Yu et al. [182] for secondary electrons from PMMA. Given the absence of data for the energy distribution of secondary electrons in the energy range of interest (0 – 50 eV), the energy of the secondary electrons is considered independent of the energy of the primary electrons and equal to the most probable energy of the distribution proposed by Seiler et al. [188, 190]. The energy of the secondary electrons is considered equal to 1 eV.

Regarding the angular distribution of secondary electrons, an isotropic (cosine) distribution is considered, following Monte Carlo calculations for PMMA [184] as well as experimental

measurements for polycrystalline surfaces [188]. Finally, regarding the energy and the direction of the (elastically) reflected electrons, specular reflection with no energy losses is considered. The same approach is adopted for ions (cf. Section 2.2.1.3).

2.2.1.3 Ion Reflection Model

Models for the reflection of ions on surfaces have been proposed [120, 138, 140, 142-144, 191] in the context of plasma etching of conventional structures of microelectronics (trenches and holes) to study etching artifacts due to surface charging, such as notching [120], twisting [130], and microtrenching [142]. Hwang and Giapis [120, 142] assumed inelastic and specular reflection model for Si and SOI substrates, following hard sphere collision kinematics. Specular and elastic reflection was considered by Zhao et al. [138] for photoresist and SiO₂ substrates. Radmilovic-Radjenovic et al. [140] also considered specular reflection for SiO₂ substrates. Wang and Kushner [130] considered both specular (at high energies) and diffusive (at low energies) reflection for SiO₂ substrates. In all of the previous works [120, 138, 140, 142-144, 191], it was considered that the incident ions deposited their charge and were reflected as hot neutral species.

Following the previous works, and in the absence of experimental information on the detailed nature of the reflection of Ar⁺ on a PMMA surface, specular and elastic reflection of Ar⁺ is considered, although Ar⁺ may be implanted or may lose energy at the collision. Additionally, it is considered that ions drop their charge at the spot of the impact and are reflected as hot neutral species [120, 130].

If \mathbf{n} is the unit normal vector on the surface and \mathbf{d} is the unit vector on the direction of the incident ion, the direction of a specularly reflected ion is given by vector \mathbf{r} , i.e.

$$\mathbf{r} = \mathbf{d} - 2(\mathbf{d} \cdot \mathbf{n})\mathbf{n} \quad (2.6)$$

The probability of specular reflection is considered [192]

$$P = 1 - \cos\theta, \quad (2.7)$$

where θ is the angle of ion incidence with respect to the normal to the surface.

2.2.1.4 Surface Charge Density Model

In the Model 4 of the surface charging module, the local surface charge density, σ , on the surface profile is calculated. σ is the link between the particle trajectories and the electric field: The electric field not only affects particle trajectories (Model 1) but is also affected by them (Model 5). When an ion or an electron impinges on the dielectric surface, its charge is transferred on it. A discretization of the surface profile to equal segments and the distribution of the particles (ions and electrons) on these segments are required for the calculation of the local surface charge density. After every charging step, the ratio of the difference of the impinging ions (times the

charge number) and electrons over the length of the local segment is multiplied with the elementary charge and added to the value of the local surface charge density. The surface charge is gradually accumulated. Given that the calculations are in 2d, and strictly speaking, a line and not a surface charge density is calculated. However, the surface has the same shape along the z axis, thus the charging should not vary along that direction [131, 146, 167]. In such a case, the line and surface charge densities are equivalent.

2.2.1.5 Charging Potential Model

The Model 5 of the surface charging module takes the surface charge density from the Model 4 and calculates the electric potential in both mediums of the computational domain (Figure 2.2), i.e. vacuum and polymeric substrate, by solving the Laplace equation,

$$\nabla^2 V_i = 0. \quad (2.8)$$

The index i stands for the medium: V_1 is the electric potential field in the vacuum and V_2 is the electric potential in PMMA.

The boundary condition at the top ($y=d$) of the simulation domain reads

$$V_1(x, d) = 0. \quad (2.9)$$

The charging field is an electric dipole field that decays very fast with distance (dependence on $1/r^3$, where r is the distance from the charge); so beyond inlet ($y=d$) there is no perturbation of the sheath potential due to charging [120, 145].

The boundary condition at the bottom ($y=c$) of the computational domain reads

$$V_2(x, c) = 0. \quad (2.10)$$

The substrate is considered grounded for convenience so all potentials are calculated with reference to it [123, 145]. However, in reality, the surface is floating with a radio frequency bias which is taken into account to the ion energy distribution function (IEDF); the IEDF depends on the sheath potential [145].

In order to mirror the simulation domain [120, 146], the following condition is imposed on both left ($x=a$) and right ($x=b$) boundary,

$$\mathbf{n} \cdot \nabla V_i \big|_{x=a,b} = 0, \quad (2.11)$$

which implies that the potential is symmetric with respect to the boundary that is imposed on. \mathbf{n} is the unit normal vector pointing outside of the simulation domain.

Furthermore, the application of the Gauss law between the two media leads to the surface charge density condition [146] imposed on the surface profile, i.e.

$$\varepsilon_1 \frac{\partial V_1}{\partial \mathbf{n}_{\text{up}}} \Big|_{(x,y) \in \Gamma} - \varepsilon_2 \frac{\partial V_2}{\partial \mathbf{n}_{\text{down}}} \Big|_{(x,y) \in \Gamma} = -\sigma, \quad (2.12)$$

where ε_1 and ε_2 are the dielectric permittivities of the two media, and \mathbf{n}_{up} and \mathbf{n}_{down} are the unit normal vectors on the surface profile Γ (Figure 2.2). σ is the surface charge density which is calculated by Model 4 (Section 2.2.1.4).

Finally, to ensure that the potential is continuous across any boundary, the following equality is imposed.

$$V_1(x, y) \Big|_{(x,y) \in \Gamma} = V_2(x, y) \Big|_{(x,y) \in \Gamma} \quad (2.13)$$

A final note on the dimensionality of the Laplace equation is made. The profile of the polymeric surface is constant along the z axis, thus the surface charge density and as a consequence the electric potential should not vary along that direction. Thus, a 2d approach can be utilized for the calculation of the electric potential.

2.2.2 Surface Etching Model

The surface etching model generally links the fluxes, the energies, and the angles of incidence of species arriving on the surface with the etching rate of the surface. Ar^+ induces physical sputtering of the PMMA. If s is a point on the arclength of the surface profile, the local etching rate is calculated by the following equation,

$$ER(s) = \int_0^\infty \int_0^{\pi/2} EY(\varepsilon_+, \omega) f(\varepsilon_+, \omega, s) J_+(s) d\omega d\varepsilon_+, \quad (2.14)$$

where $J_+(s)$ is the local ion (Ar^+) flux and $f(\varepsilon_+, \omega, s)$ is the local ion distribution as a function of the (kinetic) energy, ε_+ , and the angle of incidence, ω , of the locally impinging ions. Both of them are calculated from the results of the Model 1 at the steady state. The velocity components of an impinging ion are utilized to calculate a) the energy of the ion (ε_+) by Equation 2.1 and b) ω of the impinging ion by the equation

$$\omega = \arccos \left(\frac{\mathbf{u} \cdot \mathbf{n}_{\text{down}}}{|\mathbf{u}|} \right). \quad (2.15)$$

EY in the integral of Equation 14 is the etching (sputtering) yield (see Sections 2.2.2.1 and 2.2.2.2). Two notes are made for the surface etching model. First, the effect of the vacuum ultraviolet (VUV) radiation on the etching rate of PMMA by Ar plasma is not taken into account. This is justified as sputtering by Ar^+ is the main factor in material removal[75]; VUV radiation

has a small contribution to the etching rate especially when the temperature of the substrate is kept low and/or the ion energy increases. Additionally, the inclusion of this effect in a surface etching model is rather complex as VUV radiation induces bulk depolymerization and O₂ depletion reactions that are highly polymer structure specific and temperature dependent [76]. Second, the change of the surface chemical composition during etching is not taken into account. That is why a C equivalent etching yield is calculated (Section 2.2.2.1). The ratio of C, H, and O atoms on the polymeric surface may change during etching. The change of the surface chemical composition is not taken into account in the measurements of Yoshimura et al. [168] as well.

2.2.2.1 etching (sputtering) yield based on Yoshimura et al. experimental measurement and TRIM simulations

To the best of our knowledge, there are no data on $EY(\varepsilon_+, \omega)$ for Ar⁺ sputtering of PMMA (see Equation 2.14). Only the dependence of the etching yield of PMMA on ε_+ (Ar⁺ energy) has been measured by Yoshimura et al. [168] with ion beam sputtering experiments. In order to approximate the dependence of the etching yield on both ε_+ and ω , TRIM [189] code was utilized. By using different ω and ε_+ , the etching yield by TRIM, $EY_{\text{TRIM}}(\varepsilon_+, \omega)$, was calculated. However, the etching yield calculated by TRIM was found orders of magnitude lower compared to the experimental measurements of Yoshimura et al. This large difference is expected especially for low energy ions [193, 194]: The polymeric surface consists of weakly interconnected long polymeric chains, whereas TRIM models an amorphous solid assuming a strongly interconnected carbon network. As a consequence, a single bond breaking event within a collision cascade may release large polymer fragments in case of a real polymeric surface, whereas the removal of only single Carbon atoms is most likely during the sputtering of a strongly interconnected carbon network.

In order to have a realistic approximation of the sputtering yield of PMMA by Ar⁺, a combination of the results of TRIM and the measurements of Yoshimura et al. [168] was performed: The absolute values of the etching yield were taken from the measurements and, due to the lack of pertinent measurements, the relative angle dependence of the etching yield was taken from TRIM. Thus, the etching yield reads

$$EY(\varepsilon_+, \omega) = EY_{\text{TRIM}}(\varepsilon_+, \omega) \frac{EY_{\text{exp}}(\varepsilon_+)}{\frac{\int_0^{\pi/2} EY_{\text{TRIM}}(\varepsilon_+, \omega) d\omega}{\int_0^{\pi/2} d\omega}} \quad (2.16)$$

The ratio at the denominator of the right hand side of Equation 16 is the average etching yield for an ion energy equal to ε_+ as calculated by TRIM. EY_{exp} is the etching yield measured by Yoshimura et al. with an ion beam normal to the polymeric surface; however, even in this case, ω is not necessarily equal to 0 as it is for a perfectly flat surface. A real polymeric surface under ion bombardment cannot be perfectly flat, free of some roughness.

The etching yield coming from both the measurements of Yoshimura et al. and the calculations of TRIM is the sputtering yield of Carbon equivalent [168]. This means that the etching yield does not refer individually to the sputtered C or O or H. In the experiment, it was not possible to detect individual sputtered species separately. With TRIM, a different sputtering yield was calculated for C, O, and H. For both the experiment and the TRIM calculations the sputtering yield of C equivalent is determined as 5 times the ratio of the removed PMMA mass per ion over the monomer mass; 5 is the number of C atoms in the PMMA monomer, $C_5O_2H_8$. If a mass of a single monomer is removed from the surface per ion, the sputtering yield of C equivalent is 5. The values of the EY calculated by Equation 16 are shown in **Figure 2.5**. For ion energy greater than 60 eV, the maximum of the etching yield is at an angle of 79.3° .

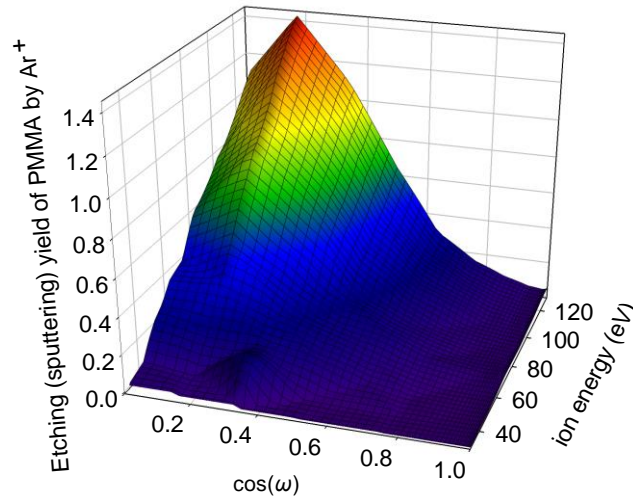


Figure 2.5. Etching (sputtering) yield of C equivalent for PMMA by Ar^+ as a function of the ion energy and the angle of ion incidence. For ion energy greater than 60 eV, the maximum of the etching yield is at an angle of 79.3° .

The etching yield of C equivalent (Equation 16, Figure 2.5) can be fitted to a function of the form

$$EY(\varepsilon_+, \omega) = g_1(\varepsilon_+) g_2(\omega) . \quad (2.17)$$

$g_1(\varepsilon_+)$ is considered the same as in the work of Yoshimura et al. [168] and reads

$$g_1(\varepsilon_+) = a_1 \left(1 - \sqrt{\frac{\varepsilon_+}{\varepsilon_0}} \right)^{5/2} \left[1 + a_2 \left(\sqrt{\frac{\varepsilon_+}{\varepsilon_0}} - 1 \right) \right] \quad (2.18)$$

where $a_1=0.725$, $a_2=0.930$, and $\varepsilon_0=20.9$ eV. $g_2(\omega)$ is extracted by fitting to the data of Figure 2.5 and reads

$$g_2(\omega) = a_3 \exp \left\{ - \left[\frac{|\cos(\omega) - a_4|}{2a_5} \right]^{a_6} \right\} \quad (2.19)$$

where $a_3=3.00$, $a_4=0.185$, $a_5=0.170$, and $a_6=1.58$. $g_2(\omega)$ in Equation 16 fits the data of Figure 2.5 very well for $\varepsilon_+ > 60$ eV. For $\varepsilon_+ < 60$ eV, i.e. at the region of low values of the etching yield, $g_2(\varepsilon_+)$ is less accurate. In particular, Equation 16 does not capture the “bump” of Figure 2.5 for ion energies from 30 to 60 eV and angle of ion incidence from 65° to 75° ($0.25 < \cos\omega < 0.45$). More accurate fitting for this region could be achieved by using a high number of adjustable parameters.

Equation 18 is coming from the work of Yoshimura et al. [168], where a fitting to experimental measurements covering ion energies from 30 to almost 500 eV was performed. The angle dependence of the etching yield, i.e. Equation 19, is coming from calculations with TRIM for ion energies from 30 to 500 eV. Thus, the etching yield formula, i.e. Equation 17, is valid from 30 to 500 eV.

Given that one of the objectives of this case study is the investigation of the effect of charging on the etching rate (Section 3.3), a critical question is whether the calculations by TRIM and/or the measurements of Yoshimura et al. are affected by surface charging. The answer is that TRIM calculations do not take into account surface charging and that for the measurements of Yoshimura et al. the surface was neutralized sufficiently by an electron gun [168].

2.2.2.2 etching (sputtering) yield based on Bruce experimental measurements

The *EY* of polymeric substrates at low ion energies (<50 eV) has not been studied in detail in the literature. Yoshimura et al. [195] measured the *EY* of PMMA and estimated that E_{th} is 20.9 eV; however, their measurements refer to Ar^+ energies above 100 eV (Section 2.2.2.1). Bruce [76] measured the etching rate of several polymeric substrates and found remarkable etching rates (30 – 40 nm/min for PMMA) even at ion energies of 20 eV, which means that the threshold ion energy should be lower. To take advantage of the experimental measurements of Bruce pertaining to lower ion energies for sputtering of PMMA by Ar plasma, the surface etching model was upgraded with a new etching yield equation described below.

The etching (sputtering) yield follows the energy dependence proposed by Steinbruchel [196] and is also angle dependent [197, 198]; etching yield reads

$$EY = Af(\theta) \left(\sqrt{E_{ion}} - \sqrt{E_{th}} \right), \quad (2.20)$$

where E_{th} is the threshold ion energy for the polymer sputtering. Following Mouchtouris & Kokkoris [192], it is assumed that $E_{th}=4$ eV and $A = 0.1$ monomers/(ion eV^{0.5}) in Equation 20; with these values, the simulation results into an etching rate close to that measured by Bruce [76] for PMMA.

θ in Equation 20 is the angle of ion incidence (with respect to the normal to the surface). Mouchtouris & Kokkoris [192] also expressed the angle dependence $f(\theta)$, shown in Figure 2.6, by a simple polynomial function aiming to approximate the measured or simulated curves of angle dependent etching yield [84, 197-202] of polymeric substrates:

$$f(\theta) = \begin{cases} a, & \theta \leq \varphi_1 \\ b_0 + b_1\theta + b_2\theta^2 + b_3\theta^3, & \varphi_1 \leq \theta \leq \varphi_2 \\ 1 + c(\theta - \varphi_2)^2, & \theta \geq \varphi_2 \end{cases} \quad (2.21)$$

The constant parameters in Equation 20 are

$$b_3 = \frac{a-1}{3\varphi_2\varphi_1(\varphi_1 - \varphi_2) - 3/2(\varphi_1 + \varphi_2)(\varphi_1^2 - \varphi_2^2) + (\varphi_1^3 - \varphi_2^3)}, b_2 = -(3/2)(\varphi_1 + \varphi_2)b_3, b_1 = 3b_3\varphi_1\varphi_2,$$

$$b_0 = 1 - b_1\varphi_2 - b_2\varphi_2^2 - b_3\varphi_2^3, \text{ and } c = -\frac{1}{(\pi/2 - \varphi_2)^2}. \text{ The parameters } a, \varphi_1, \text{ and } \varphi_2 \text{ are in rad and}$$

define the exact form of the angle dependence; if their values are known, then parameters b_0, b_1, b_2, b_3 and c can be calculated. φ_2 is the angle corresponding to the maximum etching yield, a is the ratio of the etching yield at normal incidence over the maximum etching yield. The space $[0, \varphi_1]$ defines the angle range that the etching yield is constant and equal to that at normal incidence. The reported values for φ_2 for Ar^+ sputtering of several polymeric substrates varies from 60° to 80° [84, 198-202]. a in the same works varies from 0.67 to 0.13 or even lower depending on the ion energy. φ_2 is considered equal to 75° [$\varphi_2 = (75/90) \times \pi/2$], a is considered equal to 0.3 and φ_1 is assumed equal to 20° [$\varphi_1 = (20/90) \times \pi/2$].

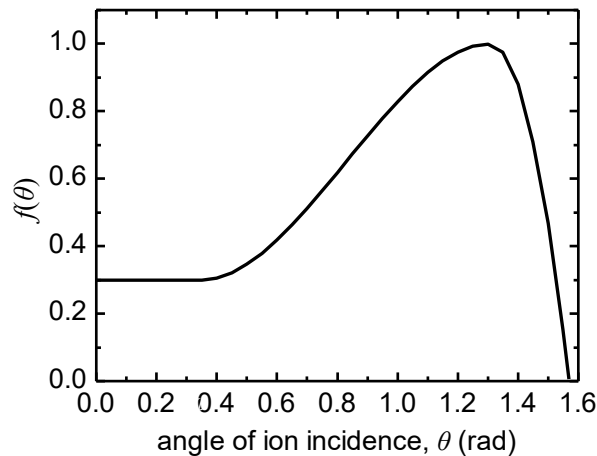


Figure 2.6. The function $f(\theta)$ of Eq. (1) vs. the angle of ion incidence, θ . The maximum is at 75° or $(75/90) \times \pi/2$ rad.

2.2.3 Profile evolution module

The local etching rate calculated by the surface etching module is fed to the profile evolution module which calculates the position of the profile at the next time instant, $t+\Delta t$. The profile evolution module is based on the level set method [172, 173]. The profile is a moving boundary which is “embedded” in the level set function, φ : φ is the signed distance from the moving boundary and the moving boundary is the zero contour of φ (see Figure 2.7). The level set method tracks the evolution of the moving boundary implicitly through the evolution of φ . Instead of a profile, a surface is tracked. The basic equation of the method describing the evolution of φ is the initial value problem,

$$\frac{\partial \varphi}{\partial t} + F |\nabla \varphi| = 0, \quad (2.22)$$

with initial condition $\varphi(\mathbf{x}, t=0)=q(\mathbf{x})$, which is extracted by the initial profile. F at \mathbf{x} is the component of the velocity in the normal direction of the contour of φ passing through \mathbf{x} and is extracted by the local etching rate. Although the velocity has physical meaning only on the surface profile, F should be defined in the whole computational domain. If F_{etch} is the velocity of the surface profile, i.e. the etching velocity (rate) coming from the surface etching model (Section 2.2.2 and 2.3.2), then the F is calculated by solving the boundary value problem

$$\nabla \varphi \cdot \nabla F = 0, \quad (2.23)$$

where $F = F_{\text{etch}}$ on the surface profile. It has to be noticed that there are several means to extrapolate the values of F in the whole computational domain. By using Equation 23, φ remains signed distance from the surface profile [84]. The signed distance is also utilized for the stop condition in the particle trajectory module [84]; tracking of a particle is stopped when φ changes sign (Section 2.2.1.1).

The complete set of computational tasks that have to be carried out for the implementation of the level set method can be found in works of G. Kokkoris [170, 171]. The numerical solution of the equations included in the profile evolution module has been achieved with a proper modification of ϕ etch code [203].

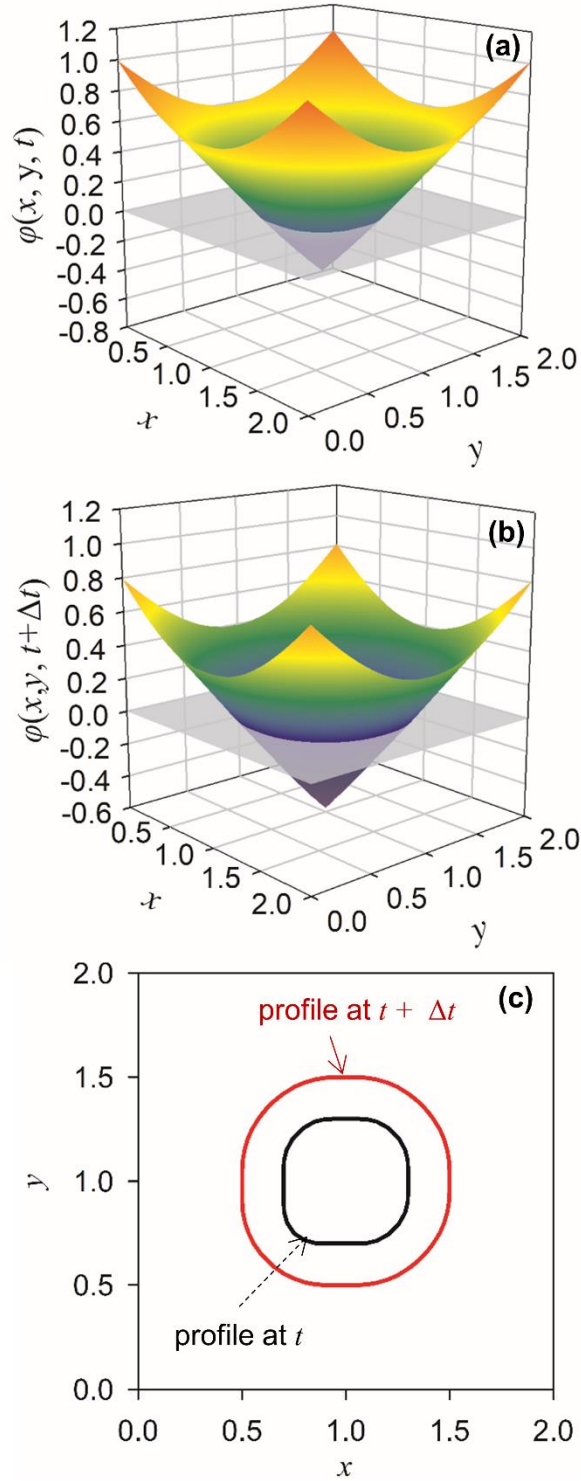


Fig. 2.7. Profile evolution with the level set method (implicit representation of the profile). The level set function, φ , a) at time t and b) at time $t + \Delta t$. c) The zero contours (profiles) of φ at t and $t + \Delta t$.

2.3 Description of the Modeling Framework: application to ion enhanced etching of PMMA with O₂ plasma

A kMC surface model is integrated in the modeling framework and is linked to the profile evolution module (Section 2.2.3 and Figure 2.8a). The inputs of the framework are the initial surface profile (as the one shown in Fig. 2.8c) and the energy and angular distributions of the species joining the surface processes (Section 2.3.1). The output is the evolving surface profile.

For the case studied in this work, i.e. plasma etching of PMMA with O₂ plasma, the kMC surface model tracks the local surface coverage by O during plasma etching and calculates the local etching rate along the profile. The former comes from the competition between the sticking of O and their removal by O⁺ on the surface under the form of O-containing reaction products; the latter is based on a synergistic and nonlinear action of ions and (adsorbed) neutral species (Section 2.3.2).

The basis of the kMC surface model is the direct kMC method (Section 2.3.2). A coarse grained continuum description of the surface is used by introducing coarse cells that incorporate a number of adsorption sites (dangling bonds) under the local mean field approximation (Section 2.3.2.1). The latter denotes that a uniform distribution of particles in the coarse cell is presumed and any local correlations among the particles in the coarse cell are omitted. The fundamental input to a direct kMC scheme is a list of possible processes associated with a rate (transition probability), which is related to the probability that the process will occur. According to the direct kMC method, two categories of processes are distinguished in the kMC model, namely the sticking of O⁺ and the sticking of O on a surface cell. The transition probabilities are calculated at each time step of the profiles evolution by tracking the trajectories of atoms and ions and the cell they finally stick taking into account remission or reflection (Section 2.3.2.2).

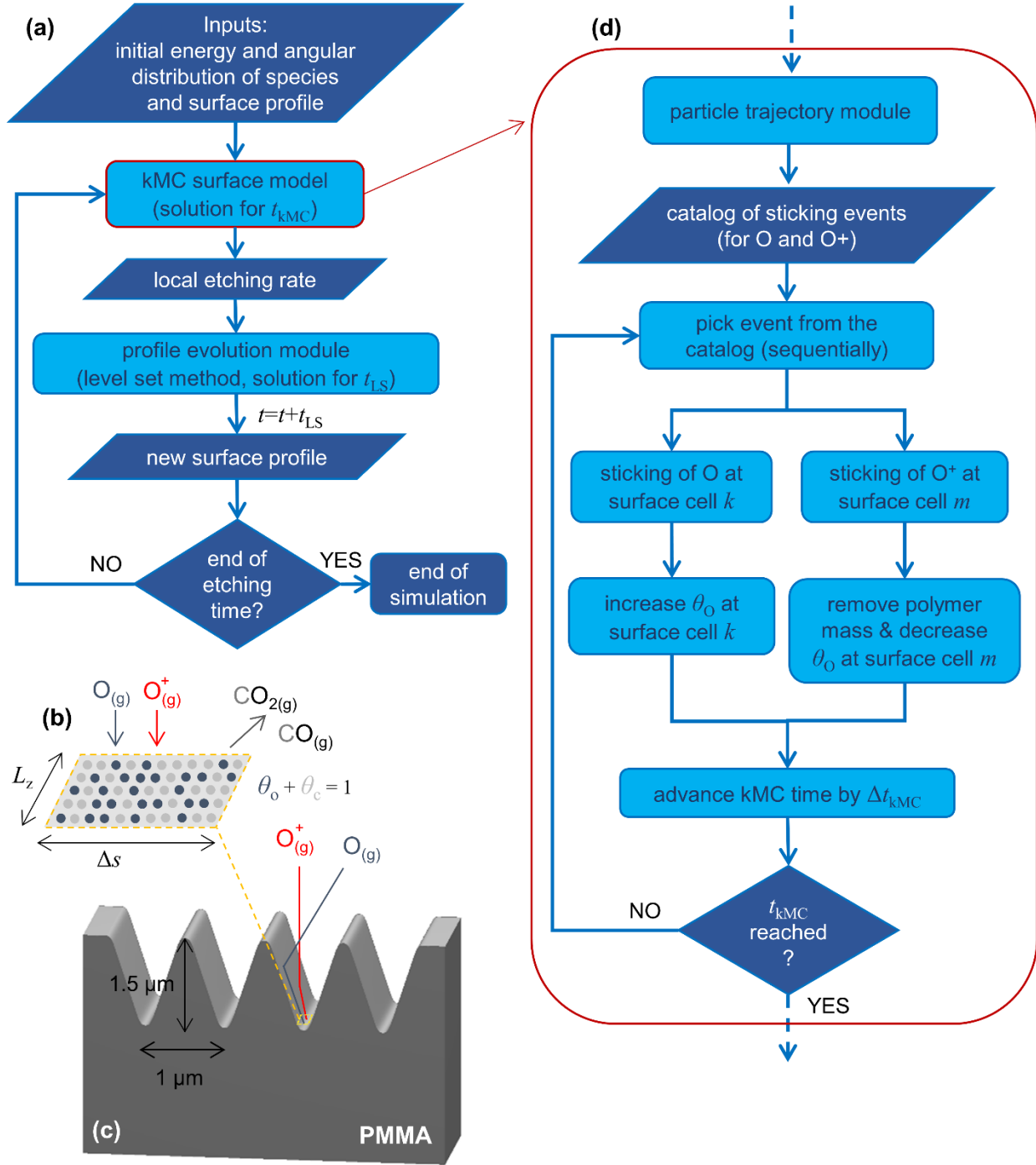


Fig. 2.8. a) The hybrid modeling framework. The kMC model is solved for t_{kMC} . t_{LS} is the time step for the numerical solution of the level set equation (Equation 2.22). b) Processes on an elementary surface etched with O_2 plasma. The grey surface sites correspond to the fractional coverage of the clean polymeric surface (C atoms), θ_c , while the blue sites correspond to fractional coverage by O, θ_o . The products of ion enhanced etching are carbon monoxide and dioxide (CO and CO_2). O^+ can be reflected and O can be diffusively reemitted. The dimensions of the elementary surface (cell) are $L_z \times \Delta s$. c) The initial surface profile used in the current study;

it comes from a sinusoidal function with amplitude equal to $0.75\ \mu\text{m}$ and period equal to $1\ \mu\text{m}$.
d) Flow chart of the kMC simulation.

The local etching rate, which is extracted by running the kMC surface model for t_{kMC} , is fed to the profile evolution module [204, 205] which “produces” the profile at the next time step, $t + t_{\text{LS}}$; t_{LS} is the time step for the numerical solution of the level set equation and its relation to t_{kMC} is discussed in Section 2.4. The profile evolution module (Section 2.2.3) is based on the level set method. It is additionally used for tracking local variables (i.e. O surface coverage) of the evolving surface profile (Section 2.3.3).

Specifically, the level set method [104, 105] is used for three tasks. The first is the evolution of the surface profile (Section 2.2.3), the second is the calculation of the signed distance function from the evolving interface (Section 2.2.1.1) and the third is the conservation of local variables of the evolving surface profile (through their transport) from the current to the next profile (Section 2.3.3). As the evolving profile is embedded in an implicit function (level set function), unless this transport takes place, any past information on the profile is lost during the evolution.

The practical implementation of the framework is discussed in Section 2.3.5.

2.3.1 Surface processes during ion enhanced etching of PMMA with O₂ plasma

Before proceeding to the discussion of the components of the framework, the surface processes during etching of PMMA substrates in O₂ plasmas are described and a mathematical formulation is introduced. The kMC model of the hybrid modeling framework (Section 2.3.2) should take into account these processes and verify the formulation (Section 5.3).

The reactive species joining the surface processes are O and O⁺. The adsorption of O₂ is negligible compared to the adsorption of O [206-208]. The dominant etching mechanism of PMMA is ion-enhanced etching which lies on a synergistic and nonlinear action of ions and (adsorbed) neutral species. Ion-enhanced etching coexists with physical sputtering by O⁺, pure chemical and photo-induced (by UV photons) etching. However, the ion energy (close to 100 eV) and the surface temperature (300 – 400 K) during plasma etching allows the neglect of sputtering [208] and pure chemical etching [206, 207] respectively. Similarly, etching induced by UV photons [206, 207] can be also neglected when compared to ion-enhanced etching.

The PMMA polymeric chain comprises of a carbon skeleton on which volatile components (i.e. H and O) are attached via covalent bonds. Attuned to the work of Bes et al. [206], we consider that the etching mechanism of PMMA in O₂ plasma involves two steps, namely a rapid initial step of desorption of the volatile components followed by a longer-lasting step of oxidation of the carbon atoms once exposed to plasma. The second step is the rate determining step of PMMA etching and, thus, governs the etching kinetics. Indeed, as carbon is the exclusive chemical element on the PMMA polymeric chain which is inherently non-volatile, the ultimate oxidation of the carbon skeleton constitutes the determining step of the etching of the polymeric chain. In this sense, the interaction of O and O⁺ coming from the plasma with O and H atoms bonded in the monomer structure of PMMA is not considered in our computations.

Ultimately, the etching rate reads,

$$ER = \frac{m_{\text{PMMA}}}{5\rho_{\text{PMMA}}} EY_C j_+ = \frac{m_{\text{PMMA}}}{5\rho_{\text{PMMA}}} \beta_0 (\sqrt{E_+} - \sqrt{E_{\text{th}}}) f(\omega) \theta_O j_+ \quad (2.24)$$

where EY_C is the etching yield of carbon atoms (C) and is determined as the ratio of C removed per incident ion. ρ_{PMMA} is the mass density of PMMA and m_{PMMA} is the mass of the PMMA monomer. 5 in the denominator is the number of C in the monomer ($\text{C}_5\text{H}_8\text{O}_2$). EY_C depends on the ion energy, E_+ , the angle of ion incidence, ω , and the surface coverage by O, θ_O . E_{th} is the threshold energy for ion enhanced etching, β_0 is the constant factor of EY_C and j_+ is the ion (O^+) flux. θ_O is defined as the ratio of the density of adsorption sites occupied by O, σ_O , over the total density of adsorption sites on the surface, σ_S (equal to $2n_c^{2/3}$, n_c is the atomic carbon density of PMMA [206]), and comes from the competition between the sticking of O and the removal of O by O^+ on the surface under the form of O-containing reaction products (Figure 2.8c). It is calculated by a surface site balance, which reads

$$\sigma_S \frac{d\theta_O}{dt} = (1 - \theta_O) s_O j_O - 1.5 \beta_0 (\sqrt{E_+} - \sqrt{E_{\text{th}}}) f(\omega) j_+ \theta_O \quad (2.25)$$

j_O is the flux of O and s_O is the sticking coefficient of O on a “clean” surface ($\theta_O = 0$). The sticking probability of O is $S_O = s_O(1 - \theta_O)$; non sticking O undergo diffuse reemission [209]. The sticking probability of O^+ depends on the angle of incidence (ω) and follows an almost cosine law [210]; non sticking O^+ undergo a specular and elastic reflection from the surface [82]. The factor 1.5 before β_0 is the average stoichiometry of the reaction products, i.e. CO and CO_2 [118]. Regarding the total density of adsorption sites on the surface, σ_S ($2n_c^{2/3}$), the factor 2 comes from the fact that, once stripped from their volatile components (rapid initial step), the polymer chain segments at the PMMA surface are converted into carbon chain segments with single bonds between sequential carbon atoms [206]; since each carbon atom can create four covalent bonds with up to 4 adjacent atoms, there are 2 adsorption sites available per atom of carbon which may be occupied by the O emerging from the plasma.

The time required for θ_O to reach a steady state value (transition time) is $\sim 5\tau$, where τ is the time constant of Equation 2.25, and reads

$$\tau = \frac{\sigma_S}{1.5 \beta_0 (\sqrt{E_+} - \sqrt{E_{\text{th}}}) f(\omega) j_+ + s_O j_O} \quad (2.26)$$

The values of the s_O and β_0 are 0.13 and 0.3721 are coming from fitting of the etching rate to measurements at different operating conditions (pressure, power) in a plasma reactor [9]. E_{th} is 4 eV [209], $\rho_{\text{PMMA}}/(5M_{\text{PMMA}})$ is equal to 35.5×10^{27} atoms/m³ [211], while E_+ , j_+ and j_O are inputs depending on the operating conditions and the case studied.

2.3.2 The kinetic Monte Carlo surface model

Various kMC schemes have been proposed for the description of surface processes [212-219]. The interested reader can find more information in the short review of kMC methods in Appendix B. Nevertheless, none of the previously proposed schemes takes into account the morphology of the surface. In this work, a kMC methodology is developed to handle rough surface morphologies. The basis of this methodology is the direct kMC method [214], which is straightforward in principle. For a surface with N_L lattice cells and for a number of N_P potential surface processes, the j_{th} process at the i_{th} cell is picked out with a probability

$$p_{ij} = \frac{\Gamma_{ij}}{\sum_{j=1}^{N_P} \sum_{i=1}^{N_L} \Gamma_{ij}} = \frac{\Gamma_{ij}}{\Gamma_{tot}} \quad (2.27)$$

where Γ_{ij} is the rate of the j_{th} process at cell i , and Γ_{tot} is the sum of process rates over the entire lattice. All Γ_{ij} are estimated a priori. The direct kMC method includes two steps: In the first step, a pair (I, J) is picked out by employing a random number from a uniform distribution, $\zeta_1 \in (0, 1)$, according to

$$\sum_{i=1}^{I-1} \sum_{j=1}^{n_j} p_{ij} + \sum_{j=1}^{J-1} p_{Ij} < \zeta_1 < \sum_{i=1}^{I-1} \sum_{j=1}^{n_j} p_{ij} + \sum_{j=1}^J p_{Ij} \quad (2.28)$$

In the second step, the time is increased by the amount of

$$\Delta t_{kMC} = -\frac{\ln \zeta_2}{\Gamma_{tot}} \quad (2.29)$$

where $\zeta_2 \in (0, 1)$ is a random number from a uniform distribution. Δt_{kMC} is the finite time interval during which the picked process occurs.

A major challenge of on-lattice kMC simulations (see Appendix B for more information) is to create a complete catalog of all possible processes along with their rates or transition probabilities. The same is true for our case, where two processes, i.e. $N_P=2$, are defined, namely the sticking of O^+ (process p_{O+}) as well as the sticking of O (process p_O) on the surface.

2.3.2.1 Coarse graining

Before proceeding to the determination of the transition probabilities of processes p_O and p_{O+} , it is crucial to regulate the system from a spatial point of view. The aim of the kMC model is to compute the local etching rate which is then fed to the profile evolution module (level set method). A coarse grained adjustment of the surface is necessary as the level set method constitutes a continuum description of the evolving profile. An atomistic representation of the

surface would impose noise to the local etching rate, which would be practically unmanageable by a deterministic profile evolution module.

According to the coarse grain approach, the surface is divided in m coarse cells; details for coarse grain kMC approach can be found in Appendix B.4. When a surface cell is not covered by adsorbed O, the number of dangling bonds (adsorption sites), b , at each coarse cell, read

$$b = \sigma_s \Delta s L_z, \quad (2.30)$$

where $\Delta s L_z$ is the area of the given cell with Δs being the dimension of the cell along the arclength of the surface profile and L_z the dimension of the cell along z axis (see Figure 2.8b).

The effect of different coarse-graining levels in the z -direction and along the arclength of the surface profile on the results are discussed in Appendix C.

The coupling of the two components of the framework allows the kMC surface model to take into consideration the profile shape (or the surface morphology) and extend the potential of previous kMC surface models in the literature which assume that the surface is flat.

2.3.2.2 Estimation of the transition probabilities by a particle trajectory module

The transition probabilities of the processes of sticking of O^+ and O on a surface cell i (processes $p_{i,O}$ and p_{i,O^+}) is defined as the rate of sticking impacts (events) of O^+ and O on cell i , i.e.

$$\Gamma_{ij} = \frac{N_{ij}}{t_{\text{kMC}}}, \quad (2.31)$$

where j is O^+ (O) and N_{ij} is the number of finally sticking O^+ (O), i.e. the number of sticking events for O^+ (O) on cell i during the time interval of the kMC model, t_{kMC} .

N_{ij} are calculated by a particle trajectory module where the trajectories of O and O^+ (particles) are numerically computed by solving a system of ordinary differential equations derived from the second law of Newton [84]. After arrival on the surface, O^+ and O either stick or rebound (through reflection or diffuse reemission respectively) from the surface depending on their sticking probabilities (Section 2.3.1). The inputs of the particle trajectory module are the energy and angular distribution of particles and the surface profile. The output of the particle trajectory module is a catalog of the sticking events, N_{ij} , containing the particle identity (O^+ or O) in conjunction with the index of the surface cell where sticking takes place. The order of the events of the catalog is random, stemming from the random choice of the initial particle identity before its trajectory being tracked. The times the combination (particle identity, surface cell i) appears in the catalog implicitly encapsulates its probability to be selected in accordance to Equation 2.28. Each component of the catalog is chosen sequentially, thus, the utilization of Equation 2.29 to pick out an event is circumvented.

The processes $p_{i,O}$ and p_{i,O^+} depend on a) the sticking probability of O^+ and O , b) the ratio of the fluxes of O^+ and O , and c) the position of the cell i on the surface. Concerning the latter, generally, kMC models do not take into account the morphology of the surface assuming it to be flat. In the case of a rough surface profile where shadowing of the neutral and ion fluxes take place, the rates of the processes depend also on a global property of the surface, i.e. its morphology.

2.3.2.3 The algorithm

The flowchart of the kMC simulation is demonstrated in Figure 2.8d. At each step, the events (processes j at cell i) are sequentially identified from the catalog and the time evolution of θ_O and removed polymer (substrate) mass are tracked.

Assuming that at time t_1 , with $0 \leq t_1 \leq t_{kMC}$, the number of the adsorbed O at a surface cell i is $N_{O,ads}(i, t_1)$ and that the next component of the catalog is “ O sticking at the surface cell i ”. The number of adsorbed O at this surface cell is increased by 1, i.e. $N_{O,ads}(i, t_2) = N_{O,ads}(i, t_1) + 1$, and θ_O is calculated by the formula

$$\theta_O(i, t_2) = \frac{N_{O,ads}(i, t_2)}{b}, \quad (2.32)$$

where $t_2 = t_1 + \Delta t_{kMC}$ (Equation 2.29).

Let's presume now that at t_2 the next component of the catalog is an event “sticking of O^+ at cell i ”. Upon sticking of O^+ , substrate material with mass equal to

$$\Delta m = EY_C(i, t_2) \frac{m_{PMMA}}{5} \quad (2.33)$$

will be removed, where the denominator (5) denotes that number of C in the monomer, and $EY_C(i, t_2) = \beta_0(\sqrt{E_+} - \sqrt{E_{th}})f(\omega)\theta_O(i, t_2)$. The instantaneous etching rate is calculated by the slope of the curve showing the removed polymer mass versus time. Simultaneously with the material removal, the number of adsorbed O is reduced and consequently θ_O is also updated, precisely

$$\theta_O(i, t_3) = \frac{N_{O,ads}(i, t_2) - 1.5EY_C(i, t_2)}{b}, \quad (2.34)$$

where $t_3 = t_2 + \Delta t_{kMC}$ (Equation 2.29).

2.3.3 Transport of local variables of the evolving surface profile

Tracking of local variables (e.g. surface coverage, surface charge density) of an evolving profile is straightforward with Lagrangian methods of profile evolution (e.g. with the string method) where an explicit representation of the profile is used. In the string method, the discretization is based on a series of nodes (see Figure 2.9) and the evolution takes place through the movement of the nodes according to the local vector of the etching velocity (which is normal to the profile). The tracking of a local variable on the profile is realized through the movement of the nodes: each node carries, transports all local variables and information of the profile from the current to the next time step.

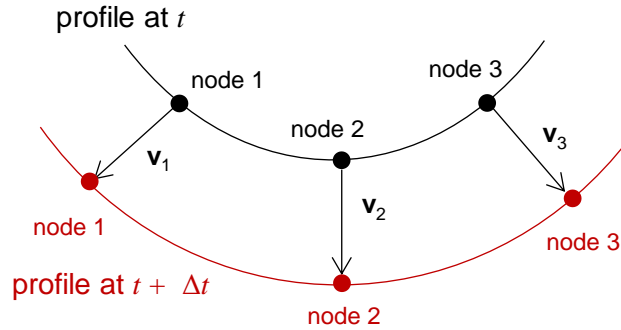


Figure 2.9. Profile evolution with the string method (explicit representation of the profile), not used in this work but shown to explain the concept of transport of variables. Discretization and movement of an evolving profile is based on nodes. The local variables are tracked through the nodes. \mathbf{v} is the vector of the local velocity node velocity (e.g. etching velocity).

Although it has several advantages over Lagrangian methods for profile evolution, the level set method is not easily applied to problems in which local variables of the profile (e.g. surface coverage) need to be tracked. This is because the evolving profile is embedded in an implicit function and hence any parameterization of the profile, any past information on the profile, is disregarded. Hence, the transport of local variables of the profile requires special methodologies [220].

The proposed methodology for the transport of a scalar local variable of the profile, S_{profile} , includes two steps: In the first step, Equation 23 is numerically solved but this time F is substituted with S ; S stands for the extension of S_{profile} in the whole computational domain. The formulation of the equation, i.e. $\nabla \varphi \cdot \nabla S = 0$, essentially means that the contours of S are normal to those of φ . In other words, S_{profile} (and S) remains constant along curves which are normal to the evolving profile. Given that function φ is advancing following F , which is the normal component of the profile velocity (only the normal component is effective, the tangential component does not contribute to the profile movement), it is rational (reasonable) to consider that a point on the surface profile is moving normally to the profile, i.e. along on the contours of S : the point follows a path where S is constant or the extension (extrapolation) of S follows the normal movement of the point.

In the second step, after the extension of S in the whole computational domain, the local values of S_{profile} on the new profile are calculated by an interpolation of S on the coordinates of the new profile. In this work, transport of the surface coverage by O atoms, θ_{O} , is performed, i.e. $S_{\text{profile}} = \theta_{\text{O}}$. The transport of θ_{O} decreases the time required for the solution of the kMC model (Section 4.1.2) decreasing the computational cost of the hybrid framework. In Figure 2.10, the contours of the level set function φ (the surface profile is the zero contour of φ) along with the contours of θ_{O} are shown; due to equation $\nabla \varphi \cdot \nabla \theta_{\text{O}} = 0$, the contours of φ are normal to those of θ_{O} .

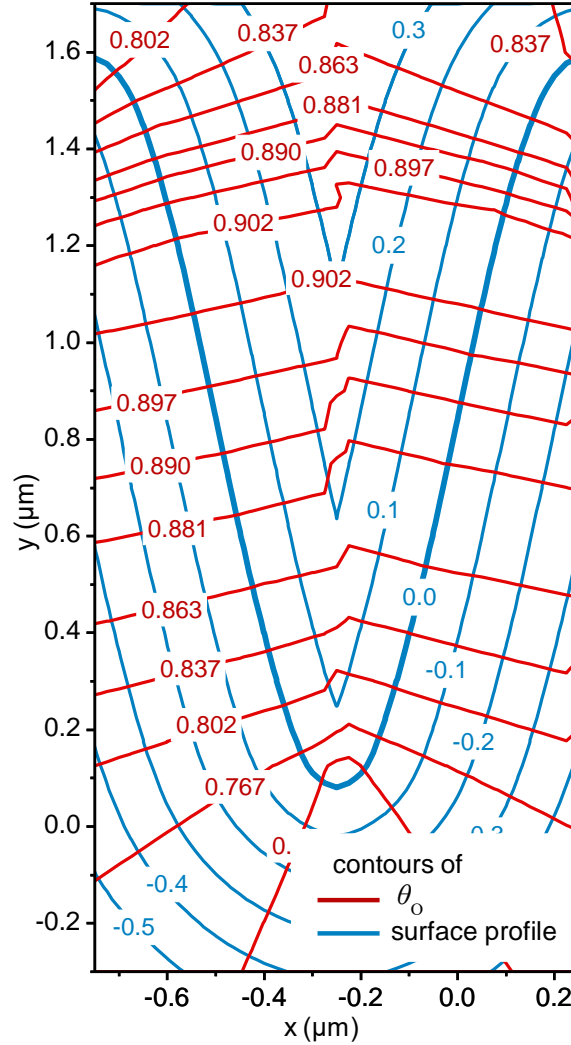


Figure 2.10: Contours of the level set function φ and contours of θ_{O} . The zero contour is the surface profile. The direction of F (Equations 22 and 23) is tangential to the contours of θ_{O} .

2.3.4 The time intervals (scales) of the framework

An obvious choice for t_{kMC} and t_{LS} , i.e. the time interval for the kMC simulation and the time step for the profile evolution, is $t_{\text{LS}} = t_{\text{kMC}}$. However, this would lead to a huge computational cost for the kMC: the total etching time is typically in the order of tens or hundreds of seconds. If the focus is on the computational efficiency, then t_{LS} should be as high as possible and t_{kMC} should be as low as possible. The high bound of t_{LS} is posed by the CFL criterion. t_{kMC} should be high enough for the right calculation of the etching rate, i.e. to get a representative value of the etching rate for t_{LS} . Hence, t_{kMC} should be greater than the time required to get the surface coverage, and thus the etching rate, to steady state, t_{ss} . If $t_{\text{ss}} \ll t_{\text{LS}}$, then running kMC model for $2-3t_{\text{ss}}$ and calculate the etching rate for the interval $[t_{\text{ss}}, 2t_{\text{ss}}]$ would yield a representative value of the etching rate for t_{LS} .

The transport of the local values of θ_{O} from the current profile to the profile at the next time step (Section 2.3.3) decreases t_{ss} and thus t_{kMC} : Through the transport and given that the profile is not drastically altered after t_{LS} , the initial local values of θ_{O} on the profile would be very close to their steady state values, inducing a decrease of t_{ss} . If no transport takes place, then the initial local values of θ_{O} will be equal to zero (or some other value) and much more time to reach steady state would be required.

2.4 Implementation

Regarding the particle trajectories calculations, a suitable multistep method with variable step size is used for the pertinent system of ordinary differential equations. Parallel computing techniques, such as parallel loops and code vectorization, are utilized to curtail the computational time.

The solution of the Laplace equation is implemented by the finite element method. The basis functions are linear. A mesh of triangular elements is constructed. It should be noted that it is not efficient to make all the triangular elements of the same size. At regions where the gradient of the potential is high (close to the surface profile), smaller triangles are used. On the other hand, in areas of small gradient of the potential (away from the surface profile), larger elements are utilized. A mesh of about 26000 elements is found enough to have a mesh independent solution. The computations are realized by COMSOL [221]. However, in order to accelerate the solution of the Laplace equation in the latest edition of the framework, a pertinent code has been developed in Matlab.

The kMC surface model is implemented with a homemade code in Matlab. The code of the profile evolution module and the transport of local surface properties is in C++.

All modules of the framework are coupled and cooperate with each other through a homemade code in Matlab.

2.5 Conclusions

A hybrid modeling framework, coupling stochastic and deterministic modules, was developed to simulate profile evolution during plasma etching. This chapter discussed the components of a hybrid modeling framework, through its application to two different case-studies, namely Ar and O₂ plasma etching of PMMA substrates with an initially sinusoidal, resembling a rough, profile. Although the details varied depending on the case study, the basic idea was that a surface etching model linked the local flux, energy, and the angle of incidence of the plasma species to the local etching yield and rate. The local etching rate calculated by the surface etching model was then supplied to a profile evolution module which computed the successive positions of the profile.

The framework was first applied to Ar plasma. The etching mechanism of PMMA was physical sputtering by Ar⁺. The angle and energy dependence of the etching (sputtering) yield of PMMA by Ar⁺ was devised combining experimental measurements [168] and calculations by TRIM (transport of ions in matter) code [189]. Particular importance was attached to the effects of plasma induced surface charging on roughness evolution. SEEE and ion reflection were also addressed. Regarding the SEEE, filling the relevant gap in the literature, an original model for the secondary electron emission yield, δ , and the backscattering coefficient, n , was developed combining available information for PMMA and other polymers in the energy range which is of interest in plasma etching. Regarding the reflection of Ar⁺ on a PMMA surface, a simple model of non-interacting collisions was considered, i.e., specular reflection of the ions on the surface with no energy losses.

The framework was also applied to O₂ plasma chemistry. The etching mechanism of PMMA was ion enhanced etching which was based on a synergistic and nonlinear action of ions and (adsorbed) neutral species. A kMC surface etching model was integrated in the framework and was coupled with the profile evolution module. The kMC model described the surface processes during O₂ plasma etching and was used for the calculation of the local etching rate along the profile. The novel aspect of the model was that it took into account the surface morphology in the calculation of the transition probability of a process through the calculation of the trajectories of the species joining the surface reactions.

The profile evolution module was based on the level set method. The novel element of the profile evolution module, not previously used in etching and deposition processes, was the use of the level set method for the transport of local properties of the profile (e.g. surface coverage) from a time step to the next which is not straightforward. The purpose of the transport was to effectively reduce simulation time.

This chapter has been published as a part of the following articles:

a) G. Memos, G. Kokkoris, Modeling of Charging on Unconventional Surface Morphologies of PMMA Substrates during Ar Plasma Etching, Plasma Processes and Polymers 13 (2016) 565-578.

- b) G. Memos, E. Lidorikis, G. Kokkoris, The interplay between surface charging and microscale roughness during plasma etching of polymeric substrates, J Appl Phys 123 (2018) 073303.**
- c) G. Memos, E. Lidorikis, G. Kokkoris, Roughness evolution and charging in plasma-based surface engineering of polymeric substrates: The effects of ion reflection and secondary electron emission, Micromachines 9 (2018).**
- d) G. Memos, E. Lidorikis, E. Gogolides, G. Kokkoris, A hybrid modeling framework for the investigation of surface roughening of polymers during oxygen plasma etching, Journal of Physics D: Applied Physics 54 (2021) 175205.**

3. Modeling of charging on unconventional surface morphologies of PMMA substrates during Ar plasma etching

3.1 Introduction

The focus of this chapter is on the surface charging of unconventional polymeric surface morphologies. The term unconventional stands for the roughness produced on initially flat polymeric substrates during plasma etching. The charging potential, the local ion fluxes, and the local etching rate are calculated on a **snapshot** of an evolving rough polymeric surface. Profile evolution is out of the scope of this chapter. The case study is Ar plasma etching (sputtering) of a PMMA substrate with a sinusoidal profile resembling a rough profile, i.e. a case where the etching mechanism is physical sputtering with a strong dependence of the etching yield and rate on the angle of ion incidence (see Figure 2.5 and Equation 2.14). The effect of charging and the aspect ratio (AR) of the sinusoidal profiles on the etching rate is investigated; the AR is defined as the ratio of two times the amplitude over the half the period of sinusoidal profile. The use of a sinusoidal profile to model a rough surface is not new in the literature. In previous works [74, 76], an equilibrium dominant wavelength and the amplitude of roughness have been used to describe a rough surface. The dominant wavelength is the period of our sinusoidal profile and the amplitude of roughness is two times the amplitude of the sinusoidal profile.

Given that charging and etching occur simultaneously, another objective of this chapter is to investigate the time scale of charging (the time that charging requires to reach a steady state condition, i.e. charging time); in particular, to assess, based on the time scales, if the two phenomena, i.e. charging and etching, can be studied decoupled. This will be crucial for the results of Chapter 4; if the charging phenomenon evolves very fast and arrives at steady state in a time much lower than the time step of the evolution of the surface profile, Δt , the solution of the charging module can be decoupled from the solution of the profile evolution module facilitating the calculations.

Additionally, the effect of the thickness of the dielectric (PMMA) on a) the local charging potential, b) the local ion and electron fluxes, and c) charging time are examined. This has not been previously investigated; previous works for conventional structures in semiconductor industry, i.e. trenches and holes, addressed the effect of the AR [163, 164] and the surface conductivity [133] on the charging time.

The rest of the chapter is structured as follows: Section 3.2 includes the model verification by a comparison with published results for a SiO₂ trench [157]. Section 3.3 includes the modeling results for PMMA surfaces with sinusoidal profiles; the local ion flux and energy, the local etching yield and rate are calculated. The effect of charging and AR are demonstrated in Section 3.4. Section 3.5 includes an investigation on the impact of the thickness of the polymeric (dielectric) layer on surface charging. The conclusions are summarized in Section 3.6.

3.2 Surface charging module verification

In order to verify the results of the surface charging module, results from a seminal work by Hwang and Giapis [157] are used as a benchmark. Hwang and Giapis developed a surface charging model for the calculation of charging potential during SiO_2 trench etching under Ar plasma. The structure used for the verification of the results is a trench with AR equal to 3 (ratio of depth, $1.5\ \mu\text{m}$, to width, $0.5\ \mu\text{m}$, see Figure 3.1).

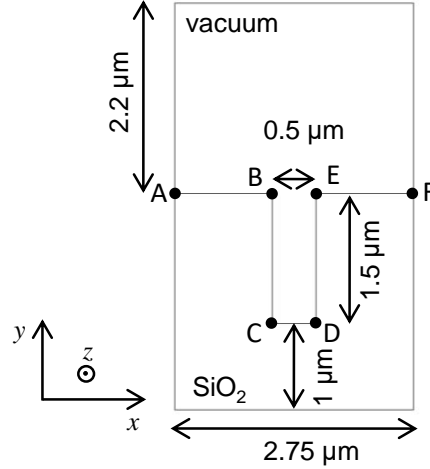


Figure 3.1. The trench geometry used for the comparison of the results with the work of Hwang and Giapis [157]. The points A, B, C, D, E, and F define the trench profile.

Both the ion energy (IEDF) and angular distribution (IADF) as well as the electron energy (EEDF) and angular distributions (EADF) are exactly the same with those in the aforementioned work. In particular, the IEDF is a bimodal distribution with average energy equal to $90\ \text{eV}$ and the IADF is a narrow normal distribution; the product of these two distributions, i.e. IEADF, is shown in Figure 3.2. The EEDF is a Maxwellian distribution with electron temperature equal to $4\ \text{eV}$ and the EADF is equal to $(\cos\theta)^{0.6}$ where θ is the angle defining the initial direction of electrons; the product of these two distributions, i.e. EEADF, is shown in Figure 3.3.

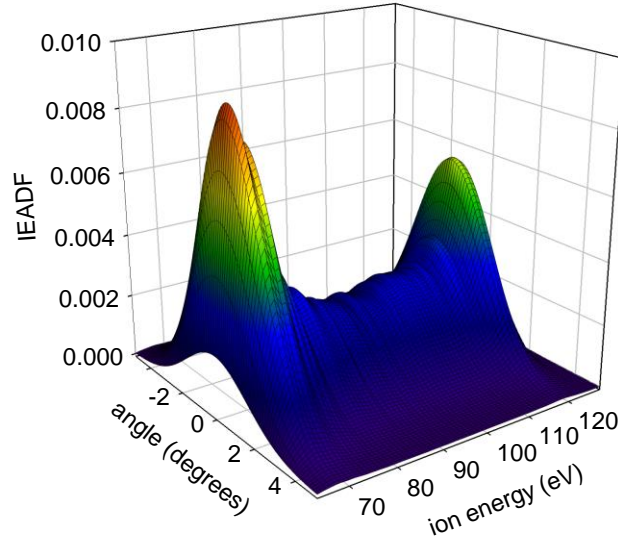


Figure 3.2. IEADF for Ar^+ being utilized in the calculations.

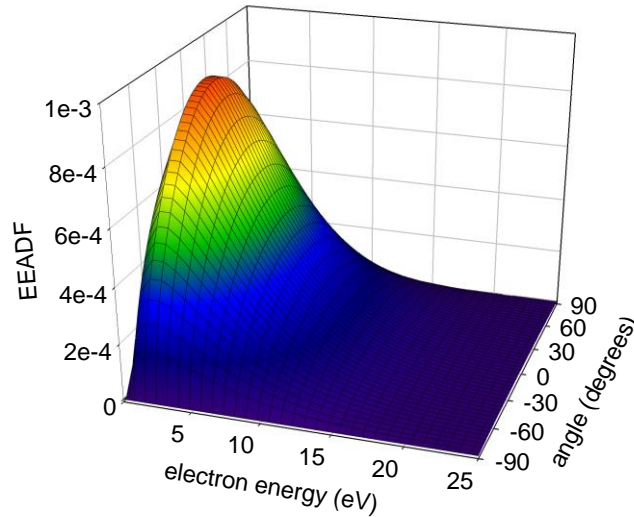


Figure 3.3. EEADF being utilized in the calculations.

In **Figure 3.4**, the charging potential on the trench profile from the surface charging module is compared and found in close agreement to the potential from Ref. [157]. It should be mentioned that there is no reported value for the thickness of the dielectric substrate in Ref. [157]. We examined different thicknesses for the dielectric substrate (see Figure 3.4) and it is found that there is no significant difference in the calculated steady state charging potentials.

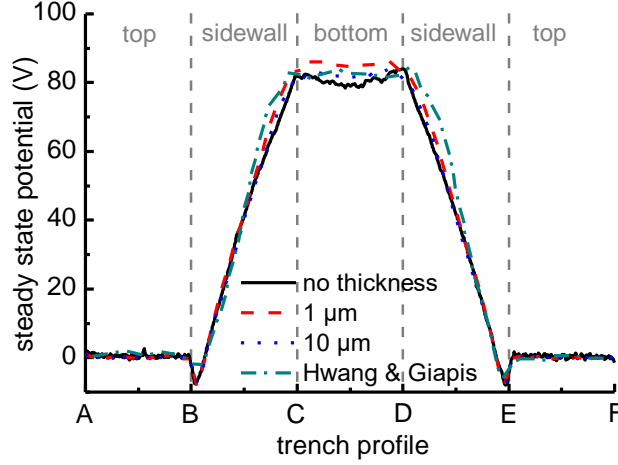


Figure 3.4. Charging potential along the trench profile of Figure 3.2 for different thicknesses (0, 1, and 10 μm) of the dielectric substrate. The results of Hwang and Giapis [157] are also shown. The same x axis with the work of Hwang and Giapis [157] has been used: The length scales have been normalized by the corresponding length of a particular segment (top, sidewall, and bottom).

As far as the IEDF of ions arriving at the trench bottom is concerned, there is a quite good agreement between our results and those of Ref. [157]. The comparison is demonstrated in **Figure 3.5** which also includes the initial IEDF. Figure 3.5 illustrates the remarkable decrease of the initial average ion energy at the trench bottom due to charging potential; the average impinging energy is reduced about 4 times, from 90 eV to 23 eV.

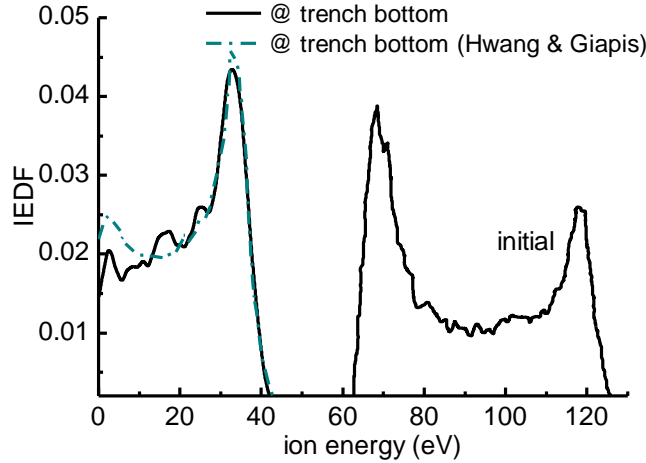


Figure 3.5. The IEDF at the trench bottom compared to the results of Hwang and Giapis [157]. The comparison with the initial IEDF demonstrates that the charging potential strongly affects the ion energy.

3.3 Surface charging on rough surfaces with sinusoidal profiles

The first unconventional surface morphology under study is a 2d sinusoidal PMMA surface with amplitude 0.75 and period 1, i.e. with an AR equal to 3 (Figure 3.6). We define the AR of the sinusoidal profile as the ratio of two times the amplitude over half the period. This definition is

consistent with the trench AR, if we see the trench as a part of a ‘square wave’. The IEADF for Ar^+ as well as the EEADF were the same as those utilized in Section 3.2.

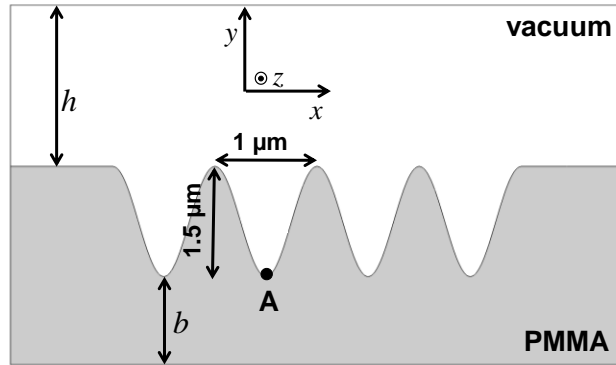


FIG. 3.6. The computational domain in which the two media are shown (vacuum, PMMA). h is the height of the vacuum space and b is the thickness of the PMMA layer. h is $2.2 \mu\text{m}$ and b is $0.1 \mu\text{m}$, $1 \mu\text{m}$ (this figure), $10 \mu\text{m}$, and much larger than h . Point A defines the center of the surface valley where the local ion and electron fluxes and charging potential are shown versus time in Fig. 3.14.

The charging potential in the simulation domain and along the surface profile at steady state are depicted in Figs. 7a and 7b. As in the trench case, the maximum potential is at the bottom of the profile valleys. There is ~44% reduction in the steady state potential at the profile valleys (~45V, see Figure 3.7b) compared to the potential at the trench bottom (~80 V, see Figure 3.4); both the sinusoidal profile and the trench have the same AR (3). The potential reduction in the case of the sinusoidal profile is due to the change in the profile slope which induces mitigation of electron shadowing. The depletion of the electron flux is smaller and so flux balance is achieved for a lower positive charging potential.

Due to the reduction of the potential at the profile valleys, the IEDF at the valleys covers a range of greater energies (18 to 90 eV, Figure 3.7c) compared to the case of trench (0 to 45 eV, Figure 3.5).

In Figure 3.8, the effect of charging on the local ion flux (Figure 3.8a), the local average ion energy (Figure 3.8b), the local average angle of ion incidence (Figure 3.8c), the local etching yield (Figure 3.8d), and the local etching rate (Figure 3.8e) is demonstrated through a comparison to the case without charging. The local average values of ion energy and angle of ion incidence are calculated by the pertinent local distributions.

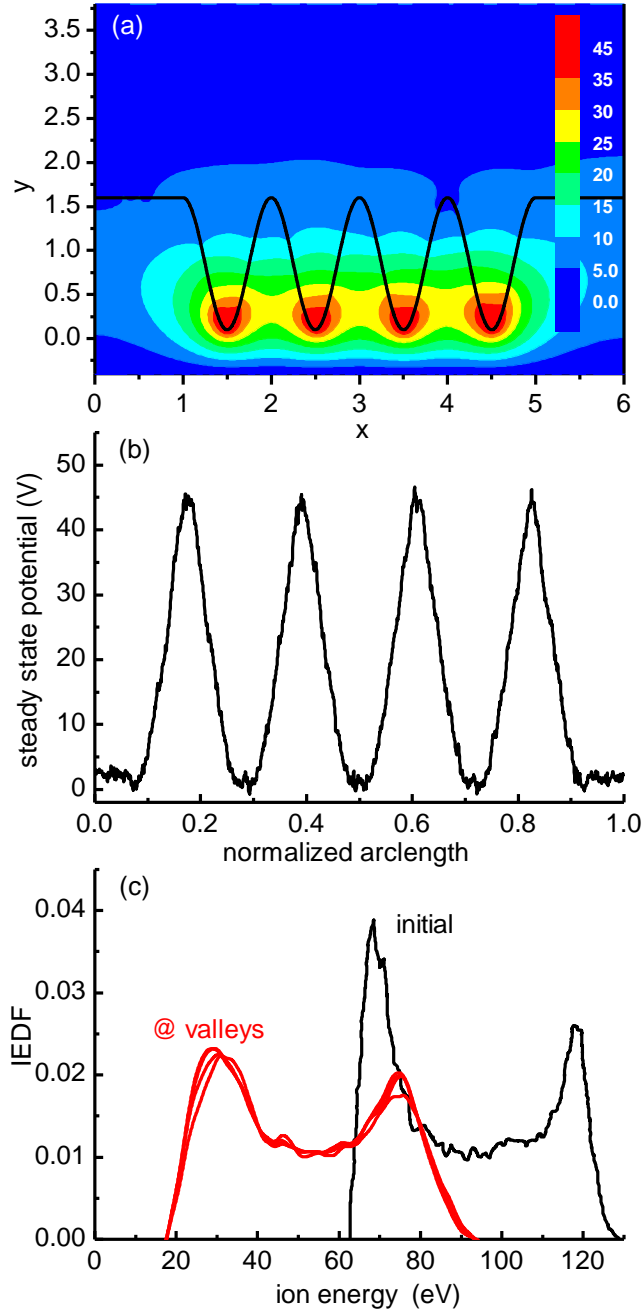


Figure 3.7. Charging potential (in V) a) in the simulation domain and b) along the normalized arclength of the sinusoidal profile at steady state. c) IEDFs at the profile valleys compared to initial IEDF.

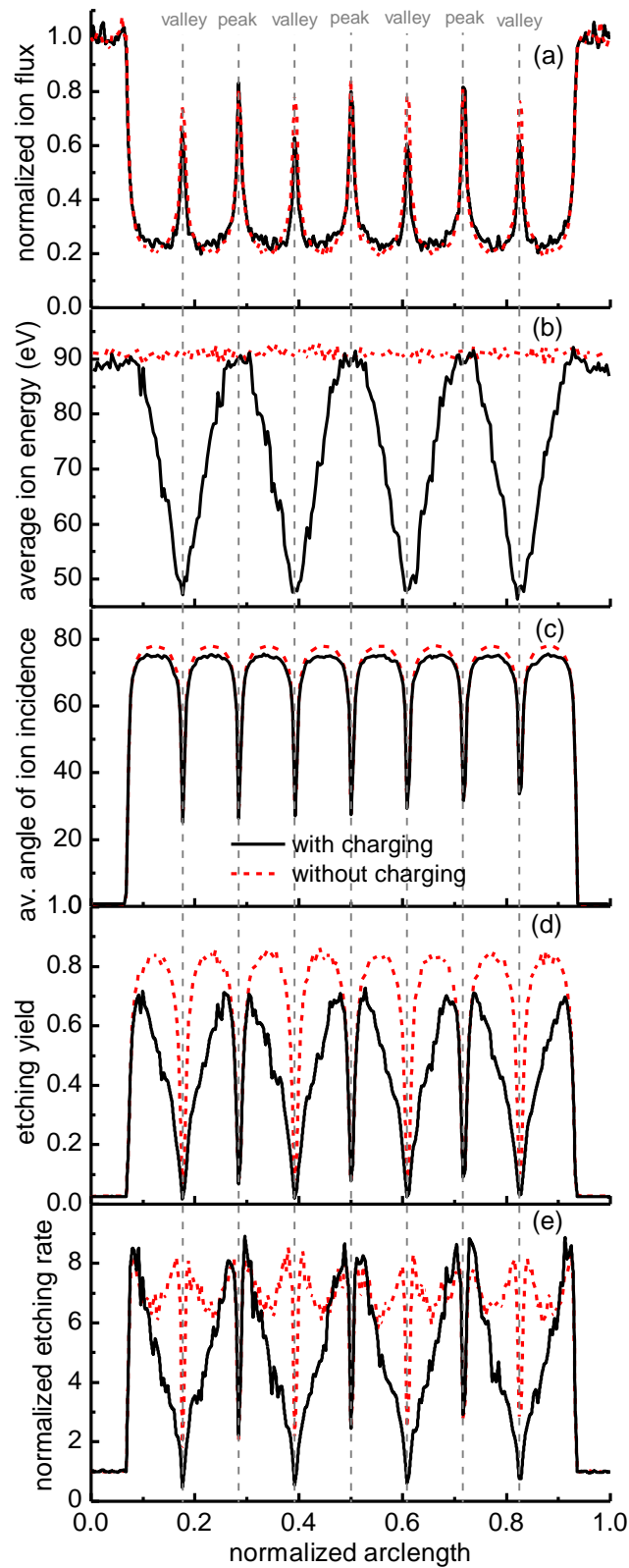


Figure 3.8. a) Normalized (to open area or flat region value) ion flux, b) average energy of impinging ions, c) average angle of ion incidence, d) etching yield, and e) normalized (to open

area or flat region value) etching rate along the normalized arclength of the sinusoidal surface profile with and without charging.

The normalized ion flux along the sinusoidal profile with and without charging is depicted in Figure 3.8a. There is a small reduction ($\sim 16\%$) of ion flux on the profile valleys compared to the case without charging. It has to be noticed, that although there is no electron shadowing (and thus no charging potential) on the profile peaks, the ion flux on these regions is not equal to the ion flux on the flat regions. The origin of this difference is the finite size of the profile segments. The profile slope is zero, i.e. the profile is flat, only at the exact location of the profile peaks and not at the finite sized profile segments at the peaks utilized in the calculations. Due to the small slope of the segments close to the peaks, the local ion flux is lower compared to the flat regions; for a monodirectional (parallel to y axis) IADF, the ion flux is proportionate to the cosine of the angle of ion incidence (Equation 2.15). The same notice for the ion flux applies also for the profile valleys in the case where charging is omitted.

Compared to the small reduction of the ion flux, there is a pronounced reduction ($\sim 53\%$) in the average ion energy at the profile valleys (~ 47.5 eV, Figure 3.8b) compared to their initial average energy (90 eV), following the developed surface potential in Figure 3.7b. The developed steady state charging potential affects not only the particle trajectories but mainly their impinging energy.

The effect of charging on the local average angle of ion incidence angle is shown in Figure 3.8c. Due to the large potential at the valleys, ions are deflected to the sidewalls of the sinusoidal profile as manifested by the slight increase of the ion flux on the sidewalls (see Figure 3.8a). This deflection is demonstrated in Figure 3.8c as a slight decrease of the angle of ion incidence on the sidewalls compared to the case without charging.

In Figure 3.8d, the local etching yield along the surface profile with and without charging is shown. The etching yield is described by Equation 2.16 (see also Figure 2.5) and shows that the etching yield is noticeably enhanced for ion energy greater than 50 eV and angle of ion incidence within a narrow region around 80° . It has to be noticed that the local etching rate is calculated by integrating Equation 2.16 with the local IEADF. In the absence of charging, the etching yield is high at the sidewalls of the sinusoidal surface and very small at the flat regions, i.e. at the profile peaks and valleys. Indeed, for the almost vertical (parallel to y axis) ions impinging on the sidewalls with the high slope, the angle of ion incidence is high (Figure 3.8c) and the etching yield is enhanced. On the contrary, the angle of ion incidence at regions of the profile with zero or small slope is low, and so the etching yield is small. However, if charging is taken into account, the local etching yield decreases as we are moving on the sidewalls from the profile peaks to the profile valleys. This decrease is due to the decrease of the ion energy (Figure 3.8b), and to a lesser extent the decrease of the angle of ion incidence (Figure 3.8c). In Figure 3.8e, the etching rate (Equation 2.14) along the surface profile with and without charging is shown. If charging is taken into account, the etching rate is smaller at the valleys as well as at the sidewalls of the profile.

3.4 The effect of profile AR on surface charging

The calculations are repeated for sinusoidal profiles with AR equal to 1, 2, and 4; the same IEADF and EEADF are considered. The results when charging is taken into account are shown in Figure 3.10. The aim is to investigate the effect of the charging on the etching rate for different surface morphologies, for profiles with different roughness.

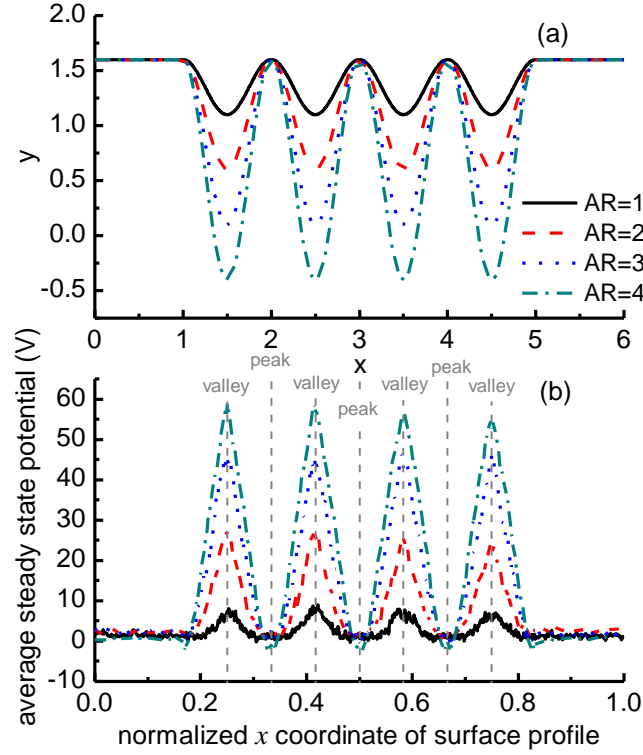


Figure 3.9. a) Surface profiles with different AR (1, 2, 3, and 4). b) Charging potential on the surface profiles along the normalized x coordinate of the profiles (Figure 3.9a). The use of the x coordinate instead of the arclength is made for ease of comparison among results for different AR.

The surface profiles as well as the charging potential along the arclength of the profiles are shown in Figure 3.9a and 3.9b respectively. As the AR increases, the charging potential at the valleys also increases because the electron shadowing is enhanced. Thus, current balance is achieved for a larger positive charging potential; as a consequence, the larger the AR is, the greater the ion energy decrease will be (Figure 3.10b) by virtue of ion deceleration. The increase of the AR also induces an increase of the local average angle of ion incidence (Figure 3.10c) due to the increase of the sidewall slope. Due to this increase of the angle of ion incidence, there is a decrease of the ion flux at the profile sidewalls with AR (Figure 3.10a); for an anisotropic (parallel to y axis) IADF, the local flux is proportional to the cosine of the angle of incidence.

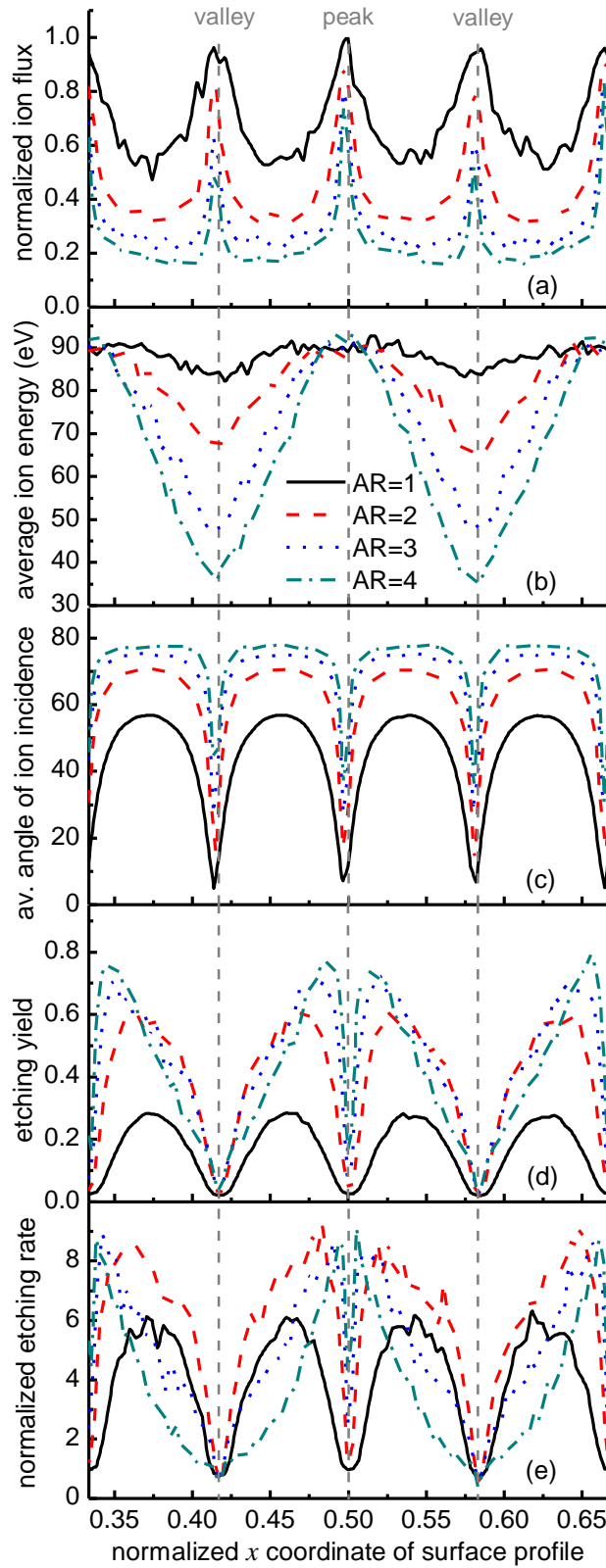


Figure 3.10. a) Normalized (to open area or flat region value) ion flux, b) average energy of impinging ions, c) average angle of ion incidence, d) etching yield, and e) normalized (to open area or flat region value) etching rate along the normalized x coordinate of the sinusoidal surface

profile (Figure 3.12a). Results for sinusoidal profiles with AR 1, 2, 3, and 4 are shown. Only the region of the profiles corresponding to the two middle periods is shown. Charging is taken into account. The same results without charging are included in figure 3.11.

According to the surface etching model (Section 2.2.2.1), the decrease of the ion energy contributes to the decrease of the etching yield while the increase of the angle of ion incidence contributes to the increase of the etching yield (Figure 2.5). The outcome of these two competitive effects is the local etching yield shown in Figure 3.10d. It has to be noticed that in the absence of charging, the ion energy is constant and does not vary with AR, i.e. one of the two effects is not taken into account. For AR greater than 1, the curves in Figure 3.10d are very close except for the sidewall regions close to the peaks; at these regions, the increase of the sidewall slope dominates over the decrease of the ion energy.

In Figure 3.10e, the local etching rate (Equation 2.14) is shown. The local etching rate at the sidewalls increases when the AR increases from 1 to 2. The effect of the (increasing) angle of ion incidence (Figure 3.10c) dominates over the effect of the (decreasing) ion energy (Figure 3.10b) and flux (Figure 3.10a). For greater AR, the local etching rate decreases as the effect of the (decreasing) ion energy and flux dominates over the effect of the (increasing) angle of ion incidence.

In the case of rough surfaces, an overall etching rate is usually measured experimentally. The local etching rate shown in Figures 3.10e and 11e is not a measurable quantity. However, it can be used to calculate an overall or reduced etching rate of the rough profiles of Figure 3.9a; the latter comes from the integration of the local etching rate over the rough surface reduced to the projection of the rough surface to a flat. Given that all surface profiles of Figure 3.9a are the same along the z axis, the reduced etching rate reads

$$ER_{\text{red}} = \frac{\int_{z_1}^{z_2} \int_{x(s_1)}^{x(s_2)} ER(s) ds dz}{\int_{z_1}^{z_2} \int_{x(s_1)}^{x(s_2)} dx dz}, \quad (3.1)$$

where s_1 is the arclength at the end of the first flat region and s_2 is the arclength at the beginning of the right flat region (Figure 3.9a); the flat regions have been excluded from the calculation so as to resemble the results of a periodic rough profile. z_1 and z_2 are the limits of the etched surface on z axis. $x(s_1)$ and $x(s_2)$ are the x -coordinates of s_1 and s_2 respectively.

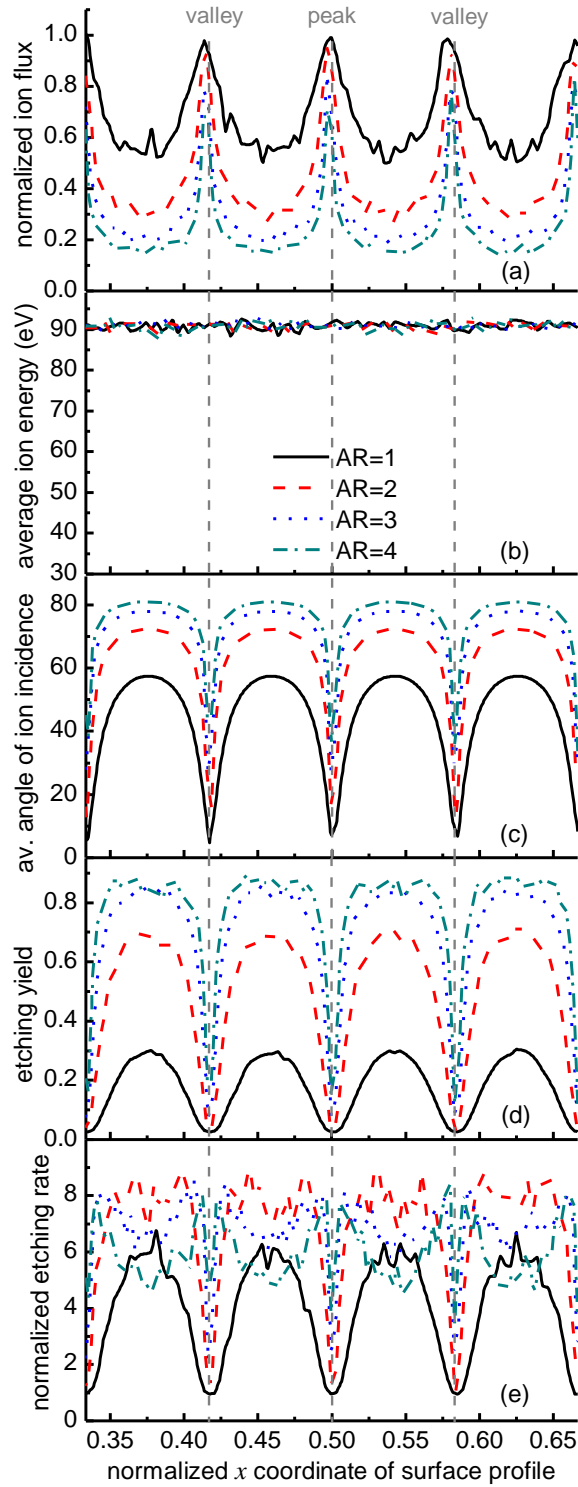


Figure 3.11. a) Normalized (to open area or flat region value) ion flux, b) average energy of impinging ions, c) average angle of ion incidence, d) etching yield, and e) normalized (to open area or flat region value) etching rate along the normalized x coordinate of the sinusoidal surface profile. Results for sinusoidal profiles with AR 1, 2, 3, and 4 (depicted in Figure 3.9a) are shown. Only the part of the profile corresponding to the two middle periods is shown. Charging is not taken into account.

ER_{red} is shown versus the AR of the sinusoidal profile in Figure 3.12. In the same figure, the ER_{red} without charging is also shown; in this case, the increase of the profile arclength and slope dominates over the decrease of the ion flux at the profile sidewalls, and the ER_{red} increases versus AR. In the case of charging, a saturation occurs: ER_{red} is almost constant for AR greater than 2 and at least up to 4. The origin for this saturation is the additional decrease of the ion energy; a decrease which is not considered when charging is not taken into account.

Figure 3.12 shows that charging affects ER_{red} . The latter is calculated from 12.2 % to 35.9 % greater when charging is not taken into account for AR greater than 2. Finally, it has to be noticed that the increase of the AR does not correspond to an increase of the etching time. AR is not necessarily a monotonic function of etching time; as etching time proceeds, we may move back and forth on the x axis of Figure 3.12.

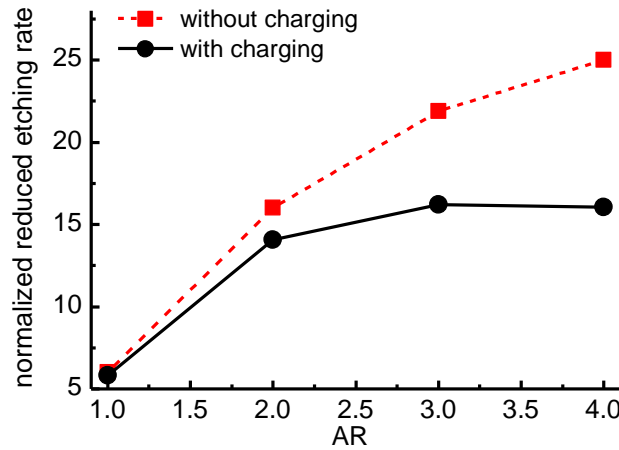


Figure 3.12. Normalized (to open area or flat region value) reduced etching rate (see Equation (1)) of the surfaces with the sinusoidal profiles (Figure 3.9a) vs. the AR of the profiles with and without charging.

3.5 The effect of substrate thickness on charging

The question to be answered is whether the thickness of the dielectric substrate affects the local charging potential and consequently the ion energy and/or the local ion and electron fluxes. If the latter is true, then the thickness will also affect the local etching rate. In Figure 3.13, the local charging potential [Figure 3.13(a)] and the normalized (to open area or flat region value) local ion and electron fluxes [Figures 3.13(b) and 3.13(c)] at steady state are shown for dielectric thickness equal to 0.1, 1, 10 μm , and for infinite dielectric thickness. The term infinite essentially refers to the case the dielectric thickness (b in Figure 3.6) is much greater than the height of the vacuum space (h in Figure 3.6), i.e. refers to the case $h/b \rightarrow 0$. The minimum value examined, i.e. 0.1 μm , is a physical low limit of the thickness value, beyond which, quantum phenomena must be taken into account [119]. From Figure 3.13, it is concluded that the thickness of the dielectric substrate does not affect the value of the local etching rate at steady state. The same conclusion was extracted in Section 3.2 for Ar^+ bombardment on a SiO_2 micro-trench [84].

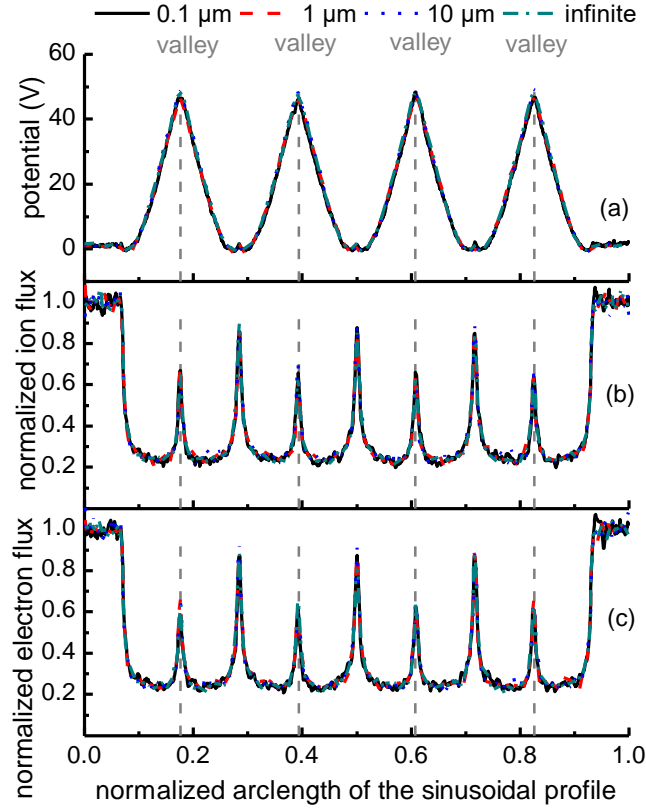


Figure 3.13. a) The local charging potential and the normalized (to open area or flat region value) local b) ion and c) electron fluxes at steady state along the normalized sinusoidal profile for different values of the thickness of the dielectric substrate (0.1, 1, 10 μm , and infinite).

Although the etching rate at the steady state would fall (due to charging) to the same level for all values of thickness, there is an underlying factor that could lead to different etching depths in an experiment: The time required to arrive at the steady state, or the charging time, may be affected by the thickness of the dielectric substrate. A long charging time may allow etching to proceed to greater depths before the steady state is reached and a strong potential is developed. The latter will happen if the charging time is comparable to the total etching time, i.e. the time that the etching process lasts.

In Figure 3.14, the ion and electron fluxes and the charging potential versus time at point A of the surface profile (see Fig. 6) are shown; the thickness of the dielectric substrate is 1 μm . The charging time, i.e. the time required for the potential distribution along the dielectric microstructure surface to arrive at a steady state (or the time that the ion and electron fluxes equalize everywhere on the surface profile), is ~ 1.5 ms and is much lower compared to the etching time which is usually on the order of minutes.

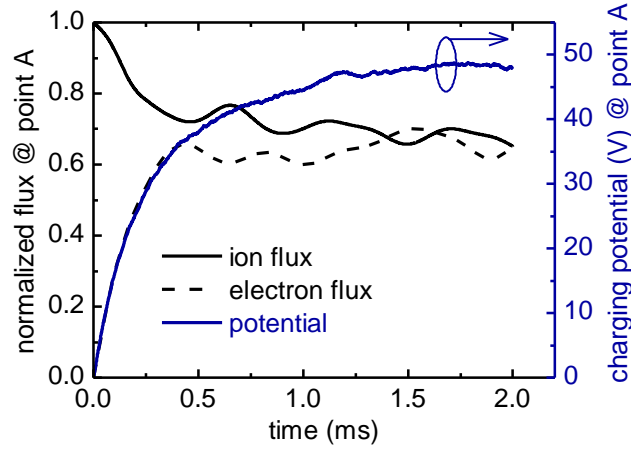


Figure 3.14. Normalized ion and electron fluxes (left y-axis) and charging potential (right y-axis) vs. time at point A (see Fig. 3). The thickness of the dielectric is 1 μm .

The charging time for several values of the dielectric thickness is shown in Figure 3.15. The greater the thickness is, the smaller the charging time is. Analytical calculations on a simplified case explain and verify this calculation (see Appendix D).

Additionally, for all values of thickness, the charging time is in the order of ms and is much smaller compared to the total etching time. This is enough to conclude that the thickness does not affect the etching rate. Although the effect of the dielectric thickness on charging time has not been studied before either in conventional or unconventional surface morphologies, the charging time in microtrenches has been calculated in previous works and has been also found to lie in the range of ms [132, 133, 139, 146, 163, 164, 222]. Moreover, the charging time is much smaller than the time required for a remarkable change of the surface morphology during plasma etching; indeed, for such a short time period (e.g. 1 ms), assuming an etching rate equal to 250 nm/min [maximum value of etching rate in Figure 4.2], the displacement of the surface profile is ~ 4 pm. This is enough to decouple the computations for charging from those for profile evolution (see Chapter 4). The same procedure has been utilized in previous works [139, 140, 146, 163, 164].

For the sake of a low computational cost it is beneficial to perform the calculations with infinite thickness, i.e. for the case $h/b \rightarrow 0$. When $h/b \rightarrow 0$, less computational time is required for the solution and additionally the calculation of the field inside the dielectric can be neglected. It can be shown (see Appendix D) that when $h/b \rightarrow 0$ the solution is equivalent to the case where the surface profile is the bottom boundary of the simulation domain.

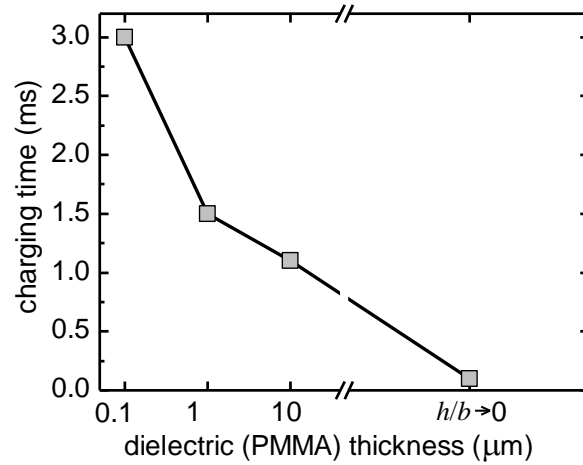


Figure 3.15. Charging time (time to reach the steady state) vs the thickness of the dielectric substrate.

3.6 Conclusions

After verification of the results of the surface charging module with a seminal work [157] in conventional structures, the surface charging module was utilized for the calculation of charging on surfaces with sinusoidal profiles. Calculations with and without charging were performed. The main difference between the two cases was the decrease of the ion energy due to the surface charging potential which was absent when charging was not taken into account. It was shown that charging did affect the reduced etching rate of a surface with a rough, sinusoidal in our case, profile.

The effect of charging on the local fluxes, energies, etching yield and rates on surface profiles with different roughness was studied. Charging is expected to affect the evolving roughness of the etched surface as well. Thus, it is necessary to take charging into account during the evolution simulation of rough polymeric - and generally rough dielectric- surfaces during plasma etching. This is the subject of the Chapter 4.

It has to be noticed that the origin of the roughness of the PMMA surfaces was also out of the scope. The aim was to study the effect of charging on surfaces with different roughness without elaborating on the origin of this roughness. The measure of roughness was the aspect ratio of the surface profiles, i.e. the ratio of two times the amplitude over the half the period of sinusoidal profiles. It was shown that the aspect ratio of the surface profiles did not strongly affect the reduced etching rate for aspect ratio from 2 to at least 4.

Finally, it was found that although the thickness of the dielectric substrate affected the charging time, i.e. the time required for reaching a steady state charging potential, it did not affect the roughness evolution; the charging time was much shorter than the etching time (which is usually in the order of minutes) for all values of thickness (0.1 μm to infinite thickness for surface roughness at the microscale), especially it was calculated in the order of milliseconds.

This chapter has been published as a part of the following articles:

a) G. Memos, G. Kokkoris, Modeling of Charging on Unconventional Surface Morphologies of PMMA Substrates during Ar Plasma Etching, Plasma Processes and Polymers 13 (2016) 565-578.

b) G. Memos, E. Lidorikis, G. Kokkoris, The interplay between surface charging and microscale roughness during plasma etching of polymeric substrates, J Appl Phys 123 (2018) 073303.

4. The intertwined effects of surface charging, ion reflection, and secondary electron-electron emission on roughness evolution during Ar plasma etching of polymeric substrates

4.1 Introduction

The **first objective** of this chapter, filling the pertinent lack in the literature, is to investigate the interplay between surface charging and roughness during plasma etching of polymeric substrates; specifically, to examine the development of charging on the rough surface (profile) being etched and its effect on the roughness evolution. The evolution of surface roughness with and without charging and under two different etching mechanisms is studied. In the first etching mechanism, the etching yield depends on the ion energy and in the second one, besides the ion energy, it depends on the angle of ion incidence.

First, no mechanisms enhancing the roughness are taken into account so as to isolate the interaction of charging and roughness. Afterwards, such a mechanism, namely ion reflection (Section 2.2.1.3), is taken into account and integrated into the surface charging module of the modeling framework. Ion reflection is expected to enhance roughness [52] by increasing the flux of ions at the valleys of the surface morphology. Besides ion reflection, the mechanism of SEEE is the second amendment to the surface charging module: an original detailed model for the SEEE yield is developed for PMMA substrates in the energy range which is of interest in plasma etching (Section 2.2.1.2). SEEE and the consequent electron redistribution on the dielectric surface could affect surface charging, as demonstrated in previous simulation studies on plasma etching of dielectric trenches [166, 167]. The secondary ion-electron emission (SIEE) is not considered as it was found that, in the presence of SEEE, SIEE had an insignificant impact on the formation of the charging potential [167].

Toward the comprehension and, finally, the control of plasma induced surface roughness, the **second objective** of the current chapter, filling the relevant gap in the literature, is to record how charging is developed on the rough profile being etched and how it affects the evolving roughness of the profile, in the presence of ion reflection and SEEE. First efforts are also implemented in order to quantify the correlation between the surface roughness and the charging potential: the scaling of the charging potential to a combination of suitable statistical properties of the surface roughness is investigated.

The objectives of this chapter are attained by the modeling framework for the evolution of rough polymeric surfaces under plasma etching, which is properly extended to capture the effects of ion reflection and SEEE (Section 2.2). The model system involves etching of a PMMA substrate by Ar plasma. The etching mechanism is physical sputtering by Ar^+ .

The rest of this chapter is organized in the following way: The model system and the case study are portrayed in Section 4.2. The interplay of charging and surface roughness is investigated through the evolution of the profile, charging potential, etching rate, and root mean square roughness versus the etching time are demonstrated in Section 4.3. In Section 4.4, the interplay

of surface charging, ion reflection, SEEE, and surface roughness is studied. The conclusions are summarized in Section 4.5.

4.2 Case Study

The case study is plasma etching of a PMMA substrate with a sinusoidal, simulating a rough, profile (Figure 4.1). The etching mechanism is physical sputtering by Ar^+ . The ion energy and angle distribution functions (IEADFs) for Ar^+ as well as the electron energy and angle distribution functions (EEADFs) are the same as in Section 3.2. The mean energy of ions and electrons are 90 and 4 eV, respectively. The ion angular distribution resembles a Gaussian and the electron angular distribution is isotropic. The ion flux is $1.86 \times 10^{20} \text{ m}^{-2}\text{s}^{-1}$. The dielectric constant of PMMA is equal to 3. A substrate with a high (infinite) thickness is considered. The role of the substrate thickness on charging has been analyzed previously (see Section 3.5 and Reference [83]) and it has been found that although the thickness of the dielectric substrate affected the charging time, i.e., the time required for reaching a steady state charging potential, it did not affect the roughness evolution: the charging time was much shorter than the etching time for all values of thickness ($0.1 \text{ }\mu\text{m}$ to infinite thickness for surface roughness at the microscale).

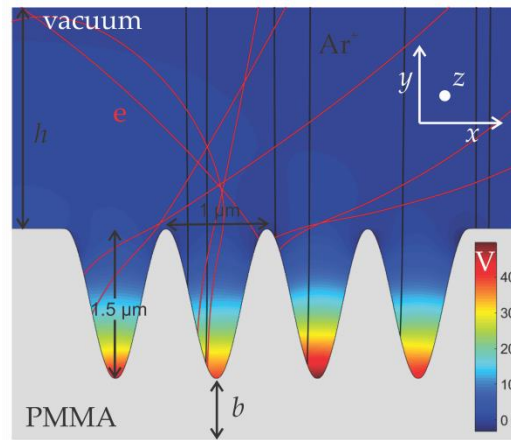


Figure 4.1. The initial sinusoidal profile of the PMMA surface. The steady state potential as well as some of the ion (in black) and electron (in red) trajectories are also depicted. h is the height of the vacuum space, and b is the thickness of the PMMA layer. h is $2.2 \text{ }\mu\text{m}$, and $b \gg h$.

4.3 Evolution of the surface profile with and without charging

The effect of charging on the evolution of the surface profile for two etching mechanisms is investigated. In the first mechanism, the etching yield depends on the ion energy (Equation 2.20 with $f(\theta)=1$) and in the second one, besides the ion energy, it depends on the angle of ion incidence (Equation 2.20).

4.3.1 Results for energy dependent etching yield

In Figure 4.2 snapshots of the surface profile for different etching times with [Figure 4.2b] and without [Figure 4.2a] charging are shown. The charging potential for the snapshots of Figure 4.2b is shown in Figure 4.2c.

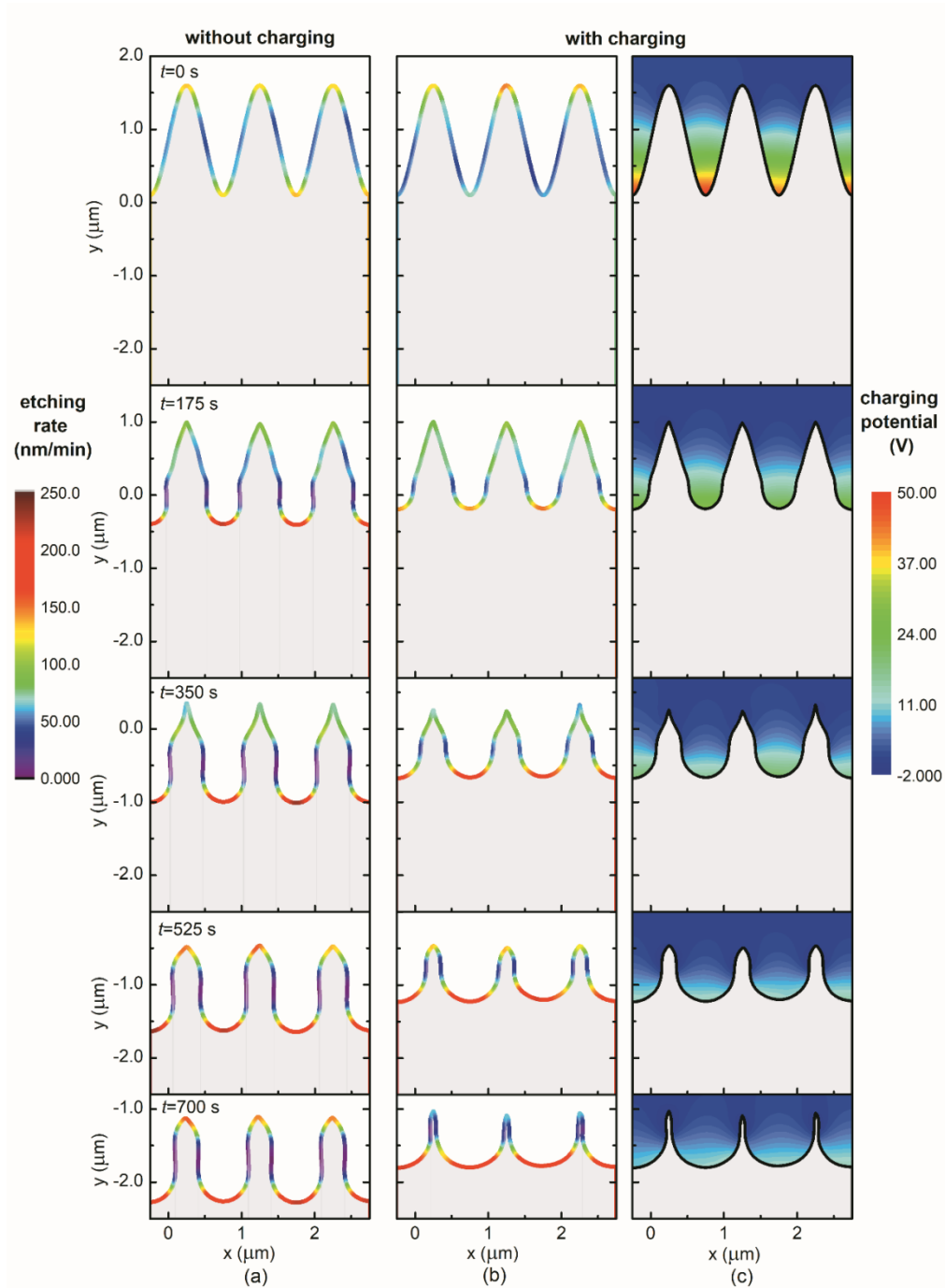


Figure 4.2. Snapshots of the surface profile for different etching times a) without charging and b) with charging, when the etching yield depends on the energy of the impinging ions. The profiles are cropped from the middle of the first valley to the middle of the last one. The color of the

profile curves denotes the magnitude of local etching rate. c) The charging potential for snapshots of Figure 4.2b is depicted in Figure 4.2c. A substrate with a high (infinite) thickness is considered.

In the case without charging [Figure 4.2a], the slope of the profile sidewall increases during etching and a columnar profile is gradually formed. In particular, the etching rate is lower at the middle part of the profile sidewall compared to the upper and down part of the sidewall (see e.g. the snapshots at 0 s, the color of the profile curve denotes the magnitude of the local etching rate) because the slope of the sidewall is greater at the middle part; the parts of the profile with high slope will receive lower ion flux compared to parts with low slope as the ion flux is proportionate to the cosine of the angle of ion incidence. Due to this difference in the local ion flux and as a consequence in the local etching rate, the down part of the sidewall is etched faster (compared to the middle part) and the slope of the sidewall increases and becomes almost vertical (parallel to y axis, see the snapshots at time ≥ 175 s). The columnar profile is retained as the ion flux received by a vertical sidewall is very small.

However, when charging is involved in the process [Figure 4.2b], the difference of the etching rate between the middle and down part of the sidewall of a profile peak is mitigated (see the snapshots at 0 s). This is because the charging potential developed at the valleys acquires a positive value capable of deflecting an amount of ions on the sidewalls. This deflection leads to an increase of the local ion flux (the angle of ion incidence is decreased) and hence to an increase of the local etching rate at the sidewalls. At the same time, the charging potential affects the energy of the impinging ions: The ion energy is lower at the parts of high charging potential, i.e. at parts of lower y coordinate [see Figure 4.2c], which induces an attenuation of the etching rate. The synergy of the ion deflection towards the sidewalls at the initial stages of the etching process with the decrease of the ion energy at parts of lower y coordinate (during the whole etching process) endows the sidewalls a smaller slope compared to the case without charging. Due to the formation of profile peaks with lower sidewall slope, the local etching rate is greater at the sidewalls and as a consequence the profile peaks are thinned faster in the case of charging.

In Figure 4.3a, the root mean square (rms) roughness of the evolving profile with and without charging is shown. The rms decreases in both cases. The rms decreases faster in the case of charging which is attributed to the greater local etching rate at the sidewall of the profile. The rms evolution in Figure 4.3a essentially quantifies the faster elimination of the profile peaks in the case of charging (Figure 4.2a and 4.2b) and shows that surface charging contributes to a decrease of the surface roughness; if charging did not exist, then the surface roughness of polymeric substrates would have been greater. Charging not only affects roughness evolution but it is also affected by it: The decrease of the surface roughness (Figure 4.2b) contributes to a decrease of the charging potential (Figure 4.2c).

In Figure 4.3b, the etching rate versus the etching time with and without charging is shown. The etching rate has been calculated by the time derivative of the mean height of the profiles. Without charging, the etching rate remains almost constant for the whole etching process. The etching rate is always smaller with charging than without; this is due to the decrease of the ion energy in the case of charging. The increase of the etching rate versus time in the case of charging is caused by the decrease of the charging potential (Figure 4.2c): The latter originates

from the gradual mitigation of electron shadowing due to the widening of the valleys of the profile.

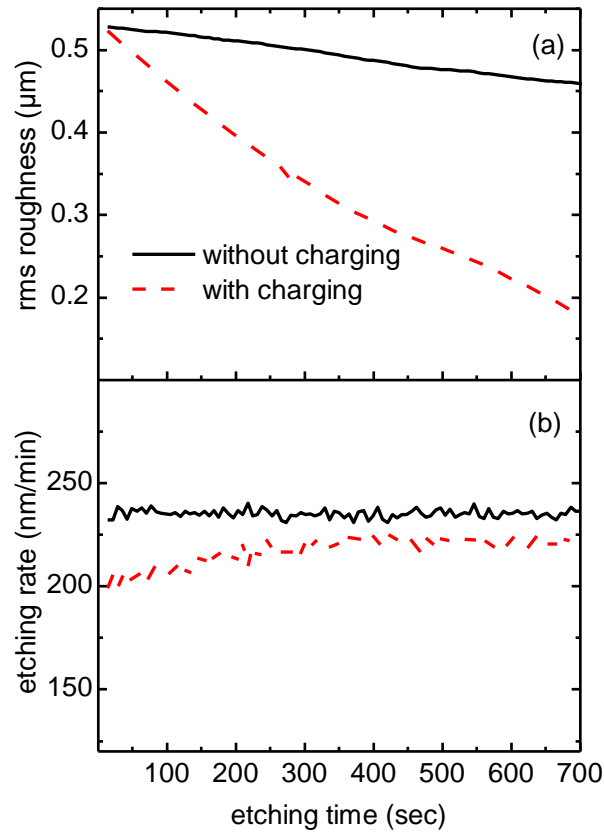


Figure 4.3. a) rms roughness and b) etching rate vs etching time (with and without charging) for the surface profiles shown in Figures 4.2a and 4.2b.

4.3.2. Results for angle and energy dependent etching yield

In Figure 4.4 snapshots of the surface profile for different etching times with [Figure 4.4b] and without [Figure 4.4a] charging are shown. The charging potential for the snapshots of Figure 4.4b is shown in Figure 4.4c.

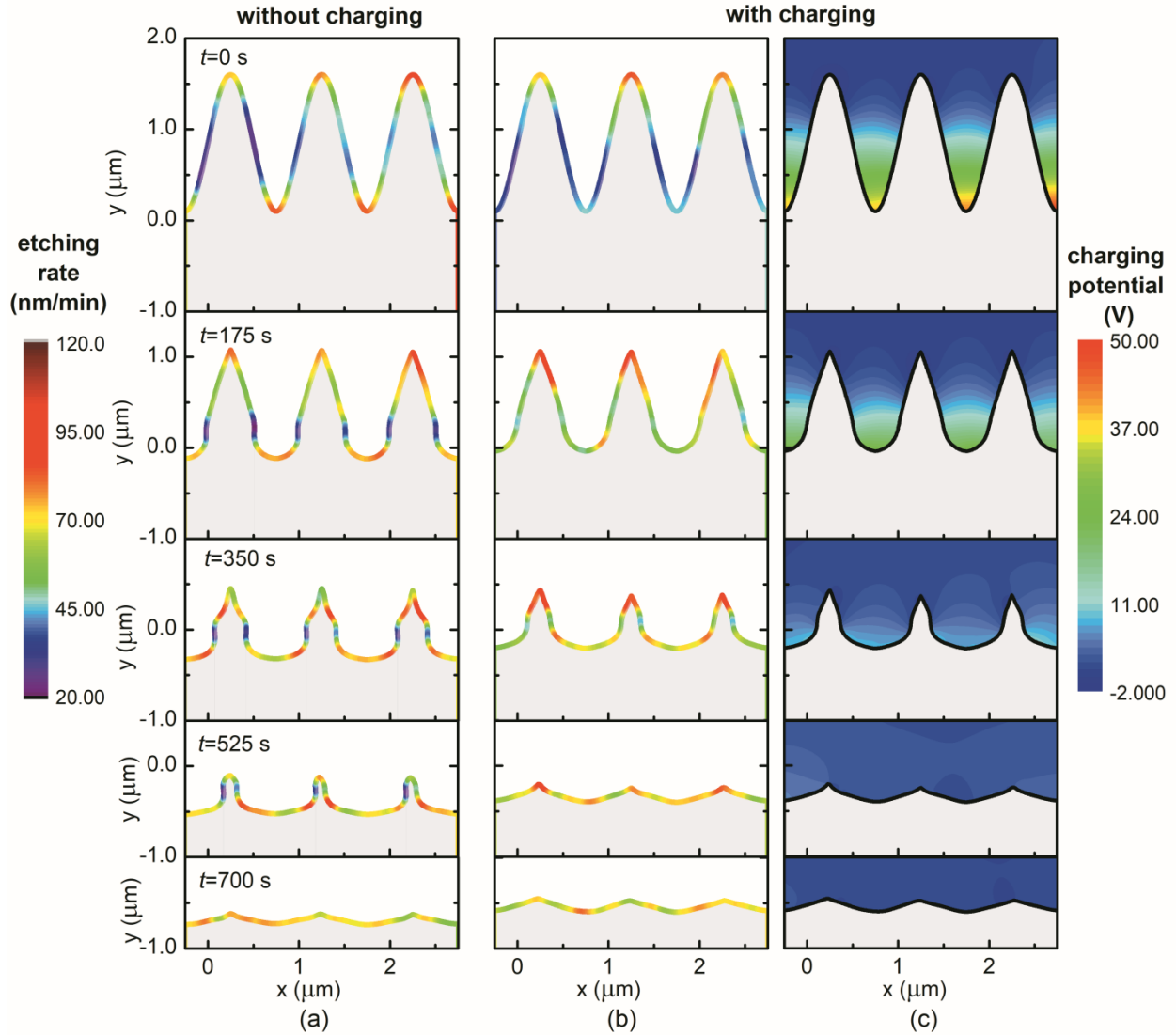


Figure 4.4. Snapshots of the surface profile for different etching times a) without charging and b) with charging, when the etching yield depends on both the energy and the angle of incidence of the impinging ions. The profiles are cropped from the middle of the first valley to the middle of the last one. The color of the profile curves denotes the magnitude of local etching rate. c) The charging potential for the snapshots of Figure 4.4b. A substrate with a high (infinite) thickness is considered.

Either with or without charging, the profile peaks are thinned during etching. The peaks are thinned slightly faster in the case of charging (Figure 4.4b). This is reminiscent of the previous case (energy dependent etching yield, Section 4.3.1). However, the dependence of the etching rate (yield) on the angle of ion incidence, i.e. on the profile slope, leads to the complete eradication of the surface peaks either charging is taken into account or it is not. At the lower part of the sidewalls, the profile slope is lower, and thus the angle of ion incidence and the etching yield are lower compared to those at the middle part. On the other hand, due to the lower profile slope, the ion flux is greater at the lower part of the sidewall compared to that at the middle part. Thus, the difference of the etching rate (i.e. the product of the etching yield with the

ion flux) between the lower and the middle part of the sidewall is mitigated and endows the sidewalls a smaller slope (compared to Figure 4.2a) although charging is not present. Due to this small slope the etching rate at the sidewalls is sustained and as a consequence the profile peaks are eliminated in almost the same rate as in the case of charging.

In Figure 4.5a, the rms roughness of the evolving profile with and without charging is shown. The rms decreases in both cases as in Figure 4.3a. However, the rms decreases only slightly faster in the case of charging compared to Figure 4.3a and this essentially quantifies the slightly faster elimination of the profile peaks in the case of charging (Figures 4.4b and 4.4a). At the final stage of the etching process ($t > 500$ s in the case of charging and $t > 670$ s in the case without charging), the rms decreases at a much lower rate; the latter is due to the almost complete eradication of the profile peaks. Up to this stage, as in the case of energy dependent etching yield (Section 4.3.1), it is shown that surface charging contributes to a faster decrease of the surface roughness. As in the case of energy dependent etching yield (Section 4.3.1), charging not only affects roughness evolution but it is also affected by it: The decrease of surface roughness (Figure 4.4b) contributes to a decrease of the charging potential (Figure 4.4c).

In Figure 4.5b, the etching rate versus the etching time with and without charging is shown. With or without charging, the etching rate decreases with etching time. This decrease is due to the decrease of the etching yield. In particular, the gradual decrease of the local slopes of the surface profile, manifested by the progressive smoothing of the profile observed in Figures 4.4a and 4.4b, leads to the consequent decrease of the angle of ion incidence. This is equivalent to shifting the value of the angle of incidence to the left on the x -axis of Figure 2.6, and, hence, equivalent to decreasing the etching yield. The decrease of the local etching yield overcomes the increase of the local ion flux induced by the same source, i.e. the decrease of the local profiles slopes. The effect of charging on the etching rate is due to the charging potential (Figure 4.4c) which decreases the ion energy and as a consequence the etching yield (see Equation 2.20). Notice that at $t = 700$ s the etching rates with and without charging are almost equal: Due to eradication of the profile peaks, the electron shadowing is mitigated, the charging potential is close to zero (Figure 4.4c), and thus the effect of charging is eliminated.

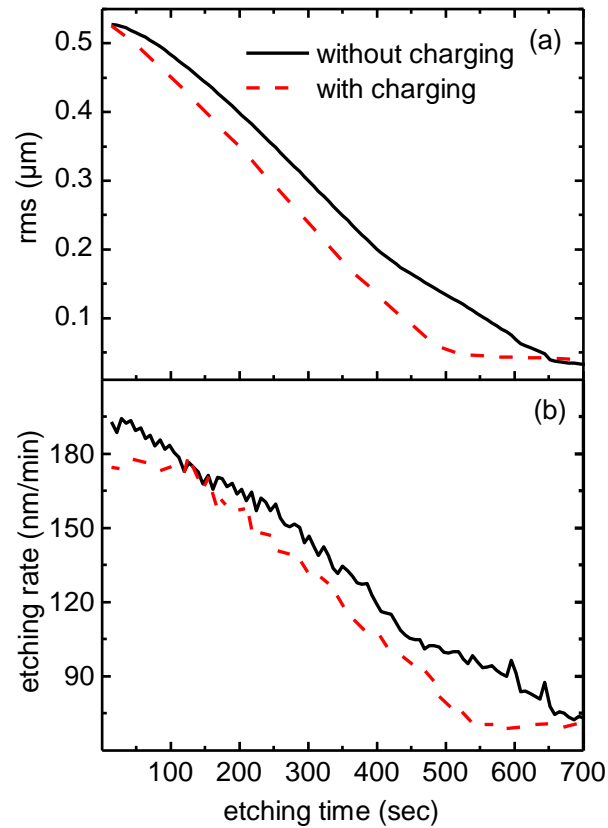


Figure 4.5. a) rms roughness and b) etching rate vs. etching time (with and without charging) for the surface profiles shown in Figures 4.4a and 4.4b.

4.4 The effects of ion reflection and secondary electron emission

Three mechanisms are considered responsible for intertwining with roughness evolution, i.e., ion reflection, surface charging, and SEEE. They are reviewed separately in terms of numerical models, which evaluate the corresponding importance of each mechanism on the total process of roughness evolution. The purpose of the simulation is to quantify the effect and, thus, to identify the role of the individual mechanisms on the roughness evolution. The etching yield depends on both the ion energy and the angle of ion incidence (Section 4.3.2).

In Figure 4.6, the profile evolution of the initial sinusoidal profile in the absence of ion reflection is depicted. Charging is omitted in Figure 4.6a, while, it is considered in Figure 4.6b; the charging potential is also included in Figure 4.6b. It is shown that the profile peaks are almost wiped out at the final stage ($t > 525$ s) either charging is considered or not. The latter is attributed to the strong angle dependence of the etching rate which mitigates the effects of charging (Section 4.3.2). Although the etching (sputtering) yield depends on both the ion energy and the angle of ion incidence (Equation 2.20 and Figure 6), the effect of ion incidence, and as consequence of the profile slope, dominates. This dominance originates from the big increase of

the etching yield at angles of ion incidence in the range of 60° - 80° . In case there is no angle dependence, a different behavior is expected (Section 4.3.1).

It has to be noticed that the peaks are reduced slightly faster in the case of charging (cf. Figures 4.6b and 4.6a). The joint action of the ion deflection toward the sidewalls with the attenuation of the ion energy at parts of lower y coordinate induces a smaller slope to the sidewalls compared to the case without charging (Figure 4.6a). Consequently, the angle of ion incidence at the sidewalls of the peaks is smaller in the case of charging approaching the maximum of the etching yield (Figure 2.6). Thus, the local etching rate is higher at the sidewalls (figures 4.4a and 4.4b), and subsequently, the profile peaks are eradicated at a faster pace when charging is involved in the process.

In Figure 4.6c, besides charging, SEEE is also included. Comparing it with Figure 4.6b, hardly few differences are distinguished in the evolving profiles. However, the charging potentials at $t = 0$ s differ. The initial profile (Figure 4.6b, $t = 0$ s) induces heavy geometric shadowing in the isotropic electron flux. Most electrons impinge on the upper region of the surface sidewalls. As the positive potential is developing in the valley region, electrons are attracted there in order to compensate the overwhelming initial current imbalance. In the absence of SEEE, such current balance is attainable for a potential of 45 V. With the inclusion of SEEE (Figure 4.6c, $t = 0$ s) the charging potential is reduced $\sim 50\%$ because a larger electron flux impinges at the valley region. Indeed, due to the emerging positive potential, it is more probable for a secondary (or a reflected) electron to terminate its trajectory at the valley region during the charging process. Thus, in order for current balance to be restored, a lower potential is needed. However, the effect of the SEEE in the charging development is mitigated as the profile evolves and eventually it is disappeared for $t > 175$ s (Figures 4.6b and 4.6c at 175 s and 350 s). After this time, the profile valleys are wide enough to reduce the electron shadowing and receive the great majority of the incident electrons. Hence, the charging potential is the same to that in the absence of SEEE (Figures 4.6b and 4.6c at 350 s).

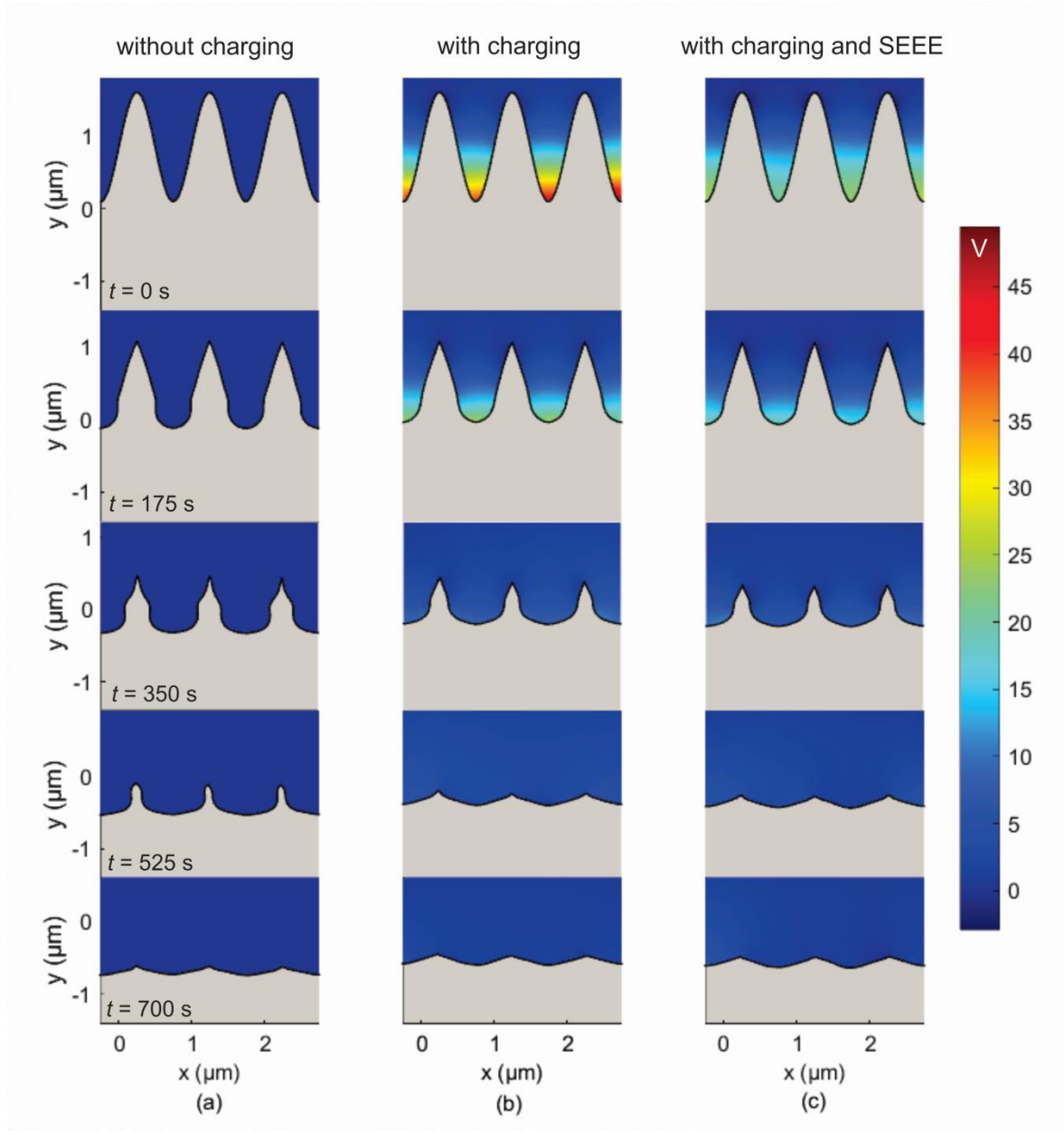


Figure 4.6. Snapshots of the surface profile for different etching times a) without charging, b) with charging, and c) with charging and SEEE, when the ion reflection is not taken into account. The profiles are cut from the middle of the first valley to the middle of the last one. The charging potential for the snapshots of Figures 4.6b and 4.6c is also depicted.

In Figure 4.7 the same results as in Figure 4.6 are shown including the ion reflection mechanism. Charging is omitted in Figure 4.7a, while it is considered in Figure 4.7b, and ultimately, in Figure 4.7c, besides charging, SEEE is also taken into account. First, by comparing Figures 4.6a and 4.7a, 4.6b and 4.7b, and 4.6c and 4.7c, it is shown that when the ion reflection is taken into account, the profile features are sustained until the end of the etching time, i.e., roughness is not eliminated. Second, when charging is taken into account, the peaks of the profile are shorter and thinner (cf. Figures 4.7b and 4.7a). Third, as in the case without ion

reflection, although SEEE initially ($t < 175$ s) induces a decrease of the charging potential, there are no apparent differences in the profiles with and without SEEE (cf. Figures 4.7b and 4.7c). This is because the available surface for electron reflection or emission towards the valleys is reduced. The SEEE mechanism just redistributes the incident electrons locally in the profile valleys and this local redistribution does not affect significantly the electron flux (and hence the electric potential).

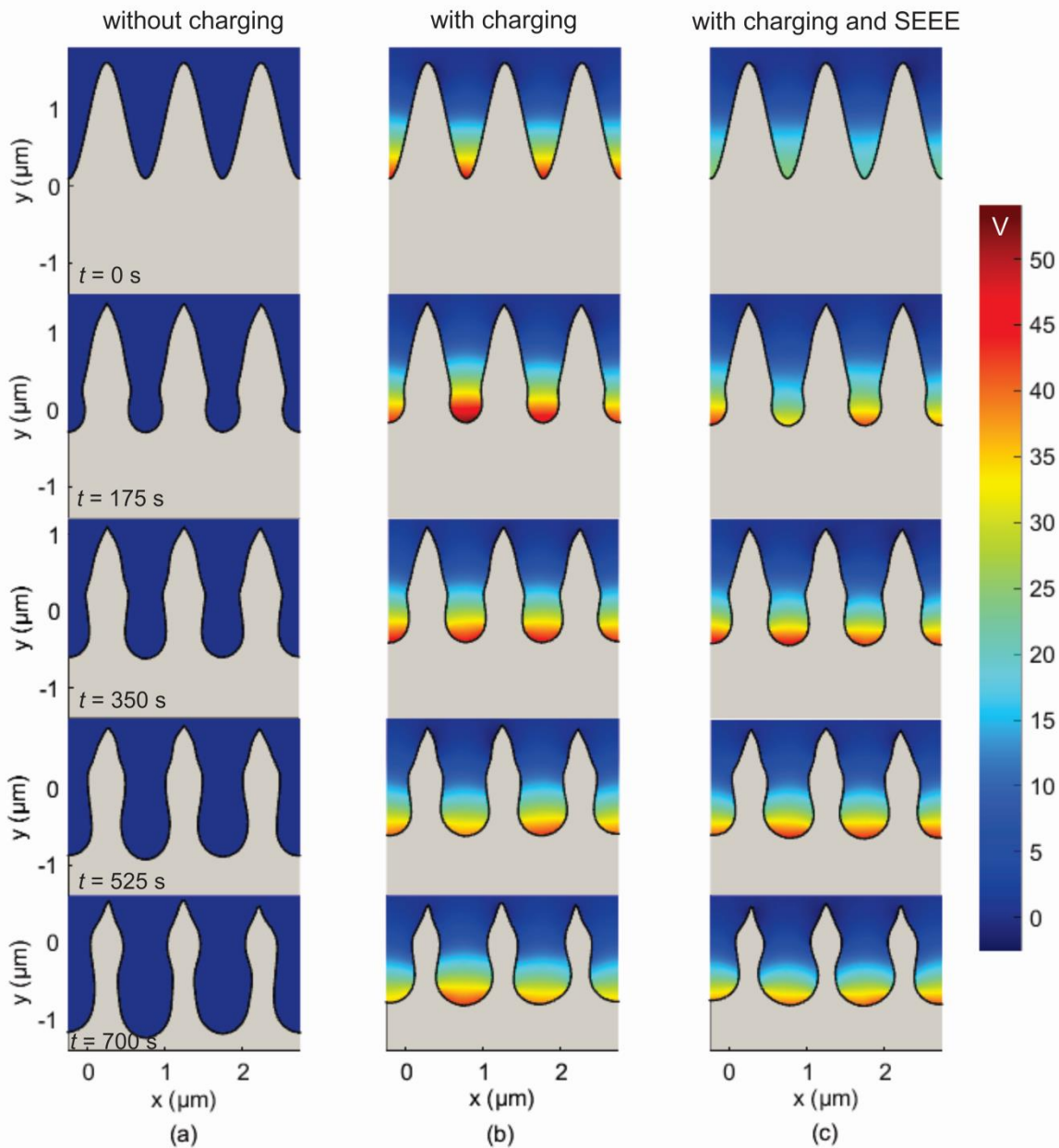


Figure 4.7. Snapshots of the surface profile for different etching times a) without charging, b) with charging and c) with charging and SEEE, when the ion reflection is taken into account. The profiles are cut from the middle of the first valley to the middle of the last one. The charging potential for snapshots of Figure 4.7b and 4.7c is also depicted.

The *rms* roughness of the evolving profiles in Figures 4.6 and 4.7 versus the etching time is shown in Figure 4.8. The eradication of the profile peaks when ion reflection is not taken into account (Figure 4.6) is manifested by the decrease of the *rms* roughness versus time. The slightly faster eradication of the peaks due to charging is substantially quantified by the marginally faster attenuation of the *rms* roughness. When ion reflection is taken into account (Figure 4.7) and in the absence of charging, the *rms* roughness increases initially but finally comes to a saturation as the “competitive forces of the process”, i.e. the angle dependent physical sputtering and the ion reflection, come to a balance. When both charging and ion reflection are considered, the *rms* roughness initially increases and after approximately 250s starts to fall. Charging not only restrains the *rms* roughness at the initial stages of etching but, subsequently, it induces a decrease of the *rms* roughness. Finally, as demonstrated in Figure 4.8, either with or without ion reflection, the effect of SEEE on the evolution of the *rms* roughness over etching time is marginal.

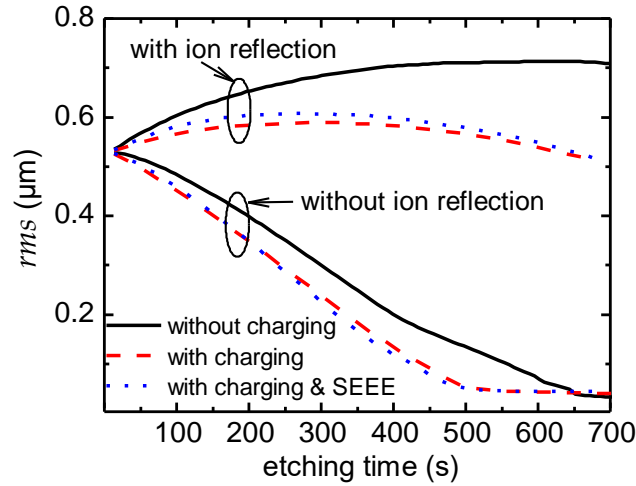


Figure 4.8. The *rms* roughness vs. the etching time for the surface profiles shown in Figures 4.6 and 4.7.

The correlation of the surface charging potential with the profile roughness has been demonstrated previously (Sections 3.4, 4.3.1 and 4.3.2). We have shown that charging is controlled by the aspect ratio for a sinusoidal profile (Section 3.4). The aspect ratio is determined as the ratio of two times the amplitude over the half period of the profile and reflects the significance of the electron shadowing effect. However, the aspect ratio cannot be defined for random rough profiles emerging in plasma based surface engineering applications. In an attempt to quantify the significance of the electron shadowing effect of such profiles on the surface charging potential, parameter *m* is proposed, which reads

$$m = \left(\frac{rms}{\lambda} \right) \frac{1}{c + skewness} \quad (4.1)$$

where λ is the distance between the surface peaks. The *skewness* of the profile quantifies the asymmetry of the distribution of the profile heights with respect to the mean profile height [223]. Generally, a surface with bumps has a positive skewness while a surface with holes has a negative skewness [50, 224]. c in Equation 4.1 is a unitless constant with a positive value (1/2 in this work) so as to avoid division by zero or very large values when the *skewness* approaches 0. m quantifies the competitive effect between the ratio rms/λ and the *skewness* on the electron shadowing. Electron shadowing is enhanced when the ratio rms/λ increases, i.e., when the surface features (e.g. bumps, peaks or holes) are greater and at close range. Electron shadowing is also expected to be heavier for lower *skewness*, i.e., for surface profile comprised mainly by valleys (or a surface morphology comprised mainly by holes).

Figure 4.9 includes the charging potential at the bottom of the valleys (average value at the four valleys) versus m for the evolving profiles shown in Figures 4.6 and 4.7. The arrows on the curves denote the time path during etching. Without ion reflection, the charging potential decreases with the decrease of m , either SEEE is taken into account or not. With ion reflection and without SEEE, there is an almost linear correlation between the potential and m . This linear correlation is disturbed when SEEE is taken into account and is restored when the SEEE effect fades away: the two curves after point A almost coincide. This coincidence is also true for the curves without ion reflection after point B. Figure 4.9 demonstrates that, besides the different mechanisms and phenomena taken into account (with or without SEEE, with or without ion reflection), the mutual interaction between surface charging and profile roughness is present in all cases examined.

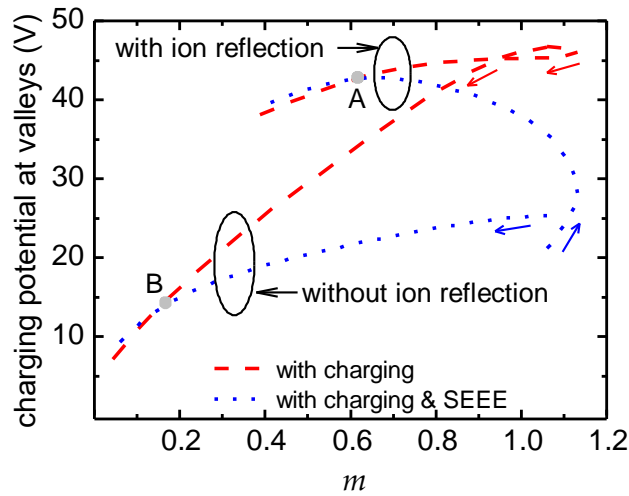


Figure 4.9. The charging potential (average value of potential at the four valleys of the profile) vs. parameter m (Equation 4.1). The arrows on the curves denote the time path during etching. Values above 500s of etching for the curves corresponding to cases without ion reflection have been removed as the profiles are almost flat (cf. Figure 4.6). The small difference (~ 3 V) observed in the initial potential between the two cases of SEEE is an expected difference between two runs of a stochastic process.

4.5 Conclusions

Toward the comprehension and, finally, the control of plasma induced surface roughness, we delved into the intertwined effects of ion reflection, surface charging, and SEEE on roughness evolution during physical sputtering of a PMMA substrate with Ar plasma. For this, a modelling framework for profile evolution of polymeric surfaces under plasma etching was utilized. The framework was extended to include SEEE and ion reflection.

The investigation showed that the roughness of an initially rough profile decreased faster if charging existed compared to the case of no charging. This practically reveals a mechanism which contributes to the decrease of surface roughness of dielectric substrates; this mechanism is not present in the case of conductive materials. Besides roughness, charging also decreases the etching rate of rough dielectric substrates. Regarding the effect of roughness on charging, the decrease of the roughness contributed to a decrease of the charging potential developed on the etched surface. The effect of charging on the roughness and the etching rate of dielectric substrates was found more intense in the case of energy (and not angle) dependent etching yield; when an angle dependence was present, the differences in the roughness with and without charging were mitigated.

The effect of SEEE on the evolution of *rms* roughness was marginal. When the ion reflection was considered, the profile features were preserved until the end of the etching time, i.e. roughness was not wiped out. In that case, charging not only constrained the *rms* roughness at the initial stages of etching but, afterwards, it led to a decrease of the *rms* roughness.

The charging potential was correlated to the profile roughness through a parameter which suitably combines statistical properties of the profile such as *rms* roughness and *skewness*. Regardless of the mechanisms and the phenomena taken into account, the charging potential showed an almost monotonic behavior with this parameter, something that revealed the mutual interaction between surface charging and profile roughness.

This chapter has been published as a part of the following articles:

- a) G. Memos, E. Lidorikis, G. Kokkoris, The interplay between surface charging and microscale roughness during plasma etching of polymeric substrates, J Appl Phys 123 (2018) 073303.**
- b) G. Memos, E. Lidorikis, G. Kokkoris, Roughness evolution and charging in plasma-based surface engineering of polymeric substrates: The effects of ion reflection and secondary electron emission, Micromachines 9 (2018).**

5. Investigation of roughness evolution during O₂ plasma etching of polymeric surfaces

5.1 Introduction

O₂ and O₂-containing plasmas offer a great potential for the surface functionalization of polymeric substrates: thermal reactive neutral species are combined with high energy ions to alter both micro/nanomorphology and composition of polymeric surfaces in a dry means of processing. Although plasma processing is an attractive option for the polymer surface modification, plasma-surface interactions are complex and the process design is usually based on a trial and error procedure. Towards comprehensive process design, a hybrid modeling framework, addressing both effects of plasmas on polymeric surfaces, is developed and applied to the investigation of O₂-plasma-induced surface roughening of PMMA (Section 5.2). A kMC surface model, considering the synergy of neutral species and ions, is used for the calculation of the local etching rate; the novel element of the model is that it takes into account the surface morphology through the calculation of the trajectories of the species joining the surface reactions. The local etching rate is utilized by a profile evolution module, which is based on the level set method, to predict the surface roughness evolution. A method for tracking local variables of the evolving surface profile (e.g. surface coverage), treating a fundamental weakness of the level set method, is used to effectively reduce the computational time. The components of the framework have been thoroughly discussed and presented in chapter 2.

In this chapter, an evaluation of the accuracy of the kMC model is performed in Section 5.3.1; the question to be answered is whether the KMC framework follows the mathematical formulation which describes the surface processes during the etching of PMMA substrates in O₂ plasmas (Section 2.3.1). Specifically, the kMC surface model implements an ion enhanced etching mechanism of PMMA etching in O₂ plasmas. The evaluation of the accuracy of the kMC model is performed through a comparison to the analytical equations describing the ion-enhanced kinetics. Section 5.3.2 handles the topic of the proper choice of time interval of the kMC model, t_{KMC} , and brings out the importance of the transfer of O surface coverage, θ_{O} , with the level set method (Section 2.3.3). The proper approach of calculating the sticking coefficient of neutrals on the surface during the particle trajectory module in order to be closer to its realistic value is given in Section 5.3.3. Section 5.4 demonstrates the effect of operating parameters and model parameters on the evolution of the surface profile and rms roughness of the surface profile. The question addressed in Section 5.5 is whether the model presented in this dissertation can capture the main trends of the experimental behavior of surface roughness of a plasma-etched PMMA substrates with O₂ chemistry. For this reason, the results of the hybrid modeling framework are compared to measurements from the literature. Ultimately, Section 5.6 discusses the capability of the hybrid framework to investigate the wetting behavior of plasma etched polymeric surfaces. The potential of the framework to address changes of the chemical

composition (oxidation) of the surface, is demonstrated, enabling the study of the wetting behavior of plasma etched polymeric surfaces.

5.2 Case study

The case study is plasma etching of a PMMA surface with a sinusoidal, simulating a rough, profile (Figure 2.8c); the amplitude of the sinusoidal profile is $0.75\ \mu\text{m}$ and the period is $1\ \mu\text{m}$. The species coming from the bulk of the plasma reactor and join the surface processes are O and O^+ . The energy, the angular distribution and the flux of O^+ are typical for plasma etching of polymeric substrates: The energy is 100 eV, the angular distribution is Gaussian with a standard deviation of 1.7° and the flux is 1.86×10^{20} ions/(m^2s). O emerge from the bulk plasma onto the surface due to random thermal motion; their angular distribution is isotropic. The ratio of O to O^+ flux is equal to 100 (base case).

5.3 Evaluation and verification of the kMC model

5.3.1 Evolution of the surface coverage and the etching rate

The first question to be answered regarding the evaluation of the kMC model is whether it follows the dynamic behavior of the surface coverage and the etching rate coming from the solution of the analytical model described by Equations 2.24 and 2.25. In Figure 5.1a the surface coverage versus kMC time, coming from a) the kMC model and b) the analytical solution of Equations 2.24 and 2.25 is shown for the flat (plane) part of the surface profile. Two problems with different initial condition for θ_0 ($\theta_{0,0} = 0, 0.5$) are solved. In Figure 5.1a, the same results for the etching rate are shown. The results of the kMC model for both θ_0 and the etching rate follow those of the analytical solutions demonstrating that the kMC model reproduces accurately the equations describing the surface processes (Equations 2.24 and 2.25).

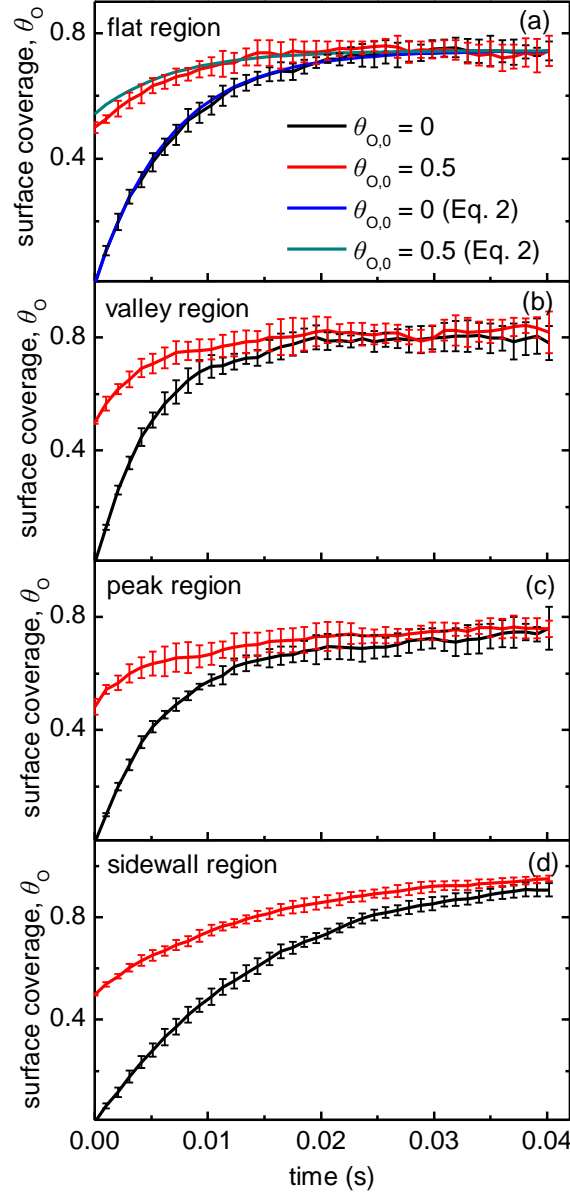


Figure 5.1. Results of the kMC model (average value of 9 runs, the error bars are the standard deviations): θ_O vs. time at a) flat region, b) valley, c) peak region and d) middle of sidewall of the surface profile (Figure 2.8c) at $t=0$. Analytical solutions of θ_O (Equation 2.25) are also depicted in Figure 5.1a. Results of θ_O vs. time starting from an initial value equal to 0.5 are also shown. The sticking coefficient of O atoms is updated (refreshed) with a period of $t_{\text{kMC}}/40 = 0.001$ s. The dimensions of the surface area are defined by $\Delta s = 0.01492$ μm and $L_Z = 0.00125$ μm (see Figure 2.8c).

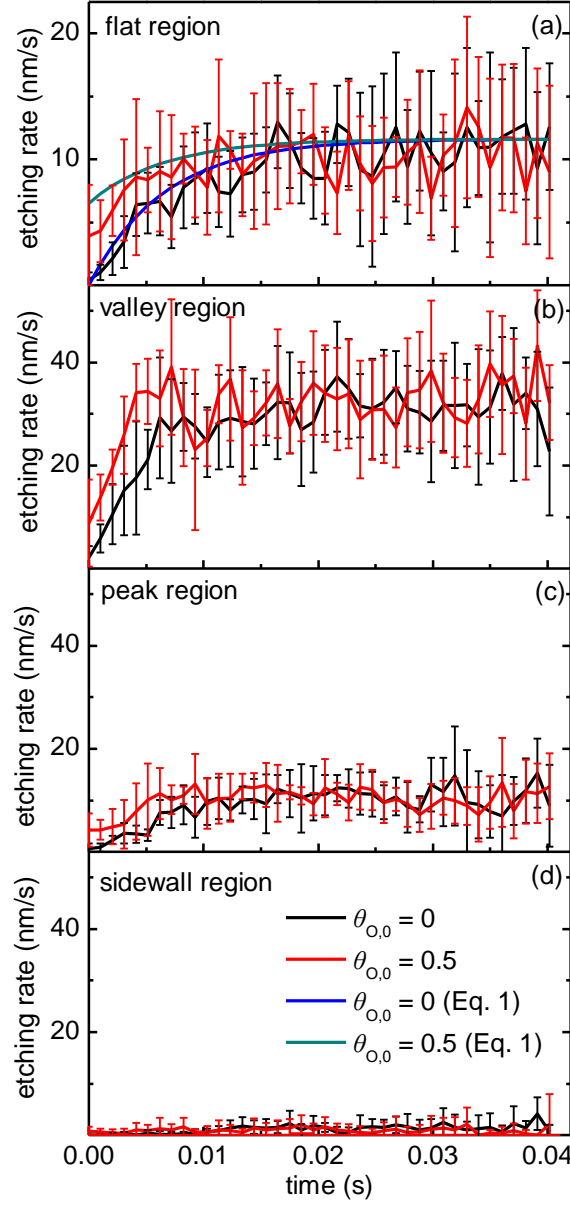


Figure 5.2. Results of the kMC model (average value of 9 runs, the error bars are the standard deviations): etching rate vs. time at a) flat region, b) valley, c) peak region and d) middle of sidewall of the surface profile (see Figure 5.8c) at $t=0$. Analytical solutions of the etching rate (Equation 2.24) are also depicted in Figure 5.1a. Results of θ_O vs. time starting from an initial value equal to 0.5 are also shown. The sticking coefficient of O is updated (refreshed) with a period of $t_{\text{kMC}}/40 = 0.001$ s. The dimensions of the surface area are defined by $\Delta s = 0.01492$ μm and $L_Z = 0.00125$ μm (see Figure 2.8c).

5.3.2 What is the proper choice of t_{kMC} ?

The relation of the time interval of the kMC model, t_{kMC} , to the time step for the numerical solution of the level set equation, t_{LS} , and to the time required for θ_O to reach a steady state value,

t_{ss} , is thoroughly discussed in Section 2.3.4. To briefly remind the reader, t_{LS} should be as high as possible and t_{kMC} should be as low as possible. Simultaneously, t_{kMC} should be high enough for the right calculation of the etching rate, i.e. to get a representative value of the etching rate for t_{LS} . Hence, t_{kMC} should be greater than the time required to get the surface coverage, and thus the etching rate, to steady state, t_{ss} . At a flat surface, the time required for θ_O to reach a steady state value (transition time) is $\sim 5\tau$, where τ is the time constant of Equation 2.25 and is given by Equation 2.26.

At the flat regions of the surface profile, both θ_O and the etching rate saturate at ~ 0.03 s for $\theta_{O,0}=0$, as shown in Figures 5.1a and 5.2a. This value is very close to 5τ required for reaching the steady state of Equation 2.25. Indeed, if the values described in the case study are substituted in Equation 2.26, 5τ is calculated ~ 0.03 s. A critical question is whether this time is enough to reach a steady state at the shadowed regions of the sinusoidal profile.

In Figures 5.1b and 5.1c the results the kMC model for θ_O versus time is shown for the valleys and the peaks of the surface profile. It seems that roughly the same time (~ 0.03 s) is needed for reaching the steady state at the valleys and peaks when the initial condition is $\theta_O=0$. Nevertheless, things are different for the sidewall region (see Figure 5.1d) where the saturation has not been reached yet. Thus, if the initial condition is $\theta_{O,0}=0$, t_{kMC} greater than 0.03 s is required to reach the steady state at the sidewall.

θ_O versus t_{kMC} is shown also for $\theta_{O,0}=0.5$ in Figure 5.1d. Under this initial condition, steady state is reached at ~ 0.035 s. In the same fashion, curves of θ_O starting 0.5 are also depicted in Figures 5.1a, 5.1b, and 5.1c. In all cases, steady state is achieved at lower times compared to the initial condition $\theta_{O,0}=0$. There is a leftward shift of all curves which can be well predicted by the analytical solution of θ_O at the flat surface (see Figure 5.1a).

In Figures 5.1b, 5.1c, and 5.1d, the etching rate at the valleys, peaks and the sidewalls is shown. The etching rate reaches the steady state at the same time period as θ_O . The etching rate also encapsulates the leftward shift of θ_O when the initial condition is $\theta_{O,0}=0.5$.

The aim of these comparisons between the two initial conditions for θ_O is to bring out the importance of the transfer of θ_O with the level set method (Section 2.3.3). After tenths of seconds, θ_O takes a value which is not zero and probably not 0.5. For example, for the surface profile after 0.5 s of etching, θ_O arrives at different values at the flat region, the valleys, the peaks and the sidewalls (0.73, 0.92, 0.76, 0.86 respectively). Through the transfer of θ_O with the level set method, these values can be used as initial conditions in the kMC model. The evolution of θ_O versus kMC time is demonstrated in Figure 5.3 for all regions. In the same figure, the results are compared to the evolution of θ_O with $\theta_{O,0}=0$. The comparison demonstrates that the route to steady state is profoundly faster when the transfer of θ_O is utilized. Thus, the t_{kMC} used for the calculations in this work is 0.02 s.

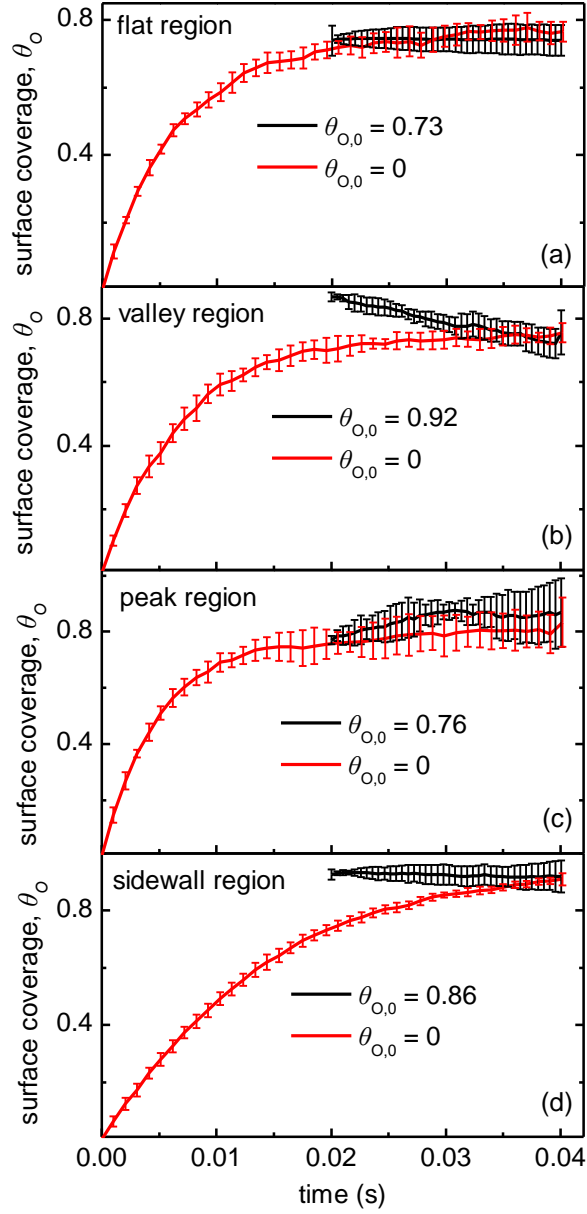


Figure 5.3. Results of the kMC model (average value of 9 runs, the error bars are the standard deviations): θ_o vs. kMC time at a) flat region, b) valley, c) peak and d) middle of sidewall region of the surface profile (Figure 2.8c) at $t=0.5$ s respectively. Two initial conditions for θ_o are considered: the first comes from the transfer of θ_o with the level set method and it is 0.73, 0.76, 0.86 and 0.92 for the flat, valley, peak and middle of sidewall regions. The second is $\theta_{o,0}=0$. To allow for better comparison, the results in the former case are shifted right by 0.02 s. The sticking coefficient of O is updated (refreshed) with a period of $t_{\text{kMC}}/40 = 0.001$ s. The dimensions of the surface area are defined by $\Delta s = 0.01492 \mu\text{m}$ and $L_Z = 0.00125 \mu\text{m}$ (see Figure 2.8c).

5.3.3 The update of the transition probabilities and the sticking coefficient of O atoms

The local values of the sticking coefficient of O are critical for the kMC algorithm as they are used for the estimation of the transition probabilities by the particle trajectory module (Section 2.3.2). The sticking coefficient is equal to $s_O(1 - \theta_O)$ (Section 2.3.2 of chapter 2), i.e. it depends on θ_O . However, the local values of θ_O vary during kMC time and thus the local values of the sticking coefficients also vary. Hence, the calculation of the transition probabilities should be also updated during kMC time. Ideally, they should be updated after the impingement of every particle on the surface. The continuous update after each Δt_{kMC} (Equation 2.23) would result in an escalating computational cost for the kMC model. A good strategy for overcoming this computational obstruction is to update the sticking coefficients and the transition probabilities periodically. In terms of computational efficiency, the proper period for this update is investigated in Figure 5.4; the evolution of θ_O (and the etching rate) on a flat region versus kMC time is demonstrated as the refresh of the sticking coefficient is repeated 1, 4, 20 and 40 times, i.e. with a period of t_{kMC} , $t_{\text{kMC}}/4$, $t_{\text{kMC}}/20$ and $t_{\text{kMC}}/40$.

In Figure 5.4a, θ_O converges asymptotically to the theoretical solution given by Equation 2.25 when the period of the update decreases. The same applies for the etching rate (Figure 5.4b). The small differences between the curves ensuing from the utilization of periods $t_{\text{kMC}}/20$ and $t_{\text{kMC}}/40$, suggests that an even smaller update period would bring no further improvement.

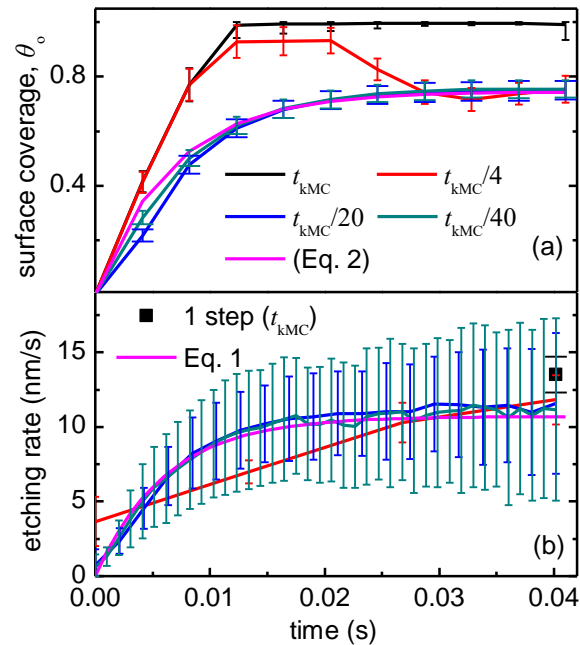


Figure 5.4. Results of the kMC model (average value of 9 runs, the error bars are the standard deviations): a) θ_O and b) etching rate vs. kMC time at the flat region of the surface profile with the sticking coefficient of O along the surface profile updated (refreshed) with a period of t_{kMC} , $t_{\text{kMC}}/4$, $t_{\text{kMC}}/20$ and $t_{\text{kMC}}/40$. The dimensions of the surface area are defined by $\Delta s = 0.01492 \mu\text{m}$ and $L_z = 0.00125 \mu\text{m}$ (see Figure 2.8c).

5.4 The evolution of the surface profile and rms roughness

In Figure 5.5, the evolution of the initially sinusoidal surface profile is shown under different conditions and model parameters. The effect of the ratio $j_O/j_{+|flat}$ (ratio of fluxes at the flat region) on the surface profile evolution is shown in Figures 5.5a and 5.5b. Two values for the ratio are considered, 100 and $\gg 100$ respectively.

In Figure 5.5a, the slope of the profile sidewall increases during etching, and a columnar profile is gradually formed. This because, the etching rate is lower at the middle part of the profile sidewall compared to the lower part, mainly, for two reasons: first, the slope of the sidewall is greater at the middle part, thus, the ion flux, which is proportionate to the cosine of the angle of ion incidence, is lower there, and, second, ion reflection increases the flux of ions towards the lower part of the surface morphology.

The pertinent curve in Figure 5.6 displays that rms roughness increases initially and then comes to a saturation. The **initial increase** of the rms roughness means that the valleys of the surface are etched faster than the peaks. The etching rate at the valleys depends on the ion flux and θ_O . Ion reflection increases the ion flux at the valleys while diffusive reemission increases θ_O at the valleys by redirecting a part of neutral flux there.

The emerging columnar profile lessens the ion reflection effect (by reducing the available surface for reflection towards the valleys) and as a result the slope of rms roughness curve decreases until a saturation occurs. At this point, the redistribution of neutral flux towards the valleys (due to diffusive reemission) sustains the **etching rate** there equal to the one at the peaks. Due to the competence between j_+ and θ_O demonstrated through Equation 2.24, there is a compensation effect in the etching rate at the valleys; the decrease of j_+ (due to the reduced available surface for reflection towards the valleys) leads to an increase in θ_O (due to diffusive reemission which directs the neutral flux at the valleys) and so the etching rate at the valleys is not further decreased.

For the case in which $j_O/j_{+|flat} \gg 100$, where the etched surface is saturated with the adsorbed neutral species everywhere ($\theta_O=1$), rms roughness is greater compared to the case $j_O/j_{+|flat} = 100$ (Figure 5.6). The appreciable slower increase of rms roughness, observed above 70 s, may indicate a trend toward saturation, however, the slope of rms roughness increases shortly, after 20 s at ~90 s. From Figure 5.5b, this transition in the behavior of rms roughness versus time corresponds to a profile changeover from columnar to tapered. This tapering ensues from the high etching rate at the valleys; θ_O is always at maximum value ($\theta_O=1$) there and so the impact of ion reflection amplification on the etching rate reaches full effect.

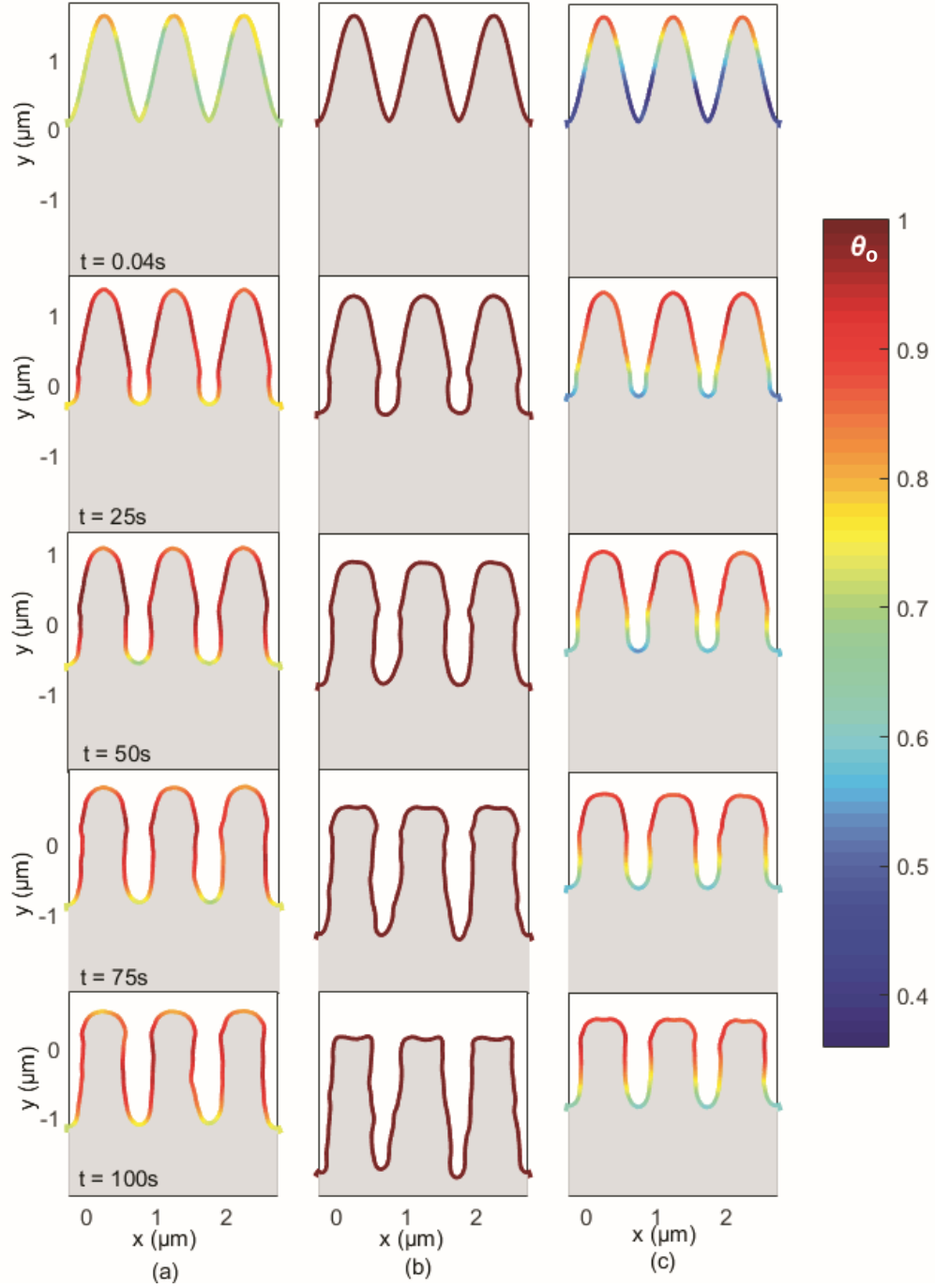


Figure 5.5. Snapshots of the surface profile for different etching times when a) $j_O/j_{+|flat} = 100$ b) when $j_O/j_{+|flat} \gg 100$ ($\theta_O=1$) and c) $j_O/j_{+|flat} = 100$ with reemission mode for O being off ($S_O=1$). The color of the profile curves denotes the magnitude of the local θ_O .

In Figure 5.5c, $j_O/j_{+|flat}$ is equal to 100 and the sticking probability of O is 1 ($S_O=1$, cf. Section 2.3.1). In this case, the effect of neutral shadowing on the profile evolution is further enhanced as no O reemission takes place. Although ion reflection directs the flux of ions to the valleys, geometric shadowing, blocks the neutral flux from reaching valleys and thus the etching rate is

much lower thereat. Additionally, the available surface for ion reflection towards the valleys is reduced as the evolution progresses. Indeed, the columnar profile renders the effect of reflection on ion flux to the valleys marginal, so neutral shadowing has an even stronger effect on the etching rate at the valleys; at this point the rms roughness starts to fall as Figure 5.6 depicts (at ~70 s). This simply means that the peaks are being etched faster than the valleys.

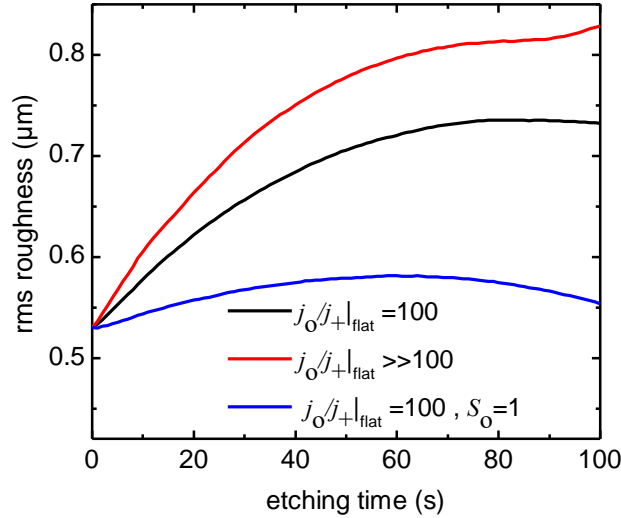


Figure 5.6. rms roughness versus time with $j_O/j_+|_{\text{flat}} = 100$, $j_O/j_+|_{\text{flat}} \gg 100$ ($\theta_O=1$), and $j_O/j_+|_{\text{flat}} = 100$ with reemission mode for O being off ($S_O=1$).

5.5 Comparison to measurements

Several experiments have been performed on the plasma etching of polymers, however, only few [17, 57] measured and recorded the evolution of the surface roughness of etched PMMA films in O_2 plasmas. The quantitative comparison of the simulation results to the roughness would require the fluxes and the distributions (angular and energy) of neutral species (O) and ions (O^+), which may come either by measurements or by calculations by a reactor scale model [225]. For the lack of the specific measurements/calculations, the question addressed in this section is whether the proposed framework can capture the main trends of the experimental behavior of surface roughness of a plasma-etched PMMA substrates with O_2 chemistry.

In Figure 5.7, the rms roughness versus etching time is shown for a combination of six pairs of (ratio $j_O/j_+|_{\text{flat}}$, ion energy) values with each pair corresponding to a different etching condition. Two values for the ratio $j_O/j_+|_{\text{flat}}$, 100 and $\gg 100$, and three values of ion energy, 100, 150 and 200 eV are considered. The first observation is the change of the growth mode for the rms roughness observed at high ratios of $j_O/j_+|_{\text{flat}}$; there are three changes (transitions) of growth mode for the rms: fast growth, followed by moderate growth, followed by fast growth. Although they may be attributed to different causes or not discussed at all, changes in the growth mode of rms roughness are encountered in the measurements of Kontziampasis et al. [17] and Sun et al. [57]

The second observation is an upward shift of the rms curve for $j_o/j_{+|flat} \gg 100$ when the ion energy is intensified. This upward shift is also observed in measurements of rms roughness with the increase of bias on the wafer carrying the sample for a high density plasma reactor (where the production of O is high and thus the ratio of $j_o/j_{+|flat}$ is also high) [226]. If $j_o/j_{+|flat}$ is lower, the framework predicts that the rms roughness is not markedly affected when ion energy varies; due to the competition between the ion energy and O surface coverage (an increase of ion energy leads to a decrease in the O coverage), there is a compensation effect in the etching rate (cf. Equation 2.24).

The third observation is an upward shift of the rms curve when the transition from the small to the large value of the $j_o/j_{+|flat}$ takes place while the ion energy is constant. The increase of the rms roughness with the increase of the source power of the plasma reactor was also experimentally observed [226]; the increase of the source power yields into further dissociation of O₂ molecules, increase of the production of O, and hence greater $j_o/j_{+|flat}$.

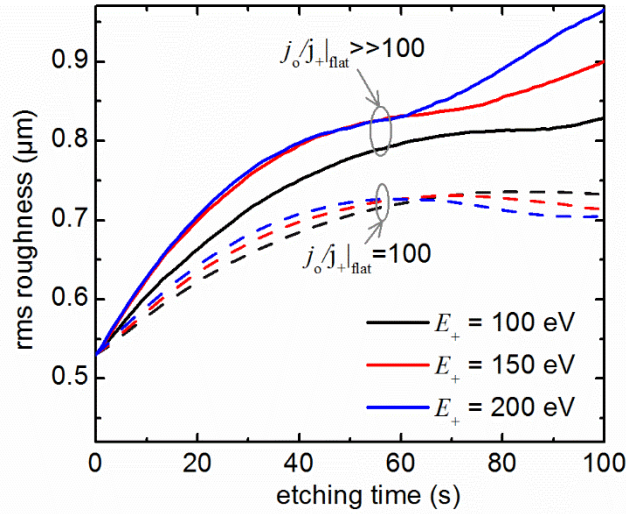


Figure 5.7. The rms roughness vs time for a combination of six pairs of ($j_o/j_{+|flat}$, ion energy) values with each pair corresponding to a different etching condition. Two values for the ratio $j_o/j_{+|flat}$, namely, 100 and $\gg 100$, and three values of ion energy (E_+), namely, 100, 150 and 200 eV are considered.

5.6 The potential of the hybrid framework to study the wetting behavior of plasma etched polymeric surfaces

O₂ and O₂-containing plasmas are commonly employed to alter the properties of polymeric surfaces. For example, the wettability of polymeric surfaces is often enhanced by using O₂ plasmas [9, 22-24]; this enhancement is attributed to both the appearance of O-containing functional groups (peroxides, alcohols, ethers, and epoxies, aldehydes, ketones and carboxylic groups) [14] on the surface as well as on the amplification of surface roughness.

Concerning the former, the increase of the wettability is related to plasma-stimulated formation of $-C(-)O-$, $-C(-)O$ and $-C(O-)=O$ bonds on the polymer surface corresponding to specific

polar functional groups [14]; in such groups, the double-bonded O available from the plasma is attached to the hydrocarbon chain and forms a hydrogen bond with water molecules, thus increasing the wettability of the surface [13]. Precisely, these polar groups (especially peroxide groups) [14] increase the surface energy by providing attachment sites for the water molecules on the surface. Ultimately, high polar contributions to surface energy are preconditions for increased wettability; these contributions grow during treatment in O₂ containing plasmas by interlocking the aforementioned functional groups on the polymer surface [12]. Concerning the latter, the change of the wettability for e.g. a hydrophilic surface can be explained through the simple Wenzel equation ($\cos\theta_w = r\cos\theta$) which predicts the change of the contact angle on the rough surface (θ_w) as a function of the Young contact angle on an unmodified surface (θ) and the roughness factor (r); the latter is the ratio of the actual surface area of the substrate to the projection of that surface onto a horizontal surface.

Can the hybrid modeling framework address the above contributions of plasma treatment on the wettability of the surface? The answer for the contribution of the surface roughness (morphology) is rather straightforward, as the output of the modeling framework is the surface profile. Assuming that the density of the functional groups at the outermost polymer surface is linked with the O surface coverage (θ_O) [12, 13], the hybrid modeling framework can also address the contribution of the former (functional groups) on the wettability.

In Figure 5.8, the average θ_O along the surface profile versus the etching time is demonstrated for three different etching scenarios presented in Section 5.4 ($j_O/j_{+|flat}=100$ and $E_+=100, 150$, and 200 eV). In all scenarios, a very steep increase of θ_O is observed in few seconds and a saturation of θ_O to an almost constant value follows. This is in agreement with previous studies [12], according to which, the maximum density of functional groups at the outermost polymer surface is achieved (completed) after a few seconds. If the plasma exposure is continued, the process passes over to etching [11, 12]. A steady state process between the introduction of functional groups and polymer etching is then established [12]. The balance of these two processes depends on the operating parameters of the given experiment [10].

Based on Figure 12, the O-functional groups on the surface for each etching scenario described above can be estimated. It seems that the O surface coverage acquires its highest value, or the O-functional groups are the most, when the ion energy obtains its lowest value (100 eV); the surface with the more functional groups is expected to be more hydrophilic. Nonetheless, this outcome does not imply that the etched surface ensuing from these operating conditions will result into a Wenzel (fully wetted) or Cassie-Baxter (partially wetted) state, as it is the combination of O-functional groups with roughness that determines, ultimately, the wetting state of the surface. In order to predict the wetting state and its robustness to transitions from one state to the other, the hybrid framework developed in this work should be combined to a computational framework which quantifies the effect of the surface morphology and the surface energy (the latter through the Young contact angle and the contact angle hysteresis) on the wetting state [227-230].

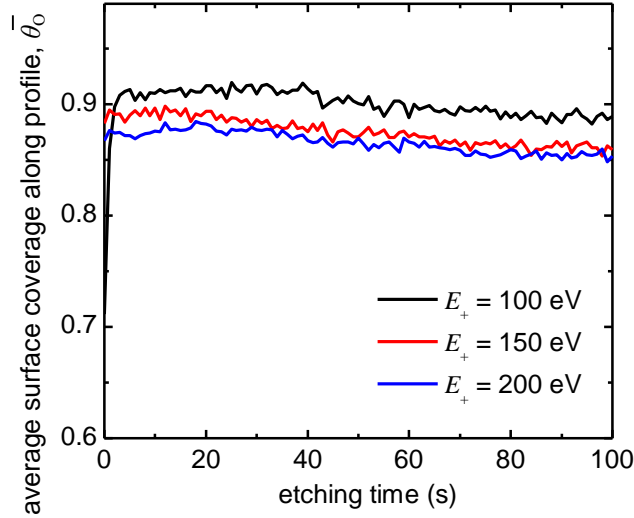


Figure 5.8. The average surface coverage of the surface vs. etching time at different conditions ($j_{\text{O}}/j_{+}|_{\text{flat}}=100$ and $E_{+}=100, 150$, and 200 eV).

5.7 Conclusions

A hybrid framework consisting of a a) kMC surface model and b) a deterministic profile evolution module was developed to simulate profile evolution during plasma etching.

The case study presented in this chapter was plasma etching of PMMA surfaces with O_2 chemistry. The results of framework focused on the development of microscale roughness. Unfortunately, there is a lack of pertinent measurements at the microscale level. To the best of our knowledge, the evolution of the surface roughness of etched PMMA films in O_2 plasmas was measured and recorded in few experimental works [57, 231] and these measurements concerned only nanoscale roughness. Although the focus of the framework was on the microscale, the results were consistent to the available measurements: The framework provided an explanation for the change of the growth mode of rms roughness versus time and captured the increase of rms roughness with source power and bias voltage [232] in high density plasma reactors.

The potential of the modeling framework to address changes of the surface wettability during plasma etching was demonstrated. The framework can simulate changes of surface morphology (roughness) and O surface coverage (linked to O-functional groups), the combination of which determines the wetting state of the surface.

This chapter has been published as a part of the following article:

G. Memos, E. Lidorikis, E. Gogolides and G. Kokkoris, (2021), A hybrid modeling framework for the investigation of surface roughening of polymers during oxygen plasma etching, Journal of Physics D: Applied Physics, 54 (2021) 175205

6 Conclusions

Toward the comprehension and, finally, the control of plasma induced surface roughness, the first purpose of the dissertation, was to record how interrelated surface mechanisms affect the evolving roughness of the surface profile during physical (mechanical) etching (sputtering) of a PMMA substrate with Ar plasma. For this reason, a computational modeling framework was developed for the evolution of a PMMA surface profile with unconventional morphology under Ar plasma etching. Particular importance was attached to the effects of surface charging by integrating a surface charging module in the framework. The framework was extended to include the mechanism of secondary electron emission and the reflection of ions on the surface.

The modeling framework was suitably modified in order to be applied to the plasma etching of a PMMA substrate with O₂ chemistry (ion enhanced etching) as well, which is widely used for the surface modification and roughening of polymeric substrates. To describe the pertinent surface processes and to calculate the local etching rates, an original kMC was developed and integrated into the modeling framework. Various operating parameters of the plasma reactor, such as the ratio of the flux of O to the flux of O⁺ (at the flat surface), the ion energy and the etching time, as well as various mechanisms, such as the re-emission of O and the reflection of O⁺ on the surface were intertwined with the evolution of topography and, finally, their interrelated effects determined the evolution of roughness. The framework was able to replicate experimental roughness development trends found in the literature in high density plasma reactors. In addition to changes in surface morphology, the framework was able to simulate changes in the O surface coverage (associated with O-functional groups created on the surface during etching), the combination of which determines the wetting state of the surface.

The novelty of the study carried out in the context of this dissertation is summarized below.

The novel contributions of the dissertation regarding the part involving etching of PMMA with Ar plasma:

- This dissertation revealed, through the relevant publications [82-84], that charging is inevitable on rough surfaces of polymeric substrates being etched by plasma. The substrate is dielectric to allow charge accumulation and the surface of the substrate is not perfectly flat. Due to the roughness there is a surface morphology which in combination with the directionality difference of positive ions and electrons impinging on the etched surface [119], enables the local imbalance of positive and negative charges.
- Even if plasma induced surface charging on conventional - with respect to the semiconductor industry - structures, i.e., trenches or holes, has been studied in previous works and its artifacts, such as notching, microtrenching, etching lag, and twisting have been examined both experimentally, theoretically, and computationally, there were no modeling framework or previous studies on the - inevitable during plasma etching - charging of polymeric (and generally dielectric) surfaces with random rough featured micro/nano scale morphology.

- The study showed that the effect of the surface charging phenomenon on the etching rate manifests itself mainly through the reduction of ion energy (ion deceleration) and to a lesser extent through changes to the trajectories of ions (ion deflection).
- From a computational point of view, the results of the current dissertation suggest that the effect of surface charging should be taken into account in the design of recipes for producing or eliminating surface roughness. A practical implication of the current dissertation is that the elimination or the reduction of surface charging will result into greater surface roughness of polymeric, and generally dielectric, substrates. This practically reveals a mechanism that contributes to the decrease of surface roughness of dielectric substrates. This mechanism is not present in the case of conductive materials.
- An original model for the SEEE mechanism was developed for PMMA substrates. The total electron yield, σ_e , the secondary electron emission yield δ , and the backscattering coefficient, η , were based on available information in the literature for PMMA and other polymers in the *range of electrons with energies* which is of interest in plasma etching (0-50eV). The total electron yield σ_e , defined as the number of emitted electrons per incident (primary) electron, was adopted from the work of Dapor [185]. It included elastically and inelastically reflected primary electrons as well as true secondary electrons. In order to separate the backscattering proportion of electrons (i.e. elastically and inelastically reflected primary electrons), the Burke's equation[183], expressing η in polymers consisting of H, C, N and O as a function of the energy of the primary electrons, was used. It was assumed that η represented **only** elastically reflected electrons in the aforementioned energy spectrum [186]. Then, for energy greater than 16 eV (threshold for the secondary electron emission process)[180, 187], δ was calculated as the difference of σ_e and η ; no dependence on the angle of electron incidence was considered [184, 188]. The energy of the secondary electrons was regarded independent of the energy of the primary electrons and equal to 1eV [188, 190]. Concerning the angular distribution of secondary electrons, an isotropic (cosine) distribution was considered [184, 188] [188]. Concerning the energy and the direction of the (elastically) reflected electrons, specular reflection with no energy losses was assumed.

Regarding the study conducted in the part of the dissertation involving etching of PMMA with O₂ plasma:

- A hybrid framework consisting of a) a kMC surface model and b) a deterministic profile evolution module was developed to simulate profile evolution during O₂ plasma etching. The coupling of the two components of the framework, allowed the kMC surface model to take into consideration the profile shape (or the surface morphology) and extended the potential of previous kMC surface models in the literature which assume that the surface is flat.
- Another novel element of the current dissertation, not previously used in etching and deposition processes, was the use of the level set method for the transport of local

properties of the profile (e.g. O surface coverage) from a time step to the next which is not straightforward. As the evolving profile is embedded in an implicit function (level set function), unless this transport takes place, any past information on the profile is lost during the evolution.

- The framework can simulate changes of surface morphology (roughness) and O surface coverage (linked to O-functional groups), the combination of which determines the wetting state of the surface.

Prospects of future research are also discussed below:

- The modeling framework is flexible as it can be applied to other polymeric substrates and/or other plasmas. It can also be applied to plasma etching of conventional structures in the semiconductor industry such as trenches. It can be utilized to study the artifacts and tackle the challenges of plasma etching of dielectric trenches, conductive trenches with a dielectric mask, and trenches on SOI wafers.
- Although the surface profile is 2d in the current study, the modeling framework can address cases of 3d surface morphologies. No change in the surface parameterization or the numerical methods is required. However, the computational cost will be higher and the requirements for parallel processing more demanding.
- Regarding plasma induced surface charging effect, although the framework has so far handled cases of microscale morphologies, it can also handle cases of nanoscale morphologies. However, in this case, one should focus on:
 - a) The sporadic nature of ion and electron flux entry in such critical dimensions. The statistical distribution of charged particles may produce a charge distribution on the dielectric surface that will severely fluctuate from point to point on the surface as times goes on. Such a spatio-temporal stochastic pattern [130, 137] of charge distribution may have a different effect on roughness evolution compared to the steady state charge distribution emerging from microscale charging.
 - b) The time scales of the different phenomena involved in the process. In the microscale, the charging time for steady state is much smaller than the time required for a remarkable change of the surface morphology during plasma etching so one can perform charging calculations without worrying about the modification of the topography due to ion bombardment. However, concerning nanoscale, charging effect may evolve in a time similar to the time required for the surface to change, so there is a strong possibility that the charging computations cannot be decoupled from those for morphology evolution.
- The plasma induced surface charging, not only affects the surface roughness developed on the etched surface, but it is also expected to affect the properties of the etched surfaces. The surface charge density developed on the etched surface was found to be stable [233] and affect the wetting properties of polymeric surfaces [47]. Experimental investigation is required to clarify the relationship between roughness and charge

retention on the surface of a polymer as well as investigation of possible applications that may arise from such technology.

- Regarding the case study involving plasma etching of PMMA surfaces with O_2 chemistry, the framework captures experimental trends in the literature; it provides an explanation for the change of the growth mode of rms roughness versus time and captures the increase of rms roughness with source power and bias voltage in high density plasma reactors. In order to generate quantitative results and to correlate them with measurements, extension of the modeling framework is required. Generally, measurements concern surface roughness statistics at different operating conditions (e.g. pressure, flow rate, power). In order to link the operating conditions with the surface roughness, a multiscale modeling framework [171, 192] is required, i.e. a reactor scale model (e.g. [234]) should be coupled to the modeling framework of the current study.
- The extension may also include additional mechanisms, such as product re-deposition [192], which can affect roughness evolution, or more detailed models, e.g., for the interaction of ions with the polymeric substrates.
- The potential of the modeling framework to address changes of the surface wettability during plasma etching was demonstrated. Strictly speaking, the wetting behavior may depend on more than one scales of roughness. An interesting extension of the current work is to analyze all scales of surface roughness and focus on the prediction of wetting state of the surface (e.g. Wenzel or Cassie-Baxter or hybrid states). For this, a) a multiscale analysis for the surface characterization [235] and b) a computational framework which quantifies the effect of the surface morphology and the surface energy (the latter through the Young contact angle and the contact angle hysteresis) on the wetting state [227-230] will be required.
- The modeling framework can also be extended by taking into account surface charging for the case study of etching of PMMA substrates with O_2 plasma. The addition of surface charging in the modeling framework for this case is challenging: surface charging induces a charging potential which evolves gradually, inducing a third time scale in the system (in addition to the time scale for the kMC simulation and the time scale for the profile evolution), and affects the trajectories of ions.
- The kMC surface model implements an ion-enhanced mechanism which is already formulated in equations. This does not mean that the application of the modeling framework is limited to such cases. It can handle cases and phenomena where the transition probabilities or the process rates depend on the local activation energies, i.e. it can serve as a platform to test complex and not explicitly formulated kinetics.

7. Appendices

A. The directionality difference between ions and electron fluxes at the wafer and the electron shadowing effect

Microstructure charging is induced by the directionality difference between ion and electron fluxes at the wafer. The origin of this difference is discussed below.

More precisely, electrons enter the sheath having a Maxwellian energy distribution.³⁹ This means that they have the same velocity in any direction towards the wafer, thus their angular distribution is isotropic. Simultaneously, due to the negative floating potential V_f developed on the electrode (Section 1.3.1), electrons are decelerated in the sheath and the vast majority of them are repelled back to the plasma. Actually, only a small fraction of electrons can cross the sheath. This fraction is comprised of electrons from the Maxwellian energy distribution that are energetic enough to overcome the negative potential V_f . In other words, only electrons with sufficient perpendicular velocity can reach the wafer

$$u_{\perp}^e \geq \sqrt{\frac{2eV_f}{m}}, \quad (\text{A.1})$$

where e is the electron charge, V_f is the (negative) floating potential of the electrode and m is the electron mass.

The direction of the aforementioned electrons can be enclosed within a narrow angle φ , denoted in figure A.1 [119]. Due to repulsion, these electrons are decelerated as they traverse the sheath and as a consequence their angular distribution expands. However, near the boundary lower sheath and so the wafer, their average energy (temperature) is the same with that of the electrons of the plasma initially due to the fact that these electrons had initially energies greater than the average [29]. Ultimately, the electron angular distribution function can be described by $\cos^n \theta$, where $n \leq 1$ and θ is the angle of incidence of electrons at the wafer [120].

On the contrary, ions, are accelerated in the presheath region to the Bohm velocity⁴⁰,

³⁹ Electrons emerge from plasma into the sheath region due to random thermal motion. The Maxwellian distribution conveniently relates a characteristic electron temperature to the average energy of electrons.

⁴⁰ Between plasma and sheath exists a quasi neutral transition region of low electric field, and the effect of this region is to increase the velocity of ions entering the sheath. This electric field penetrates plasma by a short distance, the size of an electronic Debye length (screening length). A voltage drop of $k_B T_e / (2qe)$ occurs across this distance. Here k is the Boltzmann constant, T_e is the electron temperature and e is the electronic charge. Within this screening length, ions are accelerated by this potential toward the sheath. This results in an ion flux significantly larger than just the due to random thermal motion alone. This is the Bohm criterion for a stable sheath formation, which gives the saturated ion current that is independent of the sheath potential. The saturated ion current according to the Bohm criterion is $I_{\text{ion}} = 0.6nu_B$, where n is the plasma density. [29] B. Chapman, Glow Discharge Processes, John Wiley & Sons (1980) 49-74, 139-172.

$$u_B = \sqrt{\frac{kT_e}{M}}, \quad (\text{A.2})$$

where k is the Boltzmann constant, T_e is the electron temperature and M is the ion mass. Consequently, the vertical coordinate of ion velocity,

$$u_{\perp} = u_B, \quad (\text{A.3})$$

i.e. that in the direction perpendicular to the wafer, is larger than the thermal velocity of ions in the lateral direction, that is, parallel to the wafer

$$u_p = \sqrt{\frac{kT_i}{M}}, \quad (\text{A.4})$$

where T_i is the ion temperature. As the ions cross the sheath, they are accelerated further due to attraction from V_f and so their angular distribution evolves into highly anisotropic (see Figure A.1).

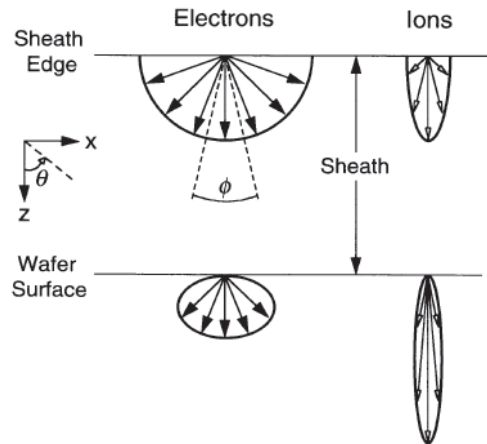


Figure A.1: Depiction of the electron and ion angular distribution functions at the sheath edge and at the unpatterned wafer surface. The anisotropy of both distributions is evident. Nonetheless, ions are much more directional than electrons. The part of the electron angular distribution that will arrive at the wafer surface is denoted by ϕ . [119]

Examples of angular distributions for ions and electrons at an unpatterned wafer are presented in Figure A.2. In the ion angular energy distribution, the domination of the normal direction is conspicuous. Contrarily, this is not happening for the case of electrons. The flux of both ions and electrons hitting normal to an unshadowed surface segment ΔS (see Figure A.3) is maximum, although there are significantly fewer electrons than ions impinging at angles near to the value $\theta = 0^\circ$, where θ is the angle particle trajectory with the surface normal. Indeed, most electrons impinge at angles larger than a few degrees from normal. The origin of microstructure charging

is the difference in the angular distributions of ions and electrons as demonstrated in the next paragraphs.

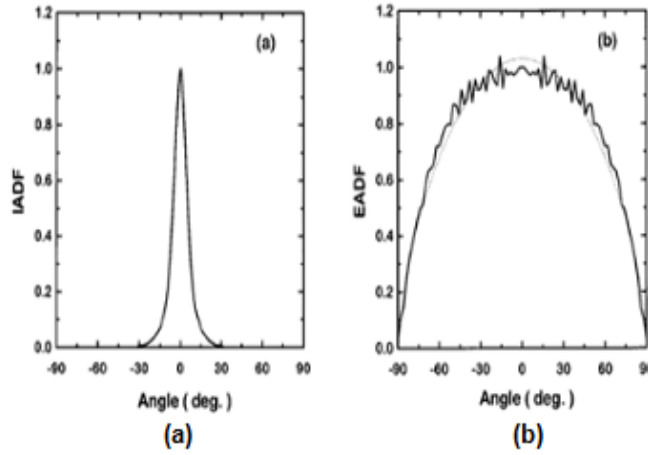


Figure A.2: (a) Ion (Cl^+) and (b) electron distribution angular distribution at the sheath lower boundary as calculated by Hwang and Giapis [120].

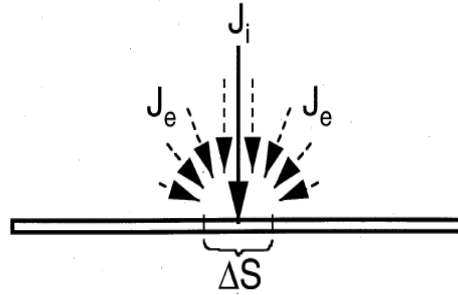


Figure A.3: Depiction of the difference in the degree of anisotropy between ions and electrons. Almost all of the ions arrive at the segment ΔS at angles of incidence smaller than a few degrees from normal, while the majority of the electrons impinge at angles that deviate significantly from $\theta = 0^\circ$. The dashed-line arrows describe electron flux while the solid-line arrows depict ion flux. Decreasing length of the dashed lines indicates smaller electron flux. Taken from [119].

Assume a dielectric line placed on a wafer surface adjacent to the surface segment ΔS . Due to their low anisotropy, electrons arrive at oblique angles of incidence on ΔS . As a result, electron flux will be diminished in this region. On the other hand, ions are highly directed, thus their traces are slightly influenced. Hence, ΔS charges up positively. As far as the material of the surface wafer is concerned, it can be conductive or insulating. In the case of a conductive material, the aforementioned current imbalance will be restored by electron transport from other unshaded areas. Additionally, the top regions of the line sidewalls will charge up negatively due to the slanting electrons trajectories. Simultaneously, this negative charge will cause ions deflection towards the lower part of the sidewall charging it up lightly positively. In the case of an insulating material, accumulation of positive charge on the segment ΔS is incurred, as

presented in figure A.4. Ions are repelled due to the emerging positive electric field while more and more electrons are attracted. When steady state is reached, the electron flux is equal to the ion flux.

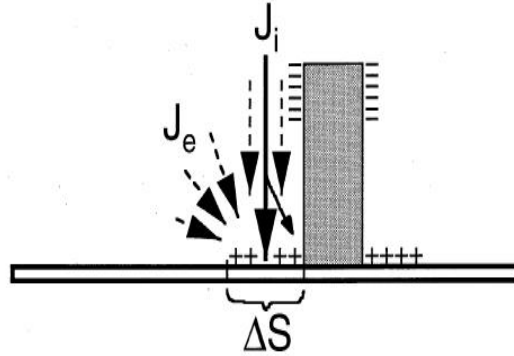


Figure A.4: Schematic illustration of steady-state current balances at an insulating surface segment next to a single insulating feature of rectangular cross section. The dashed-line arrows describe electron flux while the solid-line arrows depict ion flux. Decreasing length of the dashed lines indicates smaller electron flux. The ion and electron fluxes are not to scale. Taken from [119] .

Placing a second dielectric line, a trench is formed (Figure A.5). In this case, electron shadowing is enhanced. Actually, the closer the lines are, i.e. the larger the aspect ratio is, the more severe the shadowing is. As in the previous case, the ion flux is not affected. Consequently, the current imbalance becomes more intense. If the wafer surface is conductive, current balance is restored by electrons transport from other unshaded regions. However, in the case of an insulating surface its potential must increase much more than that of the single-line case; more ions should be deflected to achieve equal fluxes of ions and electrons.

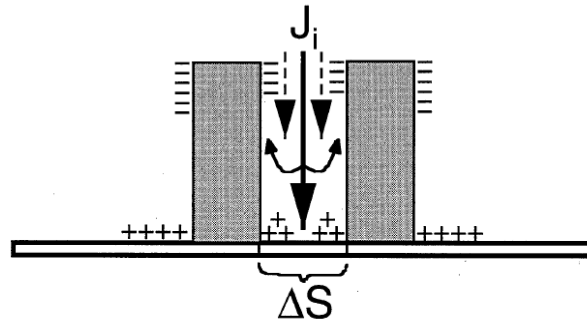


Figure A.5: Schematic illustration of steady-state current balances at an insulating surface segment confined by two insulating features, forming a trench. The dashed-line arrows describe electron flux while the solid-line arrows depict ion flux. Decreasing length of the dashed lines indicates smaller electron flux. Taken from [119].

B. A brief review on kinetic Monte Carlo schemes

B.1 Introduction - the master equation

The most important “concept” for elementary processes (e.g. adsorption, desorption, diffusion) on the surface of solids is the “adsorption site”. Kinetic Monte Carlo (kMC) simulates how the occupation of the adsorption sites evolves over time (exchange of atoms between the sites of the lattice surface and the fluid phase). The source of the kMC algorithms and a large part of the analysis of the results of kMC simulations are established on the master equation [212, 214-216, 218]. For a system (adlayer) that can switch between two states (configurations), i.e. two different ways in which adsorbates are distributed over the sites, A and B, the master equation gives

$$\frac{dp_A}{dt} = -w_{BA}P_B + w_{AB}P_A \quad (\text{B.1})$$

where t is the time, $p_{A(B)}$ is the probability of the state $A(B)$ and w_{AB} (w_{BA}) is the rate that the system goes from state $A(B)$ to state $B(A)$. The master equation describes the evolution of the probability of the system being in state A while jumping between A and B in a continuous time.

The master equation expresses a Markovian (i.e., memoryless) process where the transition to the next state does not rely on the past events of the system and hinges completely on its current state. In terms of surface kinetics, the Markov chain assumption is accurate as long as the simulated events, such as adsorption, desorption or diffusion, are infrequent. Especially, they should appear on a much longer timescale than the lattice thermal vibrations (i.e., the oscillations of *atoms* in a solid about their equilibrium positions). In this scenario, the memory of which states were formerly visited is completely lost due to the vibrations between two transitions of the system⁴¹ and, thus, the surface kinetics is accurately represented by the master equation.

kMC algorithms do not resolve analytically the master equation (equation 1) for a given system, but instead numerically model the Markov process with an approach based on stochastic dynamics. In a typical kMC simulation, the dynamics of species and their interactions are demonstrated by discrete hops from one configuration to another depended on random probabilities. These simulations are usually performed on a grid (on-lattice kMC) [214] that functions as a platform for species to interact and these interactions are based on a set of predetermined rules and the initial atomic configuration. A proper kMC algorithm should enact a correspondence between MC time and real time, as to demonstrate both the dynamics and the steady state properties of the system. The algorithm should also determine at each step, to which state the system should “hop” next. This is implemented by selecting and executing elementary

⁴¹ The more time the system allocates in one state, the more it loses sight of how it really entered there. After a while, each probable way to leave from this state consequently turns into thoroughly independent of its past before arriving the state.

surface processes with a probability⁴² proportional to their relative rates⁴³ of execution, followed by an update of the time.

B.2 Direct kMC

One of the prominent and long established kMC methods for spatial distributed systems⁴⁴ is the direct kMC method. The j th process at the i th site is picked out with a probability [214]

$$p_{ij} = \frac{\Gamma_{ij}}{\sum_{j=1}^{N_p} \sum_{i=1}^{N_L} \Gamma_{ij}} = \frac{\Gamma_{ij}}{\Gamma_{\text{tot}}} \quad (\text{B.2})$$

where N_L is the number of lattice points and N_p is the number of processes⁴⁵ happening at each site i . Γ_{ij} is the transition probability⁴⁶ of the j th process at site i , and Γ_{tot} is the total transition probability over the entire lattice. **All Γ_{ij} are estimated a priori, i.e., prior to choosing an event.** In the direct KMC method, generally, **there are two steps:**

Step 1 The (I, J) pair is picked out by employing a uniform distribution random number $\zeta_1 \in (0, 1)$ in consonance with [214]

$$\frac{\sum_{j=1}^{J-1} \sum_{i=1}^I \Gamma_{ij}}{\Gamma_{\text{tot}}} < \zeta_1 < \frac{\sum_{j=1}^J \sum_{i=1}^I \Gamma_{ij}}{\Gamma_{\text{tot}}} \quad (\text{B.3})$$

Step 2 The time is promoted by an accretion given from [214]

$$\Delta t = -\frac{\ln \zeta_2}{\Gamma_{\text{tot}}} \quad (\text{B.4})$$

where $\zeta_2 \in (0, 1)$ is a different uniform distribution random number. Δt is the finite time interval during which the picked process occur. An excellent discussion on the details of the establishment of equation of Δt in terms of Γ_{tot} is given by R. Lesar [213].

⁴² Probability of a process: process rate divided by the total rate of all possible processes.

⁴³ Rate of a process: inverse of the average time between two successive events of this process.

⁴⁴ Systems that often compromise a substrate where adsorption, desorption, diffusion among sites of the substrate can take place; there are spatial variations of the concentrations of species within the system.

⁴⁵ Processes: chemical reactions in well-mixed systems; in distributed systems these can describe reactions, transport processes, and other steps.

⁴⁶ In the kMC literature the descriptions “rate” and “transition probability” are adopted equivalently.

A bottleneck of the direct KMC method for lattice systems emanates from the extent of the system due to the vast number $N_p \times N_L$ of transition probabilities $\{ \Gamma_{ij} \}_{i=1, j=1}^{N_L, N_p}$. Picking a process j at a site i , according to equation 3, may consume substantial computational time. Moreover, at each trial, the whole transition probability matrix $\{ \Gamma_{ij} \}_{i=1, j=1}^{N_L, N_p}$ has to be amended. These pick and update procedures curb the direct kMC method to systems of a small-scale lattice size and a small number of processes.

B.3 n-fold direct kMC

The n -fold method stems from the fact that in many lattice systems, the interactions are short ranged, and thus each site supports only a limited number of probable processes, i.e., the number of processes for which $\varepsilon_{ij}=1$ is often much lower than N_p , where $\{ \varepsilon_{ij} \}_{i=1, j=1}^{N_L, N_p}$ is the participation indices of site i , i.e., whether process j happens on the i th site, $\varepsilon_{ij}=1$, or not, $\varepsilon_{ij}=0$. Specifically, **step 1** is modified as follows:

Step 1 (n-fold): Let Γ_j describe the transition probability per unit time of the j th process and n_j the number of sites appertaining to this process (class). Then one has [214, 236]

$$n_j = \sum_{i=1}^{N_L} \varepsilon_{ij} \quad (\text{B.5})$$

The j th class is picked out with a probability [214, 236]

$$p_j^{\text{class}} = \frac{\sum_{i=1}^{N_L} \Gamma_j \varepsilon_{ij}}{\sum_{k=1}^{N_p} \sum_{i=1}^{N_L} \Gamma_k \varepsilon_{ik}} = \frac{\Gamma_j \sum_{i=1}^{N_L} \varepsilon_{ij}}{\sum_{k=1}^{N_p} \Gamma_k \sum_{i=1}^{N_L} \varepsilon_{ik}} = \frac{n_j \Gamma_j}{\sum_{k=1}^{N_p} n_k \Gamma_k} = \frac{n_j \Gamma_j}{\Gamma_{\text{tot}}} \quad (\text{B.6})$$

utilizing a random number $\zeta_1 \in (0, 1)$ from a uniform distribution [214, 236]

$$\frac{\sum_{i=1}^{j-1} n_i \Gamma_i}{\Gamma_{\text{tot}}} < \zeta_1 \leq \frac{\sum_{i=1}^j n_i \Gamma_i}{\Gamma_{\text{tot}}} \quad (\text{B.7})$$

In view of all sites in a class are tantamount regarding the transition probability, a site, say m , from the picked class is randomly selected utilizing a second random number $\zeta_2 \in (0, 1)$ [214, 236]

$$m = \text{floor}(n_j \zeta_2) + 1 \quad (\text{B.8})$$

Here the command “floor” demonstrates rounding of the real number $n_j \zeta_2$ to the nearest lower integer.

A benefit of the n -fold direct method is that one has to look among the probabilities of a small number of classes to select a class and utilize a second random number to choose a site from that class. This renders the identification procedure (which process and which site) very effective.

B.4 Coarse grain kMC

In microscopic kMC simulations, an extensive number of microscopic sites, are covered by different atoms with a maximum of one atom per site. However, in some circumstances the system required behavior, property, or response is intrinsically at the mesoscale, i.e. its entire atomistic description is inapplicable for the given application. Coarse-grain models provide an effective means to model and simulate such cases; for instance, coarse-grained kMC simulations make feasible the linking of microscopic scale phenomena at an interface with continuum simulations of a fluid adjacent the interface [237]. The basic intention is to capture the properties of a system to a desired precision (i.e. to capture large-scale features, while preserving microscopic information on intermolecular forces and particle fluctuations), whilst decreasing the complexity adequately to render computer simulations of that model possible.

The coarse-graining approach was cultivated most broadly by the Vlachos group [237-244]. The idea is to assemble microscopic neighboring sites into coarse cells (collection of sites). A coarse cell does not designate an occupation of a single site, but, for each type of adsorbate, the number of such adsorbates in the cell is specified and their population coverage in the cell is described. The adsorbate may be allowed to interact with, react with, and diffuse to nearby cells. The processes (i.e., adsorption, desorption, and diffusion) are executed according to their transition probability. This execution may substitute one atom for another different atom or diffuse an atom from one cell to its adjacent cell, thus modifying the population coverage. The latter is updated, the transition probabilities are recalculated according to it and the procedure is repeated; in this fashion, surface kinetics are forged in terms of population coverages of different types of adsorbates.

This drives to vast acceleration in comparison to a microscopic kMC simulation. For instance, much less time need to be devoted on simulating diffusion [212]: diffusional hops within the cells need not be simulated. They do not alter the population of the adsorbates within a cell (i.e., they do not alter the configuration of the new coarse-grained lattice), and can therefore be neglected. However, spatial coarse graining produces errors due to loss of information [241] within a coarse cell, i.e., due to the local mean field (well-mixed) assumption [214, 216].⁴⁷ These errors can be curtailed by adaptive mesh [239-241] and multigrid methods [242].

⁴⁷ Uniform distribution of particles is presumed and any local correlations among particles in a coarse cell are omitted.

B.5 τ -leap method

The coarse-grained kMC method still adheres to the one process-at-a time concept of the microscopic kMC method. While time acceleration is still attained, as mentioned above, further acceleration can be achieved through temporal coarse graining. This can be obtained by executing multiple processes at once utilizing the τ -leap method [245, 246]. This method was developed for kMC simulations of reaction rate equations (processes), for spatially uniform (well-mixed) systems.⁴⁸ The basis of the τ -leap method is that rather than executing one reaction in every microscopic time interval, a coarse time increment (τ) is selected, during which, a large number of reactions are fired at once. The reactions that are bundled together are presumed to be independent of each other, i.e., the incidence of one does not influence the others. In general, this is an approximation. It has been demonstrated, however, that the errors imported are insignificant provided that the relative change in the population of all chemical species at each step is slight [246]. This is the so-called leap condition. Obviously, the application of the τ -leap method to a microscopic lattice violates the leap condition since the population at each selected site alters from one to zero or vice versa during an event, i.e., the changes are large.

It has been proposed, however, that spatial coarse graining can overcome this problem [244]. In the spatial coarse-grained kMC method, one adopts adequately large coarse cells that encompass a large number of sites under the local mean field assumption. Then the application of the τ -leap method becomes unambiguous. The τ -leap CGMC method enables to take coarse time steps by firing multiple processes at each time for all cells. This approach extends the τ -leap method from well mixed systems (spatially homogeneous) [245, 246] to spatially distributed. This is the key ingredient that can surmount the bottleneck of one process at a time of the microscopic kMC method and permit time synchronization of multiple processors or parallel simulations on single and multi-GPUs [247].

Nevertheless, temporal coarse graining of a microscopic kMC simulation is attainable without disregarding the leap condition. Specifically, the combination of the well-known n -fold method, which generates groups of processes (classes), and the τ -leap method permits one to take coarse time steps in microscopic kMC simulations by firing multiple processes at once [236]. This method does not demand spatial coarse graining.

C. The effect of different coarse-graining levels in the z -direction *and* along the arclength of the surface profile

C.1 The effect of coarse-graining level in the z direction

The principal concept within our coarse grain kMC model is that several adjacent dangling bonds (adsorption sites for O atoms) are grouped to form a single coarse cell. The collection of coarse cells forms a new lattice in which each coarse cell contains b adsorption sites and is characterized by an occupancy fraction, namely by θ_0 ($0 < \theta_0 < 1$). The basic assumption is that

⁴⁸ There are no spatial variations of the concentrations of species within the system.

each configuration with the same occupancy number within a coarse cell has equal probability and that no spatial correlations exist among the adsorption sites (mean field approximation).

Figures C.1a and C.2a depict the evolution of θ_0 and the etching rate at a flat region of the surface profile for different coarse graining levels along the z -direction (Figure 2.8c). In particular, L_z is considered equal to 0.00015625 μm , 0.000625 μm and 0.00125 μm while the coarse-graining level along the arclength of the surface profile is kept constant. Concerning the flat region (Figure C.1a and C.2a), as L_z increases (i.e. as the surface cell area increases), not only the statistics are improved, i.e. the error bars decrease, but also the curves approach the theoretical values for θ_0 and etching rate respectively, however, at the expense of computational cost (time). When L_z increases, the error bars also decrease for θ_0 and the etching rate at the valley, the peak and the sidewall region (Figures C.1b, c and d and Figures C.2b, c and d respectively). In all cases, the results for L_z equal to 0.000625 and 0.00125 μm are very close suggesting that greater L_z would bring no further improvement. Although the results for L_z equal to 0.00015625 μm are not so close with the results of the other two cases, the error bars are sufficiently overlapping. So, in this work, L_z is equal to 0.00015625 μm , as this value is small enough to avoid an escalating computational time cost on the simulation and concurrently large enough to allow for an accurate solution.

C.2 The effect of coarse-graining level along the arclength of the surface profile

Figures C.3a and C.4a depict the evolution of θ_0 and the etching rate at a flat region of the surface profile for 3 different coarse graining levels along the arclength of the surface profile, namely Δs is considered 0.001492 μm , 0.01492 μm , and 0.1507 μm , while keeping the coarse-graining level in the z -direction constant. The smaller Δs is, the larger the error bars are due to statistical noise. The smaller Δs approaches atomic scale, as it includes ~ 5 adsorption sites (an ion can remove ~ 4.5 adsorption sites when $\theta_0=1$). θ_0 converges asymptotically to the theoretical solution as Δs increases (Figure C.3a). The same applies for the etching rate (Figure C.4a).

Regarding the sidewall region of the profile, the statistics are improved as the coarse graining level is increased. At the same time, by changing the length of the coarse cell, the local curvature of the surface profile changes and the degree of geometric shadowing of the coarse cell alters for the valley and peak region (Figures C.3b and c): the larger the level, the smaller the degree of shadowing of the cell. Hence, the cell steady state condition is modified also.

Consequently, Δs must be small enough in order not to impose a limit on the fidelity of the surface profile representation (i.e. geometric shadowing of particles) and concurrently large enough (i.e. not an atomistic representation of the evolving profile) in order to avoid large statistical fluctuations superimposed on the surface coverage and etching rate evolution. Hence, in this work, $\Delta s = 0.01492 \mu\text{m}$.

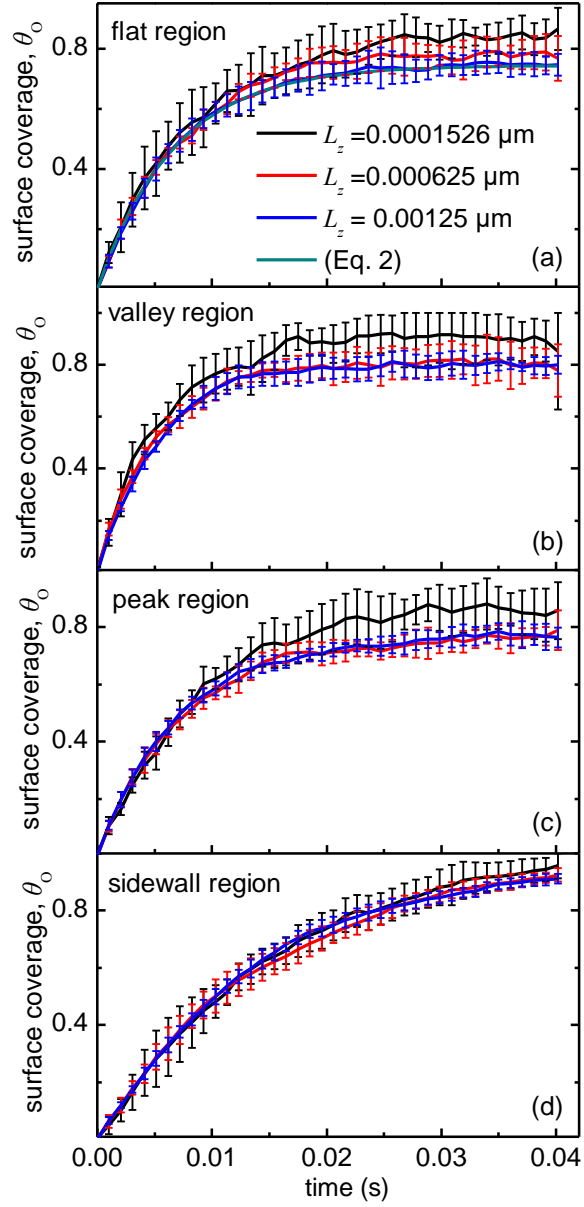


Figure C.1. Results of the kMC model (average values of 9 runs): θ_O vs. time at a) flat region, b) valley, c) peak region and d) middle of sidewall of the surface profile for L_z equal to 0.00015625, 0.000625 and 0.00125 μm ($\Delta s = 0.01492 \mu\text{m}$). Analytical solutions of θ_O (Equation 2.25) are also depicted in Figure C.1a. The sticking coefficient of O atoms (S_O) along the surface profile is updated with a period of $t_{\text{kMC}}/40$.

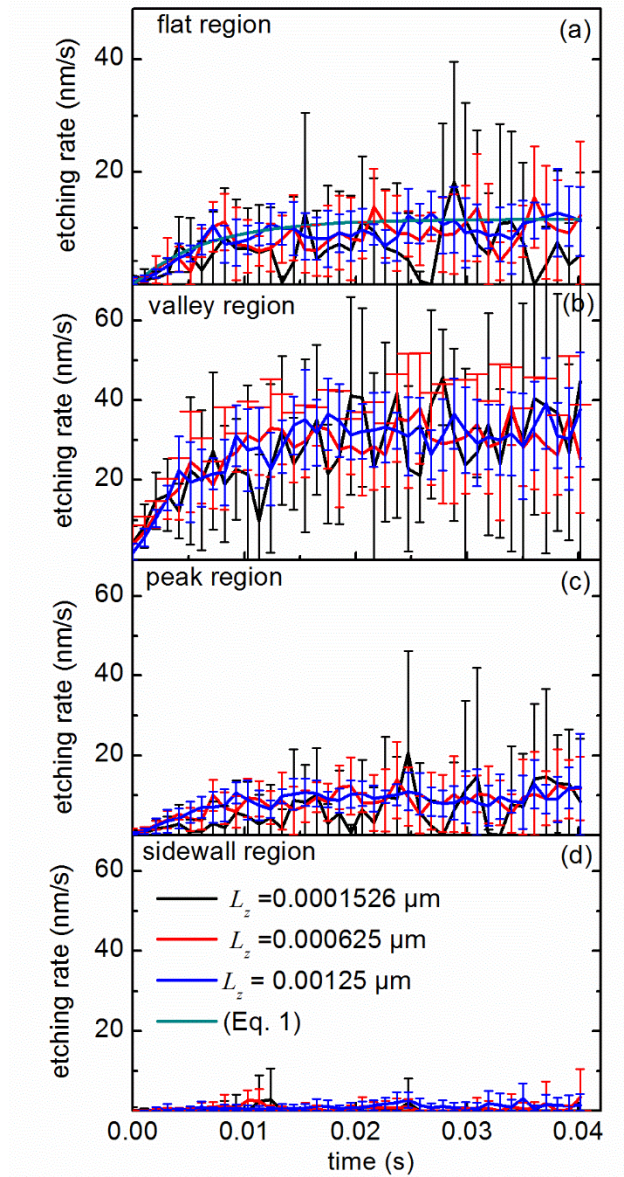


Figure C.2. Results of the kMC model (average values of 9 runs): etching rate vs. time at a) flat region, b) valley, c) peak region and d) middle of sidewall of the surface profile (see Figure 2.8c) for L_z equal to 0.0001526, 0.000625 and 0.00125 μm ($\Delta s = 0.01492 \mu\text{m}$). Analytical solution of etching rate (Equation 2.24) is also depicted in Figure C.2a. The sticking coefficient of O atoms (S_O) along the surface profile is updated with a period of $t_{\text{kMC}}/40$.

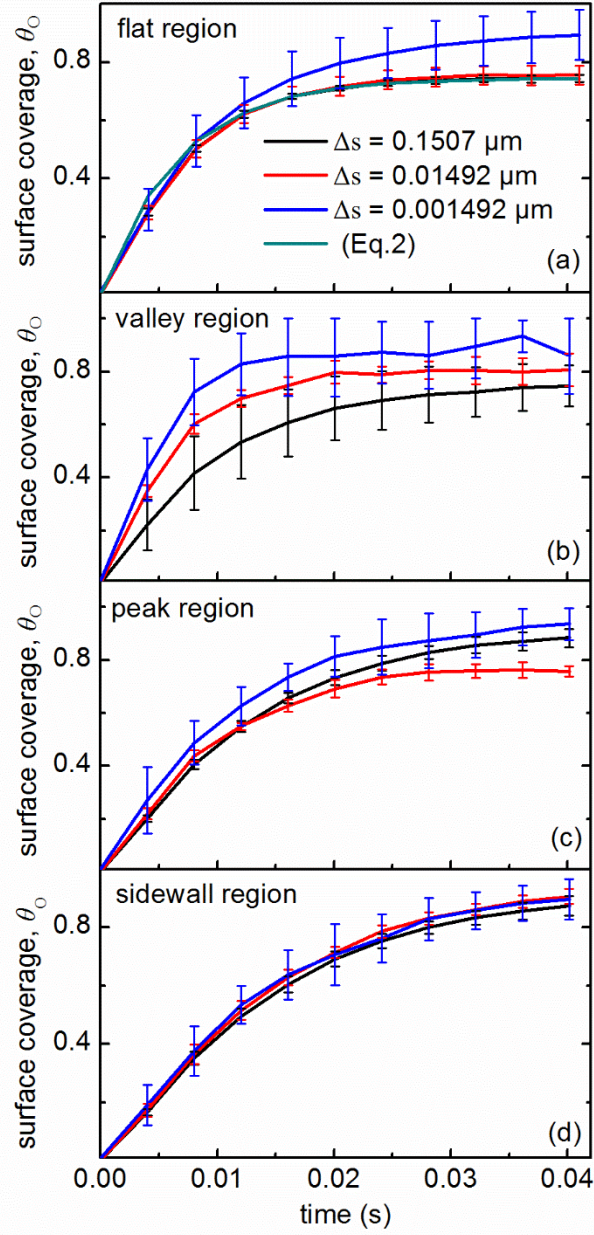


Figure C.3. Results of the kMC model (average values of 9 runs): θ_O vs. time at a) flat region, b) valley, c) peak region and d) middle of sidewall of the surface profile (Figure 2.8c) for $\Delta s = 0.001492 \mu\text{m}$, $0.01492 \mu\text{m}$, and $0.1507 \mu\text{m}$ ($L_z = 0.00015625 \mu\text{m}$). Analytical solutions of θ_O (Equation 2.25) is also depicted in Figure C.3(a). The sticking coefficient of O atoms (S_O) along the surface profile is updated with a period of $t_{\text{kMC}}/40$.

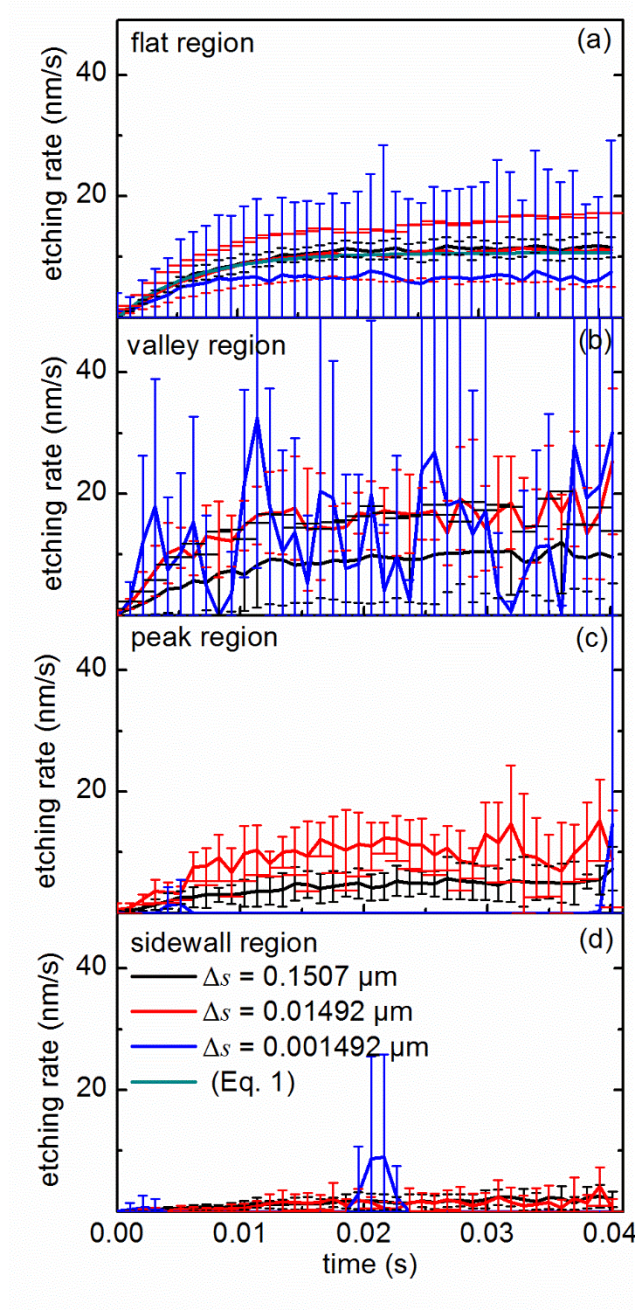


Figure C.4. Results of the kMC model (average values of 9 runs): etching rate vs. time at a) flat region, b) valley, c) peak region and d) middle of sidewall of the surface profile (Figure 2.8c) for $\Delta s = 0.001492 \mu\text{m}$, $0.01492 \mu\text{m}$, and $0.1507 \mu\text{m}$ ($L_z = 0.00015625 \mu\text{m}$). Analytical solutions of etching rate (Equation 2.24) is also depicted in Figure C.4a. The sticking coefficient of O atoms (S_O) along the surface profile is updated with a period of $t_{\text{kMC}}/40$.

D. The effect of dielectric thickness on the charging time through an analytical approach

The aim of the following analysis is the justification of the decrease of the charging time (i.e. the time required to arrive at a steady state condition) when the thickness of the dielectric substrate increases. For this, a simplified case allowing for analytical treatment will be utilized: A flat interface between a vacuum space (medium 1) and a dielectric substrate (medium 2) is considered (Figure D.1). The surface is bombarded with a flux of monoenergetic positive ions; no electrons (or negative ions) arrive on the surface. Gradually, a positive charge density builds up on the interface and a charging potential is developed. The effect of the developing electric field coming from this potential on the flux and the energy of the ions will be gradually enhanced. At steady state, the ion flux on the interface must be zero, because, owing to the absence of an electron flux, this is required for maintaining the current balance. This will happen when the charging potential on the interface arrives at a value equal to the E_+/q_+ , where E_+ and q_+ is the energy and the charge of the ions. **The faster this charging potential is built up, the lower the charging time is.**

The surface charge density scales with the number of ions arriving on the interface and consequently with time. If the surface charge density on the interface due to ion bombardment is $\sigma(t)$ after a time space t , then the charging potential on the interface is (through the solution of the Laplace equation with the method of separation of variables)[83]

$$V_s(t) = \frac{\sigma(t)h}{\varepsilon_0 \cdot (\varepsilon_{r1} + \varepsilon_{r2} \frac{h}{b})} \quad (D.1)$$

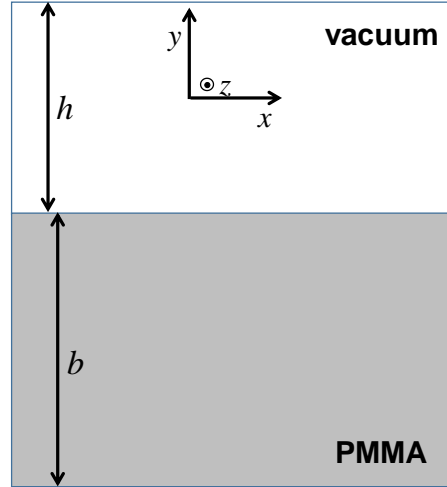


Figure D.1. The rectangular domain utilized for the analytical solution.

where ε_0 is the permittivity of free space. ε_{r1} and ε_{r2} are the relative permittivities in vacuum (which is equal to 1) and in medium 2, h is the height of the vacuum space and b the thickness of the dielectric/polymeric substrate (see Figure D.1).

From Equation D.1, for the same surface charge density (time), the thicker substrate results into a greater charging potential on the interface. Thus, **the charging potential is built up faster and the charging time is lower for the thicker substrate**. Additionally, for a dielectric substrate with an infinite thickness, or better when $h/b \rightarrow 0$, Equation D.1 becomes

$$V_s(t) = \frac{\sigma(t)h}{\epsilon_0\epsilon_{r1}}. \quad (D.2)$$

When $h/b \rightarrow 0$, the solution of the Laplace equation is the same as when the interface is the bottom boundary of the simulation domain. The scale length for the variation of potential in medium 2 can be regarded as infinite compared to the scale length for the corresponding variation in medium 1 or, equivalently, the electric field in medium 2 can be considered as zero. Thus, in order to calculate the charging potential at steady state, it is not necessary to solve the Laplace equation in the dielectric substrate.

8. References

- [1] N. Vourdas, A. Tserepi, E. Gogolides, Nanotextured super-hydrophobic transparent poly(methyl methacrylate) surfaces using high-density plasma processing, *Nanotechnology* 18 (2007) 125304.
- [2] U. Schulz, P. Munzert, R. Leitel, I. Wendling, N. Kaiser, A. Tünnermann, Antireflection of transparent polymers by advanced plasma etching procedures, *Opt. Express* 15 (2007) 13108-13113.
- [3] A. Chen, K. Kaviani, A.W. Rempel, S. Kalluri, W.H. Steier, Y. Shi, Z. Liang, L.R. Dalton, Optimized Oxygen Plasma Etching of Polyurethane-Based Electro-optic Polymer for Low Loss Optical Waveguide Fabrication, *Journal of The Electrochemical Society* 143 (1996) 3648-3651.
- [4] V.C. Rucker, K.L. Havenstrite, B.A. Simmons, S.M. Sickafoose, A.E. Herr, R. Shediach, Functional Antibody Immobilization on 3-Dimensional Polymeric Surfaces Generated by Reactive Ion Etching, *Langmuir* 21 (2005) 7621-7625.
- [5] W.L. Murphy, T.C. McDevitt, A.J. Engler, Materials as stem cell regulators, *Nature Materials* 13 (2014) 547.
- [6] K. Metavarayuth, P. Sitasuwan, X. Zhao, Y. Lin, Q. Wang, Influence of Surface Topographical Cues on the Differentiation of Mesenchymal Stem Cells in Vitro, *ACS Biomaterials Science & Engineering* 2 (2016) 142-151.
- [7] F.F. Borghi, A.E. Rider, S. Kumar, Z.J. Han, D. Haylock, K. Ostrikov, Emerging Stem Cell Controls: Nanomaterials and Plasma Effects, *Journal of Nanomaterials* 2013 (2013) 15.
- [8] J. Yang, D.Y. Kwok, Effect of liquid slip in electrokinetic parallel-plate microchannel flow, *J Colloid Interface Sci* 260 (2003) 225-233.
- [9] N. Vourdas, A. Tserepi, A.G. Boudouvis, E. Gogolides, Plasma processing for polymeric microfluidics fabrication and surface modification: Effect of super-hydrophobic walls on electroosmotic flow, *Microelectron Eng* 85 (2008) 1124-1127.
- [10] C.M. Chan, T.M. Ko, H. Hiraoka, Polymer surface modification by plasmas and photons, *Surface Science Reports* 24 (1996) 1-54.
- [11] A. Vesel, M. Mozetic, New developments in surface functionalization of polymers using controlled plasma treatments, *Journal of Physics D: Applied Physics* 50 (2017) 293001.
- [12] J. Friedrich, *The Plasma Chemistry of Polymer Surfaces: Advanced Techniques for Surface Design*, Wiley-VCH Verlag & Co. KGaA, Weinheim, Germany, 2012.
- [13] J.R. Roth, *Industrial Plasma Engineering*, IOP Publishing 2001.
- [14] A. Fridman, *Plasma Chemistry*, Cambridge University Press 2008.
- [15] E. Gogolides, V. Constantoudis, G. Kokkoris, D. Kontziampasis, K. Tsougeni, G. Boulousis, M. Vlachopoulou, A. Tserepi, Controlling roughness: From etching to nanotexturing and plasma-directed organization on organic and inorganic materials, *Journal of Physics D: Applied Physics* 44 (2011) 174021 (174013pp).
- [16] N. Vourdas, D. Kontziampasis, G. Kokkoris, V. Constantoudis, A. Goodyear, A. Tserepi, M. Cooke, E. Gogolides, Plasma directed assembly and organization: Bottom-up nanopatterning using top-down technology, *Nanotechnology* 21 (2010) 085302 (085308pp).
- [17] D. Kontziampasis, V. Constantoudis, E. Gogolides, Plasma Directed Organization of Nanodots on Polymers: Effects of Polymer Type and Etching Time on Morphology and Order, *Plasma Processes and Polymers* 9 (2012) 866-872.
- [18] *The Encyclopedia of Plasma Technology*, CRC Press Taylor & Francis Group, Boca Raton, 2016.
- [19] J.J. Végh, D.B. Graves, Molecular Dynamics Simulations of Ar⁺—Organic Polymer Interactions, *Plasma Processes and Polymers* 6 (2009) 320-334.
- [20] N. Agarwal, S. Ponoht, J. Plawsky, P.D. Persans, Roughness evolution in polyimide films during plasma etching, *Appl. Phys. Lett.* 78 (2001) 2294-2296.

- [21] M. Collaud Coen, R. Lehmann, P. Groening, L. Schlapbach, Modification of the micro- and nanotopography of several polymers by plasma treatments, *Appl Surf Sci* 207 (2003) 276-286.
- [22] K. Tsougeni, N. Vourdas, A. Tserepi, E. Gogolides, C. Cardinaud, Mechanisms of Oxygen Plasma Nanotexturing of Organic Polymer Surfaces: From Stable Super Hydrophilic to Super Hydrophobic Surfaces, *Langmuir* 25 (2009) 11748-11759.
- [23] K.N. Pandiyaraj, V. Selvarajan, R.R. Deshmukh, M. Bousmina, The effect of glow discharge plasma on the surface properties of Poly (ethylene terephthalate) (PET) film, *Surface and Coatings Technology* 202 (2008) 4218-4226.
- [24] S.H. Kim, S.W. Na, N.E. Lee, Y.W. Nam, Y.-H. Kim, Effect of surface roughness on the adhesion properties of Cu/Cr films on polyimide substrate treated by inductively coupled oxygen plasma, *Surface and Coatings Technology* 200 (2005) 2072-2079.
- [25] G. Kokkoris, N. Vourdas, E. Gogolides, Plasma Etching and Roughening of Thin Polymeric Films: A Fast, Accurate, in situ Method of Surface Roughness Measurement, *Plasma Processes and Polymers* 5 (2008) 825-833.
- [26] S.M.S. C. Y. Chang, *Ulsi Technology*, McGraw-Hill (1996) 329-330.
- [27] A. Piel, *Plasma Physics: An Introduction to Laboratory, Space, and Fusion Plasmas*, Springer (2010) 1-43.
- [28] G. Kokkoris, Ολοκληρωμένη προσομοίωση εξέλιξης τοπογραφίας κατά την εγχάραξη μικρο- και νανο-δομών με πλάσμα, (2005).
- [29] B. Chapman, *Glow Discharge Processes*, John Wiley & Sons (1980) 49-74, 139-172.
- [30] U.S. Inan, M. Gołkowski, *Principles of Plasma Physics for Engineers and Scientists* Cambridge University Press (2011) 1-19.
- [31] M.F. Cansizoglu, M. Yurukcu, T. Karabacak, Ripple Formation during Oblique Angle Etching, *THE Coatings* 9 (2019) 272.
- [32] P. Chabert, N. Braithwaite, *Physics of Radio-Frequency Plasmas*, Cambridge University Press (2011) 96-130.
- [33] D.W. Hess, Plasma–material interactions, *J Vac Sci Technol A* 8 (1990) 1677-1684.
- [34] W.L. Murphy, T.C. McDevitt, A.J. Engler, Materials as stem cell regulators, *Nat. Mater.* 13 (2014) 547-557.
- [35] K. Metavarayuth, P. Sitasuwan, X. Zhao, Y. Lin, Q. Wang, Influence of Surface Topographical Cues on the Differentiation of Mesenchymal Stem Cells in Vitro, *ACS Biomater. Sci. Eng.* 2 (2016) 142-151.
- [36] F.F. Borghi, A.E. Rider, S. Kumar, Z.J. Han, D. Haylock, K. Ostrikov, Emerging stem cell controls: Nanomaterials and plasma effects, *J. Nanomater.* 2013 (2013) 329139 (329115 pages).
- [37] I.O. Smith, X.H. Liu, L.A. Smith, P.X. Ma, Nanostructured polymer scaffolds for tissue engineering and regenerative medicine, *Wiley Interdiscip. Rev. Nanomedicine Nanobiotechnology* 1 (2009) 226-236.
- [38] J.H. Kim, H.W. Kim, K.J. Cha, J. Han, Y.J. Jang, D.S. Kim, J.H. Kim, Nanotopography Promotes Pancreatic Differentiation of Human Embryonic Stem Cells and Induced Pluripotent Stem Cells, *ACS Nano* 10 (2016) 3342-3355.
- [39] G. Kokkoris, Etching of open area surfaces. Mechanism and modeling, (2012) 3-6.
- [40] J.W. Coburn, H.F. Winters, Plasma-assisted etching in microfabrication, *Ann. Rev. Mater. Sci* 13 (1983) 91-116.
- [41] K. Nojiri, *Dry etching technology for semiconductors*, Springer, London, 2015.
- [42] H. Gokan, S. Esho, Y. Ohnishi, Dry Etch Resistance of Organic Materials, *Journal of the Electrochemical Society* 130 (1983) 143-146.
- [43] G.K. Choudhary, J.J. Végh, D.B. Graves, Molecular dynamics simulations of oxygen-containing polymer sputtering and the Ohnishi parameter, *Journal of Physics D: Applied Physics* 42 (2009) 242001242001.

- [44] A. Bès, M. Koo, T.L. Phan, A. Lacoste, J. Pelletier, Oxygen plasma etching of hydrocarbon-like polymers: Part II experimental validation, *Plasma Processes and Polymers* 15 (2018).
- [45] M.R. Sanchis, O. Calvo, O. Fenollar, D. Garcia, R. Balart, Surface modification of a polyurethane film by low pressure glow discharge oxygen plasma treatment, *Journal of Applied Polymer Science* 105 (2007) 1077-1085.
- [46] E.M. Liston, L. Martinu, M.R. Wertheimer, Plasma surface modification of polymers for improved adhesion: a critical review, *Journal of Adhesion Science and Technology* 7 (1993) 1091-1127.
- [47] E. Bormashenko, G. Whyman, V. Multanen, E. Shulzinger, G. Chaniel, Physical mechanisms of interaction of cold plasma with polymer surfaces, *J Colloid Interface Sci* 448 (2015) 175-179.
- [48] J. Drotar, Y. Zhao, T.-M. Lu, G. Wang, Surface roughening in shadowing growth and etching in 2+1 dimensions, *Physical Review B* 62 (2000) 2118-2125.
- [49] J. Drotar, Y. Zhao, T.-M. Lu, G. Wang, Mechanisms for plasma and reactive ion etch-front roughening, *Physical Review B* 61 (2000) 3012-3021.
- [50] G. Kokkoris, E. Gogolides, The potential of ion-driven etching with simultaneous deposition of impurities for inducing periodic dots on surfaces, *Journal of Physics D: Applied Physics* 45 (2012) 165204 (165209pp).
- [51] G. Kokkoris, V. Constantoudis, P. Angelikopoulos, G. Boulousis, E. Gogolides, Dual nanoscale roughness on plasma-etched Si surfaces: Role of etch inhibitors, *Phys. Rev. B Condens. Matter Mater. Phys.* 76 (2007).
- [52] O. Kouichi, N. Nobuya, T. Hirotaka, T. Yoshinori, E. Koji, Surface morphology evolution during plasma etching of silicon: roughening, smoothing and ripple formation, *Journal of Physics D: Applied Physics* 50 (2017) 414001 (414031pp).
- [53] M.E. Vlachopoulou, G. Kokkoris, C. Cardinaud, E. Gogolides, A. Tserepi, Plasma etching of poly(dimethylsiloxane): Roughness formation, mechanism, control, and application in the fabrication of microfluidic structures, *Plasma Processes and Polymers* 10 (2013) 29-40.
- [54] E. Gogolides, V. Constantoudis, G. Kokkoris, Toward an integrated line edge roughness understanding: metrology, characterization, and plasma etching transfer, 868505.
- [55] M. Fouchier, E. Pargon, B. Bardet, An atomic force microscopy-based method for line edge roughness measurement, *J Appl Phys* 113 (2013) 104903.
- [56] W. Guo, H.H. Sawin, Review of profile and roughening simulation in microelectronics plasma etching, *J. Phys. D Appl. Phys.* 42 (2009) 194014.
- [57] X. Sun, X. Li, C. Chen, K. Zhang, J. Meng, X. Wang, T. Yang, D. Zhang, F. Wang, Z. Xie, Optimized inductively coupled plasma etching for poly(methyl-methacrylate-glycidly-methacrylate) optical waveguide, *Thin Solid Films* 520 (2012) 5946-5951.
- [58] K. Ellinas, K. Tsougeni, P.S. Petrou, G. Boulousis, D. Tsoukleris, E. Pavlatou, A. Tserepi, S.E. Kakabakos, E. Gogolides, Three-dimensional plasma micro–nanotextured cyclo-olefin-polymer surfaces for biomolecule immobilization and environmentally stable superhydrophobic and superoleophobic behavior, *Chem. Eng. J.* 300 (2016) 394-403.
- [59] K. Tsougeni, A. Tserepi, G. Boulousis, V. Constantoudis, E. Gogolides, Control of Nanotexture and Wetting Properties of Polydimethylsiloxane from Very Hydrophobic to Super-Hydrophobic by Plasma Processing, *Plasma Process Polym.* 4 (2007) 398-405.
- [60] F. Palumbo, R. Di Mundo, D. Cappelluti, R. d'Agostino, SuperHydrophobic and SuperHydrophilic Polycarbonate by Tailoring Chemistry and Nano-texture with Plasma Processing, *Plasma Process Polym.* 8 (2011) 118-126.

- [61] Y.P. Li, S.Y. Li, W. Shi, M.K. Lei, Hydrophobic over-recovery during aging of polyethylene modified by oxygen capacitively coupled radio frequency plasma: A new approach for stable superhydrophobic surface with high water adhesion, *Surf. Coat. Technol.* 206 (2012) 4952-4958.
- [62] Y.P. Li, W. Shi, S.Y. Li, M.K. Lei, Transition of water adhesion on superhydrophobic surface during aging of polypropylene modified by oxygen capacitively coupled radio frequency plasma, *Surf. Coat. Technol.* 213 (2012) 139-144.
- [63] J.P. Fernández-Blázquez, D. Fell, E. Bonaccorso, A.d. Campo, Superhydrophilic and superhydrophobic nanostructured surfaces via plasma treatment, *J. Colloid Interface Sci.* 357 (2011) 234-238.
- [64] A. Vesel, I. Junkar, U. Cvelbar, J. Kovac, M. Mozetic, Surface modification of polyester by oxygen- and nitrogen-plasma treatment, *Surf. Interface Anal.* 40 (2008) 1444-1453.
- [65] I. Junkar, A. Vesel, U. Cvelbar, M. Mozetič, S. Strnad, Influence of oxygen and nitrogen plasma treatment on polyethylene terephthalate (PET) polymers, *Vacuum* 84 (2009) 83-85.
- [66] D.P. Papageorgiou, K. Tsougeni, A. Tserepi, E. Gogolides, Superhydrophobic, hierarchical, plasma-nanotextured polymeric microchannels sustaining high-pressure flows, *Microfluid. Nanofluidics* 14 (2013) 247-255.
- [67] N. Vourdas, A. Tserepi, A.G. Boudouvis, E. Gogolides, Plasma processing for polymeric microfluidics fabrication and surface modification: Effect of super-hydrophobic walls on electroosmotic flow, *Microelectron. Eng.* 85 (2008) 1124-1127.
- [68] A. Tserepi, E. Gogolides, A. Bourkoula, A. Kanioura, G. Kokkoris, P.S. Petrou, S.E. Kakabakos, Plasma Nanotextured Polymeric Surfaces for Controlling Cell Attachment and Proliferation: A Short Review, *Plasma Chem. Plasma Process.* 36 (2016) 107-120.
- [69] A. Bourkoula, V. Constantoudis, D. Kontziampasis, P.S. Petrou, S.E. Kakabakos, A. Tserepi, E. Gogolides, Roughness threshold for cell attachment and proliferation on plasma micro-nanotextured polymeric surfaces: the case of primary human skin fibroblasts and mouse immortalized 3T3 fibroblasts, *Journal of Physics D: Applied Physics* 49 (2016) 304002 (304010pp).
- [70] R. Di Mundo, M. Nardulli, A. Milella, P. Favia, R. Dagostino, R. Gristina, Cell adhesion on nanotextured slippery superhydrophobic substrates, *Langmuir* 27 (2011) 4914-4921.
- [71] R. Gristina, E. D'Aloia, G.S. Senesi, A. Milella, M. Nardulli, E. Sardella, P. Favia, R. D'Agostino, Increasing cell adhesion on plasma deposited fluorocarbon coatings by changing the surface topography, *J. Biomed. Mater. Res. Part B Appl. Biomater.* 88 (2009) 139-149.
- [72] Y.-H. Ting, S.-M. Park, C.-C. Liu, X. Liu, F.J. Himpsel, P.F. Nealey, A.E. Wendt, Plasma etch removal of poly(methyl methacrylate) in block copolymer lithography, *Journal of Vacuum Science & Technology B: Microelectronics and Nanometer Structures Processing, Measurement, and Phenomena* 26 (2008) 1684-1689.
- [73] D. Nest, T.-Y. Chung, D.B. Graves, S. Engelmann, R.L. Bruce, F. Weilnboeck, G.S. Oehrlein, D. Wang, C. Andes, E.A. Hudson, Understanding the Roughening and Degradation of 193 nm Photoresist during Plasma Processing: Synergistic Roles of Vacuum Ultraviolet Radiation and Ion Bombardment, *Plasma Processes and Polymers* 6 (2009) 649-657.
- [74] R.L. Bruce, F. Weilnboeck, T. Lin, R.J. Phaneuf, G.S. Oehrlein, B.K. Long, C.G. Willson, J.J. Vegh, D. Nest, D.B. Graves, Relationship between nanoscale roughness and ion-damaged layer in argon plasma exposed polystyrene films, *J Appl Phys* 107 (2010) 084310-084311 - 084310-084315.
- [75] R.L. Bruce, S. Engelmann, T. Lin, T. Kwon, R.J. Phaneuf, G.S. Oehrlein, B.K. Long, C.G. Willson, J.J. Végh, D. Nest, D.B. Graves, A. Alizadeh, Study of ion and vacuum ultraviolet-induced effects on styrene- and ester-based polymers exposed to argon plasma, *Journal of Vacuum Science & Technology B: Microelectronics and Nanometer Structures Processing, Measurement, and Phenomena* 27 (2009) 1142-1155.

- [76] R. Bruce, Influence of Polymer Structure on Plasma-Polymer Interactions in Resist Materials, University of Maryland, Baltimore 2010, 2010.
- [77] T.-J. Ko, W. Jo, H.J. Lee, K.H. Oh, M.-W. Moon, Nanostructures formed on carbon-based materials with different levels of crystallinity using oxygen plasma treatment, *Thin Solid Films* 590 (2015) 324-329.
- [78] D. Kontziampasis, T. Trantidou, A. Regoutz, E.J. Humphrey, D. Carta, C.M. Terracciano, T. Prodromakis, Effects of Ar and O₂ Plasma Etching on Parylene C: Topography versus Surface Chemistry and the Impact on Cell Viability, *Plasma Processes and Polymers* 13 (2016) 324-333.
- [79] T. Hatsuse, N. Nakazaki, H. Tsuda, Y. Takao, K. Eriguchi, K. Ono, Origin of plasma-induced surface roughening and ripple formation during plasma etching: The crucial role of ion reflection, *J Appl Phys* 124 (2018).
- [80] K. Ono, N. Nakazaki, H. Tsuda, Y. Takao, K. Eriguchi, Surface morphology evolution during plasma etching of silicon: Roughening, smoothing and ripple formation, *Journal of Physics D: Applied Physics* 50 (2017).
- [81] H. Tsuda, Y. Takao, K. Eriguchi, K. Ono, Modeling and simulation of nanoscale surface rippling during plasma etching of Si under oblique ion incidence, *Japanese Journal of Applied Physics* 51 (2012).
- [82] G. Memos, E. Lidorikis, G. Kokkoris, Roughness evolution and charging in plasma-based surface engineering of polymeric substrates: The effects of ion reflection and secondary electron emission, *Micromachines* 9 (2018).
- [83] G. Memos, E. Lidorikis, G. Kokkoris, The interplay between surface charging and microscale roughness during plasma etching of polymeric substrates, *J Appl Phys* 123 (2018) 073303.
- [84] G. Memos, G. Kokkoris, Modeling of Charging on Unconventional Surface Morphologies of PMMA Substrates during Ar Plasma Etching, *Plasma Processes and Polymers* 13 (2016) 565-578.
- [85] H. Tsuda, M. Mori, Y. Takao, K. Eriguchi, K. Ono, Atomic-scale cellular model and profile simulation of Si etching: Formation of surface roughness and residue, *Thin Solid Films* 518 (2010) 3475-3480.
- [86] H. Tsuda, H. Miyata, Y. Takao, K. Eriguchi, K. Ono, Three-dimensional atomic-scale cellular model and feature profile evolution during Si etching in chlorine-based plasmas: Analysis of profile anomalies and surface roughness, *Jpn. J. Appl. Phys.* 50 (2011) 08JE06.
- [87] H. Tsuda, Y. Takao, K. Eriguchi, K. Ono, Modeling and simulation of nanoscale surface rippling during plasma etching of Si under oblique ion incidence, *Jpn. J. Appl. Phys.* 51 (2012) 249901.
- [88] N. Nakazaki, H. Tsuda, Y. Takao, K. Eriguchi, K. Ono, Two modes of surface roughening during plasma etching of silicon: Role of ionized etch products, *J. Appl. Phys.* 116 (2014) 223302.
- [89] H. Tsuda, N. Nakazaki, Y. Takao, K. Eriguchi, K. Ono, Surface roughening and rippling during plasma etching of silicon: Numerical investigations and a comparison with experiments, *J. Vac. Sci. Technol.* 32 (2014) 031212.
- [90] T. Hatsuse, N. Nakazaki, H. Tsuda, Y. Takao, K. Eriguchi, K. Ono, Origin of plasma-induced surface roughening and ripple formation during plasma etching: The crucial role of ion reflection, *J. Appl. Phys.* 124 (2018) 143301.
- [91] E. Zakka, V. Constantoudis, E. Gogolides, Roughness formation during plasma etching of composite materials: A kinetic Monte Carlo approach, *IEEE Trans. Plasma Sci.* 35 (2007) 1359-1369.
- [92] G. Kokkoris, V. Constantoudis, P. Angelikopoulos, G. Boulousis, E. Gogolides, Dual nanoscale roughness on plasma-etched Si surfaces: Role of etch inhibitors, *Phys. Rev. B Condens. Matter Mater. Phys.* 76 (2007) 193405.
- [93] G. Kokkoris, E. Gogolides, The potential of ion-driven etching with simultaneous deposition of impurities for inducing periodic dots on surfaces, *J. Phys. D* 45 (2012) 165204.
- [94] A. Iwakawa, H. Ohta, K. Eriguchi, K. Ono, Numerical investigation on origin of microscopic surface roughness during Si etching by chemically reactive plasmas, *Jpn. J. Appl. Phys.* 47 (2008) 6464-6466.
- [95] H. Tsuda, Y. Takao, K. Eriguchi, K. Ono, Molecular dynamics analysis of the formation of surface roughness during Si etching in chlorine-based plasmas, *Jpn. J. Appl. Phys.* 50 (2011) 08KB02.

- [96] M. Radmilović-Radjenović, B. Radjenović, Z.L.J. Petrović, Application of level set method in simulation of surface roughness in nanotechnologies, *Thin Solid Films* 517 (2009) 3954-3957.
- [97] M. Radmilović-Radjenović, B. Radjenović, The effects of chemical (isotropic) and anisotropic etching processes on the roughening of nanocomposite substrates, *Plasma Sci. Technol.* 12 (2010) 673-676.
- [98] B. Radjenović, M. Radmilović-Radjenović, The effect of different etching modes on the smoothing of the rough surfaces, *Mater. Lett.* 86 (2012) 165-167.
- [99] B. Radjenović, M. Radmilović-Radjenović, The effects of isotropic etching on roughening and smoothing of nanostructure, *Electron. Mater. Lett.* 8 (2012) 491-494.
- [100] G. Memos, E. Lidorikis, E. Gogolides, G. Kokkoris, A hybrid modeling framework for the investigation of surface roughening of polymers during oxygen plasma etching, *Journal of Physics D: Applied Physics* 54 (2021) 175205.
- [101] W. Guo, H.H. Sawin, Etching of SiO₂ in C₄F₈/Ar plasmas. II. Simulation of surface roughening and local polymerization, *J. Vac. Sci. Technol. A* 28 (2010) 259-270.
- [102] H. Tsuda, H. Miyata, Y. Takao, K. Eriguchi, K. Ono, Three-dimensional atomic-scale cellular model and feature profile evolution during Si etching in chlorine-based plasmas: Analysis of profile anomalies and surface roughness, *Japanese Journal of Applied Physics* 50 (2011).
- [103] H. Tsuda, Y. Takao, K. Eriguchi, K. Ono, Molecular dynamics analysis of the formation of surface roughness during Si etching in chlorine-based plasmas, *Japanese Journal of Applied Physics* 50 (2011).
- [104] A. Sethian, *Level Set Methods and Fast Marching Methods. Evolving Interfaces in Computational Geometry, Fluid Mechanics, Computer Vision, and Materials Science* Cambridge University Press, Cambridge, 1999.
- [105] R.F. S. Osher, *Level Set Methods and Dynamic Implicit Surfaces*, Springer, New York, 2003.
- [106] M. Radmilović-Radjenović, B. Radjenović, The effects of chemical (isotropic) and anisotropic etching processes on the roughening of nanocomposite substrates, *Plasma Sci. Technol.* 12 (2010) 673-676.
- [107] V. Constantoudis, G.P. Patsis, A. Tserepi, E. Gogolides, Quantification of line-edge roughness of photoresists. II. Scaling and fractal analysis and the best roughness descriptors, *Journal of Vacuum Science & Technology B: Microelectronics and Nanometer Structures Processing, Measurement, and Phenomena* 21 (2003) 1019-1026.
- [108] V. Constantoudis, G. Kokkoris, P. Xydi, E. Gogolides, E. Pargon, M. Martin, Line edge roughness transfer during plasma etching: modeling approaches and comparison with experimental results, *SPIE* 2009.
- [109] Y. Zhao, G.C. Wang, T.M. Lu, *Experimental methods in the physical sciences. Vol. 37. Characterization of amorphous and crystalline rough surface: Principles and applications*, Academic Press 2001.
- [110] F.D. Egitto, Plasma etching and modification of organic polymers, *Pure and Applied Chemistry*, 1990, pp. 1699.
- [111] *Plasma deposition, treatment, and etching of polymers*, Academic Press, Inc, San Diego, 1990.
- [112] M. Zeuner, J. Meichsner, H.U. Poll, Oxidative decomposition of polymethylmethacrylate (PMMA) in plasma etching, *Plasma Sources Sci. Technol.* 4 (1995) 406-415.
- [113] O. Joubert, J. Pelletier, Y. Arnal, The etching of polymers in oxygen-based plasmas: A parametric study, *J Appl Phys* 65 (1989) 5096-5100.
- [114] M. Pons, J. Pelletier, O. Joubert, P. Paniez, Development of polymers in $\alpha < 2$ plasmas: Temperature effects and transition to imperfect anisotropy, *Japanese Journal of Applied Physics* 34 (1995) 3723-3730.
- [115] M. Pons, O. Joubert, P. Paniez, J. Pelletier, Plasma etching of polymers: A reinvestigation of temperature effects, *J Appl Phys* 70 (1991) 2376-2379.

- [116] O. Joubert, J. Pelletier, C. Fiori, T.A. Nguyen Tan, Surface mechanisms in O_2 and SF_6 microwave plasma etching of polymers, *J Appl Phys* 67 (1990) 4291-4296.
- [117] J. Pelletier, Y. Arnal, O. Joubert, Etching mechanisms of polymers in oxygen microwave multipolar plasmas, *Appl. Phys. Lett.* 53 (1988) 1914-1916.
- [118] A. Bès, M. Koo, T.L. Phan, A. Lacoste, J. Pelletier, Oxygen plasma etching of hydrocarbon-like polymers: Part I Modeling, *Plasma Processes and Polymers* 15 (2018).
- [119] K.P. Giapis, G.S. Hwang, Pattern-dependent charging and the role of electron tunneling, *Japanese Journal of Applied Physics, Part 1: Regular Papers and Short Notes and Review Papers* 37 (1998) 2281-2290.
- [120] G.S. Hwang, K.P. Giapis, On the origin of the notching effect during etching in uniform high density plasmas, *J. Vac. Sci. Technol. B* 15 (1997) 70-87.
- [121] M. Schaepkens, G.S. Oehrlein, Asymmetric microtrenching during inductively coupled plasma oxide etching in the presence of a weak magnetic field, *Appl. Phys. Lett.* 72 (1998) 1293-1295.
- [122] R.A. Gottscho, C.W. Jurgensen, Microscopic uniformity in plasma etching, *Vacuum Science & Technology B: Microelectronics and Nanometer Structures* 10 (1992) pp.2133-2147.
- [123] M. Wang, M.J. Kushner, High energy electron fluxes in dc-augmented capacitively coupled plasmas. II. Effects on twisting in high aspect ratio etching of dielectrics, *Journal of Applied Physics* 107 (2010) 023309 - 023309-023311
- [124] H. Ohtake, S. Fukuda, B. Jinnai, T. Tatsumi, S. Samukawa, Prediction of Abnormal Etching Profile in High-Aspect-Ratio Via/Hole Etching Using On-Wafer Monitoring System, *Jpn. J. Appl. Phys.*, 49 (2010) 04DB14.
- [125] N. Marchack, J.P. Chang, Perspectives in nanoscale plasma etching: What are the ultimate limits?, *Journal of Physics D: Applied Physics* 44 (2011) 174011.
- [126] C.G.N. Lee, K.J. Kanarik, R.A. Gottscho, The grand challenges of plasma etching: A manufacturing perspective, *Journal of Physics D: Applied Physics* 47 (2014) 273001.
- [127] T.G. Madziwa-Nussinov, D. Arnush, F.F. Chen, Ion orbits in plasma etching of semiconductors, *Physics of Plasmas* 15 (2008).
- [128] H. Morioka, D. Matsunaga, H. Yagi, Suppression of notching by lowering the bias frequency in electron cyclotron resonance plasma with a divergent magnetic field, *Journal of Vacuum Science and Technology A: Vacuum, Surfaces and Films* 16 (1998) 1588-1593.
- [129] V. Ishchuk, B.E. Volland, M. Hauguth, M. Cooke, I.W. Rangelow, Charging effect simulation model used in simulations of plasma etching of silicon, *Journal of Applied Physics* 112 (2012).
- [130] M. Wang, M.J. Kushner, High energy electron fluxes in dc-augmented capacitively coupled plasmas. II. Effects on twisting in high aspect ratio etching of dielectrics, *J Appl Phys* 107 (2010) 023309-023301 - 023309-023311.
- [131] J.C. Arnold, H.H. Sawin, Charging of pattern features during plasma etching, *J Appl Phys* 70 (1991) 5314-5317.
- [132] A. Shibkov, M.K. Abatchev, H.K. Kang, M.Y. Lee, Numerical simulation of local charging during plasma etching of a dielectric material, *Electron. Lett.* 32 (1996) 890-891.
- [133] J. Matsui, K. Maeshige, T. Makabe, Effect of aspect ratio on topographic dependent charging in oxide etching, *Journal of Physics D: Applied Physics* 34 (2001) 2950-2955.
- [134] H.S. Park, S.J. Kim, Y.Q. Wu, J.K. Lee, Effects of plasma chamber pressure on the etching of micro structures in SiO_2 with the charging effects, *IEEE Transactions on Plasma Science* 31 (2003) 703-710.
- [135] S.H. Lee, J.K. Lee, S.W. Jung, D.W. Kim, S.J. You, Self-consistent charge-up simulation for the microscopic feature of SiO_2 layer in rf capacitive discharge, *Curr. Appl. Phys.* 15 (2015) 1463-1471.
- [136] T. Lee, S.S. Kim, Y.S. Jho, G. Park, C.S. Chang, Electrostatic potential fluctuation induced by charge discreteness in a nanoscale trench, *Phys. Plasmas* 14 (2007) 103501.

- [137] J.A. Kenney, G.S. Hwang, Prediction of stochastic behavior in differential charging of nanopatterned dielectric surfaces during plasma processing, *J Appl Phys* 101 (2007) 044307.
- [138] Z. Zhao, Z. Dai, Y. Wang, Feature profile evolution during etching of SiO₂ in radio-frequency or direct-current plasmas, *Plasma Sci. Technol.* 14 (2012) 64-70.
- [139] T. Shimada, T. Yagisawa, T. Makabe, Modeling of feature profile evolution in SiO₂ as functions of radial position and bias voltage under competition among charging, deposition, and etching in two-frequency capacitively coupled plasma, *Japanese Journal of Applied Physics, Part 1: Regular Papers and Short Notes and Review Papers* 45 (2006) 8876-8882.
- [140] M. Radmilović-Radjenović, B. Radjenović, M. Savić, The surface charging effects in three-dimensional simulation of the profiles of plasma-etched nanostructures, *Int J. Numer. Model., Electron. Netw. Devices Fields* 24 (2011) 535-544.
- [141] H. Ohtake, S. Fukuda, B. Jinnai, T. Tatsumi, S. Samukawa, Prediction of abnormal etching profile in high-aspect-ratio via/hole etching using on-wafer monitoring system, *Japanese Journal of Applied Physics* 49 (2010) 04DB14-01.
- [142] K.P. Giapis, G.S. Hwang, Plasma interactions with high aspect ratio patterned surfaces: Ion transport, scattering, and the role of charging, *Thin Solid Films* 374 (2000) 175-180.
- [143] Z.L. Dai, G. Yue, Y.N. Wang, Study on mechanism of etching in low pressure radio-frequency plasmas, *Curr. Appl. Phys.* 11 (2011) S121-S125.
- [144] Z.L. Dai, S.Q. Zhang, Y.N. Wang, Study on feature profile evolution for chlorine etching of silicon in an RF biased sheath, *Vacuum* 89 (2013) 197-202.
- [145] T. Kinoshita, M. Hane, J.P. McVittie, Notching as an example of charging in uniform high density plasmas, *J. Vac. Sci. Technol. B* 14 (1996) 560-565.
- [146] V. Ishchuk, B.E. Volland, M. Hauguth, M. Cooke, I.W. Rangelow, Charging effect simulation model used in simulations of plasma etching of silicon, *J Appl Phys* 112 (2012) 084308.
- [147] K.P. Giapis, G.S. Hwang, O. Joubert, The role of mask charging in profile evolution and gate oxide degradation, *Microelectron Eng* 61-62 (2002) 835-847.
- [148] G.S. Hwang, K.P. Giapis, Pattern-dependent charging in plasmas: Electron temperature effects, *Phys. Rev. Lett.* 79 (1997) 845-848.
- [149] G.S. Hwang, K.P. Giapis, Ion mass effect in plasma-induced charging, *Appl. Phys. Lett.* 71 (1997) 1942-1944.
- [150] G.S. Hwang, K.P. Giapis, On the link between electron shadowing and charging damage, *J. Vac. Sci. Technol. B* 15 (1997) 1839-1842.
- [151] G.S. Hwang, K.P. Giapis, Aspect-ratio-dependent charging in high-density plasmas, *J Appl Phys* 82 (1997) 566-571.
- [152] G.S. Hwang, K.P. Giapis, The influence of mask thickness on charging damage during overetching, *J Appl Phys* 82 (1997) 572-577.
- [153] G.S. Hwang, K.P. Giapis, Prediction of multiple-feature effects in plasma etching, *Appl. Phys. Lett.* 70 (1997) 2377-2379.
- [154] G.S. Hwang, K.P. Giapis, The influence of electron temperature on pattern-dependent charging during etching in high-density plasmas, *J Appl Phys* 81 (1997) 3433-3439.
- [155] G.S. Hwang, K.P. Giapis, The influence of surface currents on pattern-dependent charging and notching, *J Appl Phys* 84 (1998) 683-689.
- [156] G.S. Hwang, K.P. Giapis, Pattern-dependent charging in plasmas, *IEEE Transactions on Plasma Science* 27 (1999) 102-103.
- [157] G.S. Hwang, K.P. Giapis, Aspect ratio independent etching of dielectrics, *Appl. Phys. Lett.* 71 (1997) 458-460.
- [158] P. Zhang, Relationship between edge roughness in mask pattern and charging in plasma etching, *Plasma Processes and Polymers* 17 (2020) 1900177.

- [159] P. Zhang, Exploring the evolution of asymmetric pattern of mask hole during plasma etching process by particle simulation method, *Results in Physics* 12 (2019) 1747-1753.
- [160] P. ZHANG, STUDY ON SURFACE CHARGING EFFECT ON MASK DURING PLASMA ETCHING PROCESS THROUGH PARTICLE SIMULATION, *Surface Review and Letters* 26 (2019) 1850168.
- [161] P. Zhang, J. Wang, Y. Sun, Z. Ding, Charging effect in plasma etching mask of hole array, *Plasma Sci. Technol.* 15 (2013) 570-576.
- [162] W. Kunstler, P. Frubing, R. Gerhard-Multhaupt, J. Cerny, J. Klemberg-Sapieha, L. Martinu, M.R. Wertheimer, A. Hollander, J. Behnisch, Surface-charging behavior of plasma-treated polymer films, 1998 Annual Report Conference on Electrical Insulation and Dielectric Phenomena (Cat. No.98CH36257), 1998, pp. 609-612
- [163] T. Shimada, T. Yagisawa, T. Makabe, Self-consistent modeling of feature profile evolution in plasma etching and deposition, *Jpn J. Appl. Phys. Part 2 Letter* 45 (2006) L132-L134.
- [164] B. Radjenović, M. Radmilović-Radjenović, 3D Etching profile evolution simulations: Time dependence analysis of the profile charging during SiO₂ etching in plasma, *J. Phys. Conf. Ser.* 86 (2007) 012017.
- [165] K. Ono, N. Nakazaki, TsudaHirohisa, TakaoYoshinori, K. Eriguchi, Surface morphology evolution during plasma etching of silicon: roughening, smoothing and ripple formation, *J Phys D* 50 (2017) 414001.
- [166] A.P. Palov, A.M. Yu, T.V. Rakhimova, D. Shamiryan, Charging and the secondary electron–electron emission on a trench surface: broadening and shift of ion energy spectrum at plasma trench etching, *Journal of Physics D: Applied Physics* 43 (2010) 075203 (075207pp).
- [167] A.P. Palov, Y.A. Mankelevich, T.V. Rakhimova, D. Shamiryan, Charging of Submicron Structures during Silicon Dioxide Etching in One- and Two-Frequency Gas Discharges, *Plasma Physics Reports* 36 (2010) 891-901.
- [168] S. Yoshimura, Y. Tsukazaki, M. Kiuchi, S. Sugimoto, S. Hamaguchi, Sputtering yields and surface modification of poly(methyl methacrylate) (PMMA) by low-energy Ar⁺/ CF⁺ 3ion bombardment with vacuum ultraviolet (VUV) photon irradiation, *Journal of Physics D: Applied Physics* 45 (2012) 505201.505201-505201.505210.
- [169] www.srim.org.
- [170] G. Kokkoris, A. Tserepi, A.G. Boudouvis, E. Gogolides, Simulation of SiO₂ and Si feature etching for microelectronics and microelectromechanical systems fabrication: A combined simulator coupling modules of surface etching, local flux calculation, and profile evolution, *Journal of Vacuum Science and Technology A: Vacuum, Surfaces and Films* 22 (2004) 1896-1902.
- [171] N. Cheimarios, G. Kokkoris, A.G. Boudouvis, Multiscale modeling in chemical vapor deposition processes: Coupling reactor scale with feature scale computations, *Chemical Engineering Science* 65 (2010) 5018-5028.
- [172] J.A. Sethian, *Level Set Methods and Fast Marching Methods. Evolving Interfaces in Computational Geometry, Fluid Mechanics, Computer Vision, and Materials Science.* 2nd ed, Cambridge University Press, Cambridge, 1999.
- [173] S. Osher, R.P. Fedkiw, *Level Set Methods and Dynamic Implicit Surfaces*, Applied Mathematical Sciences, Volume 153, Springer, New York, 2003.
- [174] J.P. Vigouroux, O. Lee-Deacon, C. Le Gressus, C. Juret, C. Boiziau, Surface processes occurring during breakdown of high-voltage devices, *IEEE T. Electr. Insul.* EI-18 (1983) 287-291.
- [175] W.L. Martinez, A.R. Martinez, *Computational Statistics Handbook with MATLAB®*.
- [176] J.A. Sethian, Fast marching methods, *SIAM Rev.* 41 (1999) 199-235.
- [177] Z.G. Song, C.K. Ong, H. Gong, Secondary and backscattered electron yields of polymer surface under electron beam irradiation, *Appl Surf Sci* 119 (1997) 169-175.

- [178] É.I. Rau, E.N. Evsta'eva, M.V. Andrianov, Mechanisms of charging of insulators under irradiation with medium-energy electron beams, *Phys Solid State* 50 (2008) 621-630.
- [179] M. Boubaya, G. Blaise, Charging regime of PMMA studied by secondary electron emission, *Eur. Phys. J. Appl. Phys.* 37 (2007) 79-86.
- [180] Y. Masaaki, M. Kosuke, K. Yasuaki, K. Hiroaki, H. Yoshihiko, Analysis of Charging Phenomena of Polymer Films on Silicon Substrates under Electron Beam Irradiation, *Japanese Journal of Applied Physics* 47 (2008) 4890 - 4892.
- [181] Y. Lin, D.C. Joy, A new examination of secondary electron yield data, *Surf Interface Anal* 37 (2005) 895-900.
- [182] K.K. Yu, G.J. Zhang, N. Zheng, Y. Raitses, N.J. Fisch, Monte Carlo Simulation of Surface-Charging Phenomena on Insulators Prior to Flashover in Vacuum, *IEEE Transactions on Plasma Science* 37 (2009) 698-704.
- [183] E.A. Burke, Secondary Emission from Polymers, *IEEE trans Nucl Sci* 27 (1980) 1759-1764.
- [184] M. Dapor, M. Ciappa, W. Fichtner, Monte Carlo modeling in the low-energy domain of the secondary electron emission of polymethylmethacrylate for critical-dimension scanning electron microscopy, *SPIE*, 2010, pp. 9.
- [185] M. Dapor, Spectra of electrons emerging from PMMA, *GIT IMAGING & MICROSCOPY* 18 (2016) 38-39.
- [186] A. Palov, F. Haruhisa, H. Sanju, Monte Carlo Simulation of 1 eV–35 keV Electron Scattering in Teflon, *Japanese Journal of Applied Physics* 37 (1998) 6170.
- [187] A.J. Dekker, *Solid State Physics*, Prentice-Hall 1962.
- [188] H. Seiler, Secondary electron emission in the scanning electron microscope, *J Appl Phys* 54 (1983) R1-R18.
- [189] Y. Masaaki, N. Takahiro, K. Hiroaki, A Monte Carlo Calculation of Secondary Electron Emission from Organic Compounds, *Japanese Journal of Applied Physics* 43 (2004) 4004-4008.
- [190] H.v. Seggern, Charging Dynamics of Dielectrics Irradiated by Low Energy Electrons, *IEEE trans Nucl Sci* 32 (1985) 1503-1511.
- [191] M. Wang, M.J. Kushner, High energy electron fluxes in dc-augmented capacitively coupled plasmas. II. Effects on twisting in high aspect ratio etching of dielectrics, *J Appl Phys* 107 (2010).
- [192] S. Mouchtouris, G. Kokkoris, Multiscale Modeling of Low Pressure Plasma Etching Processes: Linking the Operating Parameters of the Plasma Reactor with Surface Roughness Evolution, *Plasma Processes and Polymers* 14 (2017) 1600147-1600147
- [193] S. Große-Kreul, C. Corbella, A. von Keudell, B. Ozkaya, G. Grundmeier, Surface Modification of Polypropylene (PP) by Argon Ions and UV Photons, *Plasma Processes and Polymers* 10 (2013) 1110-1119.
- [194] S. Große-Kreul, C. Corbella, A. von Keudell, Chemical and Physical Sputtering of Polyethylene Terephthalate (PET), *Plasma Processes and Polymers* 10 (2013) 225-234.
- [195] S. Yoshimura, Y. Tsukazaki, M. Kiuchi, S. Sugimoto, S. Hamaguchi, Sputtering yields and surface modification of poly(methyl methacrylate) (PMMA) by low-energy Ar⁺/ CF⁺ 3 ion bombardment with vacuum ultraviolet (VUV) photon irradiation, *Journal of Physics D: Applied Physics* 45 (2012).
- [196] C. Steinbruchel, Universal Energy-Dependence of Physical and Ion-Enhanced Chemical Etch Yields at Low Ion Energy, *Applied Physics Letters* 55 (1989) 1960-1962.
- [197] D. Zhang, S. Rauf, T.G. Sparks, P.L.G. Ventzek, Integrated equipment-feature modeling investigation of fluorocarbon plasma etching of SiO₂ and photoresist, *Journal Of Vacuum Science & Technology B* 21 (2003) 828.

- [198] J.S. Han, J.P. McVittie, J. Zheng, Profile Modeling Of High Density Plasma Oxide Etching, *Journal Of Vacuum Science & Technology B* 13 (1995) 1893-1899.
- [199] A.M. Barklund, H.O. Blom, Influence of polymer formation on the angular dependence of reactive ion beam etching, *Journal of Vacuum Science & Technology A* 10 (1992) 1212-1216.
- [200] J.A.G. Baggerman, R.J. Visser, E.J.H. Collart, Ion-induced etching of organic polymers in argon and oxygen radio-frequency plasmas, *J Appl Phys* 75 (1994) 758-769.
- [201] E. Pargon, D. Nest, D.B. Graves, Ar⁺ bombardment of 193 nm photoresist: Morphological effects, *Journal Of Vacuum Science & Technology B* 25 (2007) 1236-1243.
- [202] J.P. Chang, H.H. Sawin, Molecular-beam study of the plasma-surface kinetics of silicon dioxide and photoresist etching with chlorine, *Journal of Vacuum Science & Technology B* 19 (2001) 1319-1327.
- [203] www.phietch.org.
- [204] N. Cheimarios, G. Kokkoris, A.G. Boudouvis, Multiscale modeling in chemical vapor deposition processes: Coupling reactor scale with feature scale computations, *Chem. Eng. Sci.* 65 (2010) 5018-5028.
- [205] G. Kokkoris, A. Tserepi, A.G. Boudouvis, E. Gogolides, Simulation of SiO₂ and Si feature etching for microelectronics and microelectromechanical systems fabrication: A combined simulator coupling modules of surface etching, local flux calculation, and profile evolution, *J. Vac. Sci. Technol. A* 22 (2004) 1896-1902.
- [206] A. Bès, M. Koo, T.L. Phan, A. Lacoste, J. Pelletier, Oxygen plasma etching of hydrocarbon-like polymers: Part I Modeling, *Plasma Process Polym* 15 (2018) 1800038.
- [207] M. Pons, J. Pelletier, O. Joubert, P. Paniez, Development of polymers in O₂ plasmas: Temperature effects and transition to imperfect anisotropy, *Jpn. J. Appl. Phys.* 34 (1995) 3723-3730.
- [208] O. Joubert, J. Pelletier, Y. Arnal, The etching of polymers in oxygen-based plasmas: A parametric study, *J. Appl. Phys.* 65 (1989) 5096-5100.
- [209] S. Mouchtouris, G. Kokkoris, Multiscale Modeling of Low Pressure Plasma Etching Processes: Linking the Operating Parameters of the Plasma Reactor with Surface Roughness Evolution, *Plasma Processes and Polymers* 14 (2017) 1600147.
- [210] S. Panda, D.J. Economou, L. Chen, Anisotropic etching of polymer films by high energy (~100s of eV) oxygen atom neutral beams, *J Vac Sci Technol A* 19 (2001) 398-404.
- [211] N. Vourdas, Microfluidics in chemical and biological microanalysis: interaction of polymers with gaseous plasmas for their selective etching and modification, *Engineering & Technology Chemical Engineering*, National Technical University of Athens 2007.
- [212] A.P.J. Jansen, *An Introduction to Kinetic Monte Carlo Simulations of Surface Reactions*, Springer 2012.
- [213] R. Lesar, *Computational Materials Science*, Cambridge University Press 2013.
- [214] A. Chatterjee, D.G. Vlachos, An overview of spatial microscopic and accelerated kinetic Monte Carlo methods, *Journal of Computer-Aided Materials Design* 14 (2007) 253-308.
- [215] D. Marinov, C. Teixeira, V. Guerra, Deterministic and Monte Carlo methods for simulation of plasma-surface interactions, *Plasma Processes and Polymers* 14 (2017).
- [216] M. Andersen, C. Panosetti, K. Reuter, A practical guide to surface kinetic Monte Carlo simulations, *Frontiers in Chemistry* 7 (2019).
- [217] N. Cheimarios, G. Kokkoris, A.G. Boudouvis, Multiscale Modeling in Chemical Vapor Deposition Processes: Models and Methodologies, *Archives of Computational Methods in Engineering* (2020).
- [218] V. Guerra, D. Marinov, Dynamical Monte Carlo methods for plasma-surface reactions, *Plasma Sources Sci. Technol.* 25 (2016).
- [219] D. Marinov, Kinetic Monte Carlo simulations of plasma-surface reactions on heterogeneous surfaces, *Frontiers of Chemical Science and Engineering* 13 (2019) 815-822.
- [220] D. Adalsteinsson, J.A. Sethian, Transport and diffusion of material quantities on propagating interfaces via level set methods, *J. Comput. Phys.* 185 (2003) 271-288.

- [221] K. Anselme, P. Davidson, A.M. Popa, M. Giazzon, M. Liley, L. Ploux, The interaction of cells and bacteria with surfaces structured at the nanometre scale, *Acta Biomater.* 6 (2010) 3824-3846.
- [222] J. Matsui, N. Nakano, Z.L. Petrović, T. Makabe, The effect of topographical local charging on the etching of deep-submicron structures in SiO₂ as a function of aspect ratio, *Appl. Phys. Lett.* 78 (2001) 883-885.
- [223] G.-C.W. Yiping Zhao, and Toh-Ming Lu, Characterization of Amorphous and

Crystalline Rough Surface" Principles

and Applications, Academic Press, United States of America, 2001.

- [224] J.A. Sánchez-García, L. Vázquez, R. Gago, A. Redondo-Cubero, J.M. Albella, Z. Czigány, Tuning the surface morphology in self-organized ion beam nanopatterning of Si(001) via metal incorporation: From holes to dots, *Nanotechnology* 19 (2008) 355306 (355309pp).
- [225] S. Mouchtouris, G. Kokkoris, A hybrid model for low pressure inductively coupled plasmas combining a fluid model for electrons with a plasma-potential-dependent energy distribution and a fluid-Monte Carlo model for ions, *Plasma Sources Science and Technology* 25 (2016) 025007.
- [226] D. Kontziampasis, Micro/nanomodification of polymers with plasma for bioanalytical applications, Department of Materials Science & Engineering, University of Ioannina
- 2013.
- [227] V. Krokos, G. Pashos, A.N. Spyropoulos, G. Kokkoris, A.G. Papathanasiou, A.G. Boudouvis, Optimization of Patterned Surfaces for Improved Superhydrophobicity through Cost-Effective Large-Scale Computations, *Langmuir* 35 (2019) 6793-6802.
- [228] G. Pashos, G. Kokkoris, A.G. Papathanasiou, A.G. Boudouvis, Wetting transitions on patterned surfaces with diffuse interaction potentials embedded in a Young-Laplace formulation, *J. Chem. Phys.* 144 (2016) 034105.
- [229] G. Pashos, G. Kokkoris, A.G. Boudouvis, A modified phase-field method for the investigation of wetting transitions of droplets on patterned surfaces, *J. Comput. Phys.* 283 (2015) 258-270.
- [230] G. Pashos, G. Kokkoris, A.G. Boudouvis, Minimum Energy Paths of Wetting Transitions on Grooved Surfaces, *Langmuir* 31 (2015) 3059-3068.
- [231] D. Kontziampasis, V. Constantoudis, E. Gogolides, Plasma Directed Organization of Nanodots on Polymers: Effects of Polymer Type and Etching Time on Morphology and Order, *Plasma Process Polym* 9 (2012) 866-872.
- [232] D. Kontziampasis, Micro/nanomodification of polymers with plasma for bioanalytical applications, Department of Materials Science & Engineering, University of Ioannina, Ioannina, 2013.
- [233] W. Kunstler, P. Frubing, R. Gerhard-Multhaupt, J. Cerny, J. Klemberg-Sapieha, L. Martinu, M.R. Wertheimer, A. Hollander, J. Behnisch, Surface-charging behavior of plasma-treated polymer films, 1998 Annual Report Conference on Electrical Insulation and Dielectric Phenomena (Cat. No.98CH36257), 1998, pp. 609-612 vol. 602.
- [234] S. Mouchtouris, G. Kokkoris, A hybrid model for low pressure inductively coupled plasmas combining a fluid model for electrons with a plasma-potential-dependent energy distribution and a fluid-Monte Carlo model for ions, *Plasma Sources Sci. Technol.* 25 (2016) 025007.
- [235] V. Belaud, S. Valette, G. Stremdoerfer, M. Bigerelle, S. Benayoun, Wettability versus roughness: Multi-scales approach, *Tribology International* 82 (2015) 343-349.
- [236] D.G. Vlachos, Temporal coarse-graining of microscopic-lattice kinetic Monte Carlo simulations via τ leaping, *Physical Review E - Statistical, Nonlinear, and Soft Matter Physics* 78 (2008).
- [237] M.A. Katsoulakis, A.J. Majda, D.G. Vlachos, Coarse-grained stochastic processes for microscopic lattice systems, *Proceedings of the National Academy of Sciences of the United States of America* 100 (2003) 782-787.

- [238] M.A. Katsoulakis, A.J. Majda, D.G. Vlachos, Coarse-grained stochastic processes and Monte Carlo simulations in lattice systems, *Journal of Computational Physics* 186 (2003) 250-278.
- [239] M.A. Katsoulakis, D.G. Vlachos, Coarse-grained stochastic processes and kinetic Monte Carlo simulators for the diffusion of interacting particles, *Journal of Chemical Physics* 119 (2003) 9412-9427.
- [240] A. Chatterjee, M.A. Katsoulakis, D.G. Vlachos, Spatially adaptive grand canonical ensemble Monte Carlo simulations, *Physical Review E* 71 (2005) 026702.
- [241] A. Chatterjee, D.G. Vlachos, M.A. Katsoulakis, Numerical Assessment of Theoretical Error Estimates in Coarse-Grained Kinetic Monte Carlo Simulations: Application to Surface Diffusion, 3 (2005) 59-70.
- [242] A. Chatterjee, D.G. Vlachos, Multiscale spatial Monte Carlo simulations: Multigriding, computational singular perturbation, and hierarchical stochastic closures, *Journal of Chemical Physics* 124 (2006).
- [243] S.D. Collins, A. Chatterjee, D.G. Vlachos, Coarse-grained kinetic Monte Carlo models: Complex lattices, multicomponent systems, and homogenization at the stochastic level, *Journal of Chemical Physics* 129 (2008).
- [244] A. Chatterjee, D.G. Vlachos, Temporal acceleration of spatially distributed kinetic Monte Carlo simulations, *Journal of Computational Physics* 211 (2006) 596-615.
- [245] D.T. Gillespie, Approximate accelerated stochastic simulation of chemically reacting systems, *Journal of Chemical Physics* 115 (2001) 1716-1733.
- [246] A. Chatterjee, D.G. Vlachos, M.A. Katsoulakis, Binomial distribution based τ -leap accelerated stochastic simulation, *Journal of Chemical Physics* 122 (2005).
- [247] L. Xu, M. Taufer, S. Collins, D.G. Vlachos, Parallelization of tau-leap coarse-grained Monte Carlo Simulations on GPUs, *Proceedings of the 2010 IEEE International Symposium on Parallel and Distributed Processing, IPDPS 2010*, 2010.